"SPECTRAL AND BULK PROPERTIES OF TURBULENCE IN THE SURFACE LAYER OF AIR OVER THE SEA".

by

JOHN ROY GARRATT, A.R.C.S., B.Sc.

Department of Meteorology,
Imperial College of Science and Technology.

A Thesis submitted for the Degree
of Doctor of Philosophy in the
University of London,
September 1969.

"Turbulence is a human artefact".

P.A.S.

ABSTRACT

An analysis has been made of the vertical profiles of mean wind speed u, potential temperature θ and specific humidity q in the first 16 m. above a sea surface, and of the eddy fluxes of heat and momentum, velocity and temperature spectra, flux cospectra and other statistics using simultaneous observations of fluctuations of air temperature, vertical and horizontal (longitudinal) wind speed at any two of the levels 1.5 m., 4 m., and 12 m.

Profiles of u and θ are found to be dissimilar in non-neutral stability implying a variation of the eddy transfer coefficient ratio K_H/K_M agreeing, qualitatively, with the direct flux-gradient measurements. The ratio is significantly greater than unity in unstable, and less than unity in stable, stratification.

For the majority of runs fluxes of heat and momentum are approximately constant with height, the remainder having a variation implying significant horizontal gradients of wind speed and temperature. Further only when the momentum flux is approximately constant with height is there close agreement with the friction velocity evaluated independently from the wind profile. An empirical formula is suggested relating heat flux to the more readily measured quantities u_{10}, $\theta_{10}-\theta_o$.

The spectra at high frequencies are related to the Kolmogorov predictions and the Universal constants are evaluated for the velocity spectrum and structure function. Evaluation of a non-dimensional dissipation rate as a function of Ri is shown

to be consistent with a Von Karmen constant of 0.4.

Spectra and cospectra are described through the Similarity Theory and together with data from other sources they indicate a set of Universal spectra and cospectra appropriate to the surface layer and any type of lower boundary. In the -5/3 region of the velocity spectra the ratio of the vertical to longitudinal power agrees with the Kolmogorov prediction of 4/3, though there is evidence that the turbulence in this range is not isotropic.

Observations of wave spectra with fetches ~ 10 km. give the Universal constant of the equilibrium range in excellent agreement with that deduced by Phillips. There is no evidence that wave power impresses itself on the turbulence spectra at or above 1.5 m. height.

CONTENTS

List of Symbols

A	constant.
a	constant.
B	production rate of buoyancy energy term.
b	constant.
C	constant.
C_D	drag coefficient.
C_H	heat transfer coefficient.
c	wave phase velocity.
C_p	specific heat at constant pressure.
D	vertical flux divergence term.
D_i	Structure Function.
E	rate of evaporation; total turbulent kinetic energy.
F	function; fetch.
f	function; dimensionless frequency.
G	vertical gradient.
g	function; acceleration due to gravity = 981 cm sec^{-2}.
H	turbulent heat flux.
h	height of internal boundary layer; instantaneous water level at a fixed point above an arbitrary zero.
$\overline{h}$	mean water level.
h'	instantaneous fluctuation from the mean i.e. wave amplitude.
i	square root of minus one.
K	constant; eddy transfer coefficient.
k	wave number in radians cm^{-1}.
L or L_v	Monin-Oboukhov stability length.
L_w	latent heat of evaporation.
n	frequency in cycles per second.
P	index of stability; production rate of mechanical energy term.
p	pressure.
Q	humidity component of "virtual" Richardson number, Ri_v.
Q_{ij}	quadrature spectrum.
q_i	autocovariance.
q_{ij}	cross-variance
q	instantaneous specific humidity.
$\overline{q}$	mean specific humidity.
q'	fluctuation from the mean.
R	spectral correlation coefficient.
Ri	gradient Richardson number for dry air.
Ri_v	gradient Richardson number for moist air.
r_i	auto correlation coefficient.
r_{ij}	cross correlation coefficient.
r_{xy}	correlation coefficient.
S	profile shape factor.
s	fluid property.
T	instantaneous temperature; time period.
$\overline{T}$	mean temperature.
T'	fluctuation from the mean.
T_v	virtual temperature.
T_w	wet-bulb temperature.
t	time; wind duration.
Δt	data spacing time.

u instantaneous horizontal longitudinal wind component.
$\overline{u}$ mean wind speed.
u' fluctuation from the mean.
u_o surface drift velocity.
u_* friction velocity.
V instantaneous wind speed from mini-anemometer.
$\overline{V}$ mean wind speed.
V' fluctuation from the mean.
v' horizontal lateral wind component ($\overline{v} = 0$).
w instantaneous vertical velocity.
$\overline{w}$ mean vertical velocity.
w' fluctuation from the mean.
X parameter representing u, θ, q; length scale.
x downwind separation distance; Cartesian coordinate.
y Cartesian coordinate.
z height above mean water level.
z_s, z_o, z_T aerodynamic roughness parameter.
α constant.
β constant.
γ thermal diffusivity.
ϵ constant; rate of dissipation of turbulent kinetic energy per unit mass.
ζ stability parameter = z/L.
η function.
θ potential temperature (usually written for the mean value, $\overline{\theta}$).
θ_v virtual potential temperature.
θ_* scaling temperature.
κ Von Karmen's constant.
λ wave length.
ν kinematic viscosity.
ρ function; air density.
ρ_w water density.
σ standard deviation; surface tension.
τ frictional stress; response time.
τ_s sampling period.
Φ Universal vertical dimensionless gradients.
ϕ, ϕ_o wind vane angle.
ϕ_i spectrum.
ϕ_{ij} cospectrum.
χ rate of destruction of temperature fluctuations.
ξ time lag.
ψ function.

$$\sigma_u \equiv (\overline{u'^2})^{1/2}$$

$$\sigma_w \equiv (\overline{w'^2})^{1/2}$$

$$\sigma_{uw} \equiv (-\overline{u'w'})^{1/2} = u_*$$

$$\sigma_T \equiv (\overline{T'^2})^{1/2}$$

$$\sigma_{wT} \equiv (|\overline{w'T'}|)^{1/2}$$

$$\sigma_{uT} \equiv (|\overline{u'T'}|)^{1/2}$$

$$\sigma_{h} \equiv (\overline{h^2})^{1/2}$$

Reference Abbreviations

B.P. Busch and Panofsky (1968).

L.P. Lumley and Panofsky (1964).

M.Z. Mordukovitch and Zwang (1966).

P.M. Panofsky and Mares (1968).

W.B. Weiler and Burling (1968).

Z.K. Zubkovskii and Kravchenko (1967).

1.1. Air-Sea Interaction Studies

Current studies in the surface layer of the atmosphere over the sea are being made by a number of research groups attached to the following – the University of Hamburg (over the Baltic Sea); the Institute of Atmospheric Sciences, Moscow (Black and Mediterranean Seas); the University of British Columbia (Spanish Banks site, Vancouver); the University of Michigan (Lake Michigan) and the Department of Meteorology, Imperial College (Lough Neagh, Northern Ireland) under the supervision of Professor P.A. Sheppard. Some of the above groups make both air and water (e.g. wave) measurements, whilst others make only air measurements. Up to date no set of comprehensive results of the investigation into the wave characteristics and the turbulent structure of the air flow above the waves has been published but with the interest in experimental work dealing with the air-sea interaction growing it does seem that within the next few years important information will be forthcoming from the above-mentioned groups. However, Pond et al. (1966), Smith (1966) and Weiler and Burling (1968) working at Vancouver have published papers mainly on the spectral characteristics of turbulence several metres above the waves; Zubkovskii and Kravchenko (1967) on some bulk properties of turbulence as have Brocks et al. (1966) from Hamburg. The results contained in this thesis are the first comprehensive set obtained from the Lough Neagh site and it is hoped that they will stimulate further investigation as an extension of the present one using the facility of the Lough Neagh site.

In Chapter 2, the experimental site and equipment is described with full specification of the observations together with

a description of the data processing. Chapter 3 describes the analysis of vertical profiles of wind speed, potential temperature and specific humidity with particular emphasis on the turbulent transfers of momentum, sensible heat and water vapour and their relative efficiencies as a function of atmospheric stability. Chapter 4 is concerned with the bulk properties of the turbulence, describing the eddy flux measurements with particular emphasis upon the "constant-flux" hypothesis and the investigation of alternative methods of obtaining the fluxes (in addition to the eddy correlation technique). Also included is the evaluation from experimental data of the Kolmogorov Universal constants for velocity which are subsequently used in determining the dissipation rate of kinetic energy whose properties are investigated. Flux-gradient relations are used to determine the variation of K_H/K_M with stability.

Chapter 5 describes in detail the spectral properties of turbulence for velocity (the vertical and horizontal longitudinal components) and temperature fluctuations using the Monin-Oboukhov Similarity Theory. In this chapter the lack of evidence of the presence of locally isotropic turbulence in the frequency range investigated is stressed. In addition the terms in the budget equation for temperature fluctuations are estimated and the nature of turbulent transfer observed in convective conditions described. Finally Chapter 6 describes wave statistics, in particular wave spectra and the equilibrium (saturation energy) range, and the relation between wave properties and the aerodynamic roughness is discussed.

1.2. Development of Turbulence Theories of Special Interest for the Atmosphere and Ocean

The practical importance of the study of turbulence in the surface layer lies in the construction of a physical and numerical basis for the calculation of heat, momentum and moisture transfer over different types of the Earth's surface. Special problems would seem to arise in the study of processes in the surface layer over the sea where atmospheric turbulence must, in some sense, be related with the presence of wind induced waves. Knowledge of the turbulence characteristics is extremely important for the solution of many problems which include diffusion, electro-magnetic wave scattering, the "twinkling of stars" phenomenon (Tatarskii, 1961) and more comprehensive weather prediction, the latter depending critically upon the recognition and quantitative understanding of the effects upon air-mass modification at one scale produced by the turbulent motions occurring at smaller scales, from within the surface layer, (regarding the latter, see Priestley, 1967).

The study of the microstructure of the atmospheric motions requires the statistical approach because of the random motions involved and the aim of the study must be to relate the statistics to the physical processes involved (for treatises on modern statistical theories of turbulence see Batchelor, 1953 and Hinze, 1959).

The theory of turbulence progressed rapidly with the introduction of the concept of the correlation function and energy spectrum to describe the characteristics of a field of turbulence in respect of the scales of motion involved. One of the major

results of investigation in recent decades is the clear understanding that the properties of turbulent flows for various ranges of scale differ in character and require a distinctive approach. The approach may be made through the spectrum (after G.I. Taylor, Von Weisäcker) or through use of the structure function (after Kolmogorov) according to convenience because one is the Fourier transform of the other. An intuitive grasp of the major physical processes operative in different parts of the spectrum afforded the possibility of a quantitative analysis of the turbulence essentially in three regions —

I : the energy-containing (production) region,

II : the inertial sub-range (steady transfer) region,

III : the viscous (dissipation) region,

as illustrated in Fig.1.1. Kolmogorov's theory of locally isotropic turbulence for developed turbulence at high Reynold's number (Batchelor, 1947) predicted a state of Universal equilibrium for the isotropic eddies (regions II and III) whose properties are conditioned by,

(i) the inflow of energy from region I to II which equals the transfer rate of the energy across II to region III where it is dissipated by viscous forces at a rate = ε,

(ii) the viscosity.

Further if the inertial sub-range is sufficiently wide (viz. the Re is large enough) its average properties, removed from the influence of viscosity effective only at much smaller scales, will depend only upon ε.

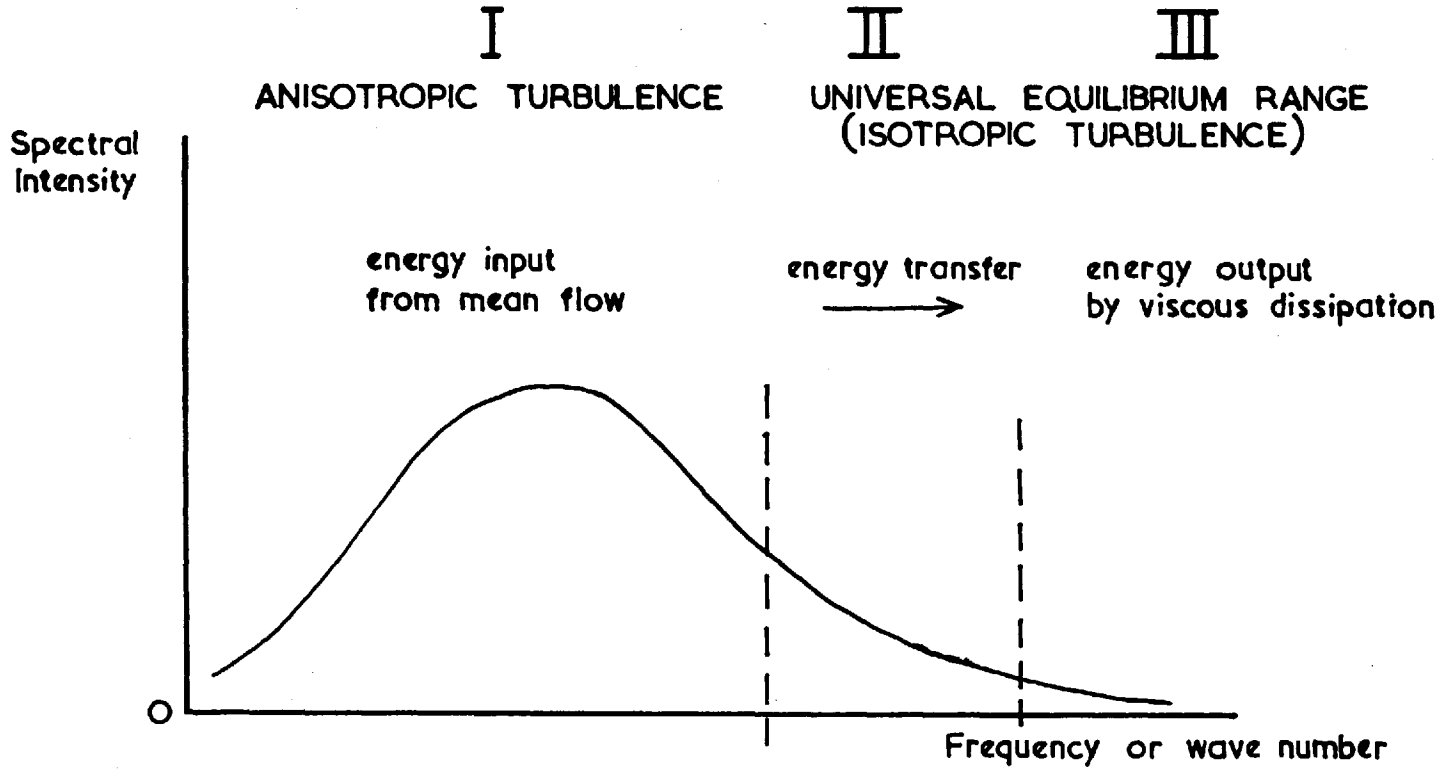

DIAGRAMMATIC REPRESENTATION OF MICROMETEOROLOGICAL SPECTRUM

FIG.1.1

Originally Kolmogorov applied his hypotheses of similarity of flow to the form of the structure function $D(x)$, the mean square velocity difference between two points in the flow separated by x, in the corresponding x inertial sub-range, viz.,

$$D_{vel}(x) \sim \varepsilon^{2/3} x^{2/3} \qquad 1.1$$

The corresponding law of the spectrum, in terms of the wave-number k is,

$$\phi_{vel}(k) \sim \varepsilon^{2/3} k^{-5/3} \qquad 1.2$$

Using similar arguments Oboukhov, in 1949, extended the theory to include temperature fluctuations. Indeed it can be expected that the theory will apply to other scalar quantities e.g. humidity, refractive index (Tatarskii, 1961). For temperature, properties in the inertial sub-range will depend additionally upon χ, the rate of destruction of fluctuations by molecular conduction, so that,

$$D_T(x) \sim \chi \varepsilon^{-1/3} x^{-5/3} \qquad 1.3$$

and,

$$\phi_T(k) \sim \chi \varepsilon^{-1/3} k^{-5/3} \qquad 1.4$$

The major contribution to the structure function at any separation x will come from eddies of size $\lambda < x$, since it will hardly be affected by eddies with $\lambda >> x$ because the eddy velocities will be the same at $\underline{r} = 0$ and $\underline{r} = x$. Choosing eddies in the inertial sub-range of k, then the structure function is not affected by eddies with

$\lambda << x$ since the eddies will be non-coherent. Thus x in the inertial sub-range is $\sim\lambda$ in the inertial sub-range. Conversely the spectral density within the inertial sub-range is determined by the correlation function at $x \sim \lambda$ and is independent of the form of the correlation at $x << \lambda$ and $x >> \lambda$.

The structure function and spectrum dependence upon x and k respectively predicted by these laws have been confirmed many times as shown in a review by L.P. p.163 —see also Chapter 5. Perhaps the best confirmation has come from measurements by Pond et al. (1966) who determined the spectra for velocity (the u component) and temperature both in the inertial sub-range and the dissipation range. The spectrum law has also been confirmed for velocity in the ocean (Grant et al., 1962) and for humidity fluctuations in the atmosphere (Elagina, 1963).

Although confirmation of the laws is generally accepted it is now thought (Oboukhov, 1962) that they are only a first approximation to reality because fluctuations in the dissipation rate of energy (and presumably in χ) should produce deviations from the theoretical laws. However estimates of this deviation (the index of k would change to -1.71 from -1.67) show it to be far below the best experimental accuracy yet obtained. An interesting feature of measured power spectra is the range of the observed laws, best seen in the u wind component and temperature which extend far into the anisotropic region —see Chapter 5. The anomalous behaviour may be related to the fact that the theory as envisaged originally applies to a three dimensional field whereas measurements are made of a one dimensional component of the velocity field

(Gifford, 1959) — however such a theory would not be valid for a scalar like temperature. It is suggested that because there is no sudden transition from anisotropy to local isotropy (i.e. the boundary between regions I and II in Fig.1.1 is not sharp) it is possible to imagine a transition region of weakly anisotropic turbulence but whose properties depend primarily upon ϵ (and χ, in the case of temperature) and only weakly upon the factors characterising the anisotropy. At larger scales these factors would determine the spectrum properties entirely.

The next important breakthrough in the advancement of turbulence theories for geophysical application came through the work of Monin and Oboukhov who developed a basic theory of similarity of atmospheric turbulence in a thermally stratified surface (constant-flux) layer. In essence the statistical properties depend upon a small number of variables which can be specified by forming scaling parameters of length, velocity and temperature (L, u_*, θ_* respectively) from the heat flux H, buoyancy parameter g/T and surface stress τ_o, as follows —

$$L = \frac{-(\tau_o/\rho)^{3/2}}{k\, g/T.\,(H/\rho C_p)} \qquad 1.5$$

$$u_* = (\tau_o/\rho)^{1/2} \qquad 1.6$$

$$\theta_* = \frac{-(H/\rho C_p)}{u_*} \qquad 1.7$$

The basic postulate of the Monin-Oboukhov Similarity Theory states that all dimensionless characteristics of turbulence in the

surface layer shall be universal functions of the parameter z/L characterising the degree of thermal stratification. § 5.2. describes the Similarity theories in more detail.

Application of this principle has received much attention in recent years (L.P. contains a survey of results as does Monin (1962) of Russian measurements) and is widely used in the present thesis. More recent results (Chapter 5) suggest that the very large-scale components of the turbulence may not obey the Similarity Theory.

1.3. Specification of Turbulence

If one considers a fluid property S and its variation with time at a point in space, then, following Reynolds (1895), the instantaneous value can be defined as being made up of a mean component $\overline{S}$ and a turbulent component S' so that S' is a fluctuation in S about a temporal mean $\overline{S}$.

The chief difficulty arises in defining the mean value, but in general this will be achieved if the sampling period τ_s is sufficiently large to contain a large number of fluctuations, such that fluctuations in $\overline{S}$ with τ_s increasing are relatively small. It is a primary requirement for the specification of turbulence that a stable mean value exists and one must appeal to observation for the minimum period which will give such a stable value.

Until recently it was generally thought that the spectrum of atmospheric motions (of the u component of the wind, for instance) remained unbroken from the smallest disturbances in the surface layer (viscous eddies) through to disturbances of the general circulation (cyclones and long waves). Recent measurements of

wind speed and temperature spectra are strong evidence for the existence of a spectral gap separating micrometeorological from synoptic motions. Such spectra of wind speed published by Panofsky and Van de Hoven (1955), Van de Hoven (1957), and of wind speed and temperature by Kolesnikova and Monin (1965) are characterised by a region of relatively low spectral intensity at periods of the order of one hour, with a micrometeorological peak occurring at periods of the order of several minutes. By choosing the sampling period somewhere between the gap and this peak (preferably as close to the gap as possible though technically this may be difficult) one substantially mitigates the difficulties encountered in determining mean values independent of sampling period and hence with the specification required.

Chou Min-Yui (1966) has carried out an analysis of experimental data to determine the optimum τ_s and concludes that, in the first 10 m. of the atmosphere, a period of about 15 minutes "is safe" for both wind and temperature. Indeed measurements within the surface layer (see B.P., P.M. and Chapter 5) suggest τ_s = 10 minutes may be sufficient though results show (§ 4.2.2.) that such a τ_s retains a significant degree of statistical variability in the flux estimates.

In practice the position of the spectral gap is highly variable depending to a large extent upon stability and in very strong convection may disappear completely (Panofsky and Deland, 1959). It depends to a lesser extent upon wind speed and aerodynamic roughness of the underlying surface. Fig.1.2 shows a spectrum measured by Van de Hoven (loc. cit.). It is quite possible that

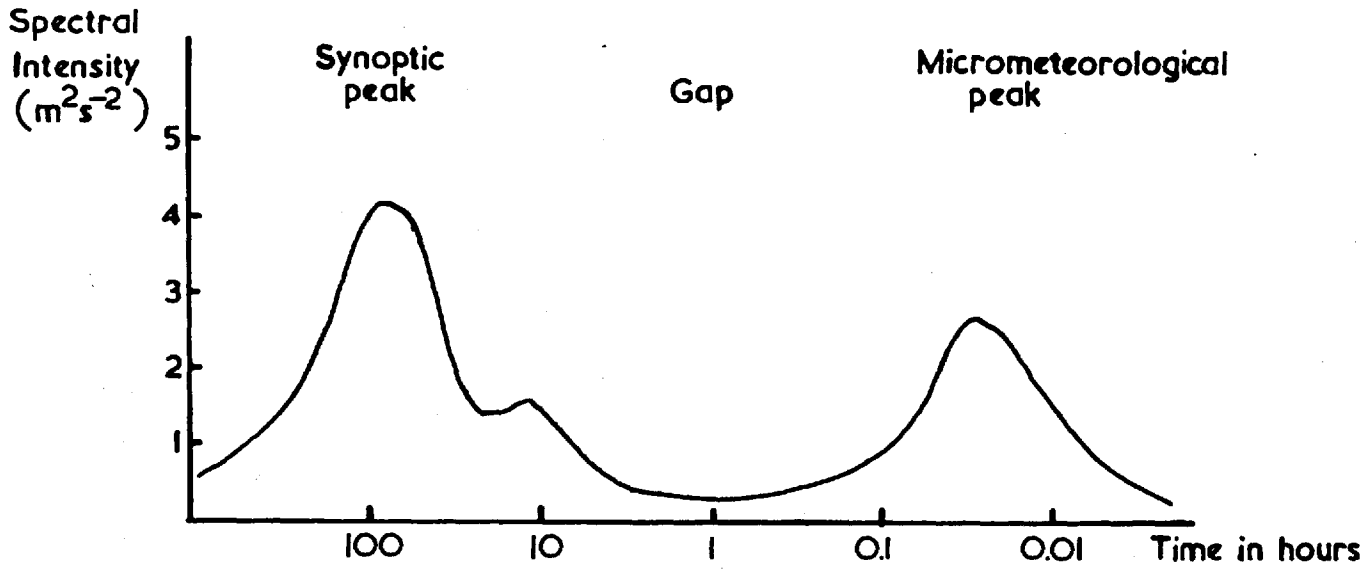

HORIZONTAL WIND SPEED SPECTRUM AT A HEIGHT OF 100m
from Van de Hoven (1957)

FIG.1.2

on some occasions $\tau_s = 10$ minutes corresponds to a period within the gap — and hence a stable mean — whilst at other times it may well correspond to a period close to the peak. In such cases, energy and flux estimates will be underestimated and when interpreting turbulence properties, and in particular when comparing results with different values of τ_s, one must be aware of this additional variable.

1.4. Large-Scale Restrictions on the Flow

1.4.1. Fetch

Only a small range of fetch can be encompassed at the present site. However surface and lower boundary layer behaviour are likely to be only weakly dependent upon fetch beyond a few kilometres and the present site is at least free from a complication on the ocean of waves being advected to a site from a source unrelated to the local wind (swell). Thus while the application of the results of this study to the ocean must be tentative, the site is well adapted to disclosing essential aspects of the interaction of wind and water.

1.4.2. Horizontal Inhomogeneity

Turbulence theories are simplified by the assumption of horizontally homogeneous mean and turbulent fields of wind speed and temperature. It is a feature of the equations for the local rates of change of wind speed and temperature (§ 4.2.3.) that such inhomogeneity, manifest as horizontal gradients in the respective properties, produces a vertical variation of the corresponding

vertical fluxes. Unfortunately no measurement is made of horizontal variations in the quantities during the periods of recording.

1.4.3. Non-Stationarity

Most theories of turbulence are greatly simplified by the assumption of stationary flow, and in practice the presence of non-stationary turbulence will complicate any investigation. The presence of non-stationary wind and temperature fields manifests itself in the presence of trends in recorded data and may, for instance, be caused by very large eddies produced by air flowing around a large obstruction (a small mountain or range of hills) many tens of kilometres upstream, or by the passage of some mesoscale phenomenon (a cumulo-nimbus) or a large-scale weather system (a front). In the case of the cumulo-nimbus the spectral gap (see Fig.1.2) is broken by the appearance of an "energy spike" and for the synoptic system the energy belongs to the low frequency side of the gap, dissociated from the micrometeorological motions. In practice it is difficult to separate the smaller-scale from the larger-scale motions unless the trend is linear, and observations are preferably made under near-stationary conditions where the spectral gap is clearly defined. A non-stationary condition is still worthy of examination by use of structure functions which at small time lag effectively act as high pass filters and are therefore independent of any trend in the data. This will also be the case for the inertial sub-range of the spectrum.

CHAPTER 2

2.1. EXPERIMENTAL WORK AT LOUGH NEAGH

Pond (1968a) has given a brief description of the instrumentation and basic features of the investigation being undertaken at the Lough Neagh site of the air-sea interaction. It is now intended to describe in much more detail many aspects of the experimental work being attempted, with full description of site and instrumentation and subsequent data analysis.

2.1.1. Description of Site

The tower upon which the instrumentation is mounted stands in about 7 m. of water some 700 m. offshore on the eastern side of Lough Neagh, in Northern Ireland. Referring to the map of Fig.2.1. it is seen that the tower lies approximately midway on a straight line joining the north land point to the south point so that the azimuthal freedom for uninterrupted air flow across the water to the tower is some 170° (190° to 360°). When air blows from beyond these extreme directions, a complication arises in the form of severe refraction of the water waves resulting in loss of equilibrium between wind and waves and, more important, boundary layer equilibrium up to the top of the tower is not attained in the shorter fetches - consequently no serious work is then attempted. The diagram also illustrates the range of fetches available for the investigations of the air-sea interaction through the studies of the mean and turbulent structure of the surface layer of air, and of the wave structure. According to past studies of the formation of the internal boundary layer (i.b.l.) when air blows from land to sea (see e.g. Elliot, 1958 and Panofsky and Townsend, 1964)

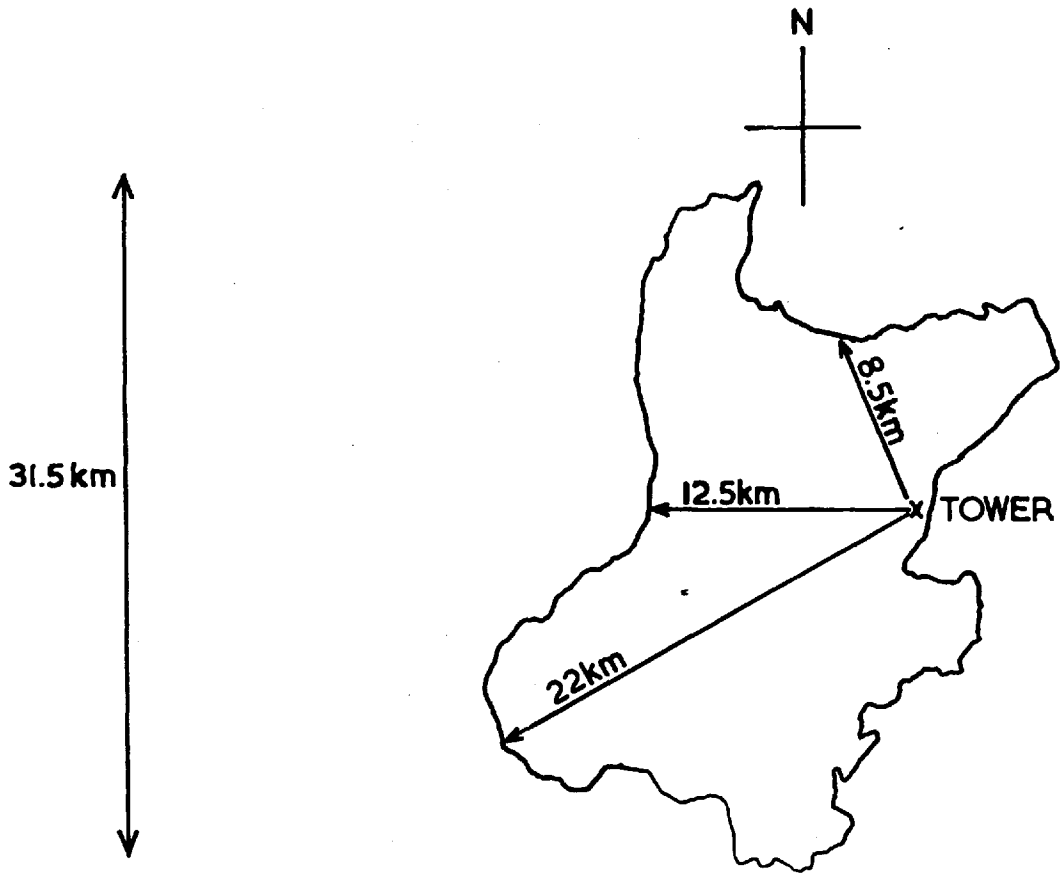

LOUGH NEAGH,
N. IRELAND.

FIG. 2.1

the height of the modified boundary layer (h) should increase approximately linearly with the increase in fetch (F), viz., $h/F \simeq .005$ to $.01$. At the minimum fetch of 8 Km., $h \simeq 50$ m. and the surface layer properties will be characteristically sea modified, with the instruments at 16 m. being well within the i.b.l. (Indeed the tower is situated such that air blowing off the north or south points reaches the tower with air below 15 m. (approx.) undisturbed by the short land traversal.)

The Lough has rather flat country immediately to its south, west, and north, but there is a mountain range (maximum height 1000 m.) some 45 Km. distant at a bearing of 290° to 310° from the tower, which may induce some extra unsteadiness of wind at the tower though there is no direct evidence of this. Certainly in its overall properties Lough Neagh represents outstandingly the best large inland water site for studies such as the present.

2.1.2. Description of Tower

Plates 1a, 1b show photographs of the tower and instrument mast looking from the west south west towards the shoreline. They show structural features and instrument positioning, and give a general indication of exposure in working conditions.

The angle-iron platform, having a 3 m. square deck with metal grille to minimise wave damage in gales, supports a triangular scaffolding tower with ladder arrangement and main supports for instrumentation facing towards the west. The platform deck is at 2.5 m. above mean water surface and the tower reaches 12 m. - an extension pole enabling instruments to be placed at

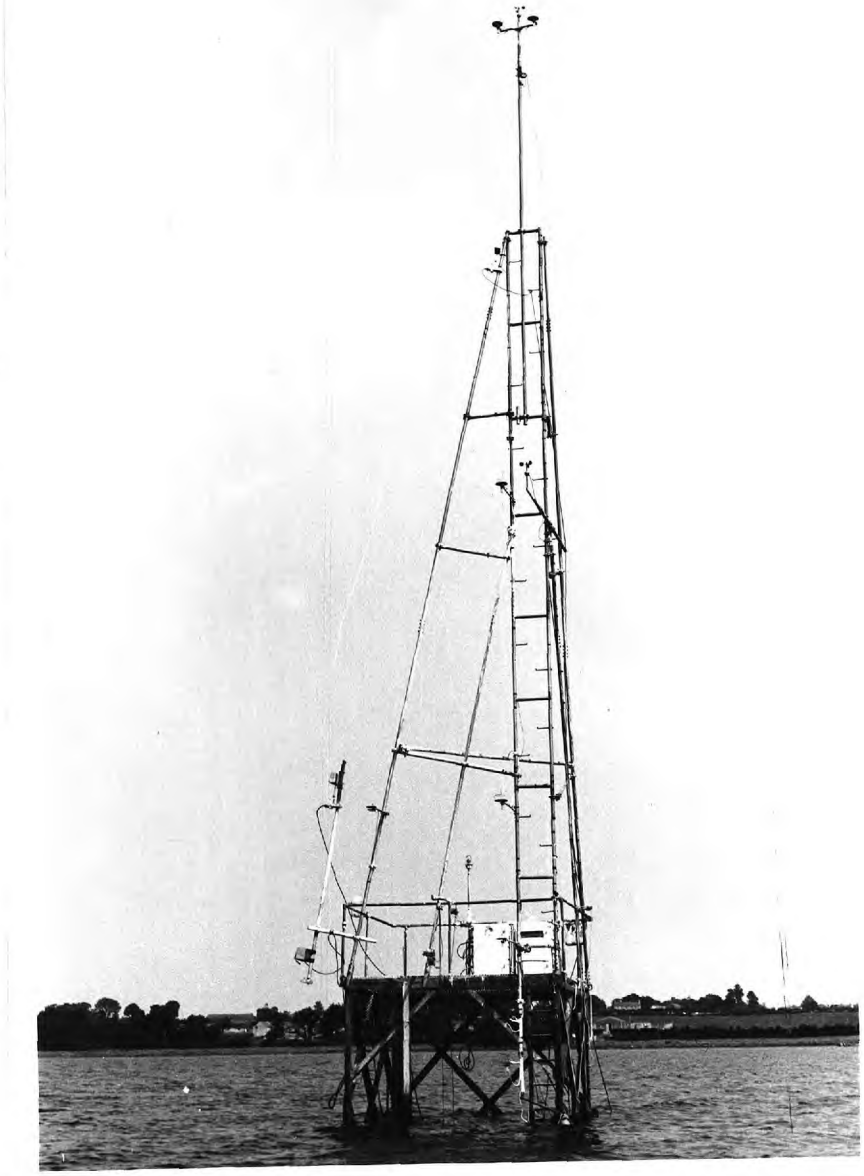

Plate Ia

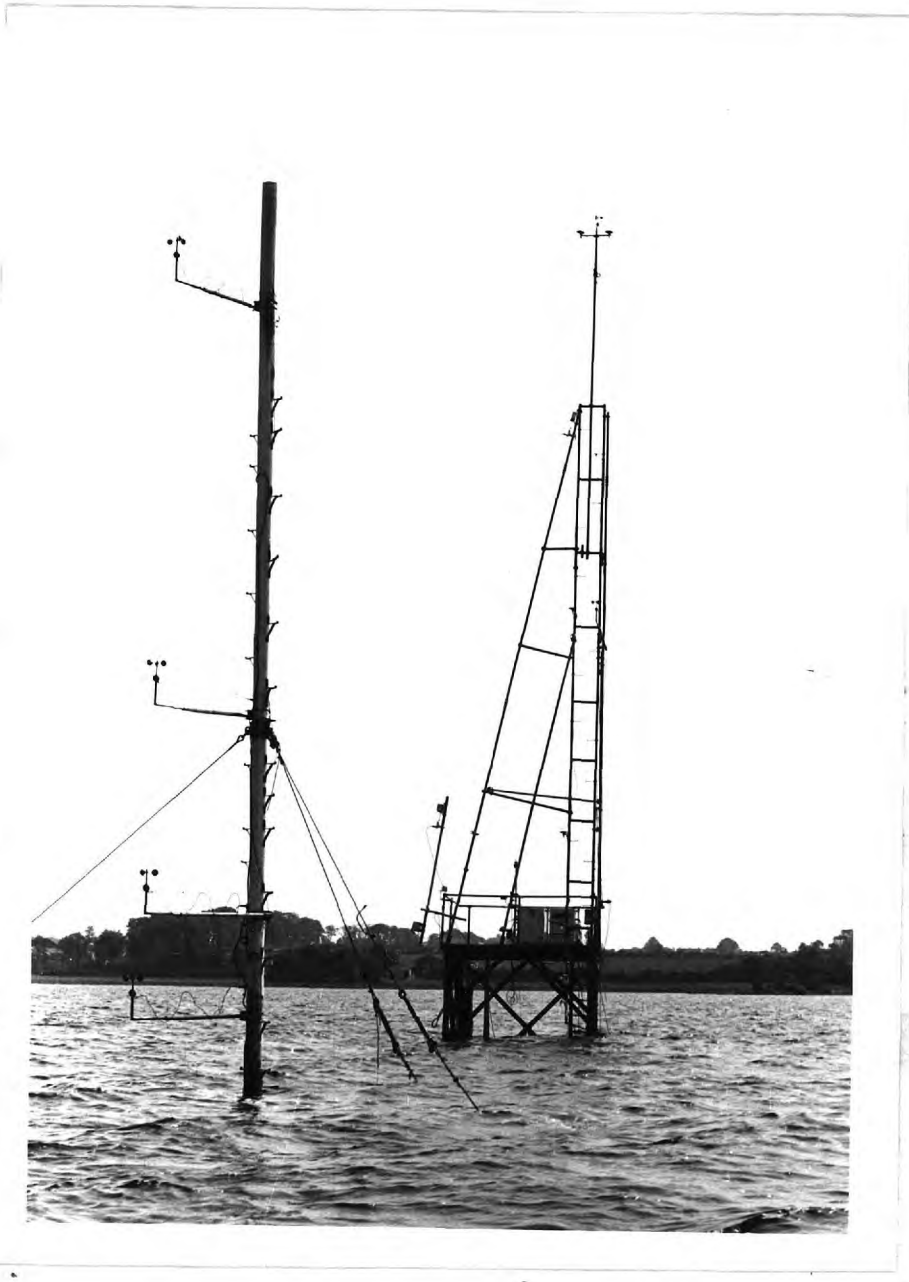

Plate Ib

the 16 m. level. In the north east corner of the platform is a "still-well" (see § 2.1.5.) and on the east side the electronic instrumentation is housed in "all-weather" covers, from which run the main cables along the sea-bed to the onshore laboratory some 700 m. away. 25 m. from the main tower towards the west stands an instrument mast, guyed to the sea-bed and designed to carry a vertical array of large-cup (profile) anemometers.

This mast is used to provide a more interference-free support for the anemometers up to 8 m. than would be provided by the tower. Less stringent exposure precautions are needed for representative measurements of the scalar quantities, temperature and humidity, and for the fluctuations.

2.1.3. Profile Instrumentation

Profile Anemometry: The anemometer consists of a set of 'Sheppard' cups mounted on a shaft which has a stainless steel ball race at the top, and a thrust jewel bearing at the bottom. Inside the spherical housing is a disc rotating with the shaft and interrupting the light from a small bulb to a photo-transistor. Anemometers are mounted on the mast at heights above the water of about 1 m., 2 m., 4 m. and 8 m. and on the tower again at 8 m. and at 16 m. The signals from each photo-transistor are taken to shore where a simple two-transistor amplifier drives an electro-mechanical counter at a rate of one count per revolution of the cups.

Profile Thermometry: Both dry- and wet-bulb thermometers are thermojunctions made from fine manganin-constantin wire, matched

for thermo-electric potential into the main lead wires. The junctions are enclosed in 20 s.w.g. stainless steel tubing welded over at the ends. The joints are welded and insulated from the steel by an epoxy-resin filling to a minimum of 10^8 ohms leakage resistance. These steel probes are mounted on thin acrylic "snouts" between radiation shields. The fine wires are welded to the heavier (30 s.w.g.) lead wires, and encapsulated within an acrylic block which holds the structure onto the mounting arm (see Plate 2a). Testing for thermal conduction error showed that in an airflow of ~ 2 m.s^{-1} the temperature at the base of the "snout" had to be raised to 100°C before an error of 0.01°C was obtained at the junction.

The wet-bulb is positioned down wind and slightly above the dry-bulb, and is covered with a close fitting wick made from cellulose tissue. A large (3 mm. diameter) wick of the same material brings water from the polythene bottle hanging below the block, up to the top surface immediately behind the wet-bulb and the small replaceable wick is fed from this point. Even in the generally clean air of Northern Ireland it is found that to obtain wet-bulb temperatures to the required 0.01°C the wick should be replaced within 48 hours, preferably every 24 hours. The large feed wick will remain good for some 14 days. To ensure maximum response of the wet-bulb system, with adequate ventilation, work should be carried out in wind speeds >2 m.s^{-1}.

The radiation shield is made from steel-mesh reinforced P.V.C. sheeting in three layers. The top-most is a plain 18 cm. circular disc, firmly attached to the support arm. The upper

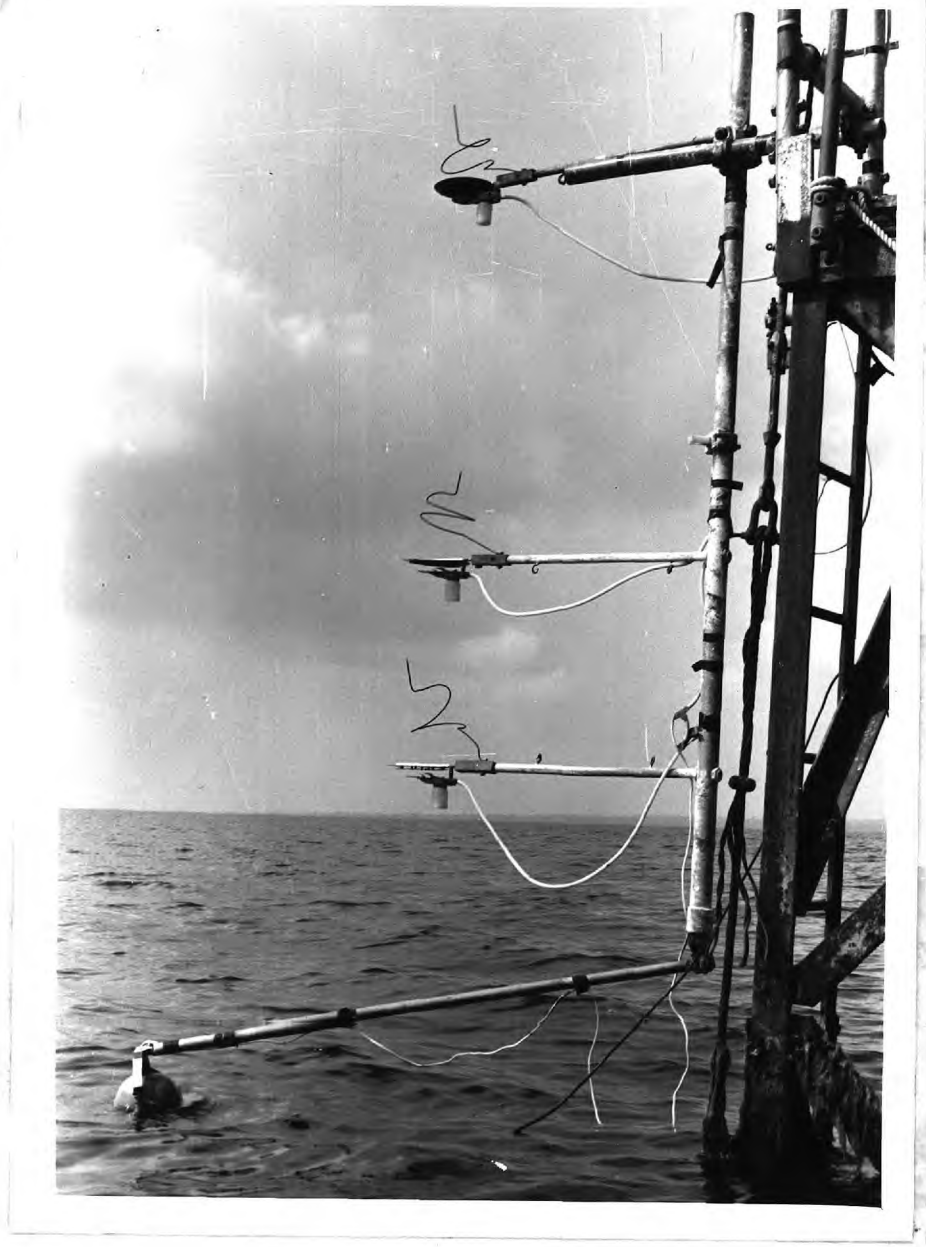

Plate 2a

surface is covered with aluminium coated polyester film of high reflectivity and good emissivity. 5 mm. below this and fastened to it by small pillars is a black painted thin polyester sheet 13 cm. in diameter. This contains the boundary layer from the top sheet and prevents reflection of radiation from below. In the centre and 1 cm. below this are the thermojunction probes. These are just outside the boundary layer from the surface above and below and are not illuminated until the sun's altitude is below 14°. 1 cm. below the probes is another black painted surface 6 cm. wide by 9 cm. long, the underside of which is again covered with a reflective film. Extensive testing of this arrangement in the laboratory and in the field shows that errors from full sunlight in light winds do not exceed 0.01°C. As all shields are identical relative errors between thermojunctions in use must be significantly smaller. The shields have proved mechanically robust and have withstood repeated assault by water waves over a period of three months plus continuous exposure (Plate 2b shows top view of low-level thermometry system with shields).

The lead wires from each junction are taken to a junction box at the 4 m. level on the tower. This box is designed to eliminate temperature gradients at its centre where the joints are enclosed. To do this it is made with walls all round consisting of five layers of alternate thick aluminium and acrylic, and tests showed errors due to temperature gradients at the centre not to exceed 0.01°C. Both the constantin and manganin leads are joined individually within this enclosure to strands of standard miniature multicore tinned copper conductors. This cable then runs to a housing at

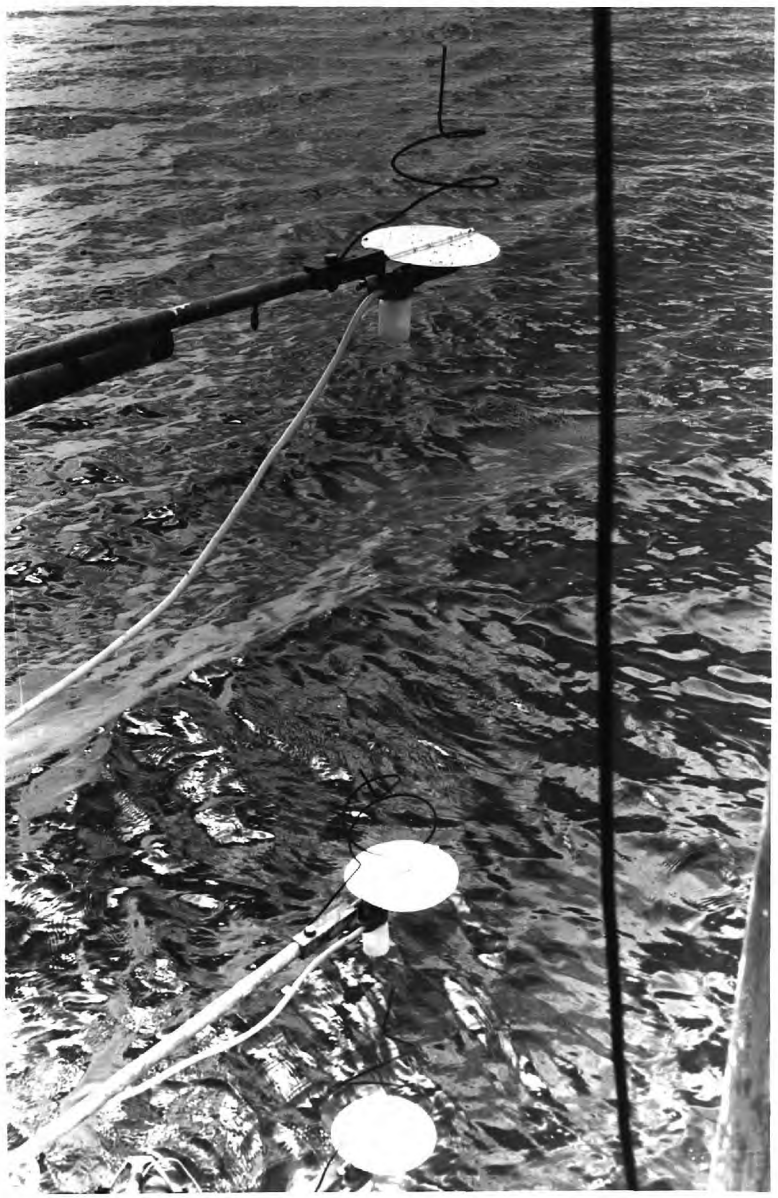

Plate 2b

the lee side of the platform where, in a heavy aluminium box, a carefully designed switching system connects the wires to make the appropriate thermocouple circuit and connects this to the input of the amplifier.

The channels so connected are as follows:-

(a) zero - a resistance equal to that of a typical thermocouple circuit.

4 m. dry to -

(b) Sea - a single junction mounted in a stainless steel pellet 2 cm. below water surface on a float. The voltage from this channel is resistively divided by a factor of ten to produce a signal compatible in amplitude with the remainder,

(c) ½ m. dry,

(d) 1 m. dry,

(e) 2 m. dry,

(f) 8 m. dry,

(g) 16m. dry,

(h) 16m. dry - repeated to give added confidence to the top-most point of the profile, and,

(i) a reference 40.3 microvolts (equivalent to 1°C) derived from a mercury cell.

4 m. wet to -

(j) Sea (as above),

(k) ½ m. wet,

(l) 1 m. wet,

(m) 2 m. wet,

(n) 8 m. wet,

(o) 16m. wet,

(p) 16m. wet.

Switching both the constantin and manganin leads of each thermojunction in this manner ensures that each thermocouple circuit when it is being read is completely independent of the others.

The selection of the channels is effected by five lines from the control system on shore, and the output from the amplifier, set to a gain of 10^4, is fed to a digital voltmeter on shore. The sequence of operations for reading one channel is as follows:-

(1) The appropriate thermocouple circuit is made and connected to the input of the D.C. amplifier,

(2) The output from this is read by the digital voltmeter,

(3) The output from the digital voltmeter is taken in serial form i.e. a train of pulses, the number of which is proportional to the reading, into a store in the main control box. The appropriate sign is maintained by off-setting the input to the d.v.m. by the equivalent of 1°C in the positive direction. Thus zero in the store is at 1°C and a range of ± 1°C can be accommodated (10°C for the 4 m. — sea reading). As soon as this number is in the store, the input channel is changed and the d.v.m. continues with the next reading,

(4) A train of pulses is fed to the store at 400 per second with the store counting either up or down, according to sign, until the zero level is reached when the train is stopped. This train is also fed to the appropriate one of 16 divide-by-eight, up or down, counting stores. As soon as a total count of 8 either positive or negative going has been reached in this store, it drives one of 32 totalising electro-mechanical counters (one positive and one negative per channel).

This sequence is completed in 94×10^{-3} seconds giving one cycle of all 16 channels in 1.5 seconds (which is about the time constant of the thermometer bulbs), and a total of 400 readings in 10 minutes. This rate is adequate to ensure a good sample. The scale values of this system are so arranged that, having allowed for any zero drift by subtracting the total in the 'zero' channel output (normally less than 10 counts) from the others, a count of 1000 ± 5 appears in the reference channel counter. The 'sea' counters contain readings in 10^{-2} °C and the others in 10^{-3} °C.

Tests performed on site give confidence in these results to better than 0.01°C (see radiation shield tests above) for the average temperature profile over 10 minutes. Deposited rain must of course be allowed to evaporate before any run is made.

Finally facilities are built onto the control box to allow:-

(1) Correction of zero drift from the shore,

(2) Remote hand switching of input channels for checking the performance of individual thermocouples,

(3) Elimination of large spurious readings from the ½ m. and/or 1 m. thermojunctions if these are wet from wave action.

The method for evaluation of profile parameters can be found in § 2.2.7.

2.1.4. Fluctuation Instrumentation

The 'trident' consists of a stainless steel support for anemometer and wind vane, with a thermometer mounted between them. All are in the same horizontal plane (see Plate 3). A steel tube holds this assembly some 29 cm. up-wind of a 5 cm. square by

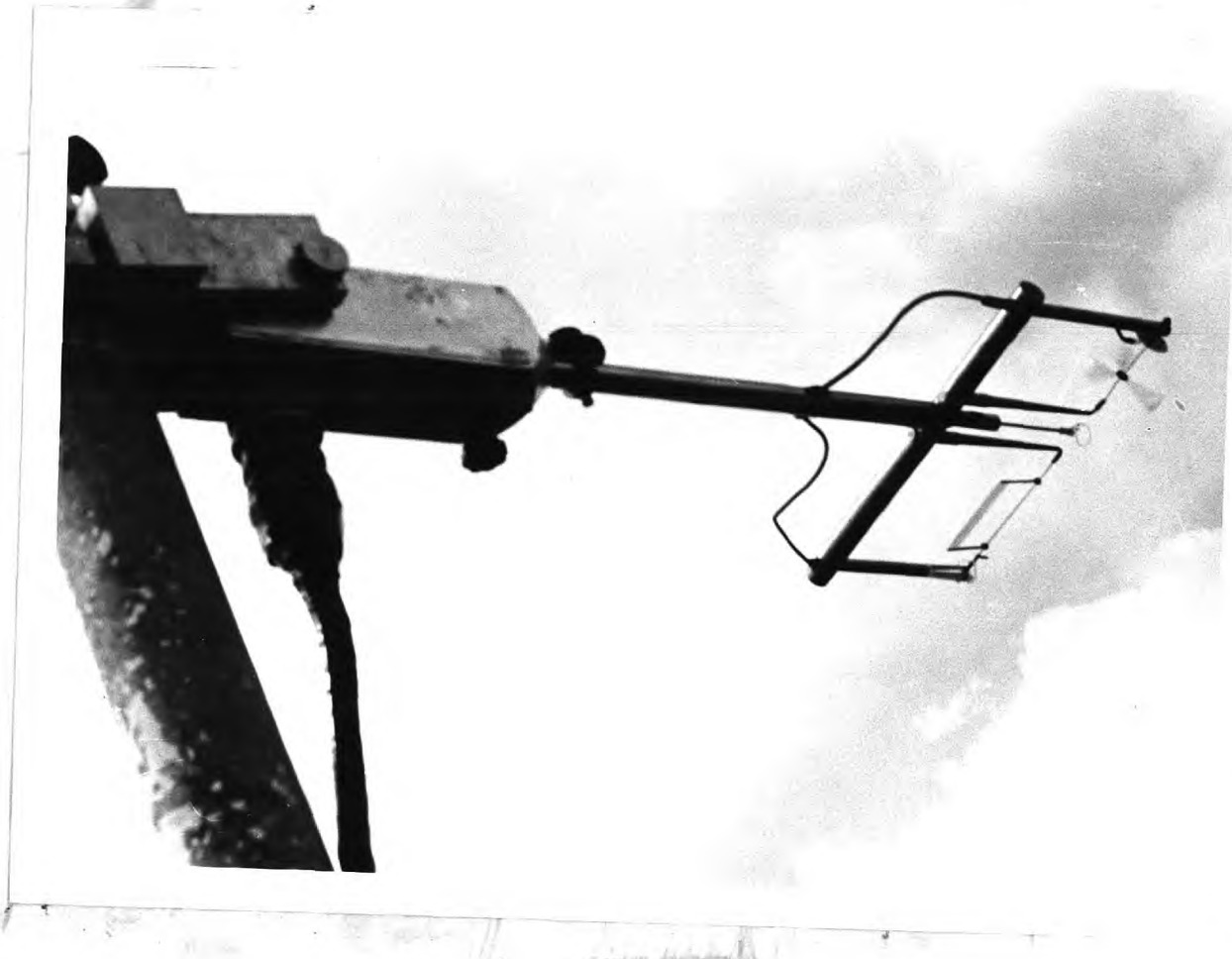

Plate 3

15 cm. long aluminium box containing all the electronics circuitry together with level adjusters and a clamp which allows attachment to any part of the tower structure.

(1) Anemometer: Three 'scoop' shaped cups (2.5 cm. long by 1 cm. wide) are fastened to a stainless steel spindle running horizontally in jewel bearings. To one end of this spindle is attached a 1.5 cm. diameter photographic disc marked at 2° intervals. A small lamp and photo-transistor (buried in the support arm) combine with this to give 180 pulses per revolution of the cup system. The system has a distance constant of 10 cm. (response time of 0.02 secs. at wind speed of 5 $m.s^{-1}$) and an output of 360 pulses sec^{-1} per $m.s^{-1}$. The pulses are amplified and squared in the mounting box.

(2) Vane: This consists of a light polyester vane with two wire support arms at its extremities fixed to a horizontal spindle running in jewel bearings. The position of the vane is measured by a loop of wire moving with the vane and progressively damping an inductance. This has been buried in the support arm and is included in an oscillator circuit which gives a frequency output changing from 7.5 $Kc.s^{-1}$ to 12.5 $Kc.s^{-1}$ with a movement of the vane from 30° down to 30° up positions, and is linear in the sine of the angle from the horizontal. The output from this oscillator (in the mounting box) is a square wave. The response time (the vanes are critically damped) for a wind speed of 4 $m.s^{-1}$ is 0.02 secs.

(3) Thermometer: This is a resistance thermometer of 12 micron platinum wire loosely wound on a 0.5 mm. nylon filament

for support, 'loosely' implying that the platinum touches the nylon only once per turn. The resistance is 255 ohms at 10°C and it is included in an oscillator circuit producing a frequency output from 1 Kc.s^{-1} to 30 Kc.s^{-1} for temperatures of 1°C to 30°C respectively. It has been estimated that Joule heating in the wire will cause a temperature rise of less than 0.01°C, and in the present work is no serious matter. The circuitry is also included in the mounting box and has a square-wave output identical in form to the other two. The response time is 0.01 secs. in a wind speed of 5 m.s^{-1}.

Thus each trident is a self-contained unit requiring a supply voltage of between 15 and 30 volts and producing three outputs suitable for transmission over the 700 m. lines to the shore. Though recording capabilities at present allow simultaneous recording from only two such instruments, three have been mounted on the tower at heights of about 1.5 m., 4 m. and 12 m. and switching arrangements allow only two of these to be selected for use as required. A monitor on the platform allows each instrument to be checked for correct performance at any time.

2.1.5. Miscellaneous Instrumentation

(1) Water Wave Recorder: The transducer for this measurement consists of a 125 s.w.g. stainless steel wire some 3 m. long suspended vertically in the water from a small winch at a height of 2 m. A 4 Kg. weight keeps the wire vertical and the winch allows simple cleaning of plant growth from the wire.

This wire is fed in a constant current mode by square waves 2 volts in amplitude. A plate in the water acts as an electrode to pick up signals, through the water, and whose amplitude is a function of the height of the water up the wire. Both the wire and the electrode form part of an oscillator circuit which produces a linear frequency change of 1 $Kc.s^{-1}$ per 10 cm. of height up the wire, from 1 $Kc.s^{-1}$ to 25 $Kc.s^{-1}$. The output is in the form of a square wave compatible with the 'trident' signals. Calibration of the system is carried out on a calm day when no seiching is present and involves determining the frequency output for fixed lengths of wire beneath the surface by simply rotating the winch through a known number of revolutions. The absolute resolution of the recorder is determined by the height of the meniscus but with such a fine wire this will be much less than the height of the smallest gravity wave (<1 mm.) present.

(2) Temperature Monitoring: Water temperature and air temperature at 4 m. height are monitored remotely from shore and shown in 0.1°C on the display of the digital voltmeter.

(3) Water Level Recording: A float in an 8" steel pipe acting as a "still-well" drives a potentiometer through a rack and pinion and the height of the water surface to a reference point on the platform deck is displayed on the digital voltmeter in mm. The height of every instrument in use is measured relative to this reference point.

2.1.6. Recording of Fluctuation Signals

In the laboratory on shore the six signals from two of

the three 'tridents' (see § 2.1.4.), together with a 10 Kc.s^{-1} time signal and another from the water wave recorder (§ 2.1.5.) are recorded on 16-channel magnetic tape running at 30 inches per sec. Later these channels are individually replayed, together with the time signal (see § 2.2.1.).

2.1.7. Calibration of Anemometers

Profile: Prior to a trip to the field site, each of about 13 large-cup anemometers is calibrated relative to a "master" anemometer in a wind tunnel at the Department. Each anemometer thus has its own calibration curve (counts per minute against wind speed) for use on site. After each trip the calibrations are checked for deviations incurred in the field, for subsequent corrections to the relevant wind speeds measured with "faulty" calibrations. Such corrections are very rare indeed.

The "master" itself has been calibrated against a pitot-static tube placed in the wind-tunnel, and the resultant calibration curve is assumed to remain constant with time (because the "master" resides permanently in the tunnel and mechanical parts are not expected to deteriorate noticeably over a period of a few years). Accuracy of the "master's" calibration at very low speeds (~2 m.s^{-1}) is questionable because of difficulty encountered in measuring the correspondingly small pressure difference; relative to each other the anemometers used in the field should be accurate to within 2–3 cm.s^{-1}.

Fluctuation: The small-cup anemometers have been calibrated against the performance of the "master" in the wind tunnel. A calibration

curve is produced (output in counts per 0.1 second against wind speed) for a typical set of cups, but checks show that this is virtually the same for all cup systems, mainly because all the cups used are produced from the same mould and the jewel bearings are near-identical.

However, use of the calibration curve in the field revealed an inconsistency; namely that at a given height the mean wind speed as recorded by the mini-anemometer $\bar{V}_u$ was always smaller (by up to 10% or so) than that recorded by the large-cup anemometer $\bar{u}$, for the same height. It must be remembered that $\bar{u}$ is obtained in a horizontal plane and $\bar{V}_u$ in a vertical one, but this difference would account for less than 1% of the observed difference $\bar{u} - \bar{V}_u$. Investigation and tests in the wind tunnel showed that the observed difference could be attributed to a slowing down of the small cups by the action of the lateral component of the wind. The not entirely acceptable solution to this problem has been to take the calibration of the small cups for any run from the mean wind speed given by the large cups at the same (interpolated) level.

2.2. DATA ANALYSIS

2.2.1 Fluctuation Data: Analogue to Digital Conversion

At some convenient time, the magnetic tape is replayed at 15 inches per second relaying the recorded signal from one channel, together with the time signal from a fixed channel, into a counter-timer. The time signal gates the system at 0.1 second intervals on the original time scale, and during this period the data signal is counted. The digital output from the counter-timer

is used to produce a punched paper tape record, one for each signal recorded. The resolution obtained on the digital output for 0.1 second readings is as follows:-

(i) Anemometer — $3\ cm.s^{-1}$

(ii) Vane — 2×10^{-3} rdn. (7')

(iii) Thermometer — 0.01°C

(iv) Wave recorder — 1 mm. height of water surface.

The data-spacing time (Δt) of 0.1 second has been used for several reasons, as follows:-

(1) Consideration of Instrumental Response

(a) Sensors with First Order Response to Sinusoidally Fluctuating Input (Anemometer and Thermometer)

The system can be represented mathematically by:

$$\frac{d\alpha}{dt} + \frac{\alpha}{\tau} = f(t), \qquad 2.1$$

where, $f(t) = \alpha_{input} \sin 2\pi nt$, the applied disturbance of frequency n, amplitude α_{input}. α is the sensor indication at time t, τ is the response time of the sensor. The solution is: $\alpha = \alpha_{output} \sin(2\pi nt + \epsilon)$ where $\alpha_{output} = \alpha_{input}[1 + (2\pi n\tau)^2]^{-\frac{1}{2}}$ and ϵ is an angular phase lag. The ratio of the indicated energy to the true energy at frequency n will then be

$$(\alpha_o/\alpha_i)^2 = [1 + (2\pi n\tau)^2]^{-1} \qquad 2.2$$

For this ratio to be, say, 0.90 (which is an adequate

accuracy in the light of the statistical variability of the energy estimates - see § 2.2.5.), $2\pi n\tau$ must $\simeq 0.3$ and with $\tau \simeq 0.01$ second, then $n \simeq 5$ cps. For $n < 5$ cps, the ratio will approach 1. To obtain estimates at this frequency it is necessary to have the data-spacing time interval $= (2n)^{-1} = 0.1$ sec.

(b) Sensor (Vane) with Second Order Response to Sinusoidally Fluctuating Input

This can be represented by (cf. (a) above):

$$\frac{d^2\alpha}{dt^2} + a\frac{d\alpha}{dt} + b\alpha = f(t) \qquad 2.3$$

where, a and b are dynamic constants of the vane; the other symbols are as before. The solution is:

$\alpha = \alpha_{output} \sin(2\pi nt + \epsilon)$ where

$$\alpha_{output} = \alpha_{input} F(n, a, b) \qquad 2.4$$

For full details of (α_o/α_i) as a function of n, a, b see MacCready and Jex (1964) or Gill (1967). Suffice it to say that for a critically damped vane (any one of those used at Lough Neagh is approximately critically damped with relatively small degree of overshoot) with time constant = 0.02 secs., then at $n = 5$ cps, $(\alpha_o/\alpha_i)^2 = 0.90 - 0.95$, again an acceptable accuracy.

It should be mentioned that the response times are inversely proportional to wind speed and the figure of 0.90 quoted in (a) and (b) above will very often be exceeded.

(2) Consideration of Resolution

The resolution gets worse as the data-spacing time decreases. For example, with $\Delta t = 0.1$ sec the resolution of the anemometer is 3 $cm.s^{-1}$ but at $\Delta t = 0.05$ sec. it is 6 $cm.s^{-1}$. Thus the extra information gained by decreasing Δt is lost because of inadequate resolution of the data signal. In the present case, at the minimum Δt determined by (1) the resolution is entirely acceptable (rough calculation, using the known form of the U spectrum at high frequencies, indicating possible noise problems for $\Delta t \simeq 0.03$ sec).

(3) Computer Time

The amount of data to be processed by computer can easily become prohibitive because of the time and cost factor of large-store digital computers. Fortunately the data available in the present work (6000 datum values per signal recorded for 10 minute periods with $\Delta t = 0.1$ sec) have been assimilated by the University of London Atlas computer without encountering prohibitive delays.

2.2.2. Vetting of Fluctuation Data

The following symbols are defined— V = instantaneous (more precisely an average over 0.1 seconds) wind speed obtained from the anemometer 'raw' data after application of a calibration factor (see § 2.1.7. and § 2.2.3.). ϕ = instantaneous angle between vane and an arbitrary fixed zero obtained from the vane 'raw' data using a calibration factor obtained in the laboratory (§ 2.1.4.). T = instantaneous temperature obtained from the thermometer 'raw' data using a calibration factor obtained in the laboratory (§ 2.1.4.).

h = instantaneous water level above an arbitrary but fixed zero obtained from the 'raw' wave data using a calibration factor obtained on site (see § 2.1.5.).

A primed symbol represents the fluctuation from the mean, as specified in § 1.3.

A simple process is carried out to remove spurious readings arising from a "drop-out" on the magnetic tape (a section of tape unable to read correctly). The elimination of spurious data is effected by setting arbitrary, but realistic upper and lower limits and discarding any reading outside this range. A new reading is then manufactured by linear interpolation between the previous and next accepted value. The limits are set as functions of the mean values as follows:

$$0.3\overline{V} \leqslant V \leqslant 1.7\overline{V}$$

$$-30° \leqslant \phi' \leqslant +30° \quad \text{where} \quad \phi' = \phi - \overline{\phi}$$

$$-1.5°C \leqslant T' \leqslant 1.5°C \quad \text{where} \quad T' = T - \overline{T}$$

$$0.3\overline{h} \leqslant h \leqslant 1.7\overline{h}$$

The next step is to evaluate the frequency distribution of each parameter which serves as a guide as to the suitability of a record for analysis. At this stage priority is given to quasi-stationary records i.e. those showing little or no trend, but for those with distinct linear trends (very few in number) a regression line is fitted to the data and new values calculated.

2.2.3. Evaluation of Orthogonal Components of Wind Speed u, w from V, ϕ

The problem of obtaining V, the true instantaneous wind

speed from the 'raw' mini-anemometer data was raised in § 2.1.7. and involves use of the wind-tunnel calibration (giving V_u) and knowledge of $\bar{u}$, so that

$$V = \frac{\bar{u}}{\bar{V}_u} V_u \qquad 2.5$$

Fig.2.2 illustrates diagrammatically the relation between u, w and V, ϕ with ϕ_o defining the true horizontal. The following equations result from consideration of the diagram —

$$u = V\cos(\phi - \phi_o) \qquad 2.6$$

$$w = V\sin(\phi - \phi_o) \qquad 2.7$$

$$\phi_r = \phi - \phi_o \qquad 2.8$$

$$\overline{\phi}_r = \overline{\phi} - \phi_o \qquad 2.9$$

In principle it is required to determine the local horizontal (or vertical) to which u, w are referred and especial consideration must be given to the evaluation of w' and, in particular, to $\overline{u'w'}$ through calculation of ϕ_o.

It must first be accepted that the frame of reference of the sensor vane cannot be predetermined with sufficient accuracy for the subsequent analysis. There then appears to be two methods available for evaluating ϕ_o, viz.,

(1) Assume $\overline{\phi}_r = 0$, so that $\phi_o = \overline{\phi}$ (equation 2.9),

(2) Assume $\bar{w} = 0$ and from equation 2.7,

$\bar{w} = 0 = \overline{V\sin(\phi - \phi_o)}$, giving,

$$\tan\phi_o = \overline{V\sin\phi} \Big/ \overline{V\cos\phi} \qquad 2.10$$

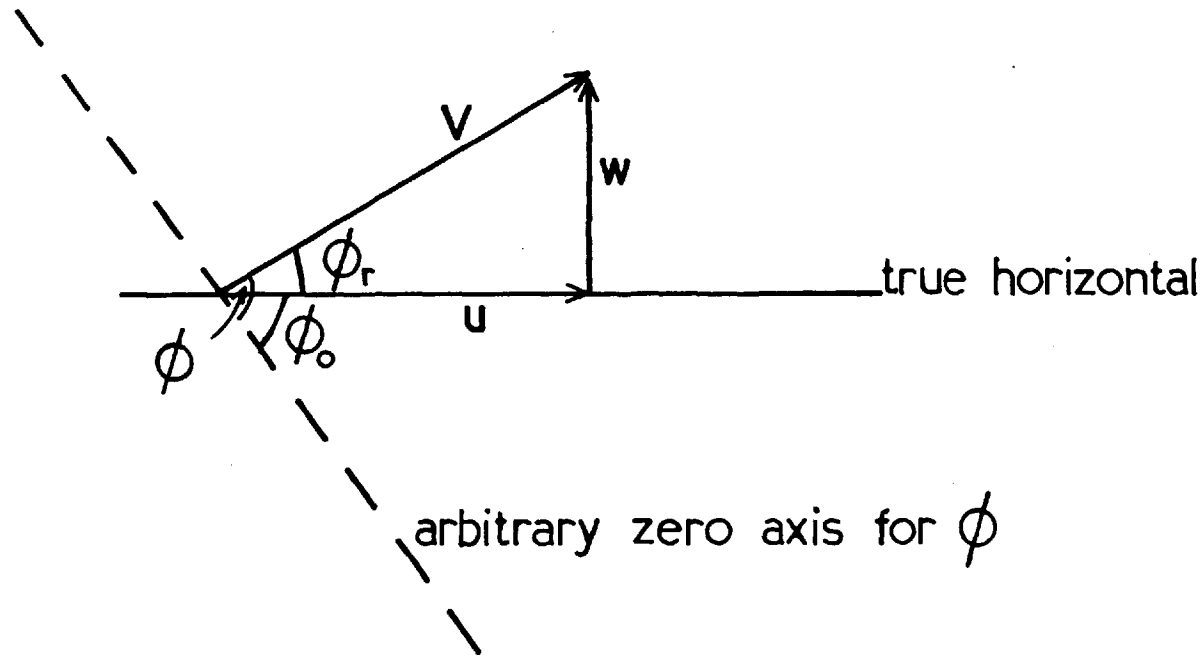
V
w
ϕ_r
true horizontal
u
ϕ
ϕ_o
arbitrary zero axis for ϕ

FIG. 2.2

Method 1 implies $\overline{w} = \overline{w}_1 < 0$, since $\overline{w}_1 \simeq \overline{V'\phi'}$ and appeal to observation indicates a negative correlation between V and ϕ (or u and w). Commonly observed values of $\overline{w}_1$ using Lough Neagh data are ~ -1 cm.s^{-1}. Method 2 implies $\phi_o < \overline{\phi}$ ($\overline{\phi}_r > 0$), an inequality which is observed in practice.

To assess the likely errors in evaluating $\overline{u'w'}$ using each method it is worth considering the following — let the uncertainty in ϕ_o be $\Delta\phi$, and write equation 2.7 for small angles ϕ_r, viz., $w = w_o = V(\phi - \phi_o)$, the true vertical velocity. The apparent (instantaneous) vertical velocity will be $w_a = V(\phi - (\phi_o + \Delta\phi))$ or $w_a = w_o - V\Delta\phi$. For small angles, 2.6 may be written $u = V$. Hence, $u_a w_a = u_o w_o - V^2\Delta\phi$, or,

$$\overline{u_o w_o} = \overline{u_a w_a} + \overline{V^2\Delta\phi} \qquad 2.11\,a$$

Since $\overline{V^2} = \overline{u}^2 + \overline{u'^2} + \overline{w'^2}$, this equation may be written —

$$\overline{u'_o w'_o} + \overline{u}\,\overline{w_o} = \overline{u'_a w'_a} + \overline{u}(\overline{w_o} - \overline{V}\Delta\phi) + (\overline{u}^2 + \overline{u'^2} + \overline{w'^2})\Delta\phi$$

$$\text{i.e.} \qquad \overline{u'_o w'_o} = \overline{u'_a w'_a} + (\overline{u'^2} + \overline{w'^2})\,\Delta\phi \qquad 2.11\,b$$

Note that 2.11 b is independent of $\overline{w_o}$, but under steady-state conditions it is reasonable to expect $\overline{w_o} = 0$. Equation 2.11 may further be written,

$$100\,\Delta(\overline{u'w'}) \Big/ \overline{u'w'} \simeq 10^3\Delta\phi \qquad 2.12$$

since $(\overline{u'^2} + \overline{w'^2}) \Big/ \overline{u'w'} \simeq 10$ (see § 4.2). For example,

to produce a 100% error in $\overline{u'w'}$, $\Delta\phi$ must equal 0.1 or 5.7°, and a 10% error requires $\Delta\phi = 0.01$ or 35 minutes. The $\Delta\phi$ used here may be identified with the mean tilt used by Pond (1968 b) and the conclusions reached herein are in quantitative agreement with those of Pond who concluded that the mean tilt must be kept $< 3°$ if the error in $\overline{u'w'}$ is to be <25%. Writing $\overline{u'^2} + \overline{w'^2} = E$, 2.11 b for method 1 becomes,

$$\overline{u'_o w'_o} = \overline{u'_1 w'_1} + E\,\Delta\phi_1 \qquad 2.11\,c$$

and for method 2,

$$\overline{u'_o w'_o} = \overline{u'_2 w'_2} + E\,\Delta\phi_2 \qquad 2.11\,d$$

It is then possible to identify $\overline{u'_1 w'_1}$ and $\overline{u'_2 w'_2}$ as estimates of $\overline{u'\,w'}$. In practice it is found that there is never more than a few per cent difference between the two implying $\Delta\phi_1 \sim \Delta\phi_2$. These angles are likely to be $\sim \Delta\phi_1 - \Delta\phi_2$ which has values .001 - .003 rdns. Substitution in 2.12 gives an error of a few per cent in $\overline{u'\,w'}$ using either method.

Method 2 was chosen to determine ϕ_o, so that $\overline{u'\,w'}$ is given by $\overline{u'_2 w'_2}$, and there is identity between $\overline{w_o}$ and $\overline{w_2}$, both being zero.

2.2.4. Power Spectrum Analysis

Consider the time variation of particular parameters at a fixed point in the flow, u(t), w(t), T(t), h(t).

Autocovariances and Spectra — for u

The autocovariance $q_u(\xi)$ is defined, at time lag ξ, $q_u(\xi) = \overline{u'(t)\,u'(t+\xi)}$ for a stationary process $u'(t)$. Defining the structure function

$$D_u(\xi) = \overline{[u'(t) - u'(t+\xi)]^2} \qquad 2.13$$

$$D_u(\xi) = 2\left(q_u(0) - q_u(\xi)\right) \qquad 2.13a$$

The autocovariance can be normalised using the variance $\overline{u'^2}$ giving the autocorrelation coefficient, $r_u(\xi) = \overline{u'(t)u'(t+\xi)} \div \overline{u'^2}$. The frequency spectrum or spectral density $\phi_u(n)$ of $\overline{u'^2}$ is defined by:-

$$\overline{u'^2} = \int_0^\infty \phi_u(n)\,dn \qquad \text{giving a normalised spectrum } F_u(n),$$

$$\overline{u'^2}\,F_u(n) = \phi_u(n), \qquad \text{so} \quad \int_0^\infty F_u(n)\,dn = 1$$

$\phi_u(n)$ and $q_u(\xi)$ are related through the Wiener-Khintchine theorem dealing with Fourier transforms (L.P. p.16), viz.,

$$q_u(\xi) = \int_0^\infty \phi_u(n)\,\cos 2\pi n\xi\,dn \qquad 2.14$$

and

$$\phi_u(n) = 4\int_0^\infty q_u(\xi)\,\cos 2\pi n\xi\,d\xi \qquad 2.15$$

the cosine transforms being used because q is an even function.

Cross-covariances and Cross-spectra (for u, w)

The cross covariance between the two series u(t), w(t),

$q_{uw}(\xi)$ is defined by, $q_{uw}(\xi) = \overline{u'(t)\, w'(t+\xi)}$ and that between w and u, $q_{wu}(\xi)$ by $q_{wu}(\xi) = \overline{u'(t+\xi)\, w'(t)}$. It is a feature of atmospheric turbulence in the surface layer that $q_{uw} \neq q_{wu}$ for $\xi \neq 0$ and q is not necessarily either odd or even. It can be written as the sum of an even and odd function $q^{+}_{uw}(\xi)$ and $q^{-}_{uw}(\xi)$ respectively where, $q^{+}_{uw}(\xi) = 0.5[q_{uw}(\xi) + q_{wu}(\xi)]$

$$\text{and} \qquad q^{-}_{uw}(\xi) = 0.5[q_{uw}(\xi) - q_{wu}(\xi)] \ .$$

Similarly the frequency cross-spectrum is written, $\Phi_{uw}(n) = \phi_{uw}(n) - iQ_{uw}(n)$ where $\phi(n)$ is the cospectrum, and Q(n) the quadrature spectrum. Analogous to equation 2.15 we have,

$$\phi_{uw}(n) = 4 \int_0^{\infty} q^{+}_{uw} \cos 2\pi n\xi \, d\xi \qquad 2.16$$

$$\text{and} \qquad Q_{uw}(n) = 4 \int_0^{\infty} q^{-}_{uw} \sin 2\pi n\xi \, d\xi \qquad 2.17$$

Note that $\overline{u'w'} = \int_0^{\infty} \phi_{uw}(n)\, dn$, so that the cospectrum measures the contribution of various frequencies to the covariance.

From the previous definitions it is possible to define a spectral correlation coefficient,

$$R_{uw}(n) = \phi_{uw}(n) \Big/ \phi_u^{1/2}(n)\, \phi_w^{1/2}(n) \qquad 2.18$$

and the coherence, $Coh_{uw}(n)$, by

$$Coh_{uw}(n)^2 = \frac{\phi_{uw}(n)^2 + Q_{uw}(n)^2}{\phi_u(n)\, \phi_w(n)} \qquad 2.19$$

If $Q_{uw} << \phi_{uw}$, then $R_{uw}(n) \simeq Coh_{uw}(n)$ so that the coherence is effectively given by a spectral correlation coefficient. The quadrature spectrum essentially gives information as to what part of a moving eddy contributed to the observations of u and w and is generally non-zero when the maximum correlation between u and w exists at a non-zero lag (as observed in the present work). The sign of the quadrature spectrum between u and w changes from the bottom to the top of eddies with transverse vorticity (L.P. p.189).

Taylor Transformation

Taylor (1938) made the assumption that the turbulence is essentially frozen into the mean flow so that a linear transformation is then possible between temporal and spatial properties of the turbulence, viz.,

$$r(x) = r(\xi) \qquad 2.20$$

when $x = \bar{u}\xi$ and,

$$\phi(k) = \frac{\bar{u}}{2\pi}\phi(n) \qquad 2.21$$

when $k = \frac{2\pi n}{\bar{u}}$. Here x is a downwind separation distance (in cm.) corresponding to the time lag ξ (in seconds) and k is a wave-number in rdns.cm^{-1}. Hence $\lambda = 2\pi k^{-1}$ defines the eddy wavelength λ in cm. The transformation is generally assumed valid if $(\overline{u^2})^{\frac{1}{2}} << \bar{u}$ and for $kz \gtrsim 1$ (Pond et al. 1966). For $kz << 1$ no precise physical interpretation of k is intended and equation 2.21 is a convenient linear transformation from a frequency to a wave number parameter.

It is now necessary to consider the computational procedures,

when u'(t) etc. are known only at discrete intervals Δt for $0 < t < T$ with Δt = 0.1 sec. and T = 10 minutes, the sampling period. The method described will be for the evaluation of a spectrum $\phi_u(n)$ but is readily modified for evaluation of other spectra and cospectra; it can be found in Pasquill (1962) — a modification of that described in Blackman and Tukey (1958). It is intended to provide a realistic analysis of a finite series of discrete observations and is based upon equation 2.15.

2.2.5. Computational Procedure for Evaluation of Spectra

With N observations at intervals of time δt the first step is to form the autocovariances Q_j for successive values of lag $j\,\delta t$ seconds, as follows,

$$Q_j = \frac{1}{N-j} \sum_{i=1}^{N-j} u'(i)\, u'(i+j) \qquad \text{for } j = 0,1,2, \ldots\ldots, m.$$

Q_j will then be known at m+1 specific lags. It follows that the spectrum function is determined only for specific frequency bands centred at,

$$n = 0, \ \frac{1}{2m\,\delta t}, \ \frac{2}{2m\,\delta t}, \ \ldots\ldots, \ \frac{m}{2m\,\delta t}$$

The Fourier transform equation (2.15) is accordingly evaluated in series form, with frequency n replaced by $h/2m\,\delta t$ and time lag ξ by $j\,\delta t$, as follows

$$L_o = (2m)^{-1}(Q_o + Q_m) + m^{-1} \sum_{j=1}^{m-1} Q_j$$

$$L_m = (2m)^{-1}(Q_o + (-1)^m Q_m) + m^{-1} \sum_{j=1}^{m-1} (-1)^j Q_j$$

$$L_h = m^{-1} Q_o + 2m^{-1} \sum_{j=1}^{m-1} Q_j \cos\left(\frac{jh\pi}{m}\right) + m^{-1} Q_m \cos\pi h$$

for $h = 1, 2, 3, \ldots\ldots m-2, m-1.$

in which it is implicit that $\sum_{h=0}^{m} L_h = Q_o$, the variance of the series.

It is desirable to perform additional smoothing of the results by means of a 3-term weighted average as follows —

$$U_o = 0.54 L_o + 0.46 L_1$$

$$U_h = 0.54 L_h + 0.23 (L_{h-1} + L_{h+1}) \qquad \text{for } h = 1,2, \ldots. m-1$$

$$U_m = 0.54 L_m + 0.46 L_{m-1}$$

These values of U_h are effectively averages of the spectral density $F(n) Q_o$ over overlapping frequency bands centred at $h/2m\,\delta t$ of width $1/m\,\delta t$ with

$$U_h = F(n) Q_o \Delta n \qquad \text{where}$$

$$\Delta n = (2m\delta t)^{-1} \qquad \text{for} \quad h = 1, 2, \ldots\ldots m-1$$

and $$\Delta n = (4m\delta t)^{-1} \qquad \text{for} \quad h = 0, m$$

It is a feature of turbulence spectra (and sea wave spectra)

that over a wide frequency range the spectral density decreases rapidly with increasing frequency (see Figs. 5.1 to 5.3, for instance) and the above spectral density estimates will then be in error because the spectrum has really been subjected to band-pass filters which are imperfect in the sense of not having definite cut-offs, but having minor lobes which produce a certain amount of leakage from one band to the next. The correction procedure is called pre-whitening and is effected by transforming the original time series $u(t)$ to one giving a spectrum not varying rapidly with frequency as follows —

$$u''(i) = u'(i) - 0.75\, u'(i-1)$$

The spectrum of the transformed series is obtained as before up to the stage of obtaining V_h estimates corresponding to U_h and the following reverse transformation,

$$U_h = V_h \left(1 + b^2 - 2b\cos(\pi h/m)\right)^{-1} \qquad \text{with } b = 0.75$$

is then applied to give estimates U_h appropriate to the original series.

The choice of number of lags is important, requiring a balance between the resolution (the greater m the greater the resolution) and the accuracy of the spectral estimates (the greater m, the greater the inaccuracy). The latter is best described by considering the number of degrees of freedom (f) of each estimate required to give a satisfactory accuracy, and a satisfactory resolution. In fact $f = 2Nm^{-1}$ approximately and with $m = N/20$ which we have used, $f = 40$ —in our case therefore $\Delta n = 1/60$ cps

(excluding the ends). This choice of m gives adequate resolution over the resultant frequency range (1/60 to 5 cps) together with relatively stable spectral estimates such that there is an 80% probability of the true (long-term) value lying between 75% and 135% of the single spectral estimate. If five consecutive estimates are averaged the number of degrees of freedom of the averaged estimate is now 200, and the above limits (for the same probability) now become 90% and 115% respectively. This averaging process is possible at the higher frequencies where single estimates become "crowded together" when frequency is plotted on a logarithmic scale. It was decided to have $f = 40$ giving $m = 300$ with $N = 6000$. This gives 301 estimates through the spectrum and all but the first ten (at the low frequency end) are averaged in groups of five with hardly any additional machine effort. The highest frequency at which an estimate is made is called the Nyquist frequency = $(2\Delta t)^{-1}$ and because of the finite energy at greater frequencies aliasing causes overestimation of the energy at frequencies $\sim(2\Delta t)^{-1}$ (Blackman and Tukey 1958) —thus estimates at the highest frequencies are discarded. A correction to the spectrum for the finite data-spacing time (suggested in Pasquill, 1962) was initially used as a test but rejected because of over-compensation, which was obvious on inspection.

2.2.6. Measurement of Profiles Over the Sea

Accurate profile measurements over the sea are technically more difficult to make than overland because of, firstly, absence of terra firma and less accessible sites, and secondly, the

requirement of greater sophistication in instrumentation and recording technique because of the need to measure accurately much smaller gradients of u and θ. In addition the interpretation of measured profiles over the sea is possibly complicated by defining suitable reference axes. Overland one defines a set of stationary reference axes with respect to an aerodynamically smooth or rough (rigid) surface, whereas over the sea there is substantial horizontal and vertical motion of the boundary surface consisting in part of a propagating gravity wave system with phase velocity ~ wind speed superimposed upon a drift current with velocity << the wind speed and produced by the direct frictional drag of the wind on the top layers of the sea. The analysis and interpretation of profiles may also depend upon the method used for measuring them of which there are basically two:-

(i) Instruments are mounted on a floating buoy or boat so as to follow the principal wave motion and remain at approximately the same height above the instantaneous water surface beneath the instrument mast. Corrections have to be made for oscillatory motions of the mast (see e.g. Deacon et al. (1956), Pond (1968 b)),

(ii) Instruments are mounted on a tower or mast standing on the sea-bed so as to remain fixed relative to earth. The height of each instrument above the water surface varies in time, but because the sampling period (10 minutes) is >> the period of the dominant gravity wave (a few seconds) the relevant reference height for each instrument can hardly be other than that above the mean water surface.

Profile measurements made over the sea up to the year 1962 are listed in Roll (1965) and from the information available, method (i) predominates. The advantage of (i) over (ii) is that use of (ii) is confined to shallow waters whereas (i) can be used in the open ocean. An advantage of (ii) is that recorded data are not subject to distortions due to oscillatory motions of the instrument mast.

It would seem logical for a system moving vertically with the wave motion but with approximately constant horizontal coordinates to choose reference axes similarly moving vertically with the waves, and to establish relations between wind etc. and height (stability) in the new coordinate system in analogy to the relations established for flow over the land (the Eulerian description). Relations between the quasi-Eulerian and Eulerian characteristics could be used for correcting vertical motion and rolling of floating constructions (Kitaigorodskii, 1967). On the other hand for a construction fixed relative to earth it seems logical to describe the characteristics in the Eulerian sense as for flow over land (there is also evidence that the wave motions have insignificant effect on transfer above a comparitively thin layer —Zilitinkevich, 1967). In this case the effect of a wave disturbed sea surface is related to an effective roughness length of the water surface. An important requirement of the theory is to relate the effective roughness length to the external parameters describing the wave motion and surface layer characteristics — for further discussion of this problem see Chapter 6.

2.2.7. Profile Data

For each 10 minute period, the counts from the six anemometers and all the wet- and dry-bulb thermometer channels are written onto a tabulated sheet, the "still-well" reading allowing for the direct determination of the heights of the instruments above the mean water surface.

(1) Determination of Wind Speed

The wind speeds are evaluated directly from the counts using the calibration curves. The wind speed is then plotted as a function of the logarithm of the height, on log-linear graph paper.

(2) Determination of Dry-Bulb Temperature

With the counts already in either hundredths or thousandths of °C (§ 2.1.3.), a zero error correction is applied to give values of $(T_z - T_4)_{DRY}$ and then $(T_z - T_o)_{DRY}$. Values of $\theta - \theta_o$ are then readily computed for all 6 heights, with the duplication at 16 m., and plotted as for wind speed.

(3) Determination of Wet-Bulb Temperature

As in the previous section, temperature differences are evaluated giving $(T_z - T_o)_{WET}$ in °C., with a resolution of 0.01°C. To determine the specific humidity differences, it is first necessary to consider the heat balance of moisture transfer at a wet thermojunction, viz.,

$$L_w(q_w - q) = C_p(T - T_w) \qquad 2.22$$

at height z, where L_w is the latent heat of evaporation,

q_w is the specific humidity of the leaving saturated air,

q is the specific humidity of the approaching air (unsaturated),

C_p is the specific heat at constant pressure of dry air,

T is the temperature of the air approaching and

T_w the temperature of the saturated air leaving the wet-bulb.

In terms of the height difference (0 to z), 2.22 can be written,

$$q_o - q_z = (q_{w_o} - q_{wz}) - \frac{C_p}{L}[(T_o - T_z) - (T_o - T_{wz})] \qquad 2.23$$

The evaluation of the second bracket on the R.H.S. is readily accomplished but that of the first is less straightforward. Writing $q_{w_o} - q_{wz} = (T_o - T_{wz})\, \partial q_w/\partial T_w$, curves of $\partial q_w/\partial T_w$ as functions of ΔT_w and T_o have been drawn using tables of saturated vapour pressure as function of T_o, and for a given situation it is only necessary to take the appropriate T_o and the approximate averaged ΔT_w between 0 and 16 m. to determine $\partial q_w/\partial T_w$. Multiplication by $(T_o - T_w)$ gives $(q_{w_o} - q_{wz})$. To this is then added the second term on the right hand side of equation 2.23 to give $q_o - q_z$. The values are then plotted as for wind speed and $\theta - \theta_o$.

CHAPTER 3

3.1. INTRODUCTION

3.1.1. Form of Analysis

Data obtained on the variation with height of the mean air properties wind speed, potential temperature and specific humidity are analysed and the relative efficiencies of the turbulent transfers of momentum, heat and water vapour investigated by appeal to a relation between the eddy transfer coefficients and a profile shape factor. The gradient Richardson number is used as a measure of the stability (degree of thermal stratification) taking the presence of humidity into consideration.

u,θ,q profiles for 100 Runs have been used of which 25 have in addition the measurement of fluctuation data at one or more heights. Because the majority of Runs are without direct flux measurement the analysis described in this Chapter purposely excludes determination of dimensionless gradients — the Universal functions Φ_M, Φ_H, Φ_V (defined § 3.1.2.) - as has been made by Charnock (1967) and Dyer (1967).

The variations of profile characteristics with Ri_v suggest a dissimilarity in the u and θ profiles in both stable and unstable stratification but in the opposite sense. Dissimilarities in the u and q profiles are not so evident and require further investigation.

3.1.2. Description of Profiles

$\overline{u}$, $\overline{\theta}$, $\overline{q}$ will be denoted by the variable $X(z)$. The height variation of $X(z)$ in the surface constant-flux layer overland and over the sea is described by the well known relation,

$$\partial X/\partial z = X_* \Phi(\zeta)/\kappa z \qquad 3.1$$

The vertical turbulent flux of X is related to the vertical gradient of X through the eddy transfer coefficient K viz.,

$$\overline{w'X'} = -K\,\partial X/\partial z \qquad 3.2$$

and when,

$$X = u\,,\ \Phi = \Phi_M\,,\ K = K_M\,,\ X_* = u_*$$
$$X = \theta\,,\ \Phi = \Phi_H\,,\ K = K_H\,,\ X_* = \theta_*$$
$$X = q\,,\ \Phi = \Phi_V\,,\ K = K_V\,,\ X_* = q_*$$

The scaling parameter X_* is related to the flux $\overline{w'X'}$ as follows:-

$$(\tau_o/\rho)^{1/2} = -\overline{u'w'} = u_*^2$$
$$(H/\rho C_p) = \overline{w'T'} = -u_*\,\theta_*$$
$$E/\rho = \overline{w'q'} = -u_*\,q_*$$

Combination of 3.1 and 3.2 for any two of u, θ, q gives equations like —

$$K_H/K_M = \Phi_M/\Phi_H \qquad 3.3$$

$$K_V/K_M = \Phi_M/\Phi_V \qquad 3.4$$

The understanding of the transfer properties of turbulence requires knowledge of the relative sizes of the K's or Φ's in all stabilities. Similarity theory requires that $\Phi = 1$ for neutral stratification ($\zeta = 0$) so that integration of 3.1 gives, for an aerodynamically rough surface,

$$(X - X_o)/X_* = K^{-1} \ln(z/z_s) \qquad 3.5$$

for $z>>z_s$, where X_o is the surface value of X and z_s is a roughness length appropriate to and varying with the property. There is good evidence that 3.5 describes X(z) in neutral stratification in the surface layer overland and it will be assumed to have validity over the sea where a logarithmic profile is also observed. For near-neutral stratification ($|\zeta| << 1$) Monin and Oboukhov (1954) proposed that

$$\Phi = 1 + \alpha\zeta \qquad 3.6$$

where α equals a constant.

Substitution in 3.1 and integrating yields,

$$(X - X_o) / X_* = \kappa^{-1} \left(\ln(z/z_s) + \alpha\zeta\right) \qquad 3.7$$

In the case of the wind profile Taylor (1960) has showed that 3.6 and 3.7 are strictly valid only for $|\zeta| \leq 0.03$ with a value $\alpha \approx 6$; at greater values of $|\zeta|$ α must be treated as a function of ζ.

Writing 3.5 for wind, for flow overland $U_o = 0$ at the origin of z but over the sea U_o may be identified with the surface drift current. Fortunately a knowledge of U_o is not necessary to determine U_* (and wind gradients) and its small size relative to u (viz. $u_o \sim u_* \sim 0.03\bar{u}$ —obtained from rough estimates at Lough Neagh; see also Bye (1967) for a more detailed account) will only marginally affect the value of z_o.

Sheppard (unpublished) has analysed logarithmic wind profiles obtained at Lough Neagh and obtained values of u_* and z_o on the

basis of 3.5 and the wind profile to 16 m. His results suggest $z_o \propto u_*^{2.7}$ with remarkably little scatter of the experimental points but the relation probably cloaks a more physically meaningful one. Thus a relationship proposed by Charnock (1955) on dimensional grounds but neglecting viscosity and surface tension gives $z_o \propto u_*^2/g$. This however has never been fully confirmed as is obvious from the contradictory results collected together by Roll (1965), but the problem of the relation between z_o and u_*, with particular relevance to the above results, will be discussed more meaningfully in Chapter 6, where wave statistics are introduced.

3.2. MEASUREMENT OF GRADIENT AND INDEX OF STABILITY

3.2.1. Gradient Measurement

The gradient of X may be required at any height z but evaluation is by no means unique. The literature contains basically two methods, viz.,

(i) Vertical gradient obtained by (a) a logarithmic finite difference method (used by Hess and Panofsky, 1966), (b) a linear finite difference method (used by Dyer, 1967),

(ii) A regression curve is fitted to the points using a power law relation from which the gradient is obtained by differentiation (used by Record and Cramer, 1966).

The method (ii) is the least accurate whilst (i)b is the most accurate in moderate and extreme instabilities. For use in non-extreme stabilities, both stable and unstable, the method (i)a has been chosen for the Lough Neagh data since it is exact in neutral stratification.

Writing 3.5 for two levels z_1, z_2 and subtracting,

$$X_2 - X_1 = K^{-1} X_* \ln(z_2/z_1) \qquad 3.8$$

Eliminating X_* between 3.1 and 3.8 for $\Phi = 1$,

$$(\partial X/\partial z)_{\bar{z}} = (X_2 - X_1) / \bar{z} \ln(z_2/z_1) \qquad 3.9$$

with $\bar{z} = (z_1 z_2)^{\frac{1}{2}}$.

By writing $\Phi = 1 + \alpha\zeta$ for small ζ it is possible to estimate approximately the error when using 3.9 in non-neutral conditions.

In this case 3.8 becomes,

$$X_2 - X_1 = K^{-1} X_* \left(\ln(z_2/z_1) + \alpha L^{-1}(z_2 - z_1) \right) \qquad 3.10$$

and,

$$(\partial X/\partial z)_{\bar{z}} = \frac{(X_2 - X_1)(1 + \alpha \bar{z} L^{-1})}{\bar{z} \left(\ln(z_2/z_1) + \alpha L^{-1}(z_2 - z_1) \right)} \qquad 3.11$$

Comparison of 3.9 and 3.11 with appropriate values of α, L, z_1, z_2 gives an error in $\partial X/\partial z$ when using 3.9 for $\zeta \neq 0$ (strictly for $|\zeta| << 1$). From knowledge of the values of $X_2 - X_1$ encountered at the three mean heights $\bar{z}$ = 1.8, 4, 12.25 m. and the experimental error in X, values of z_1, z_2 were chosen for each $\bar{z}$. Thus, initially gradients at the 4 m. level were found using height differences from 3.2 to 5 m., and 2 to 8 m. and the results averaged (differences never amounted to more than 5 per cent under all conditions). Gradients at 1.8 m. and 12.25 m. were found for height differences 1 to 3.2 m. and 10 to 15 m. respectively. Finally an overall average error in the gradient was deduced for

all stabilities viz. for heights 1.8 m. and 4 m. gradients can be up to 10 per cent in error, but on average are 5 per cent, this being an underestimate of the gradient in unstable conditions. At the 12.25 m. level the error may be as high as 100 per cent for the most unstable cases (in addition for conditions close to neutral when the changes with height of θ are of the same order as the experimental error in θ, $\partial\theta/\partial z$ will be in error to the order of 100 per cent) but on average will be 20 per cent.

3.2.2. Index of Stability - Richardson Number

3.2.2.1. Evaluation

The gradient Richardson number can be defined,

$$Ri_v = \frac{g\,T^{-1}\,\partial\theta_v/\partial z}{(\partial u/\partial z)^2} \qquad 3.12$$

in terms of the virtual potential temperature θ_v to take account of the presence of moisture in the air and its effect upon the production rate of buoyant energy. 3.12 can be written in terms of the dry potential temperature θ and specific humidity q since $\theta_v = \theta(1 + 0.61\,q)$.

The differential form is,

$$\partial\theta_v/\partial z = \partial\theta/\partial z + 0.61\,\partial(\theta q)/\partial z$$

or,

$$\partial\theta_v/\partial z = \partial\theta/\partial z(1 + 0.61q) + 0.61\,\theta\,\partial q/\partial z \qquad 3.13$$

Because $0.61\,q\,\partial\theta/\partial z \ll 0.61\,\theta\,\partial q/\partial z$, 3.13 can be written,

$$\partial\theta_v/\partial z = \partial\theta/\partial z + 0.61\,\theta\,\partial q/\partial z \qquad 3.13\,a$$

In the absence of a significant humidity gradient $\partial\theta_v/\partial z = \partial\theta/\partial z$ which is the relation generally used both overland and over the sea, even though, in the latter case, humidity terms are important (as will be shown). 3.12 may now be written,

$$Ri_v = \frac{g\,T^{-1}\,\partial\theta/\partial z}{(\partial u/\partial z)^2} + \frac{0.61\,g\,\partial q/\partial z}{(\partial u/\partial z)^2} \qquad 3.14$$

The first term on the right will be called Ri_D, and the second Q. Throughout the thesis the degree of stratification will be described in terms of Ri_v, which may often be abbreviated to Ri.

Gradient errors estimated in § 3.2.1. can be used to estimate errors in Ri_v using 3.14, viz. errors in Ri_D or Q (each effectively involves 3 gradients) will be ~15 per cent at levels 1.8 m. and 4 m. and ~60 per cent at 12.25 m., giving an error in Ri_v of 20 per cent at 1.8 m. and 4 m., and 100 per cent at 12.25 m. Errors in individual cases may be considerably greater or less than these estimates but they are sufficient pointers to the attainable accuracy in Ri_v.

3.2.2.2. Nature

Regarding the nature of the two terms Ri_D and Q, Ri_D is negative when $\theta < \theta_o$ and positive when $\theta > \theta_o$ whereas Q is nearly always negative (the case of predominant evaporation from as opposed to condensation on the sea-surface). Fig.3.1 illustrates the relative sizes of the two terms for a height of 4 m.

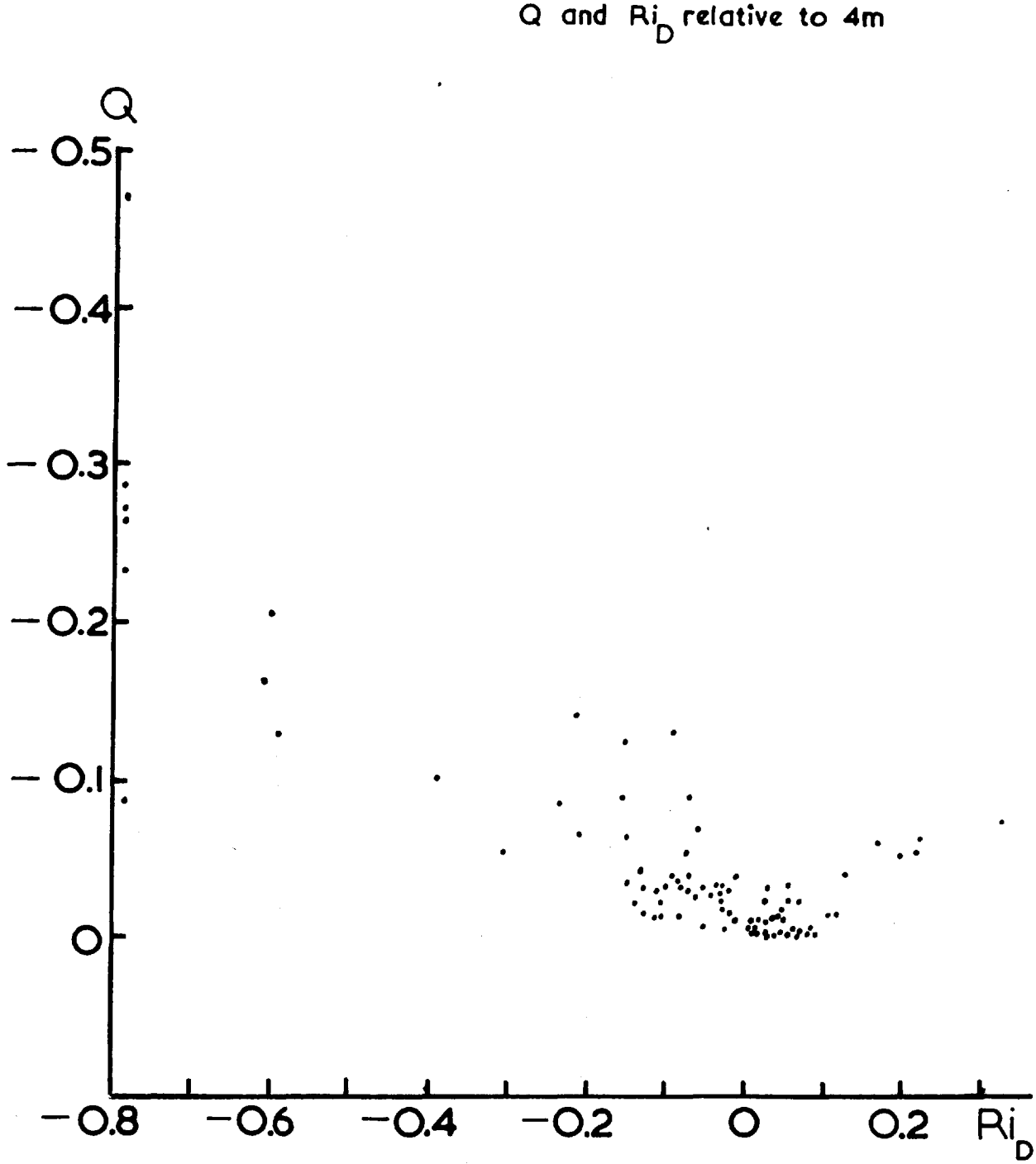

FIG.3.1

On average $Q \sim Ri_D/4$ but when Ri_D is close to zero, Q may be significantly negative. The relative sizes are also affected by the sea-surface temperature which exerts considerable influence upon the humidity gradient (§ 3.3.2.). An interesting combination of Ri_D and Q is the case when Ri_D is positive (but small) but $|Q| > Ri_D$ giving a negative Ri_v and unstable stratification overall. However, only 5 of the 100 Runs analysed fall into this category and their u, θ, q, θ_v profiles are shown in Fig.3.2. The Richardson numbers are so close to zero that the profiles are predominantly logarithmic and no profile shows the curvature characteristic of unstable stratification i.e. convexity towards the z axis. Zilitinkevich (1966), who has discussed quantitatively the importance of the Q term, has however observed such curvature in wind profiles over a reservoir when $-Q > Ri_D$.

3.3. VERTICAL PROFILES OF u, θ, q

3.3.1. Characteristic Profiles

It is inconvenient to present here all the profiles of the 100 Runs analysed and so those of the 25 Runs with fluctuation data have been chosen as representative, since they cover a wide range of stability. They are shown in Figs.3.3 and 3.4 (unstable and stable respectively) with Ri increasing — going more positive — from left to right.

There are no discontinuities in any of the profiles and evident is a similar variation of shape with stability for u, θ and q profiles, though a quantitative analysis will show that such variations do differ. The dependence of curvature upon stability

FIG. 3.2 NEUTRAL PROFILES WITH Ri_D +ve, Ri_v -ve

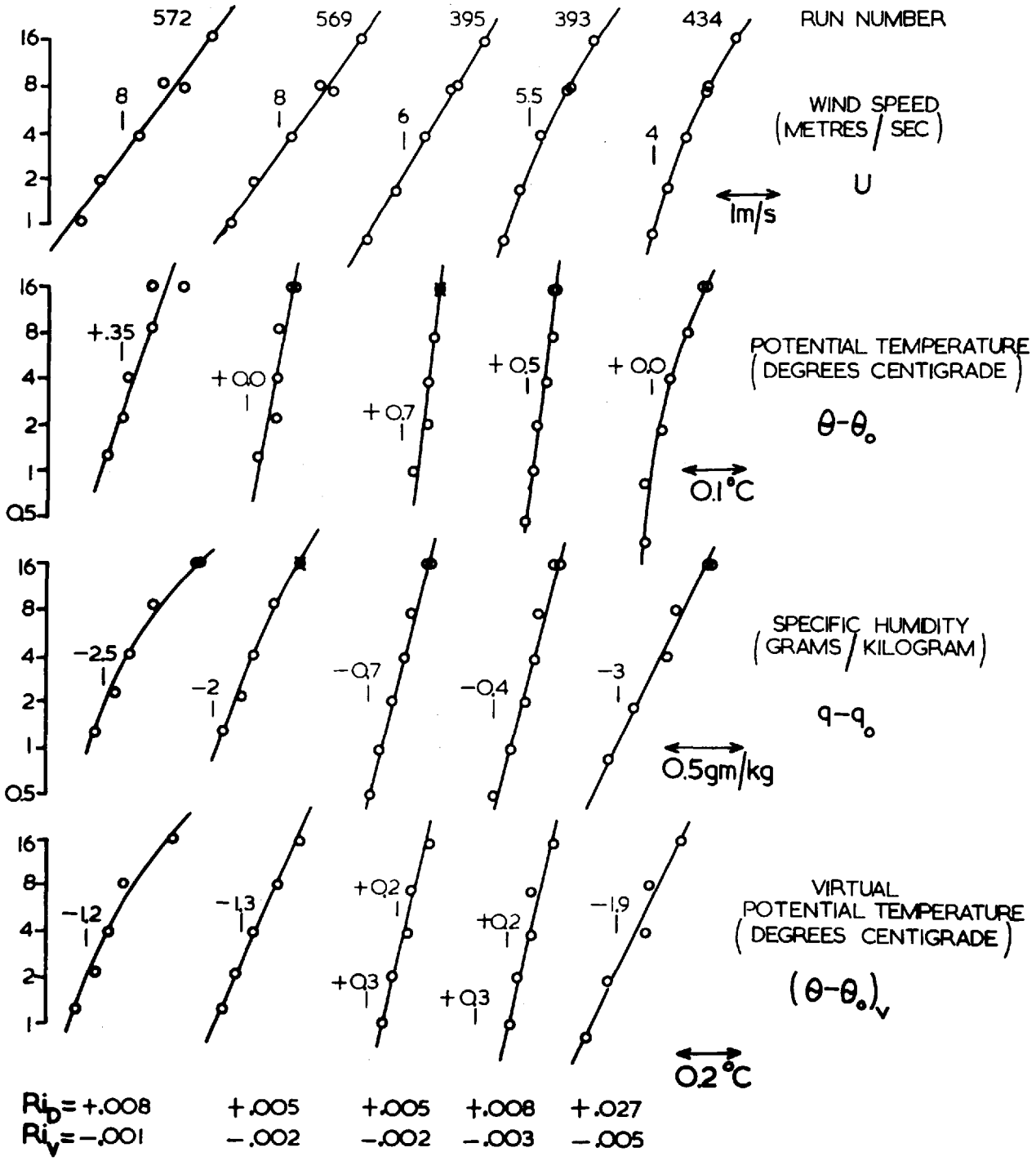

FIG.3.3 PROFILES FOR NEGATIVE RICHARDSON NUMBER

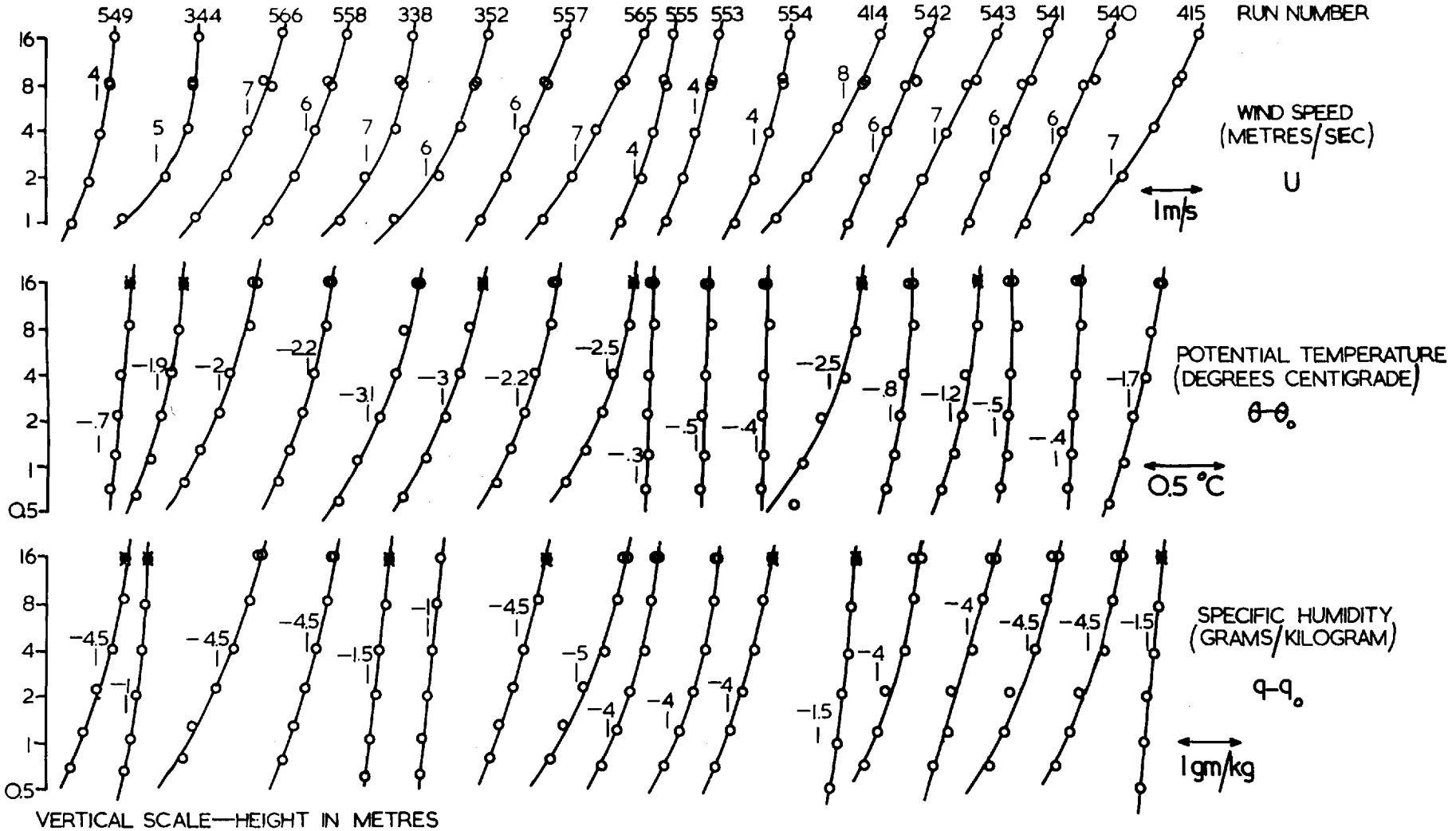

FIG.3.4 PROFILES FOR POSITIVE RICHARDSON NUMBER

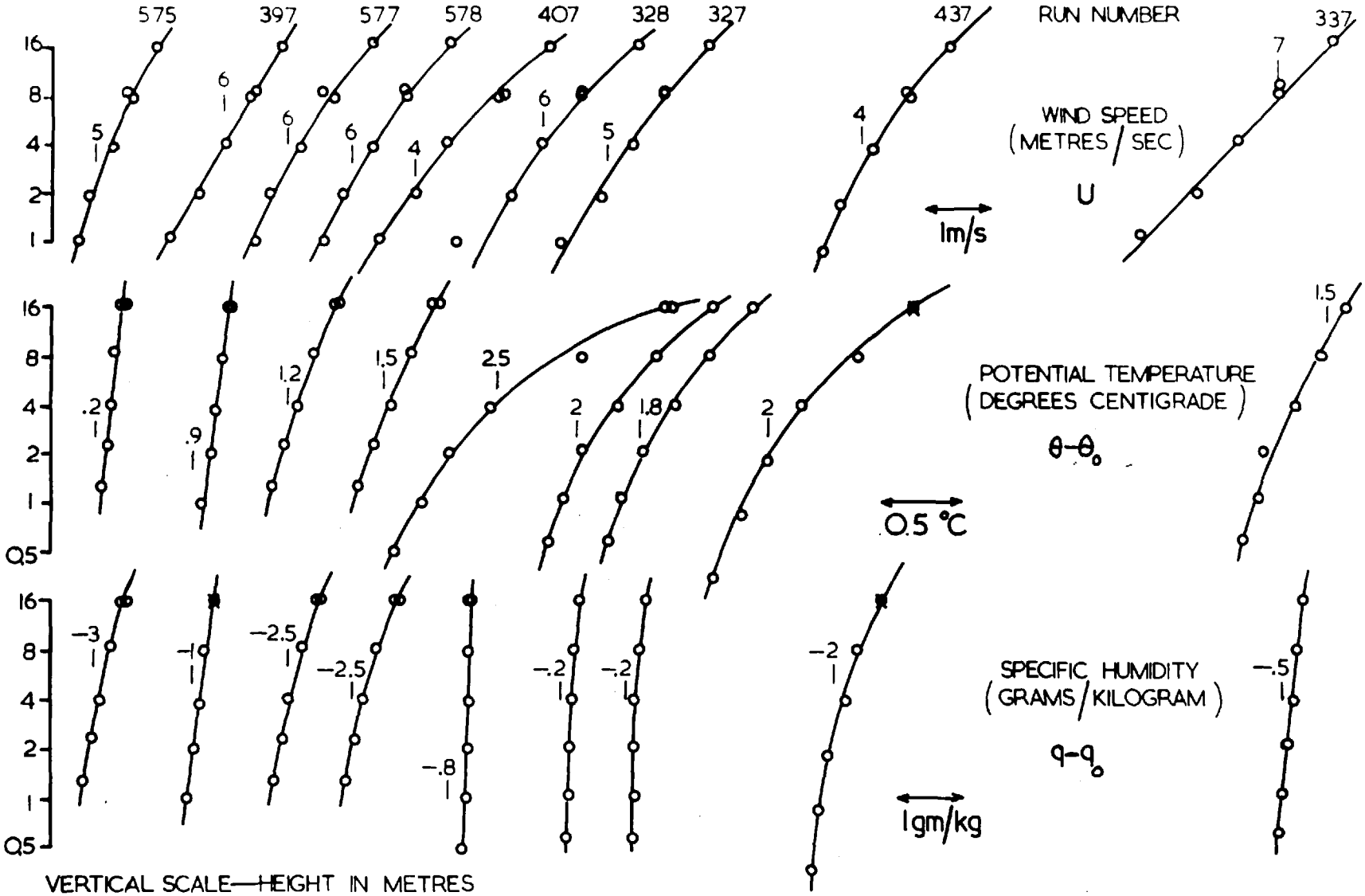

is a characteristic feature of the surface layer overland and over the sea; in the latter case, profiles published by Fleagle et al. (1958), Takahashi (1962) and Brocks (reference in Roll, 1965) together with the Lough Neagh set show such a dependence. A peculiar feature of the Lough Neagh profiles is the rare appearance of linear profiles (on a vertical logarithmic scale, of course) in moderate instability (in Fig.3.3, see Runs 549(θ), 338(q), 555(θ)) and of non-linear profiles in neutral stability (in Fig.3.4, see Run 575(u,q)). Such a behaviour may be due to two causes,

(i) The inherent subjectivity of drawing profiles (they are drawn by eye) — it may sometimes be difficult to ascertain whether or not curvature is present e.g. in Fig.3.3, Runs 344(q), 414(q) and Fig.3.4, Runs 575(q) and 578(θ). Often the choice rests on the point at the lowest or highest level, which may be in error,

(ii) There may be a degree of unsteadiness in one or more of the X fields and/or inhomogeneity in the horizontal producing a flux variation with height. These factors would cause deviations from the characteristic form of the profile.

Overall, the profiles of all 3 quantities show a consistent variation of shape with stability, as demonstrated in the next section.

3.3.2. Relations between air differences and air-sea differences

This section will simply illustrate how the gradient of X e.g. $(\partial X/\partial z)_4$ which is proportional to $X_8 - X_2$, is related to $X_4 - X_o$. In reality $X_8 - X_2$ depends largely upon the heat flux and momentum flux which in turn are closely related to the

X difference across the interfacial layer where a large percentage of $X_4 - X_o$ occurs.

It is assumed that,

(i) $u_8 - u_2$ will depend largely upon $\theta_4 - \theta_o$, u_4.

(ii) $\theta_8 - \theta_2$ will depend largely upon $\theta_4 - \theta_o$, u_4.

(iii) $q_8 - q_2$ will depend largely upon $q_4 - q_o$, $\theta_4 - \theta_o$.

Fleagle et al. (1958) have investigated such relations as functions of Ri, and Deacon et al. (1956) published results showing dependence of $\theta_{12} - \theta_4$ upon $\theta - \theta_o$ and wind speed. They are in no way dissimilar to the Lough Neagh results —

(1) $(u_8 - u_2)/u_4$ is plotted vs $\theta_4 - \theta_o$ in Fig.3.5. There exists a close relation, the ordinate at $\theta_4 - \theta_o = 0$ (equal to 0.124) implying a drag coefficient (effectively averaged over the wind speed range) relative to 10 m. = 1.16×10^{-3}. This value is consistent with independent estimates of C_D presented in § 4.2.4. from heat and momentum flux measurements.

(2) $\theta_8 - \theta_2$ is plotted vs $\theta_4 - \theta_o$ in Fig.3.6 according to whether u_4 is greater than or less than 5 $m.s^{-1}$, which conveniently separates light and strong winds. There exists a close relation with a small dependence upon wind speed. Such a relation is strongly indicative of the heat flux's (H) being determined by a function of u and $\theta - \theta_o$. In § 4.2.5. it is showed how $H/\rho C_p$ is strongly related to $u_{10}(\theta_{10} - \theta_o)$.

(3) $(q_8 - q_2)/(q_4 - q_o)$ is plotted vs $\theta_4 - \theta_o$ in Fig.3.7. The relation is less well marked, presumably due to a small wind

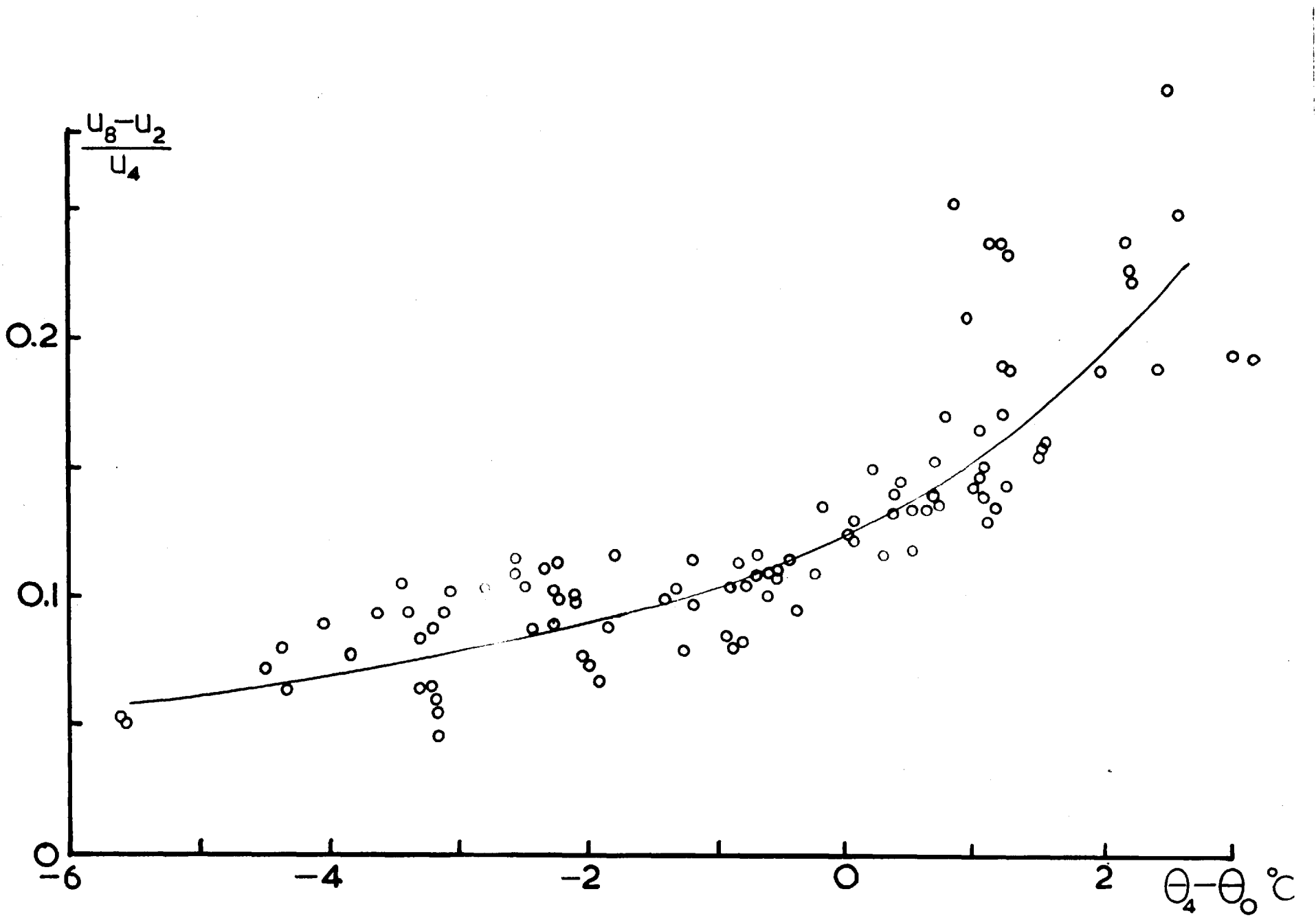

FIG.3.5

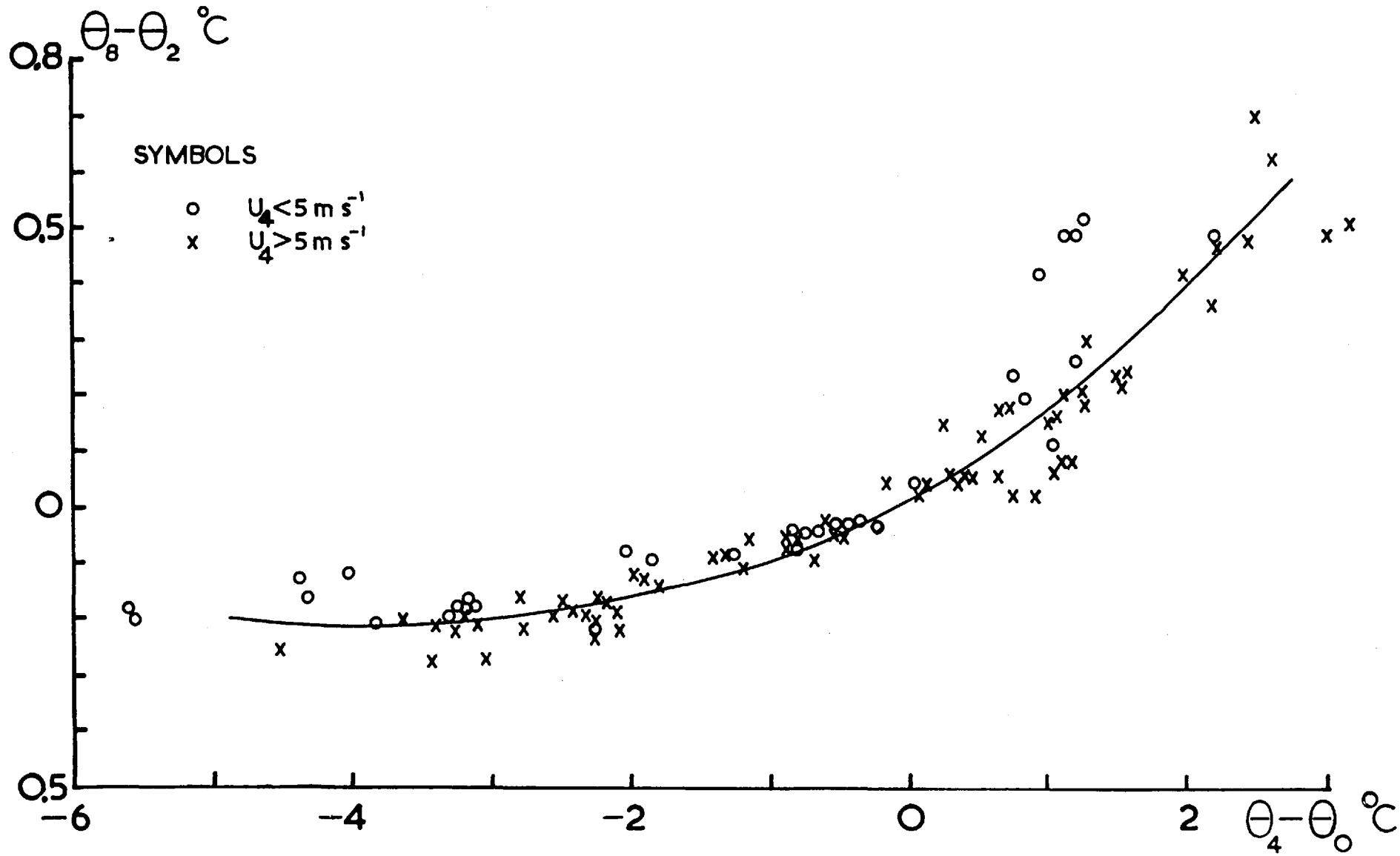
$\theta_8-\theta_2$ °C
0.8
0.5
0
0.5
SYMBOLS
o $U_4<5$ m s^{-1}
x $U_4>5$ m s^{-1}
−6
−4
−2
0
2
$\theta_4-\theta_0$ °C

FIG.3.6

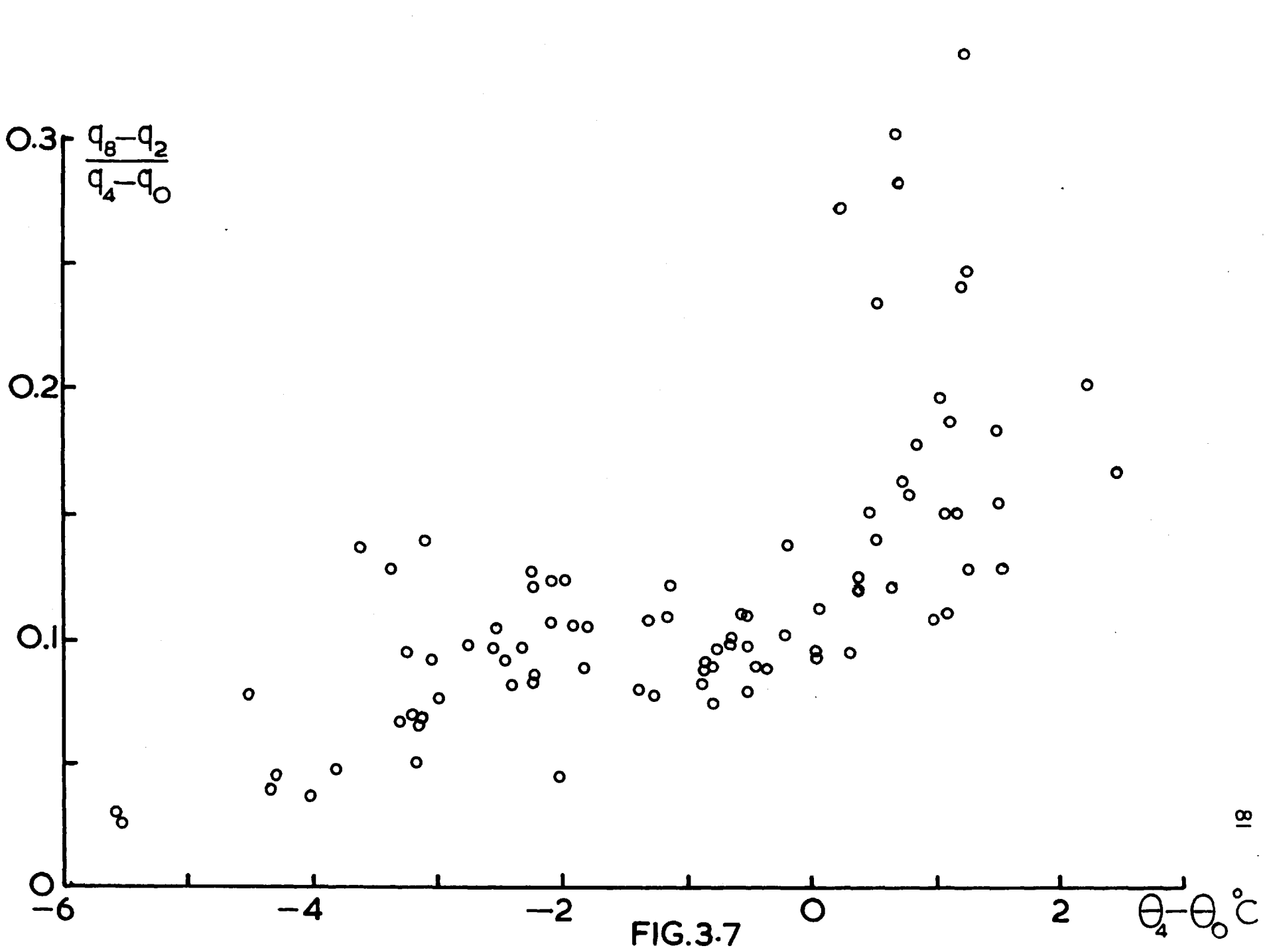

FIG.3.7

speed effect and, in addition, to variations in the sea-surface temperature which determines q_o uniquely but not q_z.

The fact that much greater gradients can be maintained for positive $\theta_4 - \theta_o$ is due to the absence of strong vertical mixing produced by convection when $\theta_4 - \theta_o < 0$.

The importance of the effect of sea-surface temperature upon the humidity profile has not been adequately stressed in the literature and it will, for instance, affect the variation of Bowen ratio with $\theta_4 - \theta_o$ (as given in Roll, p.254) considerably.

3.4. SIMILARITY OF PROFILES AND IMPLIED TURBULENT TRANSFERS

3.4.1. Introduction

The turbulent transfer of momentum, heat and water vapour in the fully turbulent layer above the boundary is characteristically several orders of magnitude more efficient than the transfer by molecular processes in the same layer. A central problem in micro-meteorological studies within the fully turbulent layer (overland and over the sea) concerns the mechanisms by which the above properties are transferred; especially knowledge on the relative efficiencies of turbulent transfer and their dependence upon the degree of thermal stratification. A measure of the relative efficiencies is implied by the ratios of any two of the eddy transfer coefficients — see equations 3.3 and 3.4 —but knowledge of these ratios, either by direct measurement or by inference, as a function of Ri or ζ is not yet firm. Any knowledge we do have relates to flow overland, and the Lough Neagh results are the first of their kind over the sea.

In 1947, Priestley and Swinbank (1947) suggested that the

influence of buoyancy was to distinguish between the transfer of heat and momentum, and that heat and water vapour would be similar. There are generally two methods of approach; firstly, use of profile measurements to infer the dependence of ratios in 3.3 and 3.4 upon Ri; and secondly, direct measurements of flux and gradient to determine K from equation 3.2. Of immediate concern is the former method; the latter one is presented in § 4.3.

The problem is to relate certain characteristics of the profiles to the K ratios and infer dependence upon Ri. If the profiles are similar ($(\partial u/\partial z)(\partial \theta/\partial z)^{-1}$ equals a constant, etc. —see § 3.4.2) the variations of the K's with height, and therefore Ri, are the same. Overland Rider (1954) could not distinguish differences in u, θ, q profiles between 0.5 m. and 2 m. nor could Sheppard (1958) do so for Swinbank's u and θ profiles between 0.5 m. and 8 m. These results are not however necessarily at variance with later measurements which, it is important to add, have been made with more refined instrumentation and greater emphasis upon site requirements. Swinbank (1964) as an aside from his discussion of the exponential wind profile found considerable dissimilarity between u and θ profiles in unstable conditions, the "degree of dissimilarity" increasing with increasing instability. Later Swinbank & Dyer (1967) published evidence for the dissimilarity of u and θ profiles in unstable air (overland) and the similarity of θ and q profiles. However there is considerable disagreement between Russian and Western workers on the transfer problem. In contrast wind and temperature profiles analysed by Zilitinkevich and Chalikov (1968) implied near-similarity over a wide range of Ri. This

disagreement is further emphasised by direct flux measurement (see § 4.3).

Over the sea, similar measurements have not been published thereby weighting the importance of the Lough Neagh results.

3.4.2. Profile Shape Factor

Writing equation 3.2 for momentum and heat transfer, and dividing one equation by the other,

$$\left(\frac{K_H}{K_M}\right)_z = \left(\frac{\overline{w'T'}}{-\overline{u'w'}}\right)_z \cdot \left(\frac{\partial u/\partial z}{\partial \theta/\partial z}\right)_z \qquad 3.15$$

If the fluxes are constant with height then K_H/K_M is constant if $(\partial u/\partial z)/(\partial \theta/\partial z)$ is constant with height (profiles similar). Writing 3.15 for 2 heights, then,

$$\frac{(K_H/K_M)_{z_2}}{(K_H/K_M)_{z_1}} = \frac{(\partial \theta/\partial z)_{z_1}}{(\partial \theta/\partial z)_{z_2}} \cdot \frac{(\partial u/\partial z)_{z_2}}{(\partial u/\partial z)_{z_1}} \qquad 3.16$$

The quantity $(\partial X/\partial z)_{z_1}/(\partial X/\partial z)_{z_2}$ is called the profile shape factor. Using equation 3.8 this may be written in terms of finite differences, viz. the apparent profile shape factor is defined (Swinbank & Dyer, 1967) for observations taken in our case between 1 m. and 16 m.,

$$S_X(z) = \frac{X_z - X_1}{X_{16} - X_1} \qquad 3.17$$

An index of similarity can be defined —

$$P_{\theta,u} = S_\theta(z)/S_u(z) \qquad 3.18$$

$$P_{q,u} = S_q(z)/S_u(z) \qquad 3.19$$

Note that if the S's are equal, $P = 1$ implying similarity of profiles. By comparing 3.1 and 3.8 it is possible to interpret S_X as follows —

$$S_X(z) \propto (\Phi)_{z^{1/2}} \Big/ (\Phi)_4 \qquad 3.20$$

for $z < 16$ m. Thus the variation of $S_X(z)$ with Ri is equivalent to the height variation of Φ as a function of Ri.

3.4.3. Normalised Profiles

For all 100 Runs, S_X was calculated from each u, θ and q profile at heights 2, 4, 8 m. (S_X being zero and one at 1 m. and 16 m. respectively). Normalised profiles were then drawn, $S_X(z)$ vs $\log_{10} z$ (ordinate), and for convenience of presentation were grouped according to the value of Ri (4 m.). 4 ranges were used, as indicated in Fig.3.8, and values of S_X averaged at each height for each Ri range.

The profile curvatures (or shape) depend strongly upon Ri and vary most at small values of Ri. This is why the variation of Ri within each range must be small in near-neutral conditions but may be relatively large elsewhere. For any one Ri range, the profiles for u, θ, q are not very different but closer inspection will suggest dissimilarity between the θ and u,q curves when $Ri < -0.2$ and $Ri > 0.05$. (§ 3.4.4, 3.4.5).

The advantage of this method is that a large group of profiles can be averaged and presented collectively as functions of one variable, Ri. The disadvantage lies in the lack of quantitative information available on the variation of S_X with Ri.

FIG. 3. 8

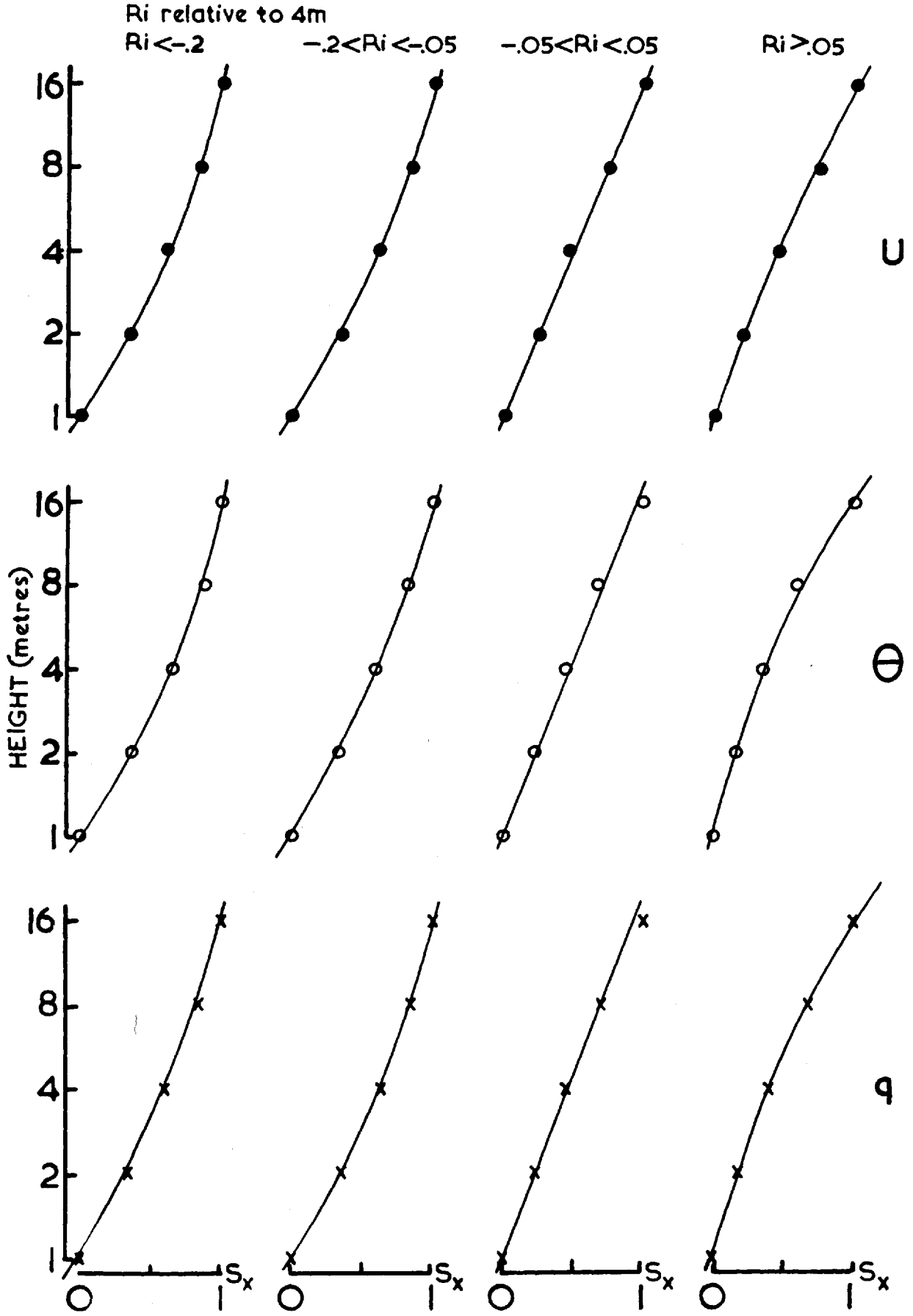
Ri relative to 4m
Ri <-.2
-.2<Ri<-.05
-.05<Ri<.05
Ri >.05
HEIGHT (metres)
16
8
4
2
1
U
Θ
q
0
1
Sx

3.4.4. Variation of Shape Factors with Ri

3.4.4.1. Individual Runs at Lough Neagh

The normalised profiles of § 3.4.3 illustrate the general dependence of S_X upon Ri, the greatest variation occurring at $z = 4$ m. For this reason it was decided to find the detailed variation of $S_X(4)$ with Ri(4). Figs.3.9, 3.10 and 3.11 give this for u, θ, q respectively for the 100 individual Runs. The considerable scatter present does not hide the increase in S_X from stable to unstable conditions with S_X becoming constant for large negative Ri. The value for negative Ri is about twice that for positive Ri implying greater height variation of Φ in the latter case (cf. equation 3.20) consistent with the known curvature of profiles.

The scatter may be due to several causes —

(i) Inherent experimental error in S_X and Ri,

(ii) Unsteadiness of the air flow.

As regards (i) the experimental error in S_X involves the ratio of differences in X each having an error (on average) of 5 per cent (§ 3.2.1) so that the probable error in S_X is 10 per cent. The error in Ri(4 m.) will be ~ 20 per cent (§ 3.2.2). The combination of these two errors would certainly explain the scatter of points in the diagrams. A small amount of scatter might be due to unsteadiness during the periods of recording, and with variations of fluxes in the vertical.

The smaller scatter in the case of S_u reflects the greater accuracy attainable in quantities like $u_2 - u_1$, than for $\theta_2 - \theta_1$ and $q_2 - q_1$. When $Ri \simeq 0$, $\theta_2 - \theta_1$ is comparable to the experimental

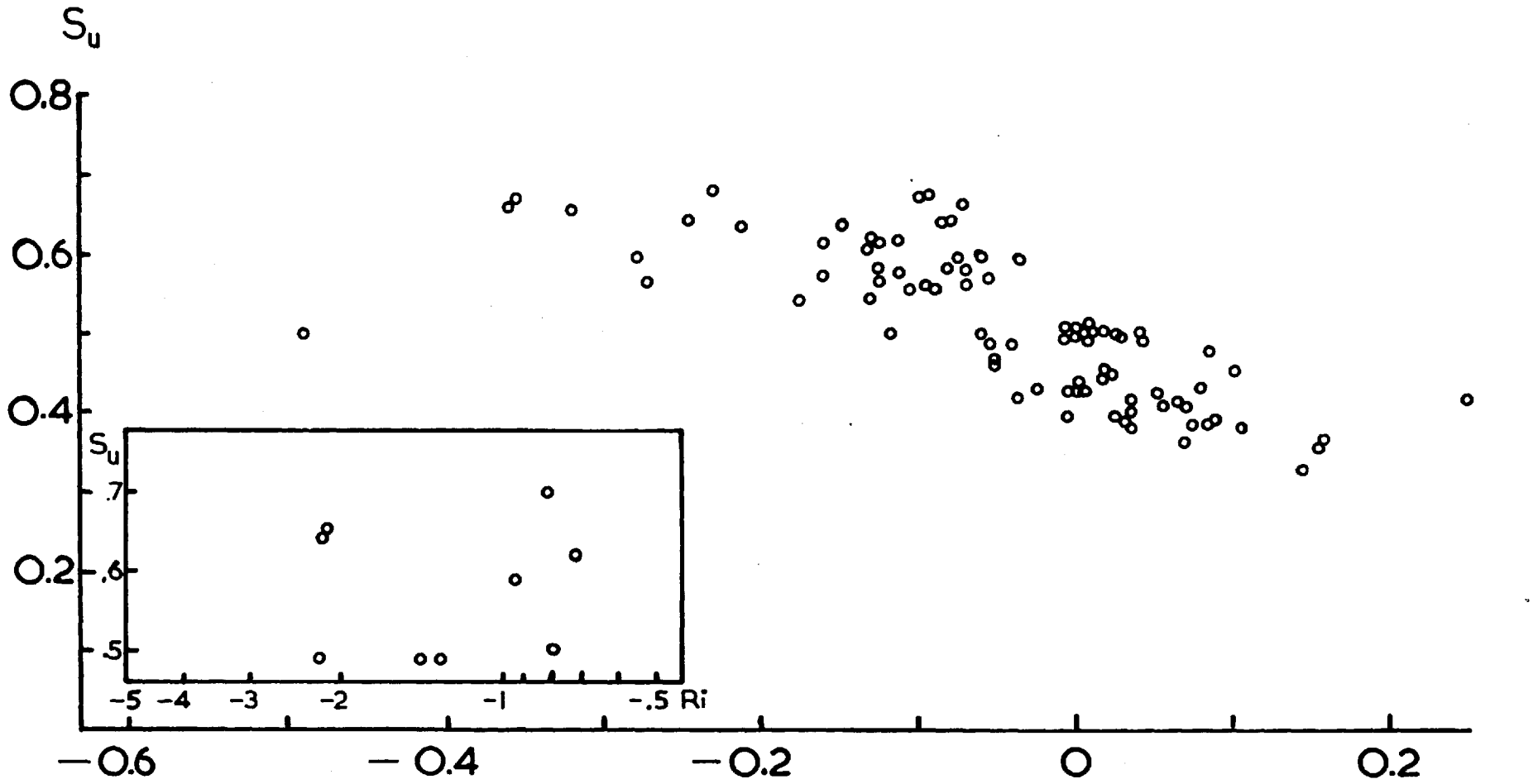

FIG.3.9

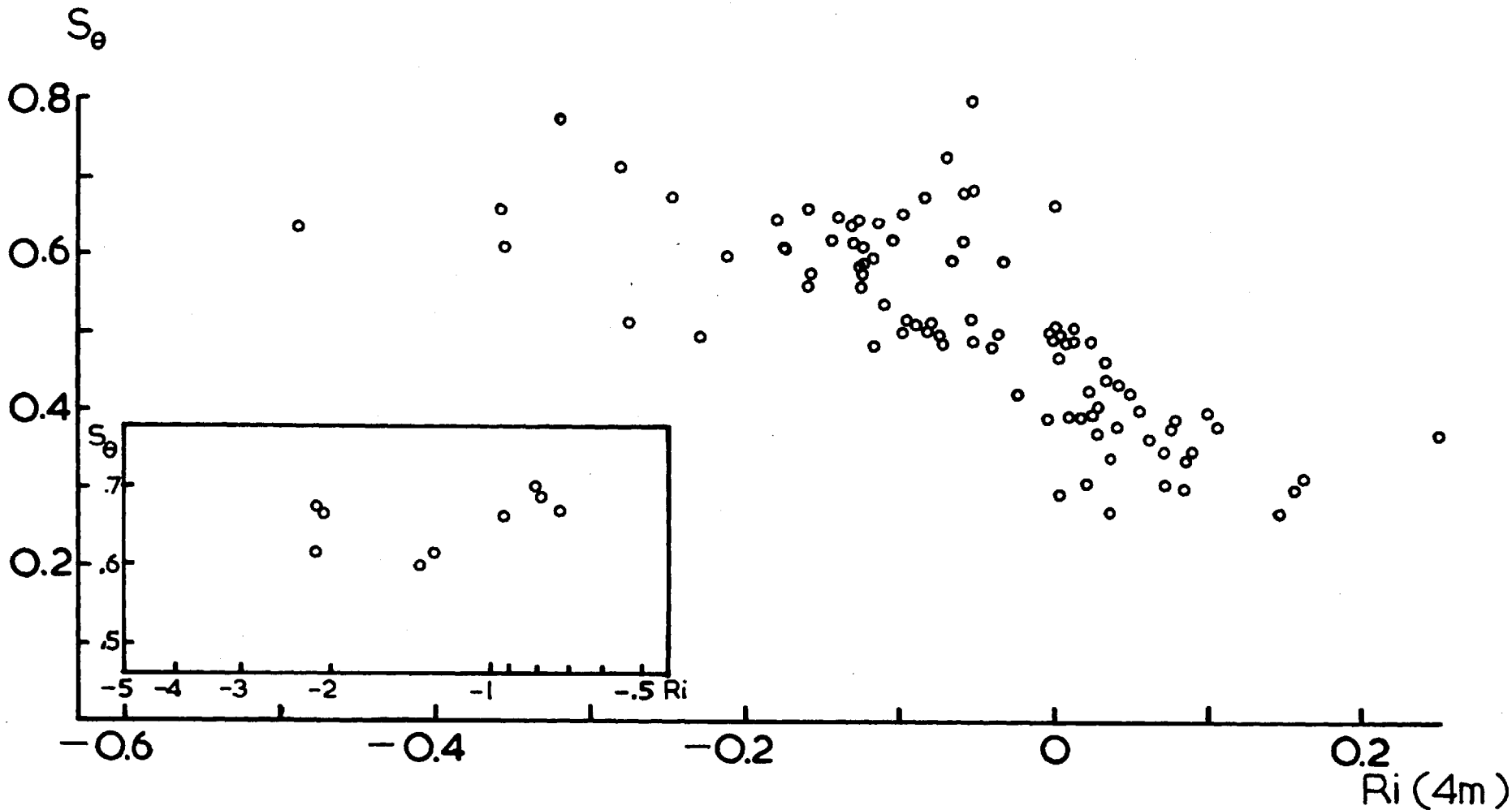

FIG. 3.10

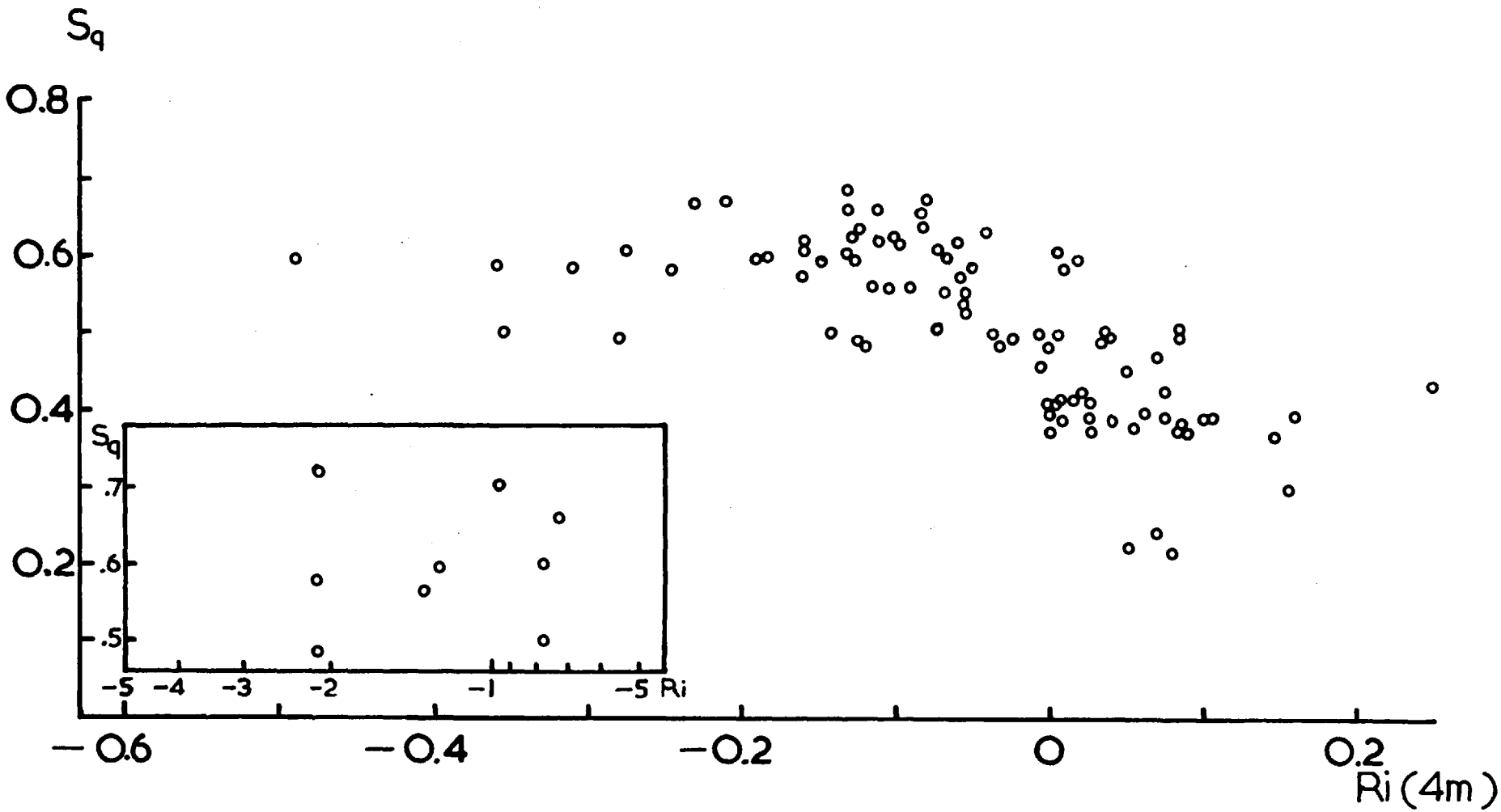

FIG.3.11

error and it is remarkable that there is not greater scatter than is present in the diagram.

3.4.4.2. Smoothed S_X - Ri curves

Computed S_X averages for several Ri ranges are shown in Fig.3.12. The mean deviation included is a measure of the amount of scatter present in Figs. 3.9 – 3.11. Analogous results (for flow overland) taken from Swinbank & Dyer (1967) are included for negative Ri together with the standard deviations. The relative size of the deviations reflects the fact that, given a comparable instrument performance in both sets of data, errors in quantities like $X_2 - X_1$ are greater over the sea where the gradients are correspondingly smaller.

Comparing the two sets of results, S_θ and S_q show a greater variation with Ri, over a comparable Ri range, overland than oversea whereas the reverse is true in the case of S_u. In both cases, $S_\theta > S_u$ for negative Ri but the relative S_q variations are significantly different, Dyer's results implying similar θ and q profiles, but dissimilar θ and u profiles, the Lough Neagh results implying similar q and u profiles but dissimilar θ and u profiles.

The apparent different behaviour for q is the outstanding feature of Fig.3.12.

3.4.5. Quantitative Assessment of Similarity

The implications of the previous section will now be investigated quantitatively using the indices of similarity defined

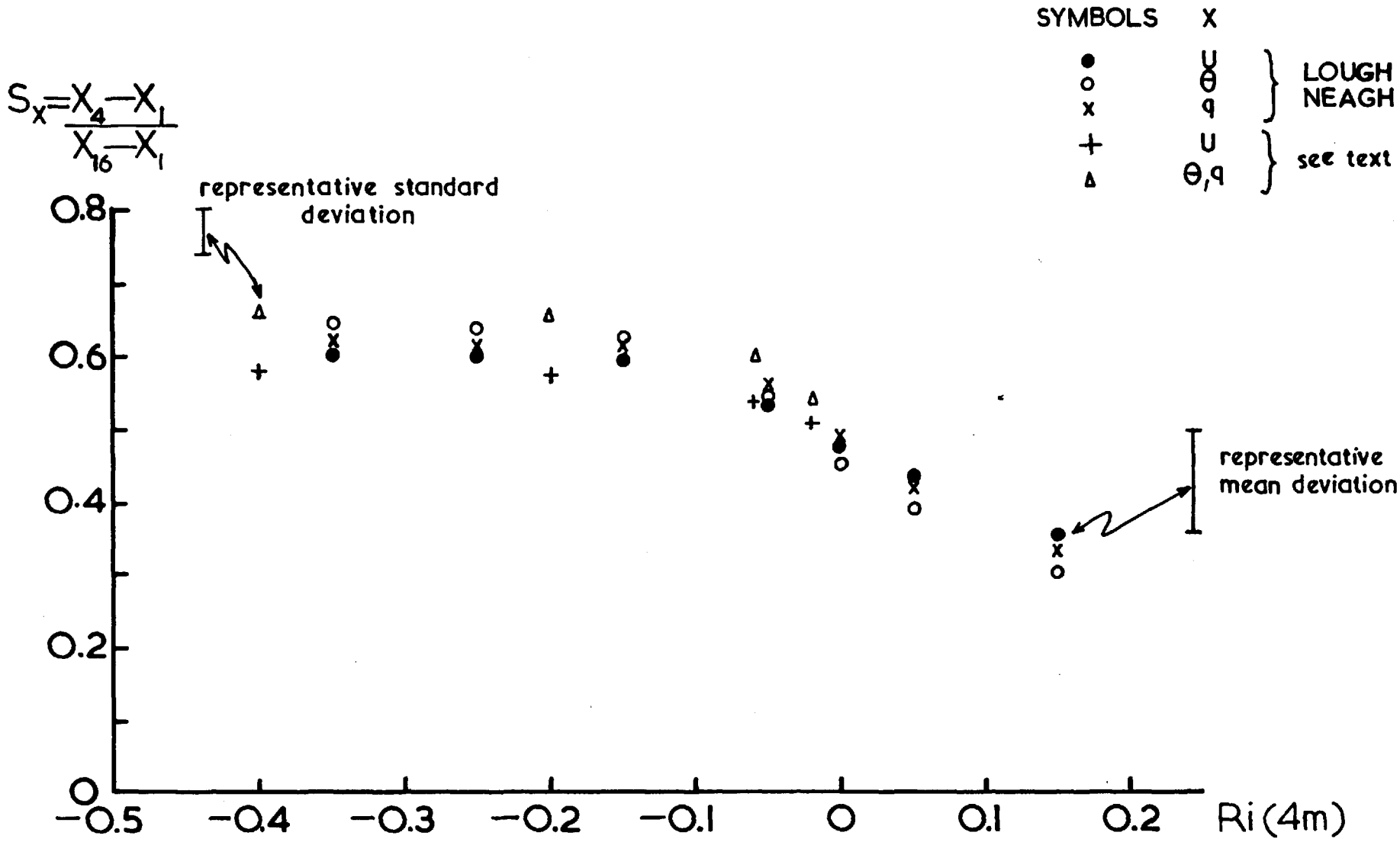
$S_x = \frac{X_4 - X_1}{X_{16} - X_1}$
representative standard deviation
SYMBOLS X
U
θ
q
LOUGH NEAGH
U
θ,q
see text
representative mean deviation
0.8
0.6
0.4
0.2
0
−0.5
−0.4
−0.3
−0.2
−0.1
0
0.1
0.2
Ri (4m)

FIG. 3-12

in equations 3.18, 3.19. Values of P have been found for each run relative to a height of 4 m., and averages formed for 4 Ri ranges. Each P is defined as follows,

$$P_{\theta,u} = \frac{S_\theta(4)}{S_u(4)} \equiv \frac{(K_H/K_M)_4}{(K_H/K_M)_2}$$

and,

$$P_{q,u} = \frac{S_q(4)}{S_u(4)} = \frac{(K_V/K_M)_4}{(K_V/K_M)_2}$$

The variations of $P_{\theta,u}$ and $P_{q,u}$ with Ri are shown in Figs. 3.13 and 3.14 respectively together with the standard deviations of P per Ri range. Regarding Fig. 3.13,

(1) $S_\theta > S_u$ when $Ri < 0$, P increasing with increasing instability. K_H/K_M therefore increases with height and consequently with increasing instability,

(2) $S_\theta < S_u$ when $Ri > 0$, P decreasing with increasing stability. K_H/K_M therefore decreases with height and consequently with increasing stability.

These two properties are consistent with direct measurements of K_H/K_M as a function of Ri —see § 4.3.1. The analysis in this section gives no information on the absolute values of the transfer coefficients. As regards Fig. 3.14, doubt must be expressed regarding the implied variation of $P_{q,u}$ with Ri, though it is comforting that it is in the same direction as $P_{\theta,u}$. The conclusion is that K_V/K_M varies little with height and is therefore approximately constant with Ri. This result must remain tentative because of the lack of direct water vapour flux measurements for comparison.

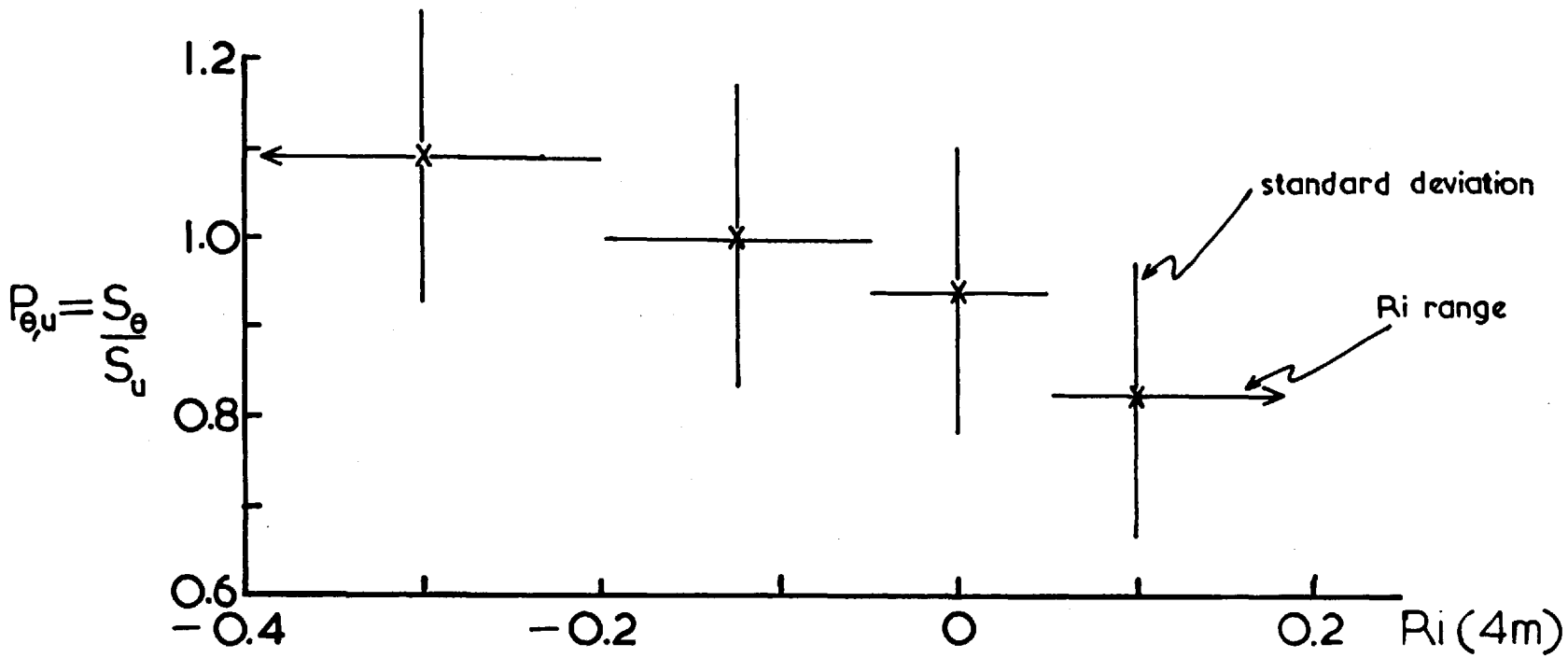
1.2
1.0
0.8
0.6
$P_{\theta,u} = \frac{S_\theta}{S_u}$
standard deviation
Ri range
−0.4
−0.2
0
0.2
Ri (4m)

FIG. 3.13

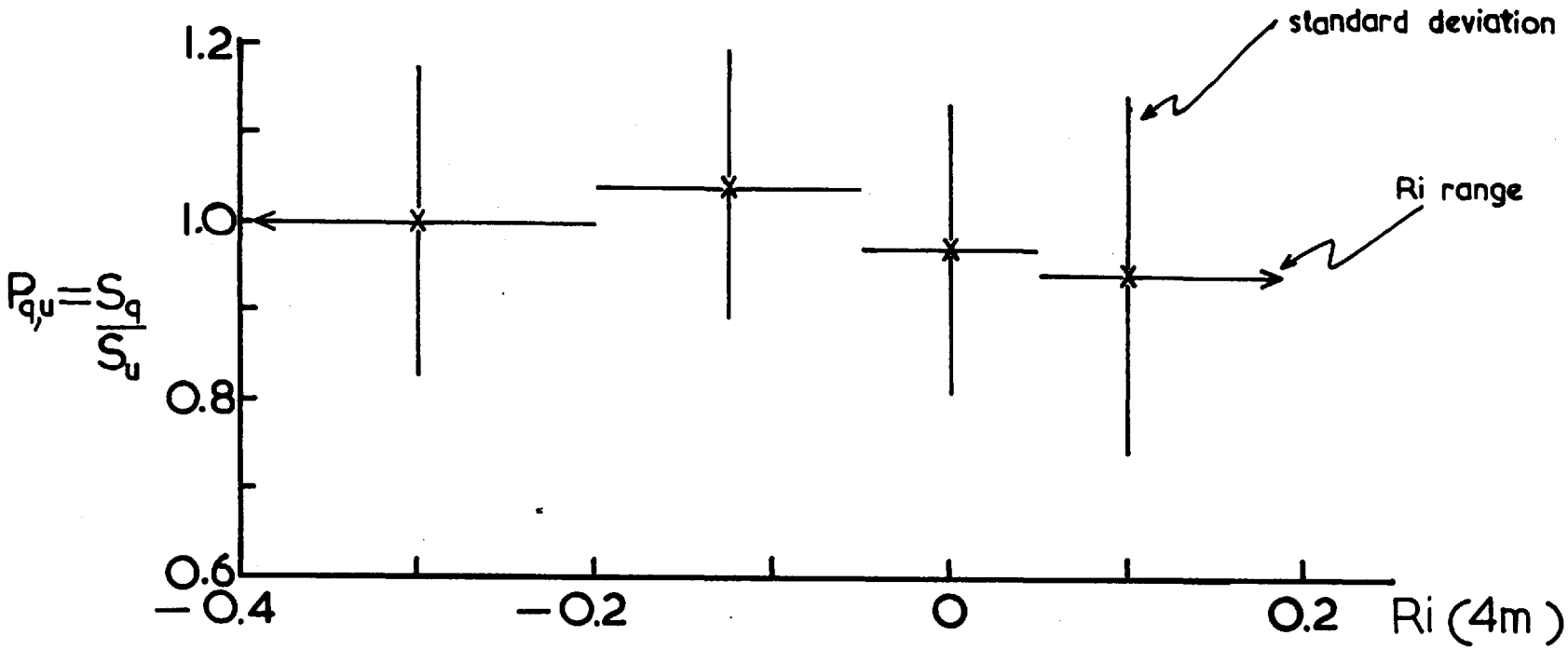
standard deviation
Ri range
1.2
1.0
0.8
0.6
$P_{q,u}=\frac{S_q}{S_u}$
−0.4
−0.2
0
0.2
Ri (4m)

FIG. 3.14

If accepted these results indicate a similar mechanism operative for the transfers of momentum and humidity (by mechanical turbulence) with an additional mechanism transferring heat (buoyancy). Earlier work overland by Pasquill (1949) and Rider (1954) generally confirmed equality of K_V and K_M but K_H was, at times in unstable conditions, found to be several times greater. It is stressed that better humidity profiles and measurements of water vapour fluxes are imperative for the Lough Neagh results to be confirmed.

4.1. Introduction

The chapter is divided into three main parts; in § 4.2. statistical properties of the turbulence are presented in the form of variances and covariances of the fluctuations which can be interpreted physically in terms of the turbulent energies (intensities) and fluxes. Particular value is placed upon relating fluxes to simpler statistics of the flow since this would have real practical value. In § 4.3. the quantitative nature of the turbulent transfers of heat and momentum is investigated using flux measurements, and compared with results in Chapter 3. In § 4.4. the nature of the dissipation rate of turbulent kinetic energy is investigated using an indirect method of estimating the dissipation rate from knowledge of the velocity fluctuation spectra. A review of material relevant to the present chapter can be found in L.P. concerning surface layer properties overland; only recently have comparable measurements made oversea become available — these are discussed in the following sections.

4.2. Turbulent Energies and Fluxes

4.2.1. Relative Magnitudes

Because turbulence in the surface layer is essentially anisotropic in nature due, in part, to the control of the ground on vertical motion there is no reason to expect the same behaviour for the statistical properties of horizontal and vertical components. This idea is borne out in practice, and is especially noticeable when considering the dependence of the statistical properties upon $\bar{u}$, z_o and z/L or Ri —the z dependence being contained in the

stability parameter. In particular similarity theory predicts that dimensionless combinations of such properties will be Universal functions of z/L. However to test such an hypothesis requires a large amount of data and, consequently, the Lough Neagh data is not particularly suited to such an exercise. However comprehensive results have been published by Russian workers --see Monin (1962), for example. They show that the z/L dependence is generally weak (this is so for velocity, but not for temperature) and so the Lough Neagh data are dealt with collectively irrespective of the value of Ri.

Firstly consider the quantity $\overline{u'^2}/\overline{w'^2}$ which is a partial measure of the anisotropy (strictly, only of the departure from equipartition of energy) — equalling unity in isotropic turbulence. Table 4.1 indicates a mean value over Lough Neagh of 3.18, compared with 3.98 measured by Z.K. over the Mediterranean Sea and a value of 10.8 measured overland by Monin (1962). It is probable that these relative values reflect the effect of roughness or inhomogeneity of surface upon the partitioning of energy, and is consistent with the idea that well away from the surface there is a tendency towards equipartition of energy. Over Lough Neagh there is no evidence that $\overline{u'^2}/\overline{w'^2}$ varies in any consistent fashion with height but for a larger height range overland (0 - 30 m.), Deacon (1955) found a tendency for the ratio to tend to 1 as z increased.

Table 4.1

Ri	$\overline{u'^2}/\overline{w'^2}$	$\overline{u'^2}/-\overline{u'w'}$	$\overline{w'^2}/-\overline{u'w'}$	$\overline{T'^2}/\left(z\frac{\partial\theta}{\partial z}\right)^2$
negative	3.18 ± 0.15	6.14 ± 0.35	2.00 ± 0.10	~ 0.5
positive				~ 4.0

Regarding the quantity $\overline{u'^2}/-\overline{u'w'}$, Fig.4.1 shows $\overline{u'^2}$ vs $-\overline{u'w'}$ for 4 Ri ranges. Table 4.1 indicates a value of 6.14 for Lough Neagh compared to 9.00 (Z.K.), whereas overland values of 4.4 and 8.4 have been quoted for Brookhaven and O'Neill sites (L.P.) in near-neutral conditions. Evidently this ratio is highly variable from one site to another, implying dependence upon some large-scale terrain factor. The disadvantage of working with quantities involving $\overline{u'^2}$ is the latter's sensitivity to unsteadiness making its behaviour unpredictable. Moreover the Lough Neagh results do not confirm those of Z.K. who found an inverse dependence of $\overline{u'^2}/-\overline{u'w'}$ upon wind speed. Later Preobrazhenskii (1968) published data for an Atlantic Ocean site, for the height range 0.5 - 5 m., showing an initial increase with wind speed to a value of about 15 (at $\overline{u}$ ~ 5 m.s^{-1}) afterwards decreasing. Thus the Russian results are not altogether consistent. It is however important to note that the Russian work was carried out, in part, at heights comparable to the wave amplitudes whereas Lough Neagh work is carried out at heights several times the wave amplitude; any wave effect will be particularly noticeable at the lowest heights. This point will be taken up again later in the thesis.

With $\overline{u'^2} = (6.14 \pm 0.35)(-\overline{u'w'})$ for Lough Neagh estimates of $-\overline{u'w'}$ are possible from the more easily measured quantity $\overline{u'^2}$ to within a probable accuracy of 5-10 per cent.

The vertical component $\overline{w'^2}$ is relatively unaffected by large-scale factors (the proximity of the surface damps out low frequency components of the fluctuations associated with unsteadiness). Concerning the ratio $\overline{w'^2}/-\overline{u'w'}$ similarity theory predicts, that

FIG.4.1

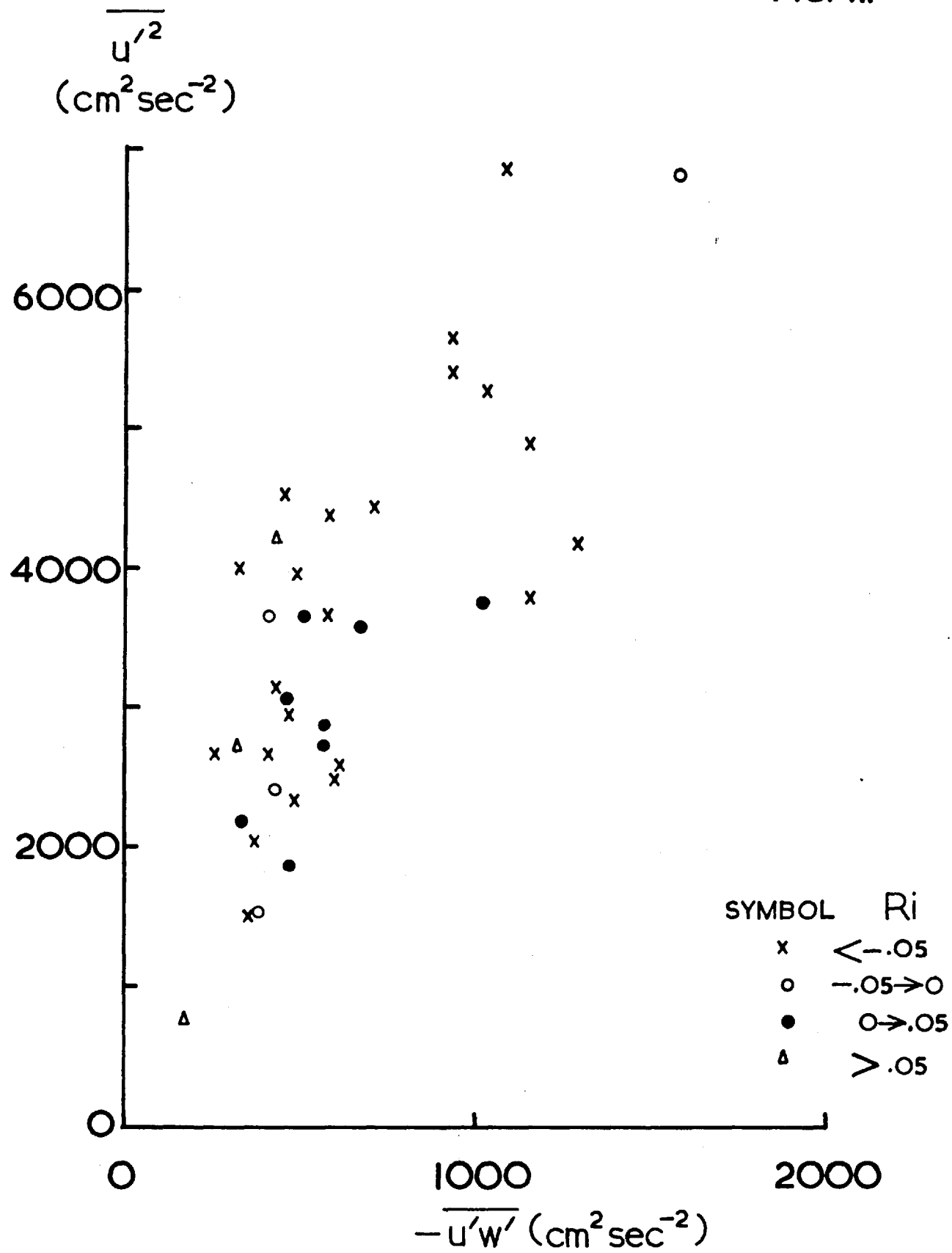
$\overline{u'^2}$ (cm^{2}sec^{-2})
6000
4000
2000
0
0
1000
2000
$-\overline{u'w'}$ (cm^{2}sec^{-2})
SYMBOL Ri
× < −.05
○ −.05 → 0
● 0 → .05
△ > .05

for ζ or Ri ~zero, it is a Universal constant. It is therefore legitimate to write $\overline{w'^2} = A(-\overline{u'w'})$ for all but extreme values of Ri. Fig.4.2 shows $\overline{w'^2}$ vs $-\overline{u'w'}$ for 4 Ri ranges, and Table 4.1 indicates a value of 2.00 for A, estimates of A made by other workers overland and oversea being given in Table 4.2. They all lie within about 20% of the Lough Neagh result.

Table 4.2

AUTHOR AND YEAR	VALUE OF A	SURFACE
Present work	2.00 ± 0.10	SEA
Z.K. (1967)	2.50	SEA
Pasquill (1962)	1.77 ± 0.10	LAND
Panofsky and McCormick (1960)	1.56	LAND
Barad (1958)	1.56	LAND

Concerning the measurement of $\overline{w'^2}$, spectral analysis indicates (§ 5.3.) that there is, in some cases (depending upon height, wind speed and Ri), a small but significant high frequency loss suggesting that A might be equal to 2.1 and not 2.0. There is not enough evidence for any real significance to be attached to the greater values of A measured oversea, though the latter could be due to the influence of waves, effectively boosting the upward motion of air and consequently $\overline{w'^2}$ relative to the horizontal component. The effect would be expected to die away at greater heights, and it may be significant that Z.K.'s value is greater than the Lough Neagh value. Again Preobrazhenskii found A to vary directly with wind speed, but no such effect is evident at Lough Neagh. For the data presented in Fig.4.2 it is found that $\overline{w'^2} = (2.00 \pm 0.10)(-\overline{u'w'})$, neglecting

FIG.4.2

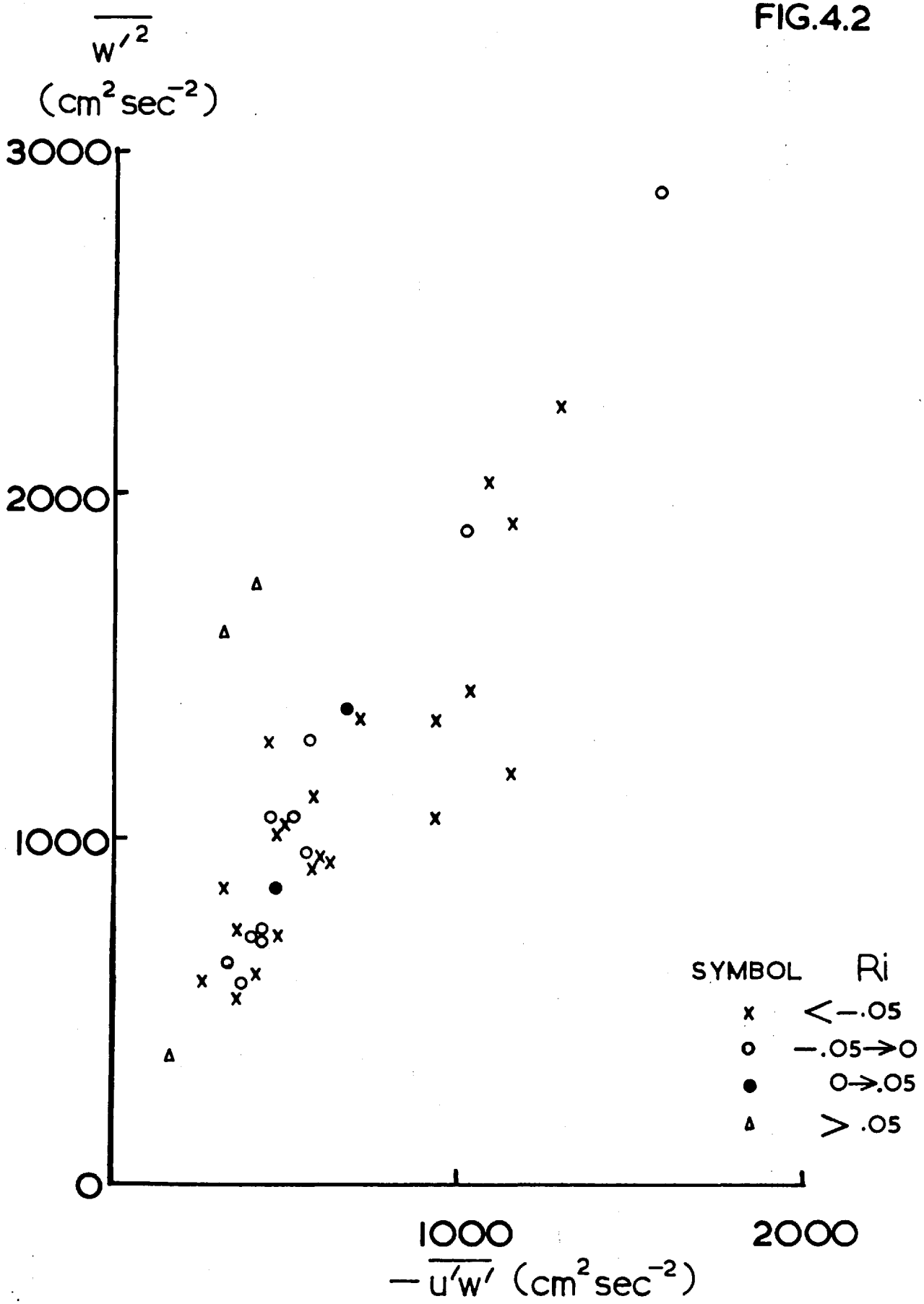
$\overline{w'^2}$ (cm^{2}sec^{-2})
3000
2000
1000
0
1000
2000
$-\overline{u'w'}$ (cm^{2}sec^{-2})
SYMBOL Ri
× < −.05
o −.05 → 0
● 0 → .05
Δ > .05

the two stable runs with anomalously high ratios thus making possible $\overline{u'w'}$ estimates to within 5 per cent from $\overline{w'^2}$ measurements. Since it is relatively easier to measure $\overline{w'^2}$ to a given accuracy (the question of an accurately determined horizontal is not so important) the method is not without merit.

The fact that it is possible to write $\overline{w'^2} = A(-\overline{u'w'})$ or $\sigma_w = A^{\frac{1}{2}} u_*$ allows $\overline{w'^2}$, strictly for neutral stability, to be expressed in terms of $\bar{u}$ and z_o, viz. using equation 3.5 gives

$$\frac{\sigma_w}{\bar{u}} = \frac{\kappa A^{\frac{1}{2}}}{\ln(z/z_o)} \qquad 4.1$$

or, relative to a height of 4 m.,

$$\frac{\sigma_w}{\bar{u}_4} = \frac{\kappa A^{\frac{1}{2}}}{\ln(400/z_o)} \qquad 4.1\,a$$

with z_o in cm.

From the Lough Neagh data, 13 near-neutral runs with logarithmic or near-logarithmic profiles were chosen and z_o evaluated using equations 3.5 and 3.7. Where σ_w was measured at more than one height simultaneously, an average value was taken and the ratio $\sigma_w / \bar{u}_4$ plotted vs $\ln z_o$ —see Fig.4.3. There is some evidence for a decrease of $\sigma_w / \bar{u}_4$ with decrease in z_o (from 10^{-2} to 10^{-4} cm. approximately). On the same diagram were plotted points deduced from published data, normalised to a height of 4 m., and covering as wide a range of z_o as possible. All the points confirm the dependence of the ordinate upon z_o according to equation 4.1 which is represented by the continuous

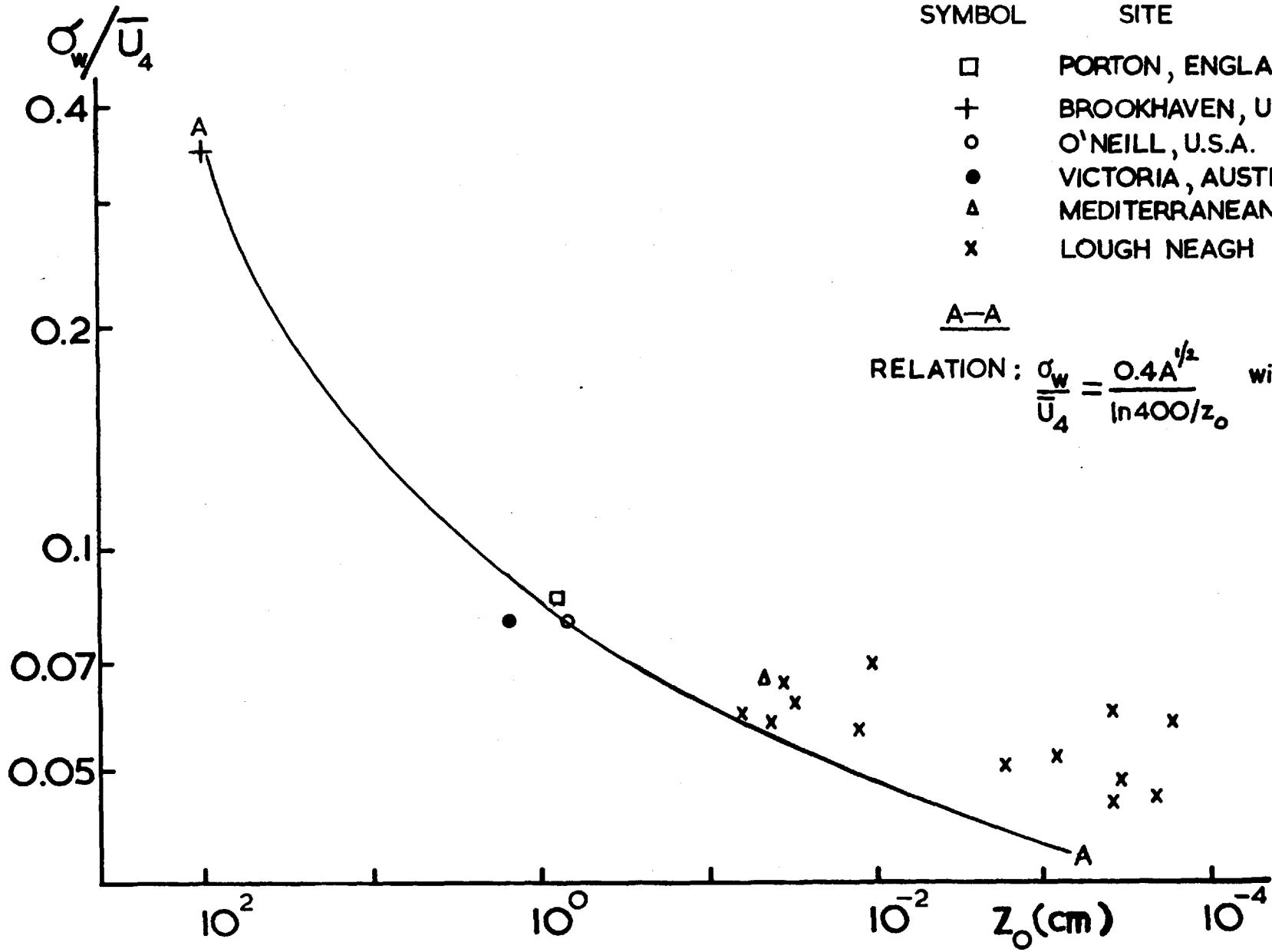
$\sigma_w/\bar{U}_4$
0.4
0.2
0.1
0.07
0.05
A
A
10^2
10^0
10^{-2}
Z_o(cm)
10^{-4}
SYMBOL
SITE
PORTON, ENGLAND
BROOKHAVEN, U.S.A.
O'NEILL, U.S.A.
VICTORIA, AUSTRALIA
MEDITERRANEAN SEA
LOUGH NEAGH
A—A
RELATION: $\frac{\sigma_w}{\bar{U}_4} = \frac{0.4A^{1/2}}{\ln 400/z_o}$ with $A^{1/2} = 1.25$

FIG. 4.3

curve AA with $A^{1/2} = 1.25$. Of special interest are the comparable sizes of z_o for Lough Neagh and the Mediterranean Sea.

Finally, the sensitivity to large-scale unsteadiness applies more so to the temperature variance $\overline{T'^2}$, limiting its usefulness. Nevertheless it should be observed that values of the dimensionless ratio $\overline{T'^2}/\left(z\frac{\partial\theta}{\partial z}\right)^2$ given in Table 4.1 agree with overland data published by Zwang (1960).

4.2.2. Flux Variability

It is important to assess the reliability of flux measurements with regard to the choice of sampling period (τ_s) and to the range of frequencies over which there is significant eddy contribution to the fluxes in question. This problem is additional to the one concerned with "tilt error" which was estimated in § 2.2.3. for $\overline{u'w'}$ to be less than 5%.

Earlier work by Deacon (1955) and results contained in Priestley (1959), Chou Min-Yui (1966) and Gurvich (1960b, 1961) together with our cospectral measurements (Chapter 5) suggest that the sampling range of 0.1 sec to 10 minutes is sufficient for heights up to tens of metres, and for moderate wind speeds and stabilities.

To illustrate the adequacy of a 10 minute sampling period, 10 minute periods were sub-divided into periods of 2,3,4,5 minutes and covariances $\overline{u'w'}$, $\overline{w'T'}$ evaluated for each sub-period as a fraction of the corresponding 10 minute period but using means for each period. The results using 4 10-minute periods for sub-intervals of 2,3,4 minutes and 23 10-minute periods for the corresponding 46 5-minute sub-intervals are shown in Fig.4.4 where the ordinate represents

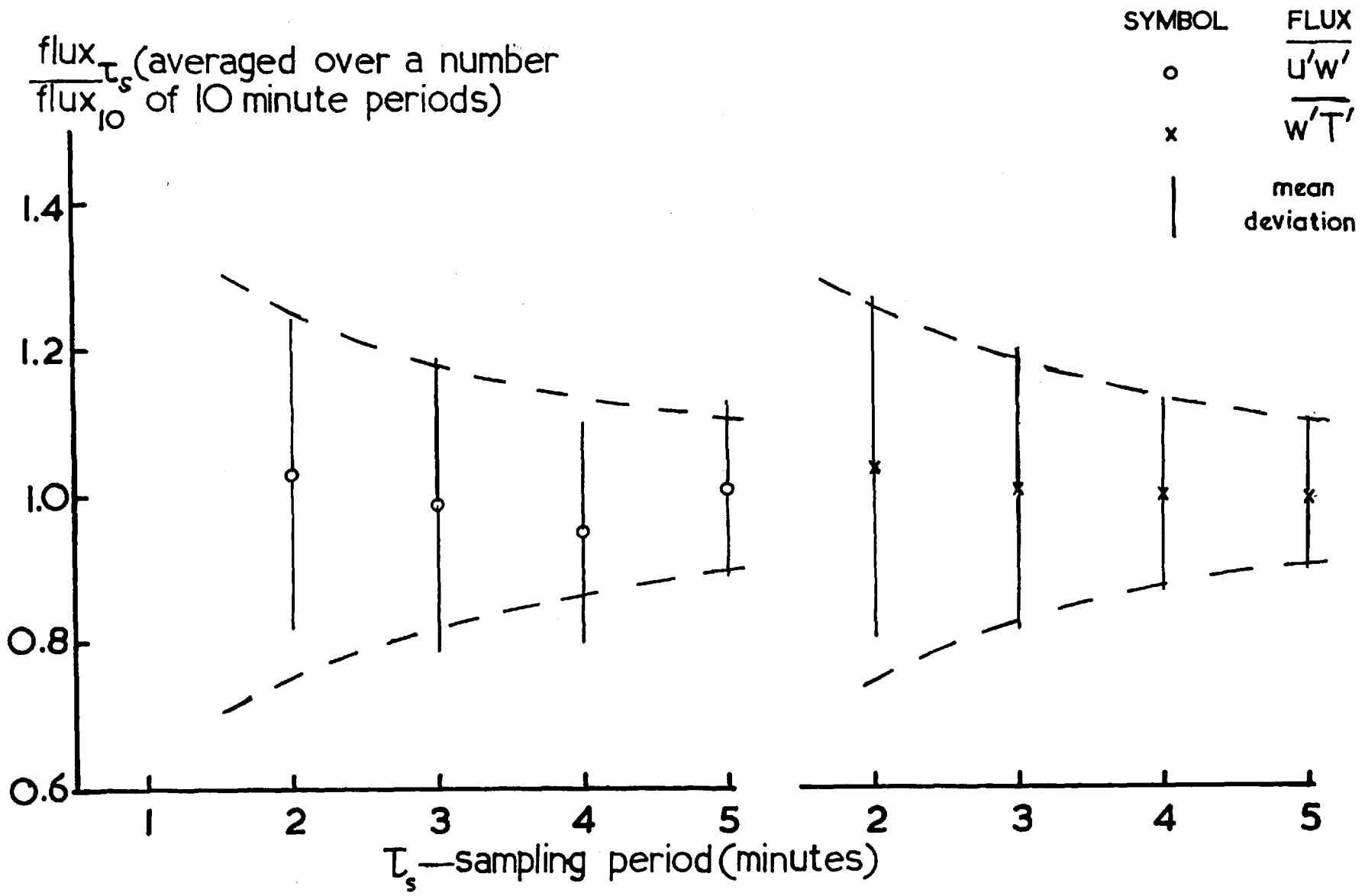
SYMBOL
FLUX
o
$\overline{u'w'}$
x
$\overline{w'T'}$
mean deviation
$\frac{\text{flux}_{\tau_s}}{\text{flux}_{10}}$ (averaged over a number of 10 minute periods)
1.4
1.2
1.0
0.8
0.6
1
2
3
4
5
2
3
4
5
τ_s—sampling period (minutes)

FIG. 4.4

the averaged ratio of the flux evaluated for a period τ_s to the flux for a period of 10 minutes. The results imply that, on average, a sampling period as small as 2 minutes is sufficient to measure all the flux contribution, for heat and momentum, for the conditions experienced at Lough Neagh. In addition the variability of the flux estimate (i.e. the mean deviation) increases with decreasing τ_s implying that for relatively reliable flux estimates the sampling period must be much greater than 2 minutes. Fig.4.5 shows a comparison of fluxes $\overline{u'w'}$ and $\overline{w'T'}$ evaluated for $\tau_s = 5$ and 10 minutes — for each 10 minute estimate there are two 5 minute ones, their difference being indicated by the vertical line separating them on the diagram. Again there does not appear to be any under-estimation of the 5 minute fluxes relative to the 10 minute. In the same way it is desirable to assess the reliability of the 10 minute fluxes compared to fluxes obtained from longer sampling periods. Reliable flux estimates for $\tau_s >>$ 10 minutes are however rather difficult to obtain because of the longer-term trends. Thus, anticipating the form of the cospectra (Chapter 5) they suggest that time periods greater than 10 minutes contribute little to the fluxes on average. Therefore the statistical variability of the 10 minute flux estimates, with respect to a long term mean flux, will be no more than 10 per cent, the variability of the 5 minute estimates relative to a 10 minute mean flux in Fig.4.4.

In conclusion it seems very probable that individual momentum and heat flux estimates (Appendix 1) will differ by no more than 10-15 per cent from the long term statistically steady value. (This maximum error is consistent with the excellent agreement

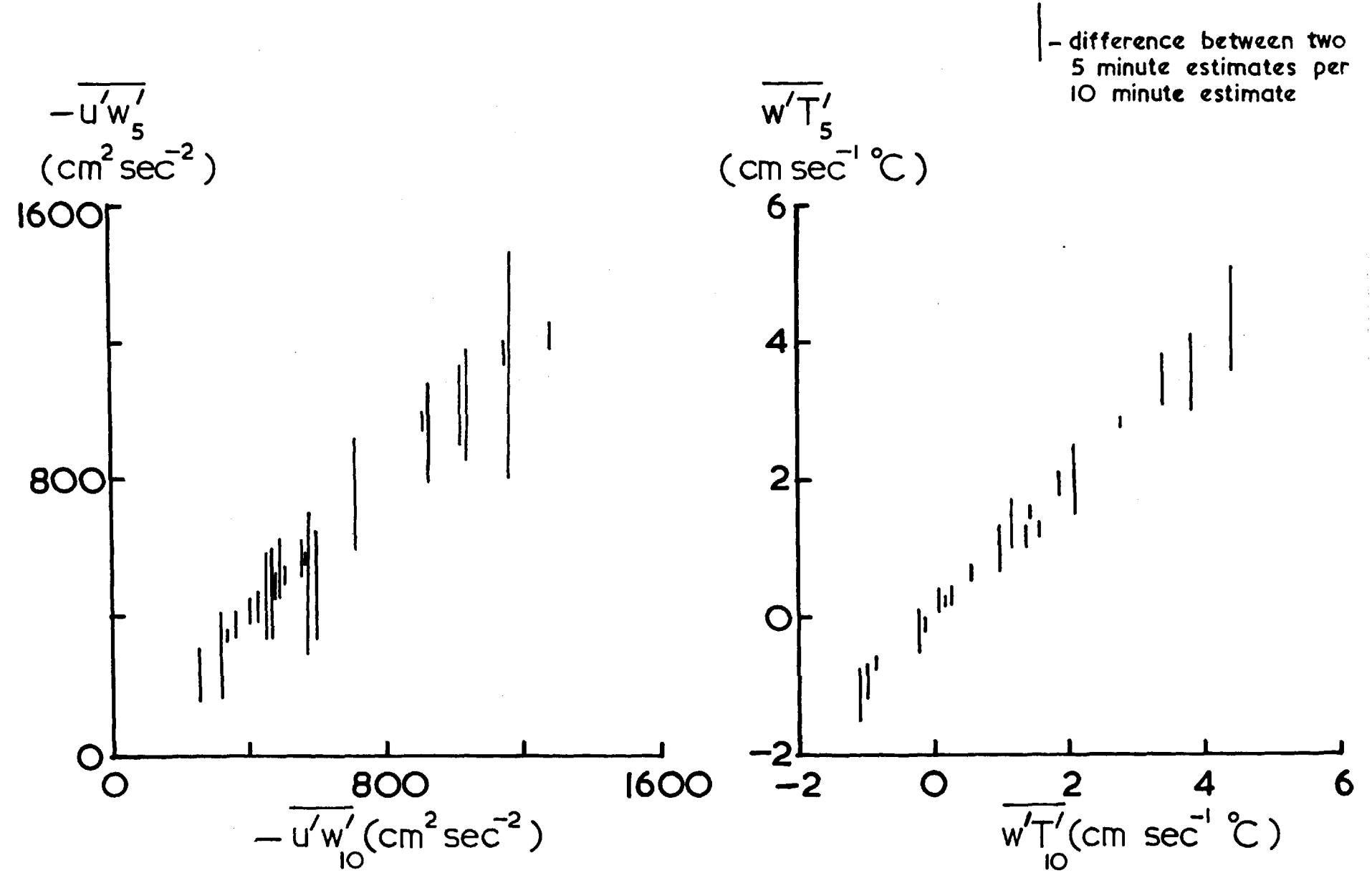
- difference between two 5 minute estimates per 10 minute estimate
$-\overline{u'w'_5}$ (cm^2 sec^{-2})
1600
800
0
0
800
1600
$-\overline{u'w'_{10}}$ (cm^2 sec^{-2})
$\overline{w'T'_5}$ (cm sec^{-1} °C)
6
4
2
0
-2
-2
0
2
4
6
$\overline{w'T'_{10}}$ (cm sec^{-1} °C)

FIG. 4.5

obtained between our estimates of the spectral constant, K_u, and those of other workers; the former requiring knowledge of $\overline{u'w'}$ — § 4.4.2.).

4.2.3. Height Variation of the Fluxes

One of the more outstanding characteristics of turbulent transfer in the surface layer that has been presumed over recent decades concerns the near-constancy of the vertical fluxes in the first few decametres above the surface. Consider the main terms in the equations for the local rates of change of $\overline{u}$ and $\overline{T}$, viz.,

$$\frac{\partial \overline{u}}{\partial t} + \overline{u}\frac{\partial \overline{u}}{\partial x} = -\frac{1}{\rho}\frac{\partial p}{\partial x} + \frac{\partial}{\partial z}(-\overline{u'w'}) \qquad 4.2$$

$$\frac{\partial \overline{T}}{\partial t} + \overline{u}\frac{\partial \overline{T}}{\partial x} = -\frac{\partial}{\partial z}(\overline{w'T'}) \qquad 4.3$$

if negligible divergence of radiative heat flux is assumed. For a steady state and horizontal homogeneity, and with $\frac{\partial p}{\partial x} \sim 1$ mb per 100 km. i.e. 10^{-2} dynes cm^{-2} per 10 m., τ and H are virtually constant up to 50 m. or so.

Measurements of the fluxes of heat and momentum at several heights in the layer 1-12 m. over Lough Neagh provided a test for the constant flux hypothesis which, in fact, has been little tested by appeal to direct flux measurements. Deacon (1955) published data showing τ and H overland between 1 m. and 29 m. were, on average, constant but from run to run varied considerably with height. More recently M.Z. (overland) made direct measurements of τ and H at 1 m. and 4 m. and found large variations from one level

to the other. They inferred that such variations were due to horizontal inhomogeneity of the wind and temperature fields, horizontal temperature gradients required to account for the heat flux variations being not inconsistent with measurements made by Rider et al. (1963) and wind gradients required to account for the momentum flux variations being, on the whole, consistent with with their own measurements. The gradients could not however account for the variations in all conditions. They further correlated the flux variations with changes in the correlation coefficients with height, implying that horizontal gradients determine the change of correlation coefficient with height. It will be seen shortly that this is not strictly true.

In both cases the measurements at the two levels had the serious disadvantage of not being simultaneous but consecutive; further Deacon found evidence for a loss of flux contribution at the low frequencies for $z = 29$ m. with $\tau_s = 5$ minutes, whereas M.Z. had $\tau_s = 10\text{-}15$ minutes.

Recently Haugen and co-workers (private communication) measured momentum fluxes at three levels simultaneously at heights 5-22 m. overland, and surface stress using a drag plate. $\overline{u'w'}$ was measured with sonic anemometers for which accurate horizontal levelling was found to be critical, "tilt errors" being particularly serious during periods of low correlation between u and w ($r_{uw} < 0.1$). Geometric levelling in the laboratory allowed the $\overline{u'w'}$ estimates to be corrected for tilt, and over a range of Ri the flux was found to be constant, on average, to within 20% over a height range of approximately 20 m.

Regarding the Lough Neagh data, Fig.4.6 shows a plot of the flux ($\overline{u'w'}$ and $\overline{w'T'}$) measured at the lower level (A or B) vs the flux measured at the upper level (B or C). For a constant-flux layer, all the points should lie on a line inclined at an angle of 45° to the abscissa axis. On the same diagram lines have been drawn to represent gradients required to produce a 50% change in the flux over 10 m. for $\bar{u} \sim 5$ m.s^{-1}. Observation shows that the horizontal gradients in equations 4.2 and 4.3 can readily produce a significant variation of flux with height but unfortunately have not been obtained at Lough Neagh. Further, runs were chosen where (a) fluxes increased, (b) decreased with height, and for each category the average percentage change was evaluated both for the fluxes and correlation coefficeints. The latter are defined, for momentum and heat,

$$r_{uw}^2 = \frac{(-\overline{u'w'})^2}{(\overline{u'^2})(\overline{w'^2})} \quad , \quad r_{wT}^2 = \frac{(\overline{w'T'})^2}{(\overline{T'^2})(\overline{w'^2})} \quad \text{respectively.}$$

The result is shown in Fig.4.7, and evidently an increase of flux with height is accompanied by an increase in correlation coefficient and conversely, as found by M.Z. However a constant flux layer does not imply constant correlation coefficient with height —see § 4.3.2.

The momentum fluxes entered in Table 4.3 (previously plotted in Fig.4.6) are assumed to have a mean error of 15% (§ 4.2.2.) and are tabulated together with horizontal wind gradients required to produce the observed change with height. Such magnitudes have been observed in practice (M.Z.) and could feasibly account for the

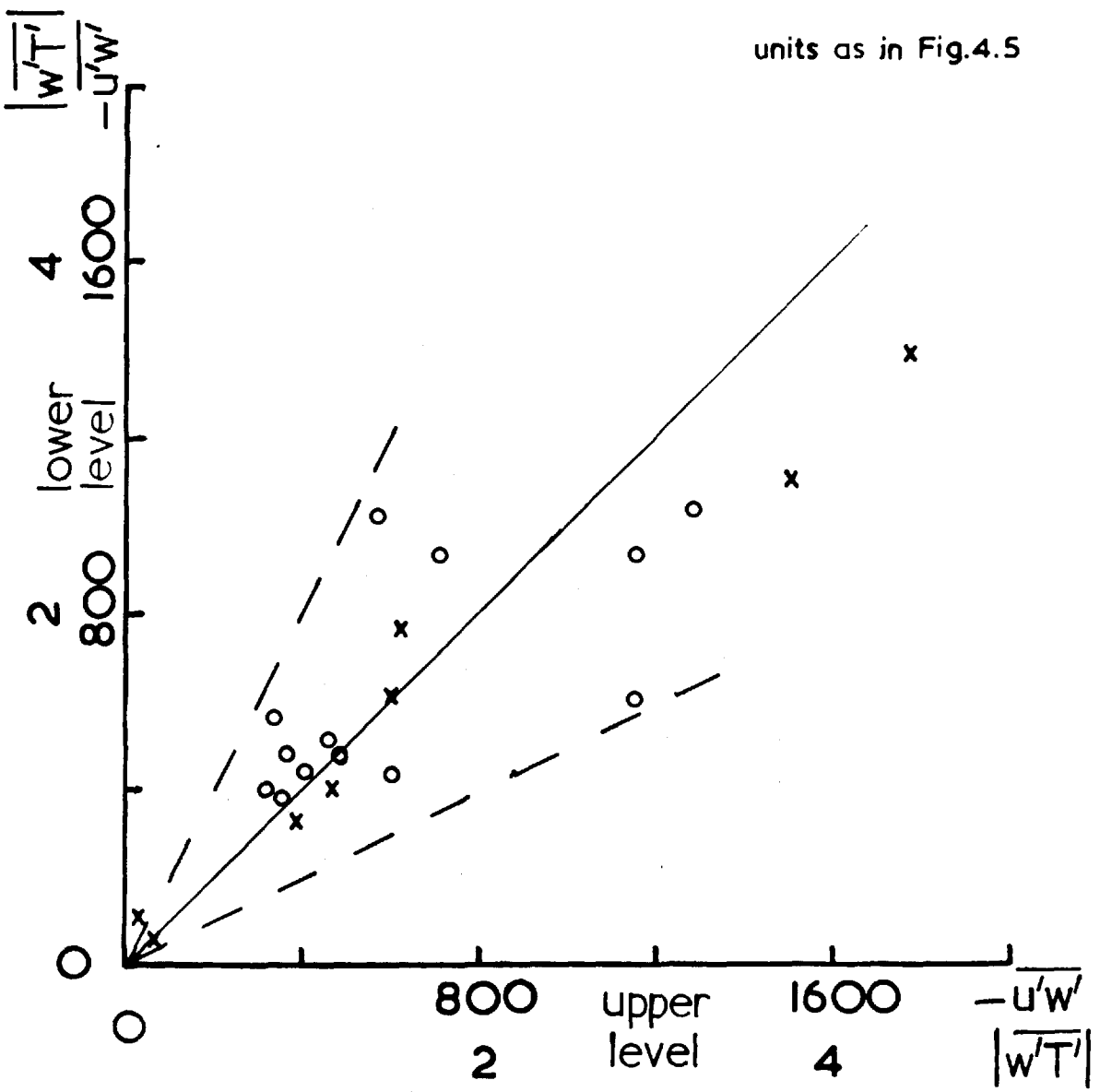

PECKED LINES —see text

$\frac{\partial u}{\partial x} \sim 1\ m\ sec^{-1}\ km^{-1}$

$\frac{\partial T}{\partial x} \sim 1^{\circ}C\ km^{-1}$

FIG. 4.6

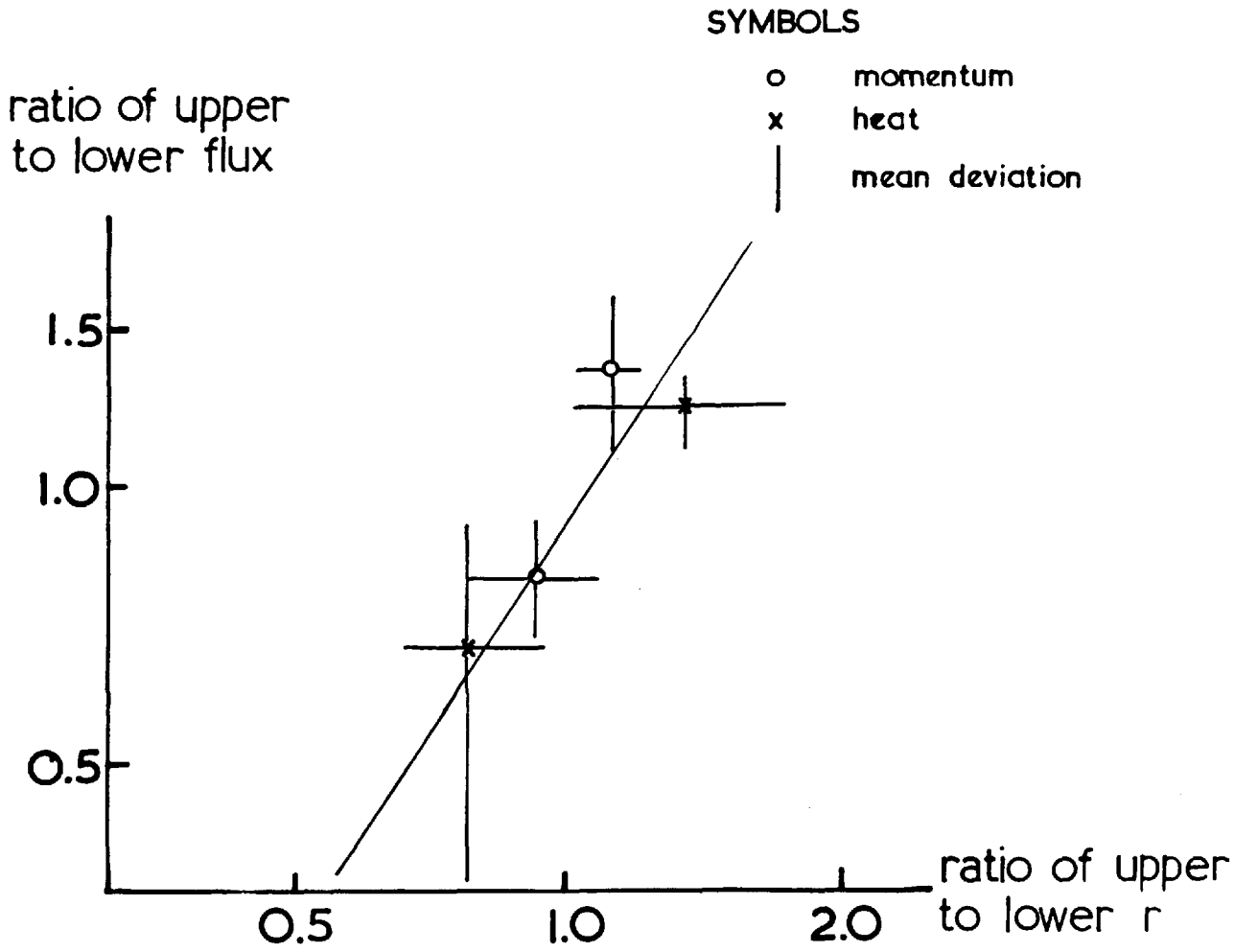

r = correlation coefficient

FIG. 4.7

Momentum Flux Table 4.3

RUN	$-\overline{u'w'}$ cm^2s^{-2}	$\partial U/\partial x$ $m.s^{-1}km^{-1}$	RUN	$-\overline{u'w'}$ cm^2s^{-2}	$\partial U/\partial x$ $m.s^{-1}km^{-1}$
(I) 540 A	403 ± 60	0.14	578 B	510 ± 75	0.09
C	317 ± 50		C	456 ± 65	
549 A	484 ± 70	1.16	(II) 541 A	426 ± 60	0.26
B	373 ± 50		C	598 ± 85	
553 A	376 ± 55	0.24	542 B	602 ± 85	1.07
B	353 ± 50		C	1150 ±165	
555 A	427 ± 60	0.17	543 B	925 ±110	0.37
B	410 ± 60		C	709 ±100	
557 B	477 ± 70	0.03	575 A	568 ± 80	1.89
C	492 ± 70		B	341 ± 50	
565 B	1034 ±150	0.42	577 A	1019 ±145	3.12
C	1285 ±185		B	568 ± 80	
566 B	929 ±130	0.38			
C	1150 ±165				

observed flux changes over Lough Neagh. Thus in Table 4.3 runs 540-578 inclusive provide evidence for a constant-flux layer allowing for a 15% error in the flux at each level, whilst runs 541-577 inclusive exhibit a significant variation with height implying horizontal wind gradients of order 1 $m.s^{-1}km^{-1}$. The separation of the runs into two groups is particularly important regarding § 4.2.4.

The heat fluxes entered in Table 4.4 (previously plotted in Fig.4.6) are assumed to have a mean error of 10% (§ 4.2.2. —the error is smaller than for $\overline{u'w'}$ because there is no "tilt error") and are tabulated together with horizontal temperature gradients required to produce the observed change with height. Such magnitudes are smaller than those observed in practice (M.Z.) and could well account for the flux changes. In Table 4.4 runs 542-578 inclusive imply

Heat Flux

Table 4.4

RUN	$\overline{w'T'}$ cm.s^{-1} °C	$\partial T/\partial x$ °C.km^{-1}	RUN	$\overline{w'T'}$ cm.s^{-1} °C	$\partial T/\partial x$ °C.km^{-1}
542 B	1.00 ± 0.10	0.03	578 B	-0.80 ± 0.08	0.03
C	1.18 ± 0.12		C	-0.95 ± 0.10	
543 B	1.56 ± 0.16	0.01	565 B	3.44 ± 0.34	0.20
C	1.49 ± 0.15		C	4.43 ± 0.44	
557 B	1.90 ± 0.19	0.07	541 A	0.28 ± 0.03	0.03
C	1.53 ± 0.15		C	0.06 ± 0.01	
575 A	-0.15 ± 0.02	zero	566 B	2.76 ± 0.28	0.21
B	-0.15 ± 0.02		C	3.79 ± 0.38	

a constant-flux layer, whilst the three remaining runs, showing a flux variation with height, suggest the presence of horizontal temperature gradients of order 0.2 °C.km^{-1}.

These results are important especially regarding the application of the Similarity Theory. The latter is strictly true only in completely steady-state and horizontally homogeneous turbulence. A rigorous treatment would therefore invalidate the Theory in unsteady or inhomogeneous fields and use of data taken in such circumstances, when subjected to analysis, would manifest itself in a relatively large amount of scatter through application of the Theory. A non-rigorous treatment using such data would require a relatively large amount to determine the statistically steady mean condition of the similarity problem in hand. In the present thesis, because of the limited number of runs available for analysis, the non-rigorous treatment is made using all runs for the analyses described in Chapters 3, 4 and 5 with the expectation of relatively large scatter present in diagrams.

4.2.4. The Momentum Flux

4.2.4.1. Comparison

Estimates of the friction velocity were obtained from a number of wind speed profiles with small curvature making use of equation 3.7, the log-linear profile. Strictly the equation applies in near-neutral conditions when $|\zeta| << 1$; if used for greater values of $|\zeta|$ Taylor (1960) has showed that, in addition to the equation's becoming more inaccurate, α in the equation must be treated as a function of ζ. Thus for negative ζ, $1 + \alpha\zeta$ falls progressively below $\phi_M(\zeta)$ as $|\zeta|$ increases and for positive ζ, $1 + \alpha\zeta$ falls progressively above $\Phi_M(\zeta)$ as ζ increases. The error in u_* when using 3.7 at such greater values of $|\zeta|$ can then be estimated from

$$\frac{u_* \text{ (estimated)}}{u_* \text{ (real)}} \sim \frac{\Phi_M(\zeta)}{1 + \alpha\zeta} \quad .$$

$\alpha(\zeta)$ has been taken from Taylor and $\Phi(\zeta)$ for $\zeta < 0$ from Charnock (1967); in the Ri range used, the likely error in u_* is $\sim 10\%$ increasing to 40% when $|\zeta| = 0.5$. The error in u_*^2 will therefore be $\sim 20\%$ for most values of Ri (relative to 4 m.) experienced. In addition errors in $\bar{u}$ must be taken into account giving u_* calculated from non-linear profiles accurate to 15% approximately and u_*^2 to 30%. This compares to a probable error in $\overline{u'w'}$ of 15%.

Fig.4.8 shows a comparison of u_*^2 and $\overline{u'w'}$ (averaged when measured at two heights) estimates. The lack of correlation evident in the diagram is disturbing, though similar scatter has been found by, for instance, Smith (1966) and Z.K. both oversea.

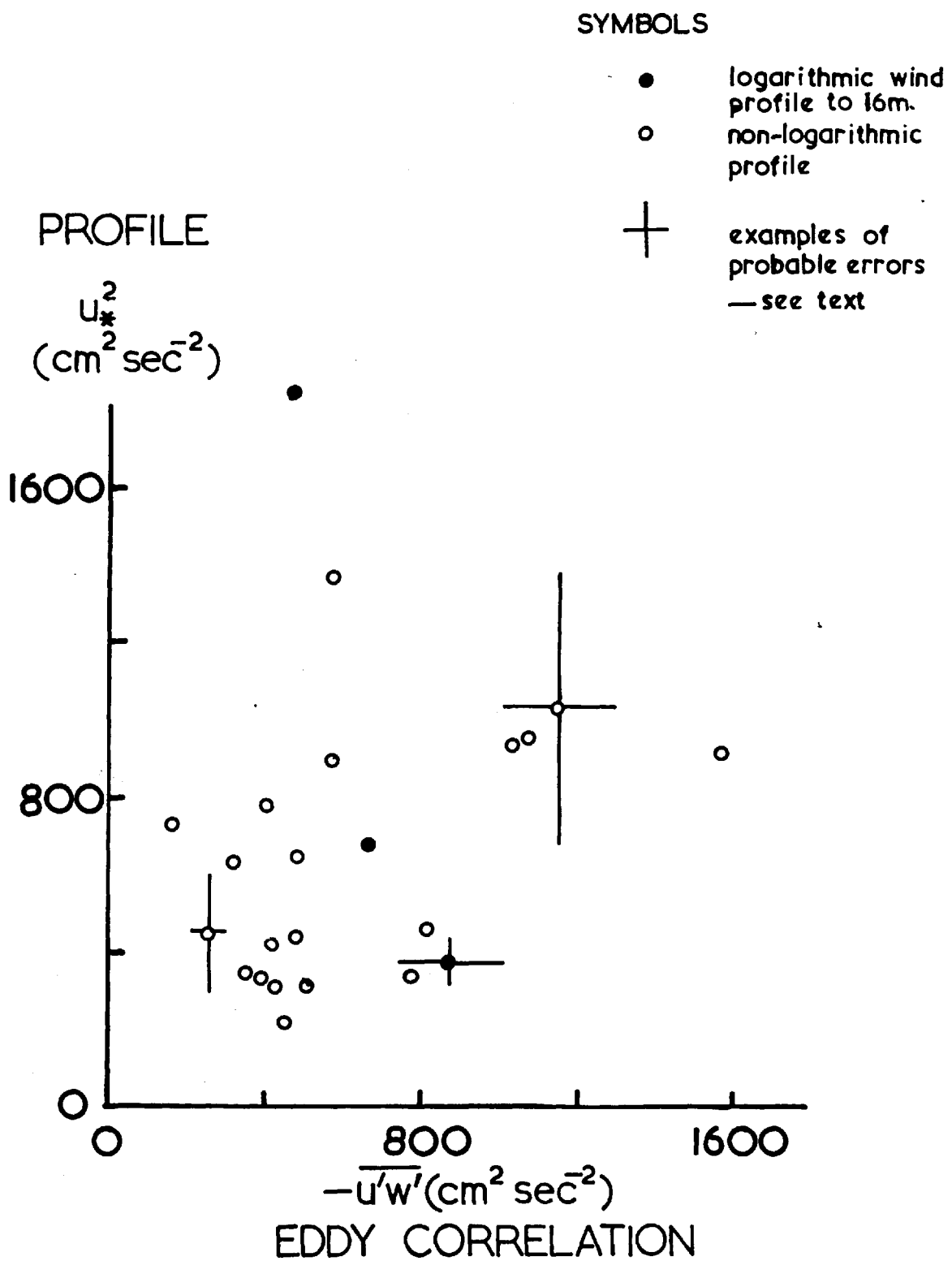
SYMBOLS
logarithmic wind profile to 16m.
non-logarithmic profile
examples of probable errors — see text
PROFILE
u_*^2 ($cm^2 sec^{-2}$)
1600
800
0
0
800
1600
$-\overline{u'w'}$ ($cm^2 sec^{-2}$)
EDDY CORRELATION

FIG. 4.8

Table 4.5

RUN	$-\overline{u'w'}$ cm^2s^{-2}	u_*^2 cm^2s^{-2}	percentage change of $-\overline{u'w'}$ with height	percentage difference between u_*^2 and $-\overline{u'w'}$
I 540	360	336	24	7
549	429	303	26	34
553	365	331	6	10
555	419	416	4	1
557	485	645	3	28
565	1160	1030	22	12
566	1040	940	21	10
578	483	440	11	9
II 541	512	307	34	50
542	876	376	62	80
543	817	455	27	57
575	455	216	50	70
577	784	335	58	80

Table 4.5 contains runs 540-578 inclusive (I) and runs 541-577 inclusive (II) as described in the previous section, with values of $\overline{u'w'}$ (averaged for the layer), u_*^2 from the profiles, the percentage change of $-\overline{u'w'}$ from one level of measurement to the other and the percentage difference between $-\overline{u'w'}$ and u_*^2. The latter two plotted in Fig.4.9 show a high degree of correlation (where there is a large difference between u_*^2 and $-\overline{u'w'}$, the difference exists between u_*^2 and both estimates of $\overline{u'w'}$ at the two levels). Such a result is important because it implies that,

(1) when the momentum flux is approximately constant with height, good agreement of the flux estimates is obtained from two completely independent methods,

(2) when large variations of flux with height are observed due to (inferred) horizontal wind gradients there is no agreement of the two methods,

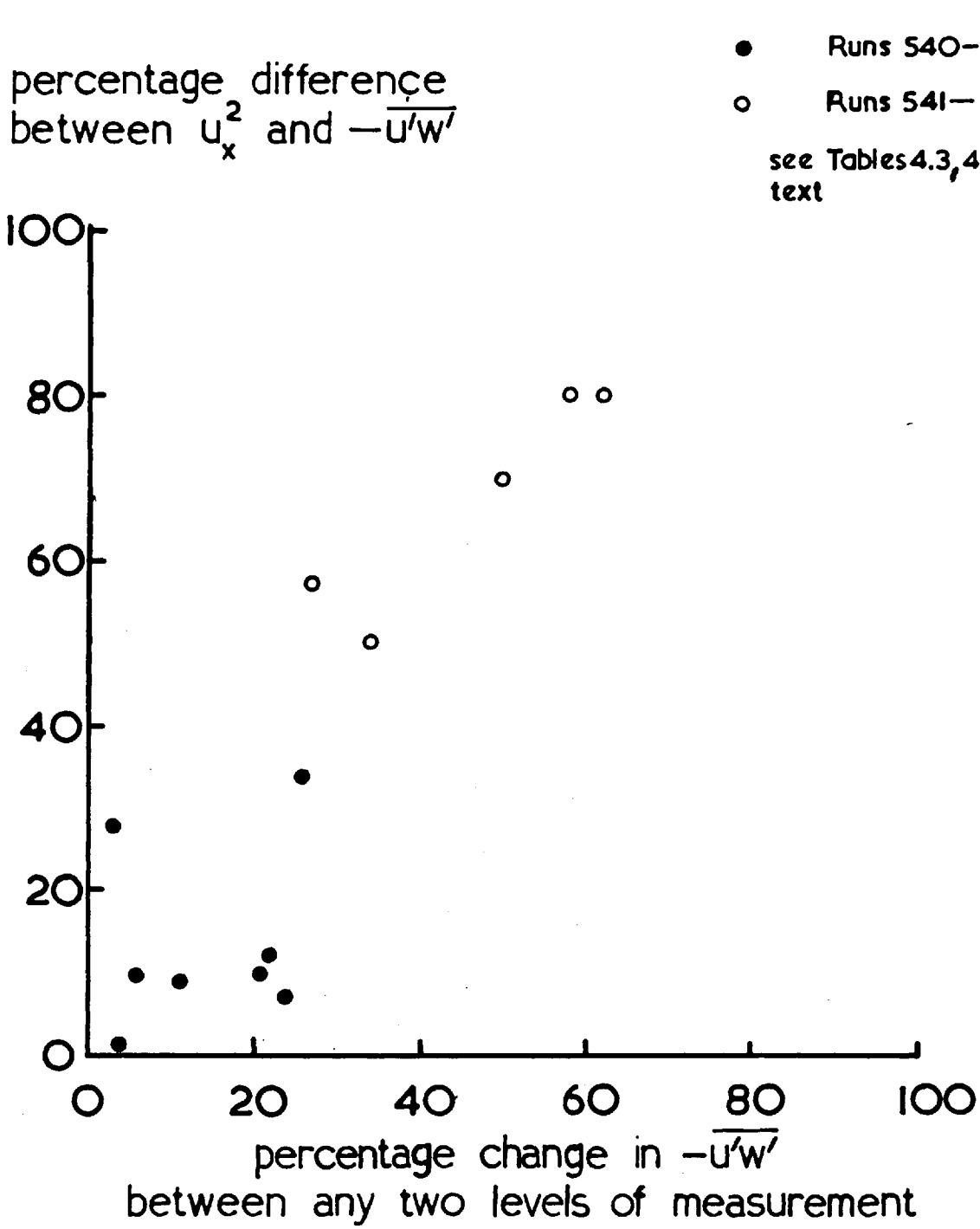
SYMBOLS
Runs 540–578 (I)
Runs 541–577 (II)
see Tables 4.3, 4.5 and text
percentage difference between u_x^2 and $-\overline{u'w'}$
100
80
60
40
20
0
0
20
40
60
80
100
percentage change in $-\overline{u'w'}$ between any two levels of measurement

FIG. 4.9

(3) The large scatter in flux estimates obtained from the two methods and observed by previous workers can be explained by (1) and (2) above which are conclusions drawn from the data in Tables 4.3 and 4.5.

The results of this section emphasise the conclusions drawn in the previous section regarding a verification of the constant-flux hypothesis in a number of runs which have each been found to yield values of u_*^2 from the wind profiles consistent with the values of $-\overline{u'w'}$ at the two levels of measurement.

4.2.4.2. Drag Coefficient

For neutral stratification the drag coefficient $C_D = (u_* / \bar{u}_{10})^2$ would be expected to be dependent upon wind speed and fetch. Data in Roll (p.161) do not provide conclusive evidence for an effect of fetch, and Sheppard (unpublished) could find none from logarithmic wind profiles obtained at Lough Neagh. We shall therefore not distinguish fetch in the following.

We show in Fig.4.10 values of C_D obtained from the covariance $\overline{u'w'}$ and $\bar{u}_{10}$ plotted against $\bar{u}_{10}$ for 4 Ri ranges, the number of near-neutral cases being too few to consider this class separately. Also shown is the probable error in C_D, this being attributed to the 15% error in $\overline{u'w'}$ deduced in § 4.2.3. The effect of thermal stratification upon the magnitude of C_D appears to be considerable, but the near-neutral points agree moderately well with the Sheppard relation. Unfortunately there are too few points and the wind speed range too narrow for a conclusion to be drawn regarding $C_D(\bar{u})$. Measurements of C_D using logarithmic wind profiles reported by Roll

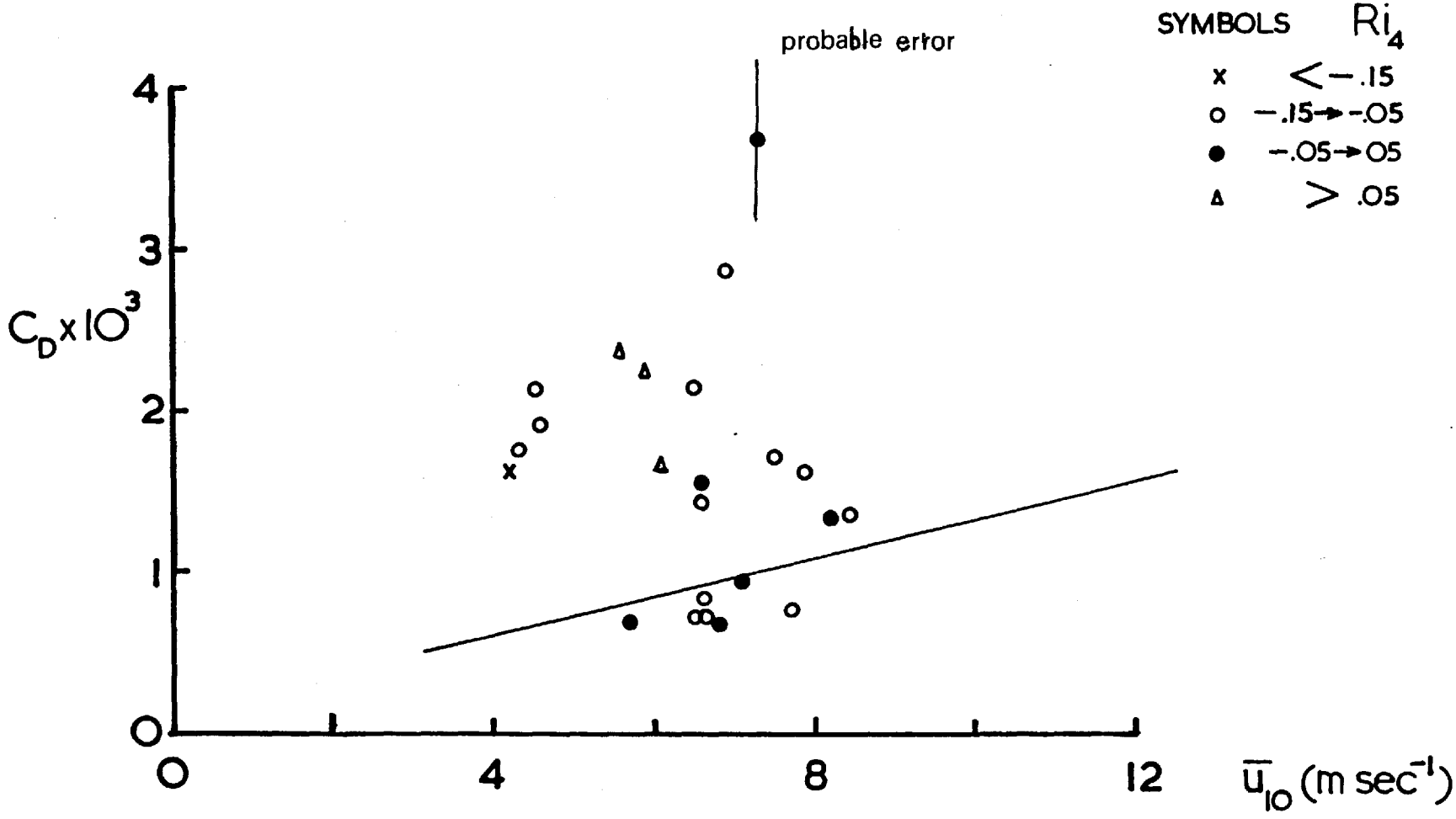

Straight line relation—— $C_D = (.12 + .12\,\bar{u}_{10}) \times 10^{-3}$

FIG. 4.10

show an increase from, on average, 1.1 to 2×10^{-3} when $\bar{u}_{10}$ increases from 5 to 20 $m.s^{-1}$ but recent measurements using the eddy correlation —see Table 4.6 — provide hardly any evidence on this question, in part perhaps because of the restricted wind speed range over which it has been possible to measure $\overline{u'w'}$ (at Lough Neagh not possible for $\bar{u} > 11$ $m.s^{-1}$ approximately because of the mechanical nature of the anemometer and vane).

Table 4.6

Author	$C_D \times 10^3$	$\bar{u}_{10}$ range ($m.s^{-1}$)
Smith (1966)	0.85	2.4 - 12.3
Weiler and Burling (1968)	1.15	1.0 - 10.0
Hasse et al. (1966)	0.70	3.0 - 8.0
Z.K.	$0.72 + 0.12\ \bar{u}_{10}$	3.0 - 9.0

In conclusion, values of C_D (near-neutral) obtained by the eddy correlation method at Lough Neagh are not inconsistent with those given by the relation $C_D = (0.12 + 0.12\ \bar{u}_{10}) \times 10^{-3}$ with $\bar{u}_{10}$ in $m.s^{-1}$ found by Sheppard using the wind profile method (see Fig.4.10 for $\bar{u}_{10} \sim 7$ $m.s^{-1}$ and $C_D \sim 1.0 \times 10^{-3}$).

4.2.5. Vertical Heat Flux

In § 4.2.2., the probable error in $\overline{w'T'}$ was estimated at 10%, and the flux was found to be approximately constant with height in the conditions experienced at Lough Neagh (§ 4.2.3.).

In this section it is proposed to relate the turbulent heat flux $H = \rho C_p \overline{w'T'}$ to relatively easily measured mean quantities which are characteristic of the flow oversea.

First, consider the gradient equation 3.1 for u and θ ; integration yields,

$$\frac{K\bar{u}}{u_*} = \int_{z_o}^{z} \Phi_M(\zeta)\, d(\ln z) \qquad 4.4$$

$$\frac{K(\theta - \theta_o)}{\theta_*} = \int_{z_T}^{z} \Phi_H(\zeta)\, d(\ln z) \qquad 4.5$$

Combining and re-arranging,

$$u_*\theta_* = -\overline{w'T'} = C_H \bar{u}\, \Delta\theta \qquad 4.6$$

where $C_H = K^2 / A_M A_H$, A_M and A_H being the integrals on the right hand side of 4.4, 4.5 respectively; and $\Delta\theta = \theta - \theta_o$. Here C_H is a heat transfer coefficient, analogous to C_D for momentum, and when $\zeta \longrightarrow 0$, $C_H \longrightarrow K^2 / \ln z_o \ln z_T \simeq C_D$ for $z_T \simeq z_o$.

More generally, 4.6 may be written,

$$\overline{w'T'} = -\bar{u}\, \Delta\theta\, f(z_o, z_T, \zeta) \qquad 4.7$$

and where ζ determines uniquely the functions Φ_M , Φ_H . Since f must be non-dimensional it can be written in terms of two variables only, viz. z_o/z_T , ζ , though the form of C_H in neutral conditions suggests modifying this to three variables, viz. z/z_o , z/z_T , ζ . To determine f it is required to know amongst other things ζ which is determined by the flux which we are trying to find. Further since f depends upon L it will depend upon $\overline{w'T'}$ and hence $\bar{u}\,\Delta\theta$ as implied by 4.6. Appeal to observation is then required to determine a

relation between $\overline{w'T'}$ and $u\Delta\theta$, the independent variable. Such a relation is shown in Fig.4.11 (simultaneous measurements of $\overline{w'T'}$ at two levels are included as two separate points on the diagram, for the same value of $\bar{u}\Delta\theta$). The experimental points are well described by the empirical relation,

$$-\overline{w'T'} = \bar{u}\Delta\theta\,(1.1 - \frac{\bar{u}\Delta\theta}{5000}) \times 10^{-3} \qquad 4.8$$

for $\overline{w'T'}$ in units of cm.sec^{-1} °C. Thus, $H = 1.3\ \overline{w'T'}$ m w cm^{-2} or $H = 18.6\ \overline{w'T'}$ m cal.cm^{-2}min^{-1}. The constant 1.1 is determined by the slope of the curve (parabola) when $\overline{w'T'} = 0$ and the dimensional constant 5000 by the curvature. Comparison of equations 4.6 - 4.8 inclusive implies,

$$f(z/z_o,\ z/z_T, \zeta) = (1.1 - \frac{\bar{u}\Delta\theta}{5000}) \times 10^{-3} = C_H \qquad 4.9$$

Firstly when $\zeta = 0$ it is expected that $\bar{u}\Delta\theta = 0$ (or very close to zero). Hence, $C_H = f(z/z_o,\ z/z_T) = 1.1 \times 10^{-3}$, consistent with values of the drag coefficient C_D in neutral conditions found earlier (see § 3.3.2.2. and § 4.2.4.2.). This implies that $f(z/z_o,\ z/z_T) = k^2(\ln z/z_o \ln z/z_T)^{-1}$. Secondly the empirical term $\bar{u}\Delta\theta \times 10^{-3}/5000$ relates to the quantity $f(\zeta)$, and one is tempted to write 4.9,

$$C_H = f_1(z/z_o,\ z/z_T) + f_2(\zeta) \qquad 4.9\,a$$

with f_1 equal to a constant at fixed z, and f_2 is directly proportional to $\bar{u}\Delta\theta$. Unfortunately there are some unacceptable

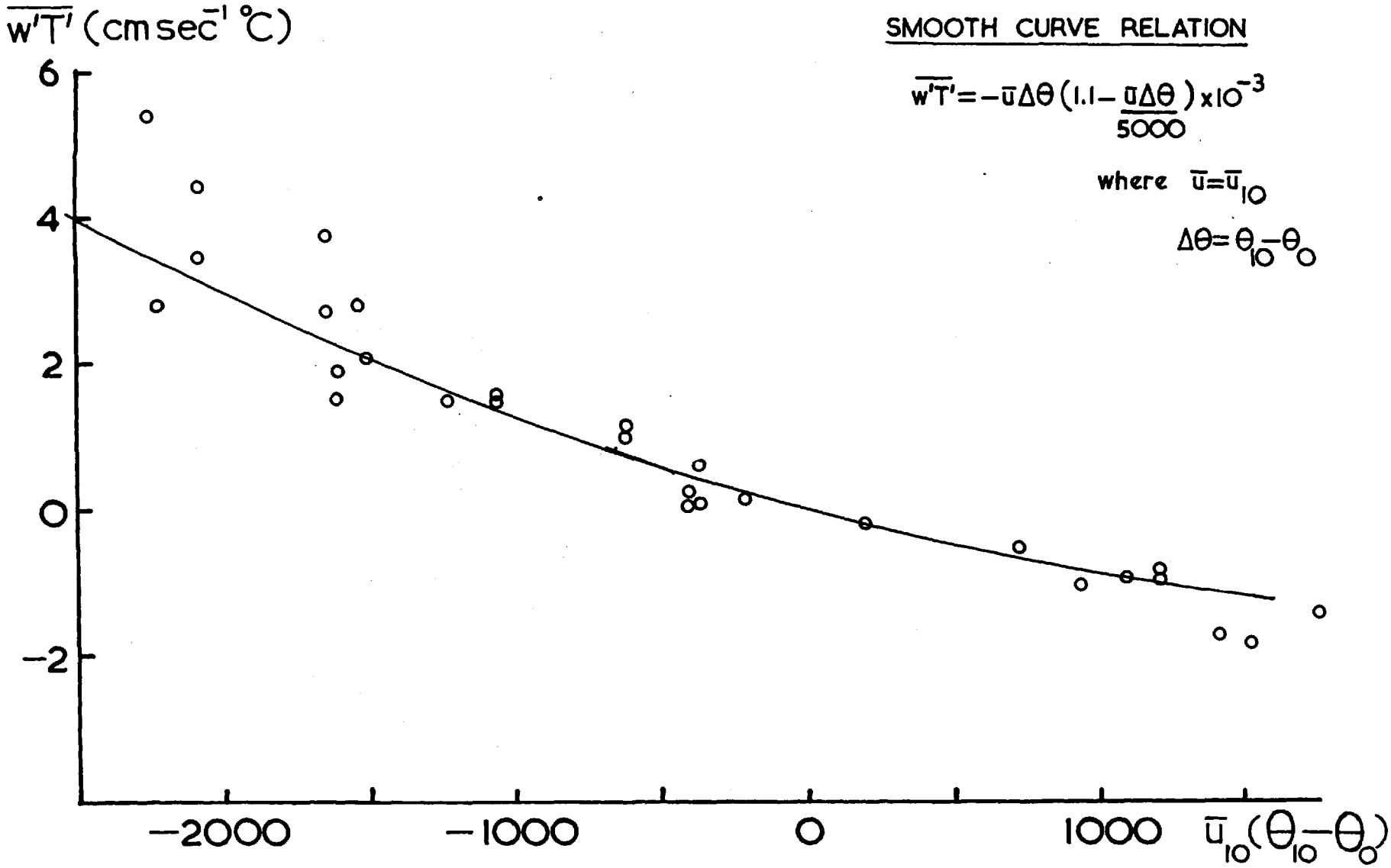
$\overline{w'T'}$ (cm sec^{-1} °C)
SMOOTH CURVE RELATION
$\overline{w'T'} = -\bar{u}\Delta\theta\left(1.1 - \frac{\bar{u}\Delta\theta}{5000}\right)\times 10^{-3}$
where $\bar{u}=\bar{u}_{10}$
$\Delta\theta=\theta_{10}-\theta_0$
6
4
2
0
−2
−2000
−1000
0
1000
$\bar{u}_{10}(\theta_{10}-\theta_0)$
(cm sec^{-1} °C)

FIG. 4.11

consequences of the empirical form of C_H in 4.9, 4.9 a above.

Firstly, $C_H = 0$ when $\bar{u}\Delta\theta/5000 = 1.1$ implying zero heat flux when $\Delta\theta = 5500/\bar{u}$ ($\bar{u} = 5.5$ m.s^{-1}, $\Delta\theta = 10°C$ and $Ri = 3.3\ \Delta\theta\ \Delta z / (\Delta u)^2 \simeq 0.11$), a critical $\Delta\theta$ increasing with a decrease in $\bar{u}$ whereas Ri(critical) implies $\Delta\theta \propto \bar{u}^2$ so the form cannot be physically correct, at least for positive $\Delta\theta$. Secondly, again for positive $\Delta\theta$, at a fixed value of $\Delta\theta$, C_H decreases with increase of $\bar{u}$, yet if C_H behaves at all like C_D it should increase with $\bar{u}$ (increasing roughness) and one would also expect it to increase because of the decrease of Ri with increase of $\bar{u}$. Thirdly, C_H is independent of wind speed in neutral conditions whereas C_D increases linearly with wind speed.

On the other hand, for unstable conditions ($\Delta\theta$ negative) the relation correctly predicts an increase in C_H with $\bar{u}$ at fixed $\Delta\theta$ and an increase with $\Delta\theta$ at fixed $\bar{u}$ due to the effect of buoyancy (and correspondingly more negative Ri).

Thus, whilst 4.8 is not physically correct in neutral and stable conditions, it is so for unstable conditions, yet being empirical is valid within the observed range of $\bar{u}\Delta\theta$. It is expected to be of practical importance in unstable conditions.

The empirical formula (4.8) can be compared with that suggested by Sheppard (1958) which emphasises the importance of molecular transfer in the interfacial layer where most of $\Delta\theta$ occurs. $C_H\bar{u}$ in 4.8 is replaced by

$$\kappa u_* \left[\ln\left(\frac{\kappa u_* z}{\gamma}\right)\right]^{-1}$$

where γ is the thermal diffusivity, but the formula gives $\overline{w'T'}$ only

to within 50 per cent using data from Appendix 1.

Finally relation 4.9 for C_H can be used for the estimation of evaporation if it is assumed $K_H = K_V$. The analogous equation to 4.6 is then,

$$\overline{w'q'} = -C_H \bar{u} \Delta q \qquad 4.6a$$

and in analogy to 4.8,

$$\frac{E}{\rho} = \overline{w'q'} = -\bar{u} \Delta q \left(1.1 - \frac{\bar{u} \Delta\theta}{5000}\right) \times 10^{-3} \qquad 4.8a$$

Thus H and E are readily available when the three quantities $\bar{u}_{10}$, $\theta_{10} - \theta_o$, $q_{10} - q_o$ are known.

Equation 4.6 makes use of the definition for θ_* given in § 3.1.2. viz. $\theta_* = -\overline{w'T'} u_*^{-1}$. With $\overline{w'T'} = -u_*\theta_*$ values of u_* and θ_* obtainable from profile measurements can be used to estimate the heat flux.

Values of u_* used in § 4.2.4.1. and θ_*, both obtained using equation 3.7 the log-linear profile, are available (values in Appendix 1) for comparison with the eddy correlation estimates of heat flux for a number of runs whose u and θ profiles have sufficiently small curvature to warrant use of equation 3.7.

The errors arising from application of 3.7 outside the stability limits specified in § 4.2.4. are applicable to θ_* so that the likely error in $u_*\theta_*$ will be ~30 per cent. Values of $\overline{w'T'}$ (averaged when two estimates are available per 10 minutes) vs $-u_*\theta_*$

are shown in Fig.4.11a. The high correlation between the two quantities is similar to that in Fig.4.11 with $\overline{w'T'}$ a function of $\overline{u}_{10}(\theta_{1C} - \theta_o)$ and reflects the fact that use of the Lough Neagh wind and temperature profiles can yield accurate estimates of the heat flux. It is further evident that the log-linear formula has useful application in the range of stabilities encountered at Lough Neagh.

4.2.6. Horizontal Heat Flux

Turbulent transfer of heat is effected in the horizontal as well as in the vertical and is given by $\rho C_p \overline{u'T'}$. The correlation between u' and T' can be deduced from knowledge of the height variation of u and θ in the surface layer, viz. consider characteristic profiles of u, θ in lapse and inversion conditions as depicted in Fig.4.12. The effect of vertical motions due to turbulence is to produce CHARACTERISTIC correlations between u' and w' (negative), between w', T' (positive in lapse, negative in inversion) and between u', T' (negative in lapse, positive in inversion). Coexistent with such correlations are skew frequency (probability) distributions, in particular of w' and T' (see § 5.5.5.) and finite correlation coefficients.

Regarding the heat fluxes, Fig.4.13 shows $\overline{u'T'}$ vs $\overline{w'T'}$ and, in general, the signs of the fluxes are as expected. The

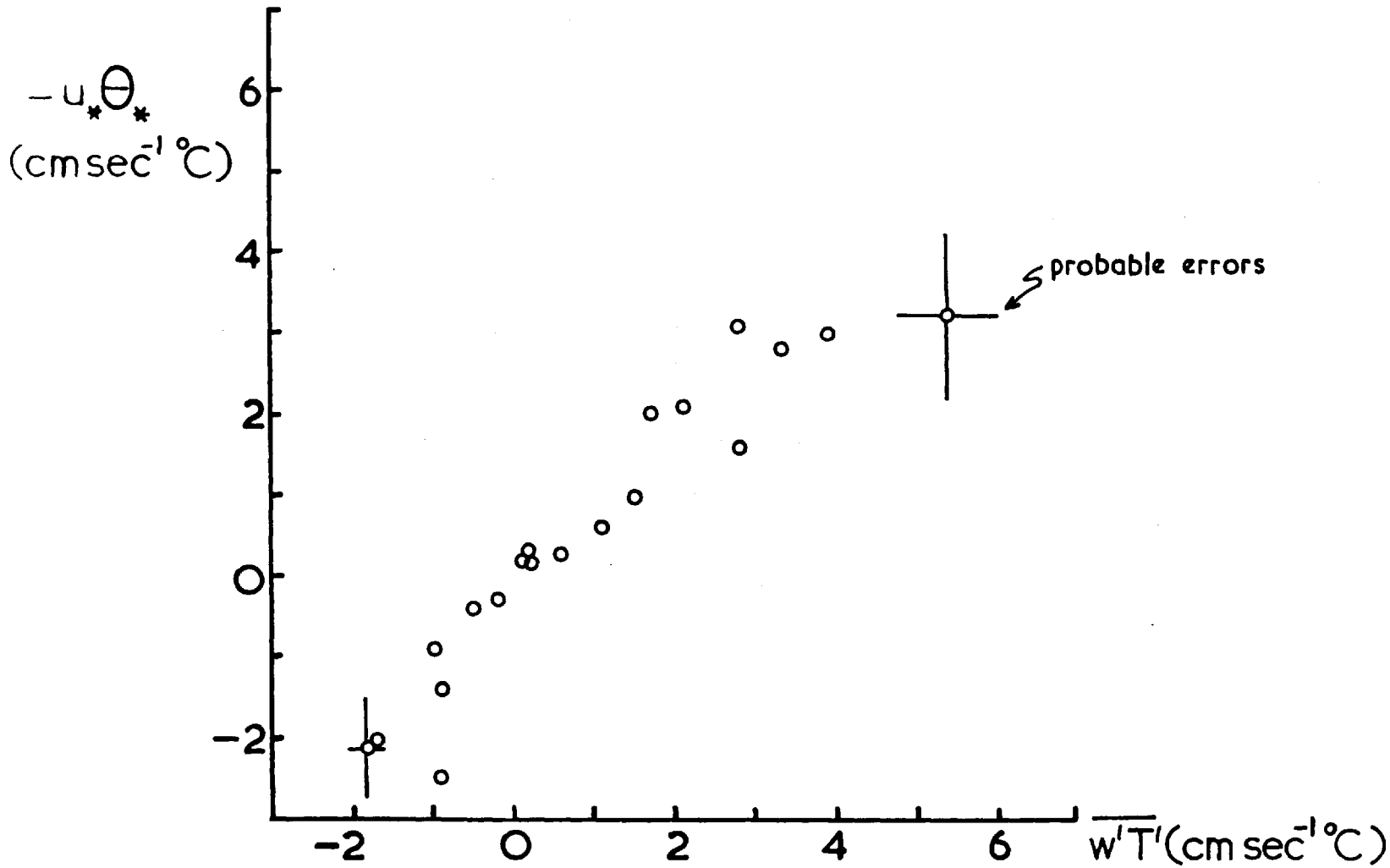
$-u_*\theta_*$
(cm sec^{-1} °C)
6
4
2
0
−2
probable errors
−2
0
2
4
6
$\overline{w'T'}$ (cm sec^{-1} °C)

FIG. 4.11a

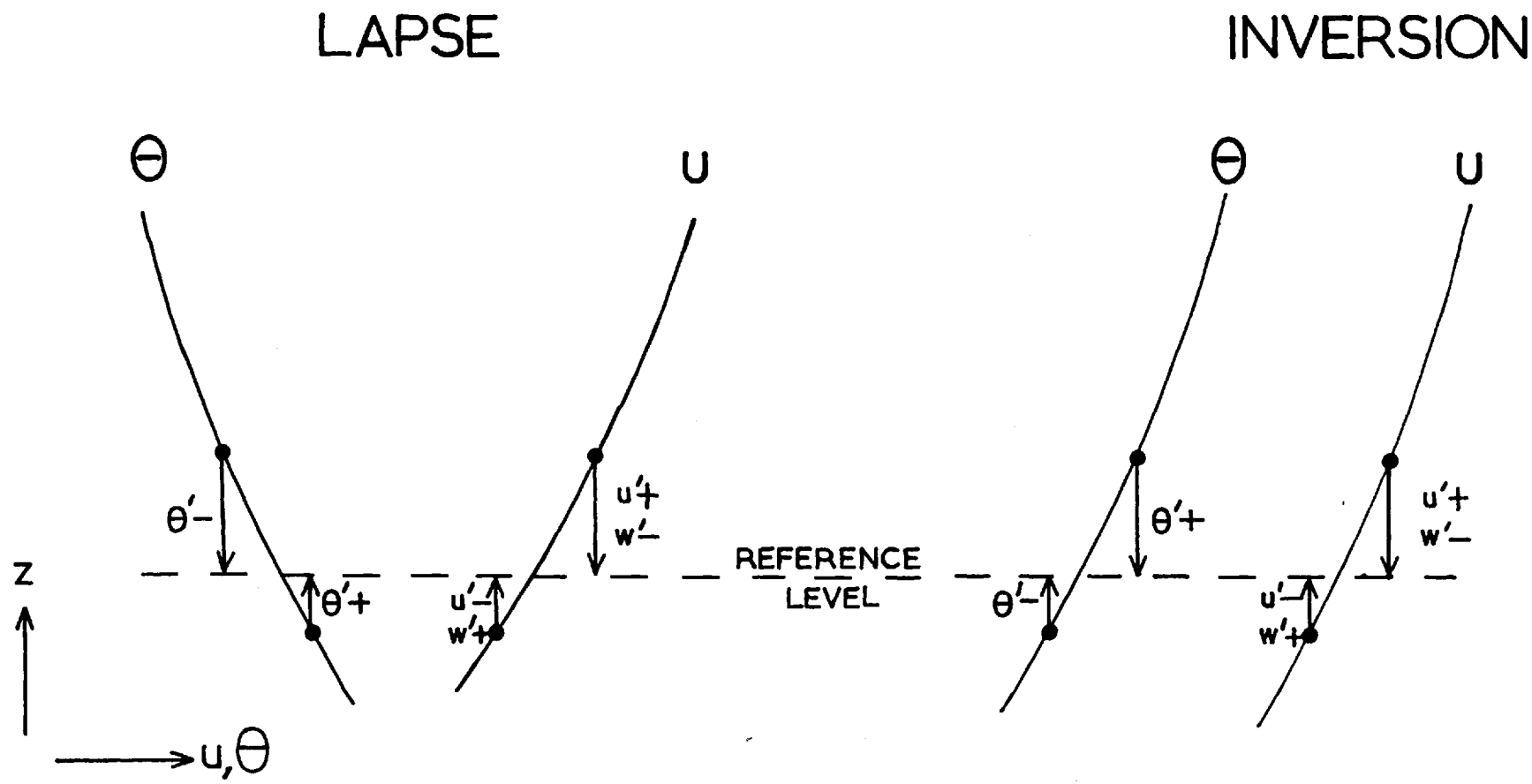

Schematic Representation of Characteristic Correlations

FIG. 4.12

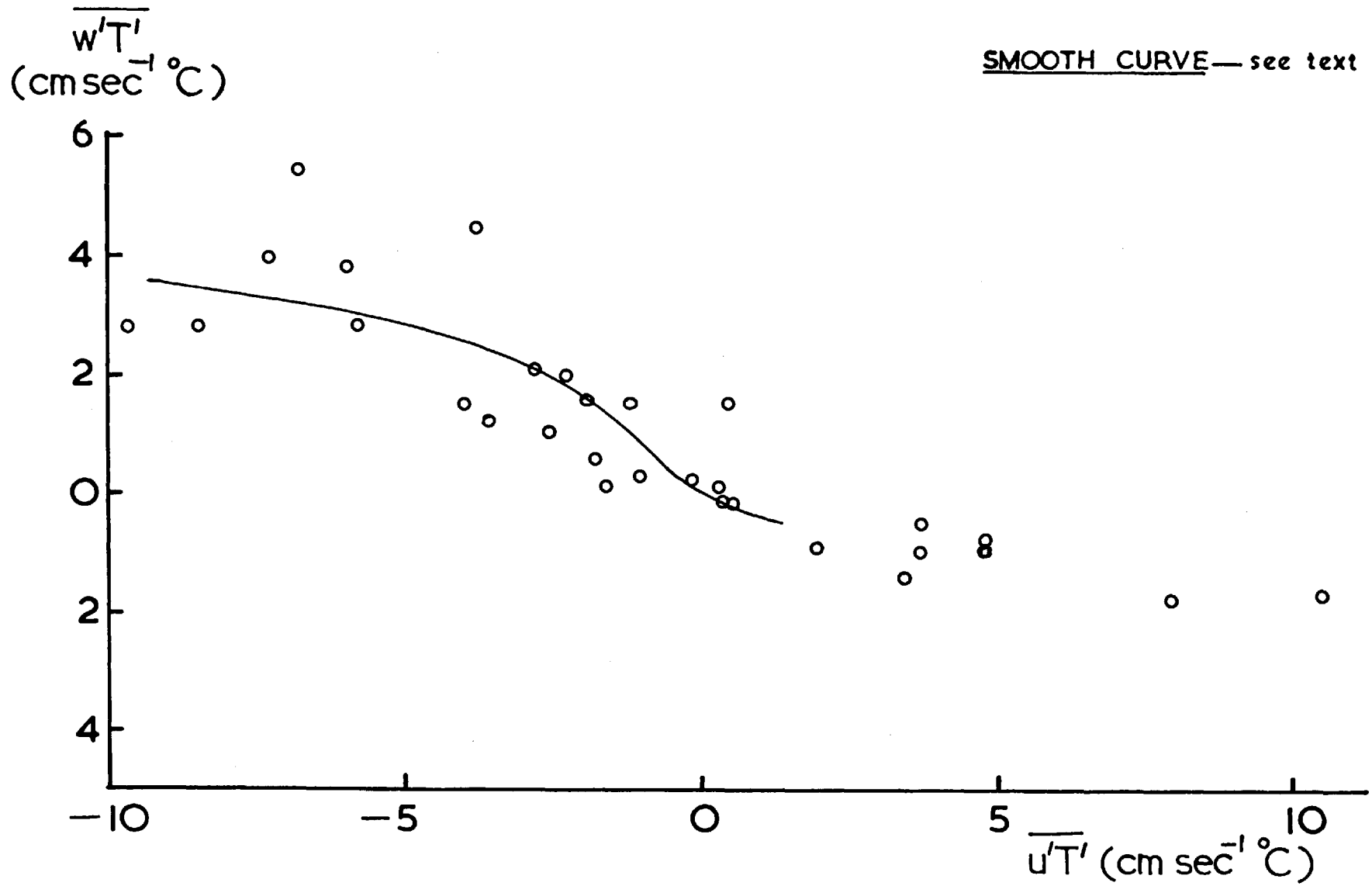
$\overline{w'T'}$ (cm sec^{-1} °C)
SMOOTH CURVE — see text
6
4
2
0
2
4
−10
−5
0
5
10
$\overline{u'T'}$ (cm sec^{-1} °C)

FIG. 4.13

Lough Neagh measurements confirm those made overland by Zubkovskii and Zwang (1966) presented in the diagram as a continuous curve taken from their paper. The results show that $\overline{u'T'}$ is several times greater than $\overline{w'T'}$ in absolute value.

Further the Similarity Theory implies that the dimensionless ratio $\overline{u'T'}/\overline{w'T'}$ should be a function of ζ or Ri. Fig.4.14 shows Lough Neagh results averaged for several Ri ranges superimposed upon which is the Russian curve produced from a much greater amount of data. The agreement between the two is very good suggesting a Universal relation.

4.3 Turbulent Transfer of Heat and Momentum

4.3.1. Eddy Transfer Coefficients

At temperatures $\sim 10°C$, the values of the kinematic viscosity and thermal diffusivity are 0.15 and 0.20 $cm^2 s^{-1}$ respectively. In contrast (see data table in Appendix 1) the eddy viscosity and conductivity —see equation 3.2 — are several orders of magnitude higher varying over a wide range (625 to 74,500 for the Lough Neagh measurements) according to the value of z, Ri and $\bar{u}$. Further, values of K reported by Swinbank (1955) overland are, for equal z, $\bar{u}$, Ri, almost a factor of ten greater than these indicating that, in general, values of K overland are significantly greater than those oversea. This is implied by the equation $K = ku_* z$ for neutral conditions, since for a given u, u_* is considerably greater overland than oversea.

Following the discussion in § 3.4. the ratio K_H/K_M is of much interest. Fig.4.15 shows K_H/K_M vs Ri with the ordinate

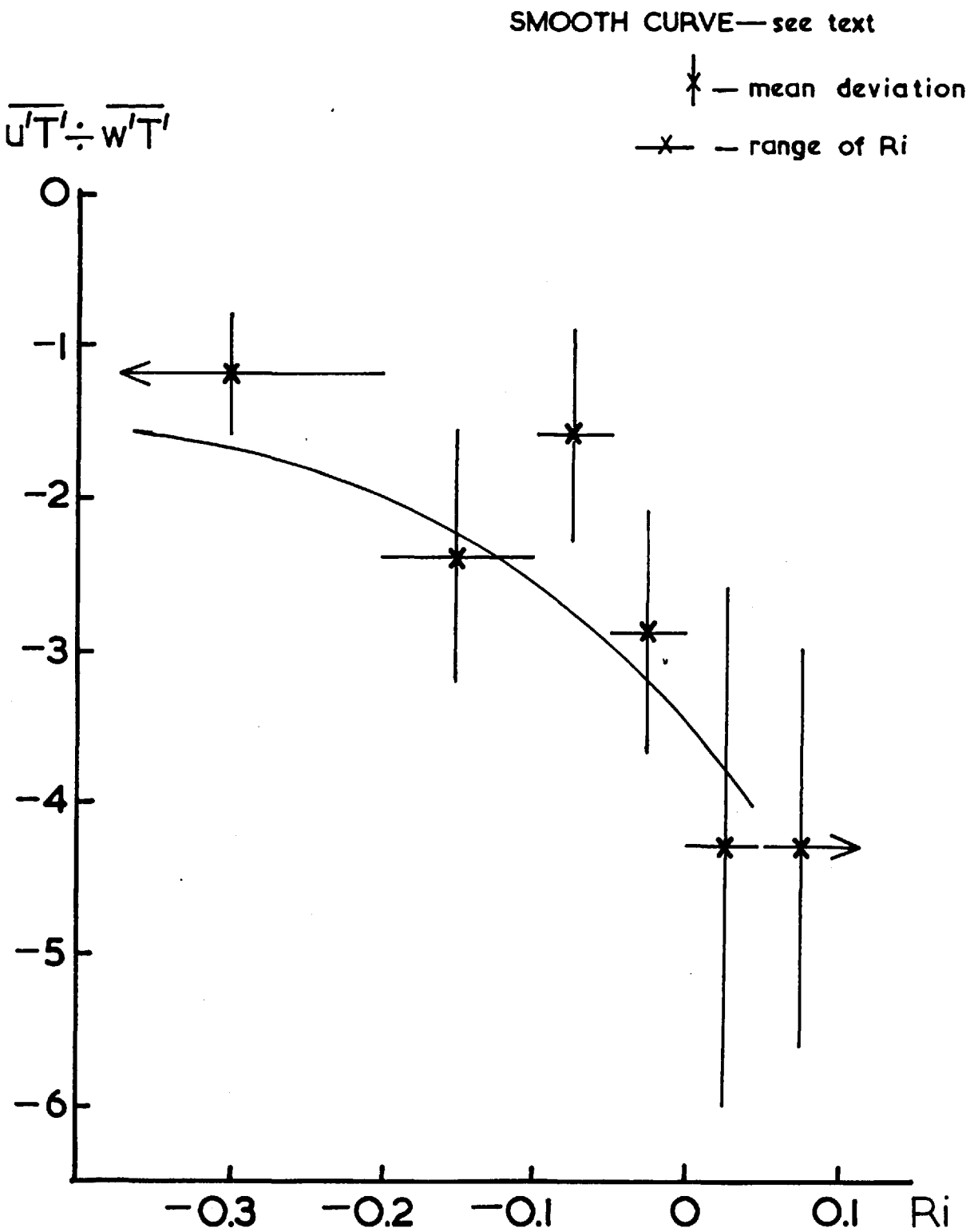
SMOOTH CURVE — see text
— mean deviation
— range of Ri
$\overline{u'T'} \div \overline{w'T'}$
0
-1
-2
-3
-4
-5
-6
-0.3
-0.2
-0.1
0
0.1
Ri

FIG. 4.14

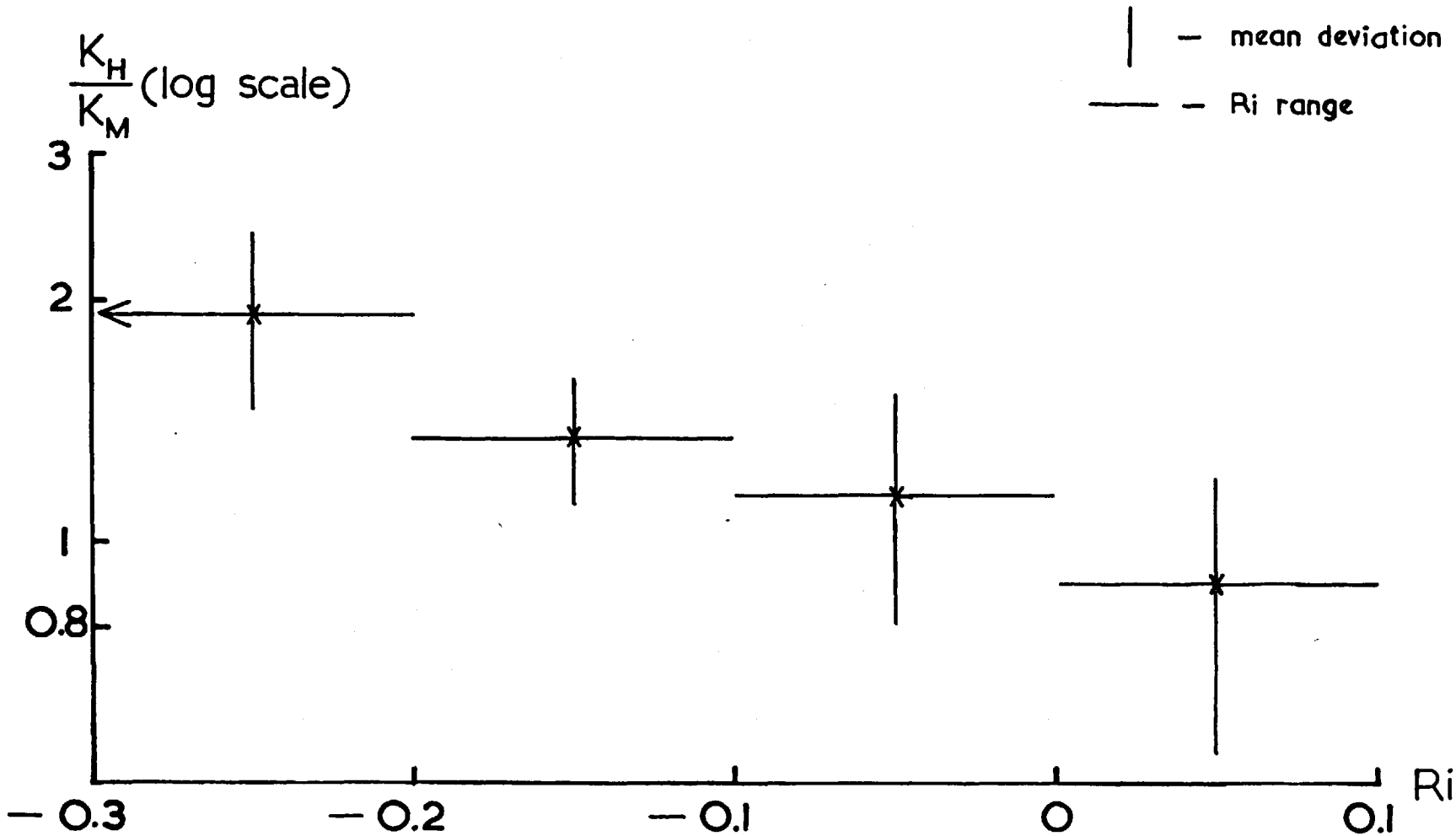
mean deviation
Ri range
$\frac{K_H}{K_M}$ (log scale)
3
2
1
0.8
Ri
— 0.3
— 0.2
— 0.1
0
0.1

FIG. 4.15

averaged for several Ri ranges. The curve clearly shows that K_H/K_M increases and decreases from unity as one goes into unstable and stable conditions respectively. The results are the first of their kind oversea, confirming the results of Western workers overland where, Charnock (1967) for instance, analysing Australian data for lapse conditions found an initially rapid increase of K_H/K_M from 1 to 2 as ζ decreased from 0 to -.3 the increase being maintained until K_H/K_M tends to 3.5 when ζ approaches -4. On the other hand Russian workers have found no significant variation of K_H/K_M with Ri; M.Z., for instance, found $K_H/K_M \simeq 1$ for $-0.8 < Ri < 0.1$.

Fig.4.15 agrees qualitatively with Fig.3.13 which shows a similar variation of S_θ/S_u with Ri. Quantitatively Fig.4.15 shows a much greater variation of K_H/K_M than is implied in the curve in Fig.3.13 and as is suggested in Fig.3.12 when comparing the Lough Neagh variation of $S_x(Ri)$ with the Australian curve. This may be a statistical effect in that the variation of $S_x(Ri)$ for $Ri < -0.3$ is determined by relatively few points and the variation of $S_\theta/S_u(Ri)$ may well be greater. It is obvious though that the profile analysis is severely restricted regarding a quantitative knowledge of $K_H/K_M(Ri)$.

4.3.2. Transfer and Correlation Coefficients

The fact that K_H and K_M are unequal in non-neutral stratification implies that turbulence distinguishes between these transfers. It is possible that such an effect is associated with unequal correlations which are manifestations of the anisotropic turbulence and its transfer properties. This idea was tested by

choosing 4 ranges of K_H/K_M (0 to 0.5, 0.5 to 1, 1 to 1.5 and greater than 1.5) and evaluating averages for K_H/K_M and r_{wT}/r_{uw} for each range. Fig.4.16 shows K_H/K_M vs r_{wT}/r_{uw} and indicates that when $K_H > K_M$, $r_{wT} > r_{uw}$ and vice versa. The straight line has been drawn to pass through the point where $K_H = K_M$ and $r_{wT} = r_{uw}$.

Now,

$$\frac{K_H}{K_M} = \left(\frac{\overline{w'T'}}{-\overline{u'w'}}\right) \cdot \left(\frac{\partial u/\partial z}{\partial \theta/\partial z}\right)$$

and,

$$\frac{r_{wT}}{r_{uw}} = \left(\frac{\overline{w'T'}}{-\overline{u'w'}}\right) \cdot \left(\frac{\sigma_u}{\sigma_T}\right)$$

It is obvious that if K_H/K_M is to be directly correlated to r_{wT}/r_{uw}, σ_u/σ_T must be correlated to $\partial u/\partial z \Big/ \partial \theta/\partial z$. Further since $K_H/K_M \simeq r_{wT}/r_{uw}$ then it is to be expected that $\sigma_u/\sigma_T \simeq \frac{\partial u/\partial z}{\partial \theta/\partial z}$. Fig.4.17 shows σ_T/σ_u vs $\left|\frac{\partial \theta/\partial z}{\partial u/\partial z}\right|$ for inversion and lapses, the correlation coefficient lying between 0.7 and 0.8 for the points shown. It therefore seems that the relative size of the K's is related to that of the r's. Since § 4.3.1. showed that $K_H > K_M$ (lapse), $K_H < K_M$ (inversion) the results of this section indicate

(i) In lapses, the effect of buoyancy is to produce a stronger correlation between w' and T' than for w' and u',

(ii) For inversions, negative buoyancy, hindering the transfer of heat relative to momentum, produces a relatively stronger correlation between u' and w'.

The effect of buoyancy upon the relative sizes of r_{wT} and r_{uw} is implied in the results published by Swinbank (1955). M.Z. however found $r_{wT} > r_{uw}$ for lapse conditions though K_H was equal to K_M.

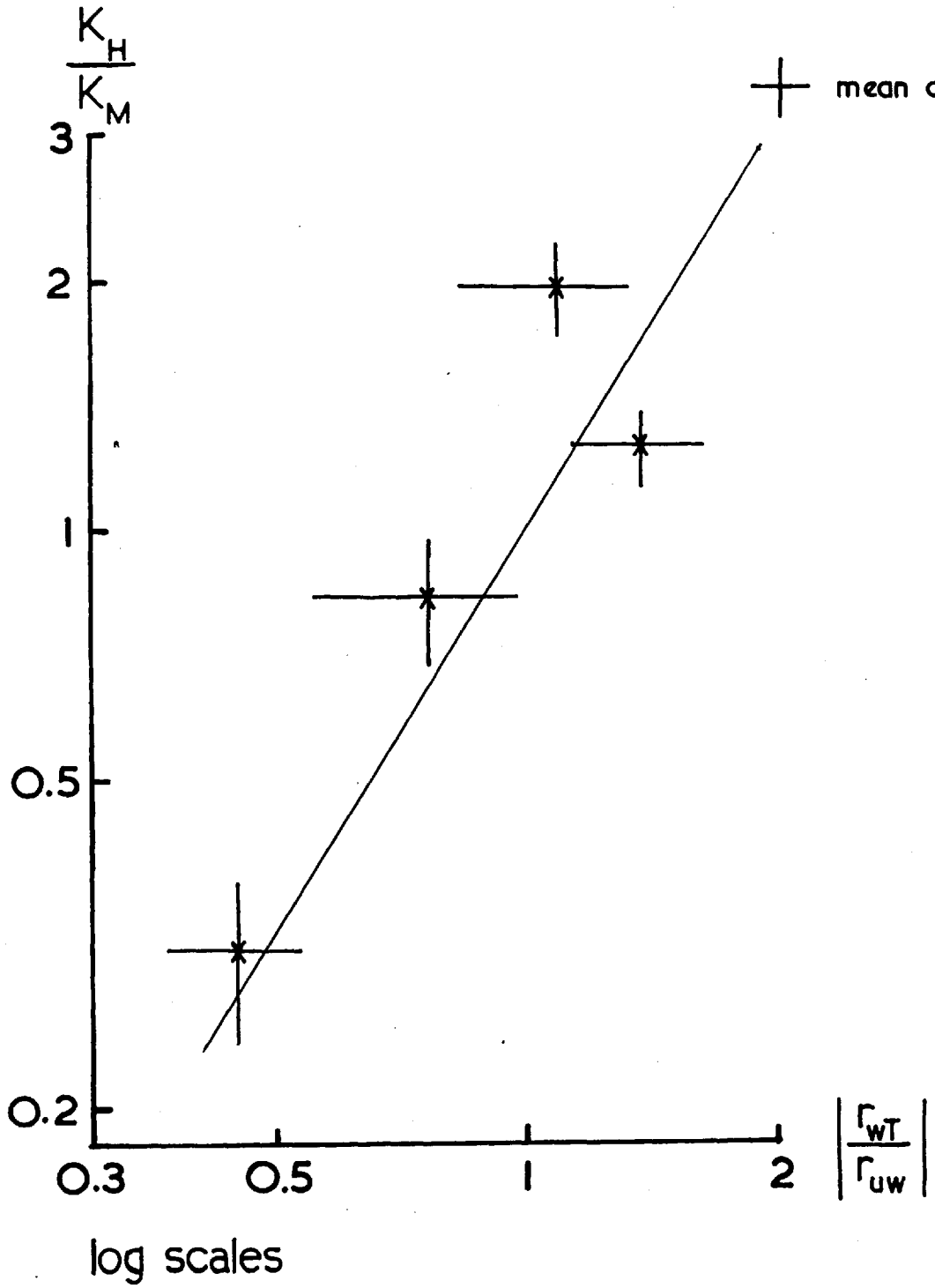
$\frac{K_H}{K_M}$
mean deviation
3
2
1
0.5
0.2
0.3
0.5
1
2
$\left|\frac{r_{wT}}{r_{uw}}\right|$
log scales

FIG. 4.16

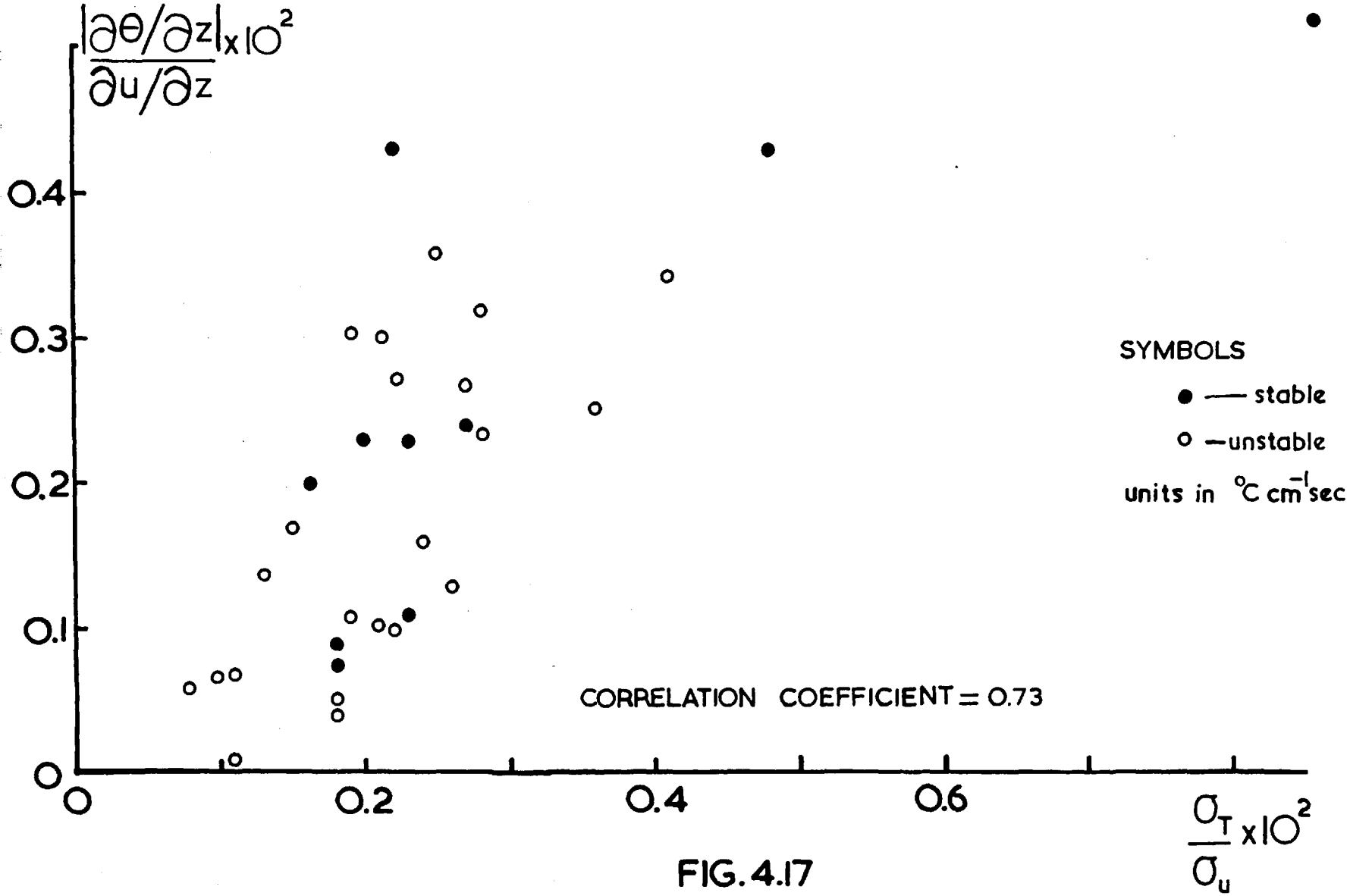
$\frac{|\partial\theta/\partial z|}{\partial u/\partial z} \times 10^2$
0.4
0.3
0.2
0.1
0
0
0.2
0.4
0.6
$\frac{\sigma_T}{\sigma_u} \times 10^2$
SYMBOLS
● — stable
○ — unstable
units in °C cm⁻¹ sec
CORRELATION COEFFICIENT = 0.73

FIG. 4.17

Because K_H/K_M is found to be a function of Ri it necessarily changes with height and so therefore will r_{wT}/r_{uw}. This result implies that the correlation coefficients change with height, as a result of the increased effect of buoyancy, be Ri positive or negative. This conclusion demands a modification of the conclusions of § 4.2.3. concerning the relation between $\partial/\partial z$ (Flux) and $\partial/\partial z$(correlation coefficient), viz. though a variation of flux with height may be related to an anomalous variation of correlation with height associated with horizontal gradients, nevertheless, in a non-neutral stratified atmosphere having horizontal homogeneity and fluxes constant with height, there will necessarily be a change of correlation with height associated with the buoyancy. In a neutral atmosphere, a change of correlation with height will be wholly associated with a variation of flux with height.

4.3.3. The Relation Between z/L and Ri_v.

Since the introduction of the Monin-Cboukhov Similarity Theory to the study of turbulence in the surface layer there have been in use generally two stability parameters, viz. z/L and Ri, each one having its advantages and disadvantages. One important requirement of the study has been to find $Ri(\zeta)$ or $\zeta(Ri)$, since on the basis of the Similarity Theory there should be a unique relation between them.

Values of z/L have been evaluated from the Lough Neagh data and compared to Ri (remembering $Ri \equiv Ri_v$) values in Fig.4.18, the probable errors in both coordinates being indicated. Values of L were calculated taking into account the humidity stratification,

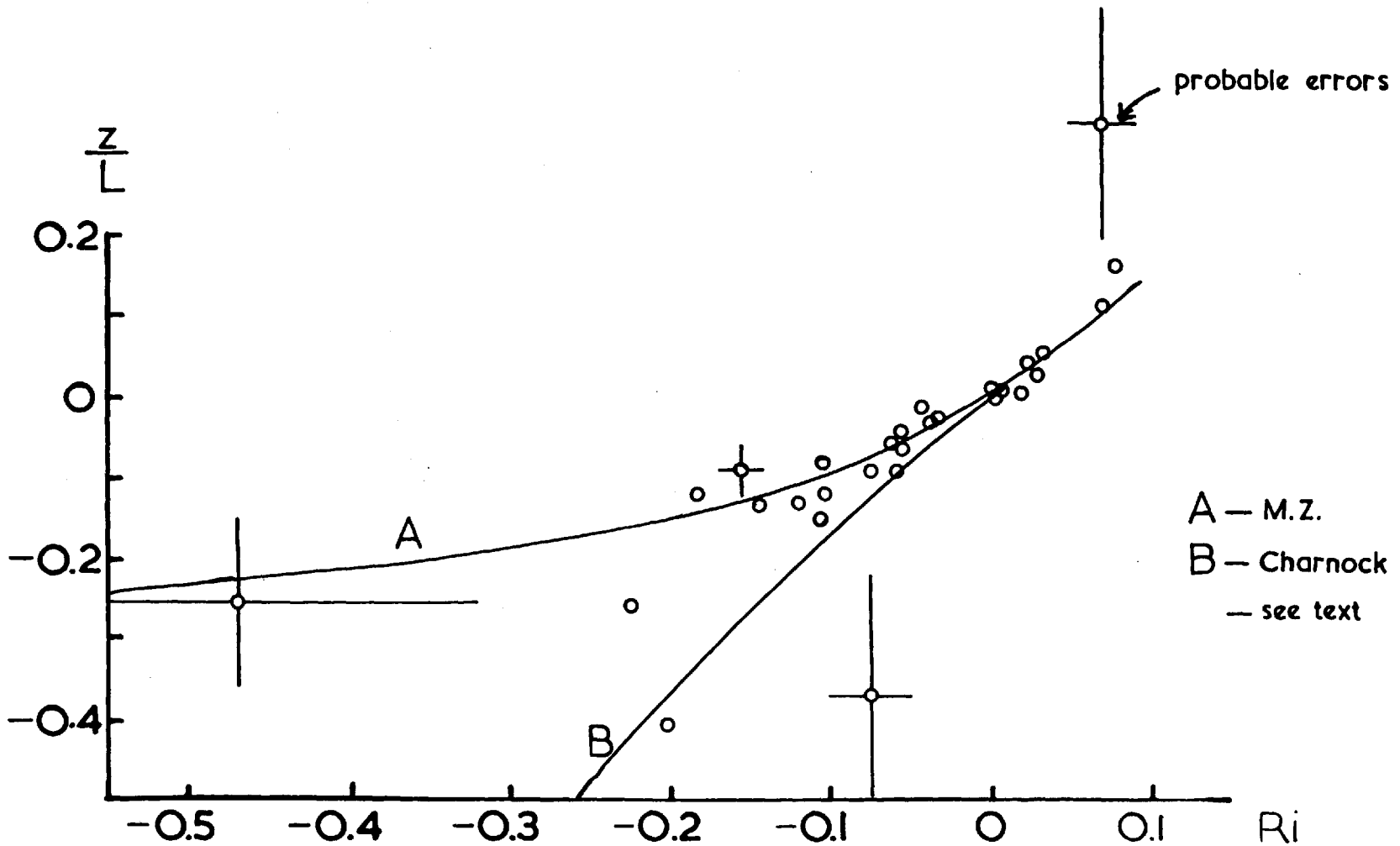
probable errors
z/L
0.2
0
−0.2
−0.4
A
B
−0.5
−0.4
−0.3
−0.2
−0.1
0
0.1
Ri
A — M.Z.
B — Charnock
— see text

FIG. 4.18

since L is defined as $-u_*^3 / k g T^{-1} \overline{w'T_v'}$. Although humidity fluxes were not measured $\overline{w'T_v'}$ can be approximately written as $\overline{w'T'}(1 + 0.61\theta \frac{\partial q}{\partial z} \left(\frac{\partial \theta}{\partial z}\right)^{-1})$ by assuming $K_H = K_V$ and which is directly calculable. Referring to the Lough Neagh points there is a high correlation between ζ and Ri for small values of Ri but considerable scatter when $Ri < -0.1$. It can be seen that points for which $\zeta << -0.1$ have relatively large probable experimental errors based on earlier estimates of the errors in flux and gradient measurements. Errors in the Ri values for these points might well be larger (cf § 3.2.2.) and could account for the scatter in the diagram. In the region of high correlation, when $Ri > 0$, $\zeta > Ri$ and when $Ri < 0$, $\zeta \simeq Ri$. Theoretically ζ and Ri are related like $\zeta = K_H K_M^{-1} \Phi_M Ri$. Thus the relative sizes of ζ and Ri will depend upon the factor $K_H K_M^{-1} \Phi_M$. For instance when $Ri < 0$, $\Phi_M < 0$ and if $K_H/K_M = 1$, $\zeta > Ri$ (see M.Z.) but if K_H/K_M increases faster than Φ_M decreases, then $\zeta < Ri$ (see Charnock, 1967). The variation of ζ with Ri determined experimentally and reported by the above authors is shown also in Fig.4.18. They illustrate the present anomalous situation regarding the variation of K_H/K_M with Ri. It is very unlikely that two regimes exist, as is implied by curves A and B in Fig.4.18 since there is no apparent physical explanation within the framework of present knowledge of surface layer turbulence behaviour. It is more likely that the difference is due to the difference in experimental technique of the determination of Ri whose consequent error (including a systematic under- or over-estimation depending upon method) can be relatively large, and to a serious fault in the Soviet method of determining fluxes since the variation of K_H/K_M with Ri has been verified by many Western workers.

4.4. The Production and Dissipation of Turbulent Kinetic Energy

4.4.1. Introduction

Turbulence in the surface layer of the atmosphere is being produced at one end of the micrometeorological spectrum in the form of relatively large eddies and simultaneously destroyed at the other end, by the action of viscosity, into heat. At intermediate scales energy is transferred by non-linear interactions from one scale to the next smaller one —see § 1.2. The equation representing the local balance of kinetic energy can be written,

$$\frac{\partial E}{\partial t} + \varepsilon = -\overline{u'w'}\frac{\partial u}{\partial z} + g T^{-1}\overline{w'T_v'} - \frac{\partial(\overline{w'E})}{\partial z} \qquad 4.10$$

where $P = -\overline{u'w'}\frac{\partial u}{\partial z}$ is the production rate of mechanical energy (through the interaction of shear and stress), $B = g T^{-1}\overline{w'T_v'}$ the production rate of buoyancy energy, the former being always positive, the latter being positive or negative depending upon the sign of $\overline{w'T_v'}$. This term is equal to $g T^{-1}\overline{w'T'} + 0.61 g \overline{w'q'}$ which can be approximated by $g T^{-1}\overline{w'T'} + 0.61 g \overline{w'T'}\frac{\partial q}{\partial z}\left(\frac{\partial \theta}{\partial z}\right)^{-1}$. The second component $= B_2$ is almost invariably positive, the first $= B_1$ alternates in sign. The term $\partial(\overline{w'E})/\partial z = D$ represents a vertical divergence of the vertical flux of kinetic energy and by nature is an advection term, all others being local. On the left hand side of 4.10 ε is the rate of dissipation of kinetic energy by viscosity, and $\partial E/\partial t$ is the local rate of change of kinetic energy being zero in steady state conditions. Time averages are implied and particular interest will be shown in the characteristics of ε. All the terms in equation 4.10, except ε, can be evaluated directly from gradient and flux (energy) measurements.

In the case of ϵ, knowledge of the form of the velocity spectra provides an indirect method for its evaluation by appeal to the Kolmogorov Laws.

4.4.2. Kolmogorov Laws

4.4.2.1. Theory

The physical basis of the Kolmogorov laws for a locally isotropic field of turbulence at high Reynold's number, as found in the atmosphere, was described in § 1.2. Of concern now is the exact form of the predictions for one-dimensional velocity fields $u'(t)$, $w'(t)$. We have (see Batchelor, 1947, for derivation) for u in the inertial sub-range,

$$\overline{(u_o - u_x)^2} = C_u \, \varepsilon^{2/3} \, x^{2/3}$$

or in terms of the u fluctuation in a steady state field,

$$D_u(x) = \overline{(u'_o - u'_x)^2} = C_u \, \varepsilon^{2/3} \, x^{2/3} \qquad 4.11$$

For w' the analogous equation has C_u replaced by $\frac{4}{3} C_u$ (this follows from Von Karman's equation, $D_w(x) = D_u(x) + \frac{1}{2} x \frac{d}{dx} (D_u(x))$ for isotropic turbulence). In terms of the temporal structure function $D(\xi)$ and using the Taylor assumption,

$$D_u(\xi) = \overline{(u'_o - u'_\xi)^2} = 2\overline{u'^2}\,(1 - r(\xi)) = C_u \, \varepsilon^{2/3} (u\xi)^{2/3} \qquad 4.12$$

In the case of the spectrum for u,

$$\phi_u(k) = K_u \, \varepsilon^{2/3} \, k^{-5/3} \qquad 4.13$$

Again for w, the constant K_u must be replaced by $\frac{4}{3}K_u$. For the frequency spectrum,

$$\frac{u}{2\pi}\phi_u(n) = K_u \varepsilon^{2/3}\left(\frac{2\pi n}{u}\right)^{-5/3} \qquad 4.14$$

and w,

$$\frac{u}{2\pi}\phi_w(n) = \frac{4}{3}K_u \varepsilon^{2/3}\left(\frac{2\pi n}{u}\right)^{-5/3} \qquad 4.15$$

Equations 4.12, 4.14 and 4.15 are the basis for evaluating ε. It will be seen in Chapter 5 that observations show $D_u(\xi) \propto \xi^{2/3}$ over a range of ξ, and $\phi(n) \propto n^{-5/3}$ for u and w above a certain (variable) frequency. For absolute estimates of ε it is imperative to know C_u and K_u which the theory states to be Universal constants for any field of turbulence.

4.4.2.2. Measurement of C/K

Lough Neagh measurements of $D_u(\xi)$ and $\phi_u(n)$ afforded the possibility of evaluating the ratio C_u/K_u from combination of equations 4.12 and 4.14. Because $\phi(n)$ is effectively a Fourier transform of $D(\xi)$ one would expect a unique relation between C_u and K_u and for C_u/K_u to be a Universal constant. A theoretical derivation of the relation is difficult but Webb (1964) showed how C might be related to K, with $C/K = 4.03$, a value well-known from earlier discussion by, for instance, Batchelor (1953) and Hinze (1959).

The results for 27 runs gave (see Table 4.9 later)

$$C/K = 3.30 \pm 0.16 .$$

This is significantly less than the value of 4 quoted above but appears to be the first experimental determination of the ratio. The theory behind C/K is fully dealt with in Appendix 3, and which predicts a value close to that given above.

4.4.2.3. The Spectral Constant (K_u)

The value of K_u generally quoted in contemporary literature lies between 0.45 and 0.50. Estimates of K_u are based on equation 4.13, or more usually 4.14, and require a determination of ε as well as $\phi(k)$ in the inertial sub-range. The best estimates of K have been made using the relation (valid for isotropic turbulence),

$$\varepsilon = 15\nu \int_0^\infty k^2 \phi(k)\, dk \qquad 4.16$$

the quantity $k^2\phi(k)$ being called the dissipation spectrum. This requires measurement of $\phi(k)$ over a wide range of k, covering the inertial sub-range and the dissipation range.

Such a method has been used for three different flow fields. Grant et al. (1962) found $K = 0.47 \pm 0.02$ for the velocity (u) field in a tidal channel, and more recently Pond et al. (1966) found $K = 0.49 \pm 0.04$ for air flow over the sea, having earlier (Pond et al. 1963) suggested a value of 0.46. Working at much lower Reynold's number in an air jet Gibsen (1963) determined $K = 0.52$ approximately. Another laboratory experiment reported by Gibsen and Schwartz (1963) for decaying turbulence behind a grid in a water tunnel, estimating ε from a decay law, suggested $K = 0.44 \pm 0.02$. The great difficulty with laboratory experiments is obtaining a high enough Re to define

a recognisable inertial sub-range. A method used by Zubkovskii (1962) in the atmosphere involved measuring $\phi(k)$ in the inertial sub-range and assuming $\varepsilon = P$ in neutral stability. This gave a value of $K = 0.50$.

A modification of this method has been used in the case of the Lough Neagh data. ε has been assumed equal to $P + B$ (note that ϕ was not measured at high enough frequencies to allow ε to be determined from 4.16). Table 4.7 shows, for 27 runs, values of $\log_{10} \phi(k)$ for $\log_{10} k = -1.8$ (always in the -5/3 region), $P + B$ and the corresponding values of K_u (three additional values were rejected for being anomalously high).

Table 4.7

RUN	$\log_{10}\phi(k)$	$P + B$ $cm^2 s^{-3}$	K_u	RUN	$\log_{10}\phi(k)$	$P + B$ $cm^2 s^{-3}$	K_u
327	3.81	50	.48	543 B	4.20	134	.60
328	3.85	75	.52	543 C	3.72	45	.42
337	3.98	120	.39	549 A	3.89	101	.36
344	3.87	37	.69	554 B	3.64	26	.49
352	3.85	74	.41	557 B	3.89	68	.47
397	3.93	106	.38	557 C	3.72	26	.59
407	3.73	37	.48	558 B	3.95	71	.52
414	4.30	194	.62	565 B	4.18	168	.47
415	4.15	272	.34	565 C	3.90	72	.46
541 A	4.10	112	.54	566 B	4.14	130	.54
541 C	3.68	29	.51	566 C	3.84	54	.49
542 B	3.79	76	.35	575 A	4.18	124	.60
542 C	3.77	52	.42	575 B	3.91	38	.58
				577 A	4.35	302	.50

These results give $K_u = 0.49 \pm 0.09$ (standard deviation). This is in excellent agreement with estimates of other workers and provides some confirmation of the average equality $\varepsilon = P + B$ at the levels

of measurement. Taking the above value with other reliable estimates given equal weight with ours it is concluded that a value of $K_u = 0.48 \pm 0.02$ should be Univerally accepted and is the value used in this thesis for determining ε.

4.4.2.4. The Structure Function Constant (C_u)

Great uncertainty surrounds the value of this constant. Values range from 0.93 (Oboukhov, 1951) to 2.2 (Zubkovskii, 1962); in the former ε was assumed equal to P and in the latter spectral measurements, assuming $\varepsilon = P$, gave K_u and hence C_u, assuming $C_u = 4 K_u$. Table 4.8 gives some other past estimates using one of the above methods.

Table 4.8

Author	Value of C_u
Batchelor, 1950	1.33
Oboukhov and Yaglom, 1959	1.59
Takeuchi, 1962	1.26
Record and Cramer, 1966	2.00

Table 4.9 shows our values of C_u using $K_u = 0.48$ for the 27 measurements of C/K. These results give $C_u = 1.58 \pm 0.19$ (standard deviation). This agrees with the results of Oboukhov and Yaglom above and is about midway between the extreme estimates quoted earlier. It is felt that this value represents a reliable estimate of C_u and is used in this thesis to determine ε.

ε was estimated from measurements of D_u, ϕ_u. ϕ_w where a Kolmogorov-like variation was observed (not observed in the case of D_w), an average being taken when two or three estimates were

available per run.

Table 4.9

RUN	C/K	C_u	RUN	C/K	C_u
327	3.19	1.53	543 B	3.09	1.48
328	3.12	1.50	549 B	3.14	1.51
337	3.42	1.64	553 A	3.23	1.55
338	3.23	1.55	553 B	3.14	1.51
344	3.37	1.62	554 B	3.23	1.55
352	3.31	1.59	554 C	2.94	1.41
397	3.50	1.68	555 A	3.14	1.51
407	3.23	1.55	555 B	3.42	1.64
414	3.37	1.62	565 B	3.37	1.62
415	3.14	1.57	566 B	3.58	1.72
540 A	3.23	1.55	575 A	3.62	1.74
541 A	3.04	1.46	575 B	3.46	1.66
541 C	2.56	1.23	577 A	3.46	1.66
			577 B	3.42	1.64

4.4.3. Energy Budget

Terms in the energy budget equation — 4.10 — have been measured, in the past, for flow overland up to heights ~ 100 m. Taylor (1952) working at levels 2 m. and 29 m. found the flux divergence term to be relatively small whilst terms ε and P were of approximately equal magnitude exceeding others by an order of magnitude. This was confirmed by measurements reported by Panofsky (1962) for levels 25 - 100 m. who further found D to have significant magnitude (~ other terms) for large negative Ri. Further data (L.P. p.125) suggested that D and B were self-cancelling and were, on average, ~ 10 per cent of P. More recently data collected by B.P. suggest $\varepsilon = P + B$ at all levels.

Lough Neagh data have been used to calculate all the terms

Table 4.10

RUN	ε cm^2s^{-3}	P cm^2s^{-3}	B_1 cm^2s^{-3}	B_2 cm^2s^{-3}	P + B cm^2s^{-3}	$\overline{w^3}\times10^{-4}$ cm^3s^{-3}	$\overline{wu^2}\times10^{-4}$ cm^3s^{-3}	$Fx10^{-4}$ cm^3s^{-3}	$\Delta F/\Delta z=D$ cm^2s^{-3}	$\varepsilon z u_*^{-3}$
327	53	56	-6	0.2	50					3.74
328	62	81	-6	0.2	75					2.95
337	90	123	-3	0.3	120					3.58
338	151	—	—	—	—					—
344	62	31	5	1	37					2.60
352	62	63	10	1	74					1.80
397	82	107	-2	1	106					1.88
407	41	42	-5	0	37					7.30
414	260	173	18	3	194					2.90
415	195	260	10	2	272					1.25
540 A	157	86	0	1	87	0.43	1.20	1.63	-32	3.48
540 C	15	16	—	—	—	-2.99	1.34	-1.65		3.21
541 A	137	106	1	5	112	0.19	0.19	0	22	2.80
541 C	41	28	0	1	29	-0.08	2.30	2.22		3.38
542 B	61	70	3	3	76	1.09	0.91	2.00	21	1.74
542 C	45	44	4	4	52	-2.25	5.94	3.69		1.40
543 B	168	124	5	5	134	0.84	1.37	2.21	-54	2.51
543 C	38	35	5	5	45	-5.59	3.56	-2.03		2.44
549 A	100	96	2	3	101	0.34	0.96	1.30	- 6	1.69
549 B	35	22	—	—	—	0.52	0.63	1.15		2.04
553 A	61	87	—	—	—	0.52	0.80	1.32	30	1.51
553 B	25	28	—	—	—	0.89	1.14	2.03		1.58
554 B	36	23	1	2	26	0.67	-0.66	0.01	15	3.70
554 C	20	—	—	—	—	0.62	0.58	1.20		—
555 A	86	103	—	—	—	1.16	1.10	2.26	-31	1.75
555 B	38	31	—	—	—	0.71	0.80	1.51		1.92
557 B	84	59	6	3	68	0.89	0.07	0.96	33	3.44
557 C	36	19	5	2	26	1.36	2.19	3.55		4.02
558 B	84	61	7	3	71	—	—	—	—	2.60
558 C	35	—	—	—	—	—	—	—		—
565 B	172	150	12	6	168	1.44	4.18	5.62	105	2.22
565 C	68	49	15	8	72	6.35	7.55	13.90		1.80
566 B	143	116	10	4	130	2.70	2.69	5.39	38	2.18
566 C	60	35	13	6	54	3.08	5.27	8.35		1.88
575 A	220	123	0	1	124	0.54	0.91	1.45	-49	2.61
575 B	65	37	0	1	38	0.12	0.16	0.28		4.14
577 A	360	304	-3	1	302	0.68	1.58	2.26	-94	1.77
577 B	135	90	—	—	—	-0.26	0.26	0		3.95
578 B	162	92	-3	1	90	0.04	0.17	0.21	10	5.62
578 C	64	36	-3	1	34	1.16	-0.16	1.00		7.95

$$F = (\overline{w'^3} + \overline{w'u'^2})$$

in 4.10 —the relevant quantities are shown in Table 4.10. D has been estimated for the appropriate layer, using $D = \Delta(\overline{w'^3} + \overline{w'u'^2})/\Delta z$,

though this rather crude method which ignores the term $\overline{w'v'^2}$ will suffice only to establish the order of magnitude of D.

$\partial E/\partial t$ never exceeded 2 $cm^2 sec^{-3}$ in our runs.

Regarding overall average values of the local dissipation and production rates taken from Table 4.10 (excluding three runs which gave anomalously high values of K_u, viz. Runs 540 A, 575 A, 578 B which were not used in the estimation of K_u earlier —§ 4.4.2.3.) these have been computed to be -

	ε $cm^2 sec^{-3}$	P + B $cm^2 sec^{-3}$
5 Runs at level A (all Ri)	153	141
14 Runs at level B (Ri -)	102	95
7 Runs at level B (Ri +)	75	74
8 Runs at level C (all Ri)	46	41

Table 4.10 indicates that estimates of D are not altogether consistent with values required to balance equation 4.10 for individual runs. This is not surprising since the method is crude and the term $\overline{w'v'^2}$ has been neglected. There are cases of flux divergence and convergence showing no variation with Ri for instance, and no conclusion on the behaviour of D can be made. For all but two cases values of $\overline{w'^3} + \overline{w'u'^2}$ are positive indicating positive flux of turbulent kinetic energy consistent with the measurements reported by Panofsky (1962).

Overall it appears that $\varepsilon \simeq P + B$ to within 5 per cent consistent with the value of K_u found from assuming $\varepsilon = P + B$. On individual occasions D may be important perhaps being associated with unsteadiness and horizontal variations of wind.

4.4.4. Characteristics of ε

4.4.4.1. Introduction

Several methods have been used in the past to estimate ε in a given situation (see L.P. p.121 and Ivanov, 1962) and it has been possible to determine the major factors upon which ε depends. Although there have been many reported measurements of ε in the surface layer and above overland hardly any have been made over the sea.

Priestley (1959) deduced from three sets of observations taken in unstable conditions overland that $\varepsilon \propto z^{-4/3}$ for a height range 10^{-1} m. to 10^{3} m. and data collected together by Ball (1961) and Ivanov (1962) generally confirmed this relation whilst showing a large amount of scatter, the reason for this scatter being described later. ε is of course strongly wind dependent and data published by Ball (1961) and Record and Cramer (1966) showed $\varepsilon \propto u^{3}$ at low levels but at heights greater than a few decametres the effect of thermal stratification became considerable resulting in no clear relation between ε and u, z.

Dimensional analysis, assuming ε depends upon u_*, z, ζ, gives $\varepsilon \sim u_*^3 z^{-1} f(\zeta)$ whereas equation 4.10 written in neutral conditions gives $\varepsilon = -\overline{u'w'}\,\partial U/\partial z = \kappa^{-1} u_*^3 z^{-1}$. It will be assumed therefore that,

$$\varepsilon = u_*^3 z^{-1} f(\zeta) \qquad 4.17$$

where $f(\zeta) \longrightarrow \kappa^{-1}$ when $\zeta \longrightarrow 0$. Equation 4.17 will be used to describe characteristics of the Lough Neagh results and results of other workers described above.

4.4.4.2. Wind Speed Dependence

Strictly, on the basis of 4.17, ε should be proportional to u_*^3. The dependence of ε upon u^3 over the sea would be complicated by the variation of roughness length with wind speed which has been established experimentally, although for the present set of data this is not so (cf. § 4.2.). In addition u_* values (from eddy correlation measurements) are not available for all runs whereas values of u are. Hence ε has been normalised to a height of 4 m. on the basis of 4.17 and plotted vs wind speed —see Fig.4.19. The variation is consistent with the relation defined in 4.17 regarding the index 3.

4.4.4.3. Height Dependence

ε has been normalised to a wind speed of 5 $m.s^{-1}$ on the basis of 4.17 and values plotted vs height. In Fig.4.20 averaged values are shown for three main levels for positive and negative Ri. On the whole an index between -1 and -4/3 would suffice to describe the relation $\varepsilon \propto z^{\beta}$. The data further suggests no significant difference in the height variation of ε in the first 16 m. over the sea for Ri of different sign. It is probable that the index β will be affected by the degree of thermal stratification increasingly with height.

Priestley's analogous overland curve with $\beta = -4/3$ is put in Fig.4.20 and a considerable separation from the Lough Neagh data is observed. This is due to differences in the roughness of the surfaces since for a given wind speed u_* in equation 4.17 will be considerably greater overland than over the sea. This effect of

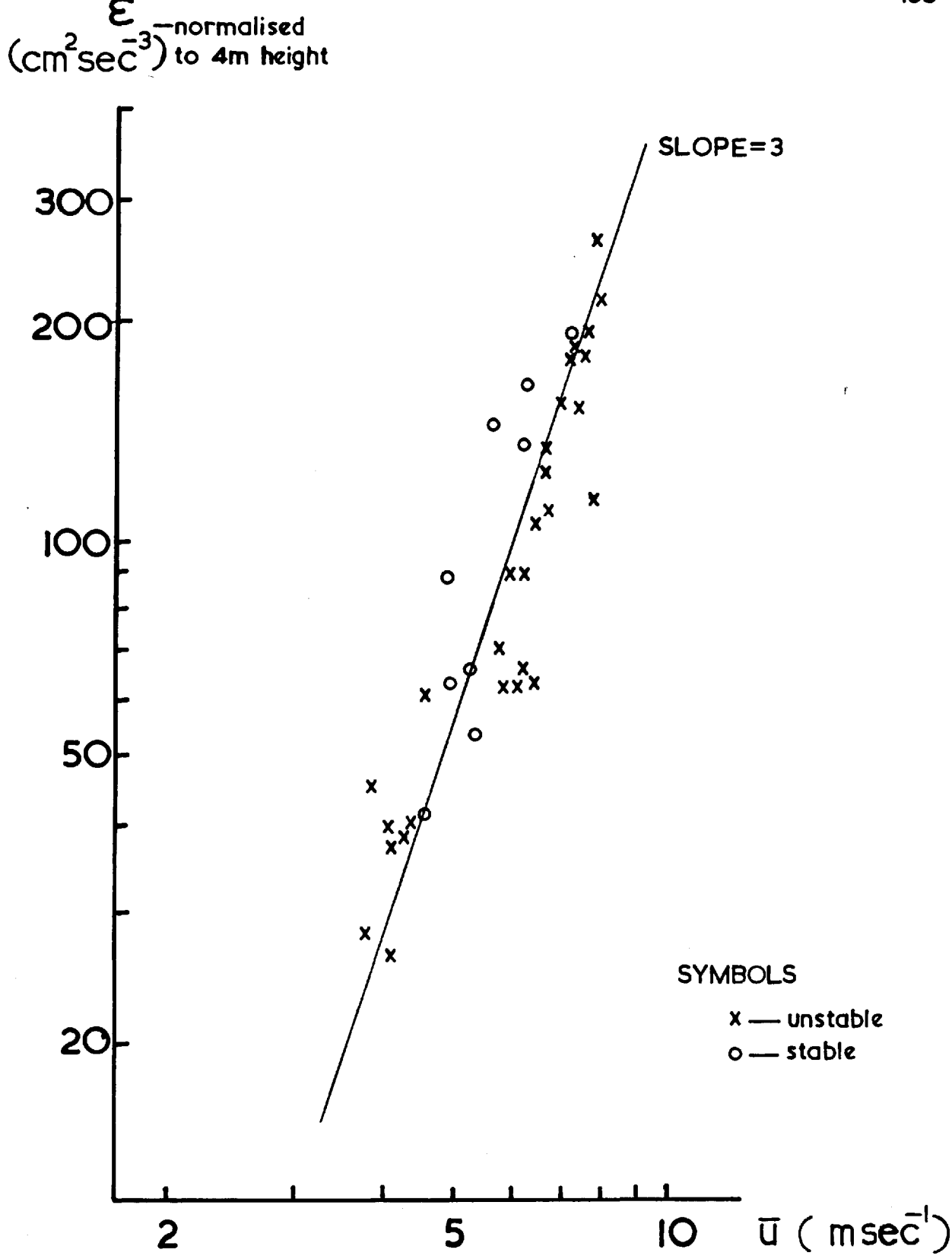
ε —normalised
(cm²sec⁻³) to 4m height
SLOPE=3
300
200
100
50
20
2
5
10
ū (msec⁻¹)
SYMBOLS
x — unstable
o — stable

FIG.4.19

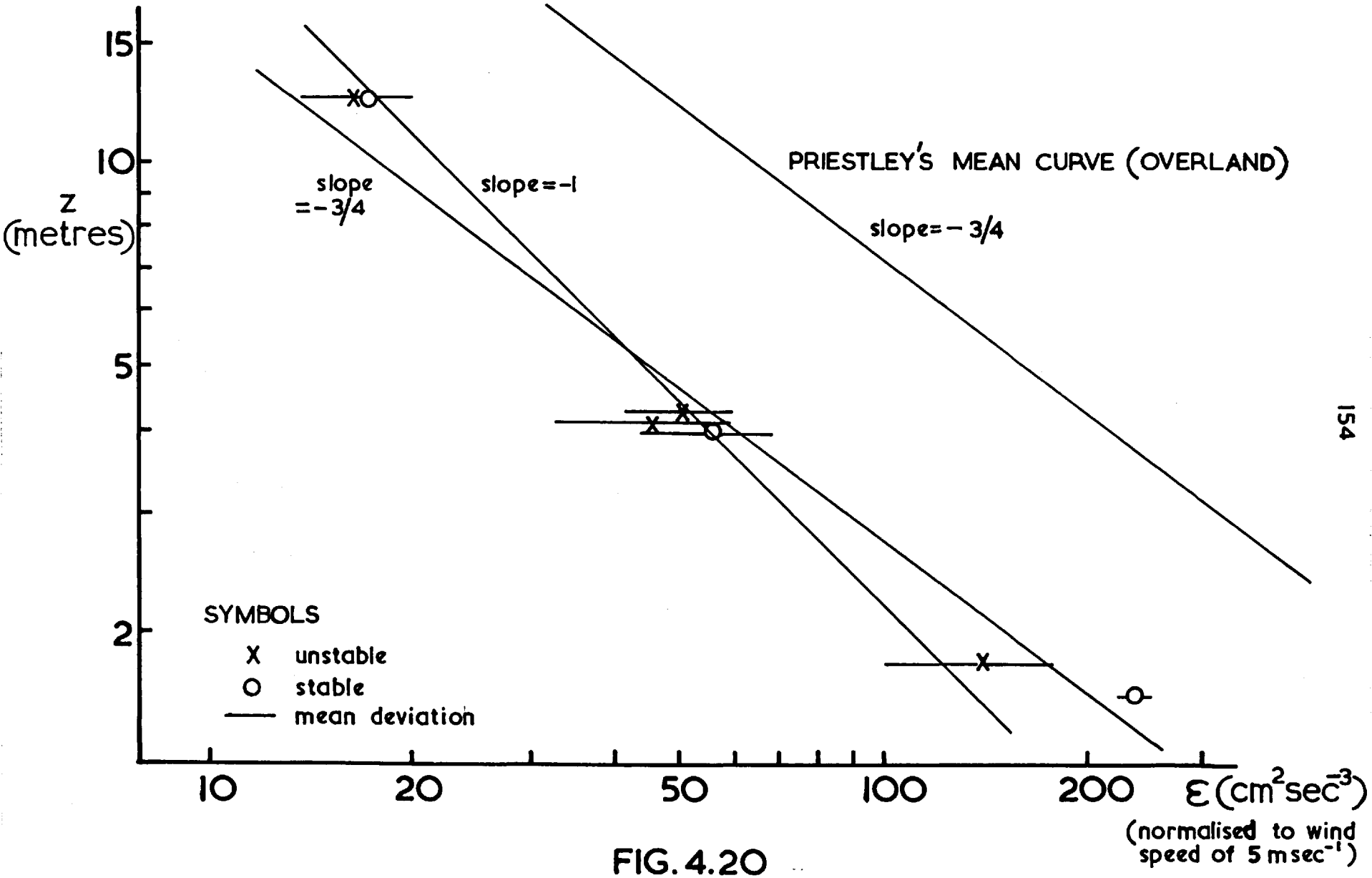
15
10
5
2
z (metres)
slope =−3/4
slope=−1
PRIESTLEY'S MEAN CURVE (OVERLAND)
slope=−3/4
SYMBOLS
X unstable
O stable
mean deviation
10
20
50
100
200
ε (cm²sec⁻³)
(normalised to wind speed of 5 msec⁻¹)

FIG. 4.20

roughness explains to some extent the large amount of scatter present in the $\varepsilon - z$ diagrams of Ball and Ivanov mentioned earlier and why Record and Cramer reported normalised ε values (obtained at Round Hill where $z_o \simeq 10$ cm.) a factor of two or more greater than those implied by Priestley's curve relating to a roughness length certainly < 1 cm.

4.4.4.4. Effect of Thermal Stratification

The effect of thermal stratification upon ε was found to be considerable by, for instance, Ivanov, Record and Cramer and implied in the results of Ball when the height was greater than several decametres. Ivanaov found, for heights $\sim$ several hundreds of metres, that, at a given wind speed and height, ε was greatest in convective conditions and least when the stratification was near-neutral. Similar behaviour is to be found in the data published by Record and Cramer at a height of 40 m. whilst at a lower height (16 m.) the behaviour was reversed. This latter behaviour is confirmed by the Lough Neagh results for heights 1 - 12 m. and is best shown with the use of equation 4.17 with $f(\zeta)$ replaced by $f(Ri)$.

Values of $f(Ri) = \varepsilon z u_*^{-3}$ —u_* being computed from the eddy covariance — have been evaluated and averages found for five Ri ranges. The result is shown in Fig.4.21. The diagram implies $f(Ri) = 2.5$ in unstable and neutral conditions, implying a Von Karman constant equal to 0.4, and $f(Ri)$ increasing to a value of about 5 in moderately stable conditions. The variation of $f(Ri)$ with Ri agrees very well with the results of B.P. showing $k \varepsilon z u_*^{-3}$ as a

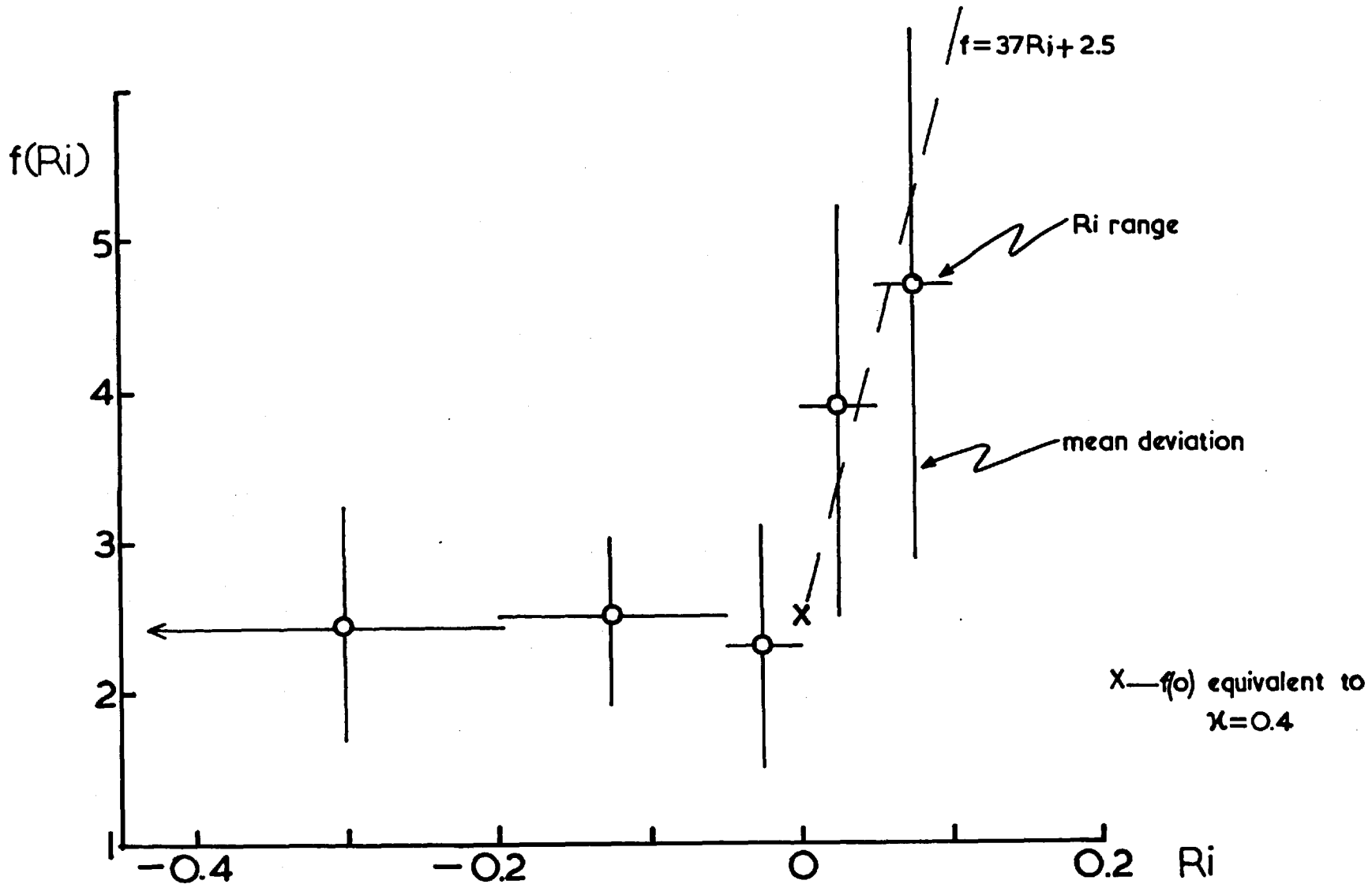
f=37Ri+2.5
f(Ri)
Ri range
mean deviation
X—f(o) equivalent to
X=0.4
5
4
3
2
1
−0.4
−0.2
0
0.2
Ri

FIG. 4.21

function of ζ for several sets of data.

ε is therefore best described by the relation, analogous to 4.17,

$$\varepsilon = u_*^3 z^{-1} f(Ri) \qquad 4.17a$$

where, $f(Ri) = 2.5$ when $Ri \leq 0$,

$f(Ri) = 37\,Ri + 2.5$ when $Ri > 0$.

4.4.4.5. Characteristic Scales Defined by ε

An interesting parameter of the flow is the time scale $t_o = E/\varepsilon$ and the corresponding length scale $X_o = \bar{u} t_o$. In decaying turbulence $dE/dt = \varepsilon$, so that for a constant dissipation rate t_o represents the total decay time and X_o the distance travelled before all the turbulence has decayed. In the case of quasi-steady state turbulence it can be interpreted as follows. If the production rate of the kinetic energy is suddenly decreased (e.g. when air flows from a rough surface to a less rough surface) or there is a sudden drop in the wind speed the energy spectrum will partially decay and re-adjust to a new level appropriate to the new production rate. The time taken for the total re-adjustment $\sim E/\varepsilon$. This will also be the time taken for the wind profile to re-adjust itself to the new roughness up to a height z (i.e. the time taken for the internal boundary layer to grow to a height z). Thus $\bar{u}\,E/\varepsilon$ will be equivalent to the fetch required to give a characteristic profile up to a height z. For $z = 4$ m., a typical value of E/ε for $\bar{u} = 5$ m.s^{-1} is 70 seconds and therefore $X_o = 350$ m. For $z = 12$ m., $E/\varepsilon \sim 220$ seconds and $X_o \sim 1.1$ km. The ratio $z/X_o \simeq 0.01$ which

is consistent with the slope of the internal boundary layer viz. height ÷ fetch (see § 2.1.1.).

5.1. Introduction

Little knowledge exists of the form of the spectra and cospectra of fluctuating quantities in the surface layer of the atmosphere over the sea, though that we do have suggests no obvious reason why, qualitatively, their features should differ greatly from those over the land. The Lough Neagh results discussed herein generally confirm this view; they extend significantly existing knowledge of the spectral characteristics of turbulence over a water surface. Thus the diagrammatic representation of a composite spectrum of atmospheric motions at low levels (see Fig.1.2) should suffice for any underlying surface.

The emphasis on the interpretation of turbulence spectra and cospectra in the surface layer has been, and is maintained in the present work,

(a) to obtain information in the inertial sub-range, especially concerning the Kolmogorov Laws,

(b) to determine the dominant scale of eddy effecting the transfer of heat and momentum and contributing to the turbulent 'energies', due regard being paid to the sampling period,

(c) to find a Universal representation for spectra obtained over a wide range of conditions using Similarity Theory.

Much of the information on the above has been obtained from experiments over the land. However the most impressive investigation of the inertial sub-range (and dissipation range) was made over the sea (Spanish Banks, near Vancouver) at a height of a few metres for velocity and temperature by Pond et al. (1966). At the same site Smith (1966) and W.B. obtained measurements of

the (co)spectra of the u,w components for sampling periods ~ 30 minutes showing characteristics relevant to (b) above.

Overland, many sets of velocity spectra have been published showing a -5/3 region as an extension of the inertial sub-range behaviour; in many cases the inertial sub-range being outside the frequency response of the apparatus (see, for instance, MacCready 1962). Monin (1962) showed that spectra for velocity and temperature obtained in U.S.S.R. exhibited a similar behaviour, and further, that their properties were consistent with Similarity Theory arguments. With regard to (b) Gurvich (1960 a, b, 1961) published measurements of w spectra and flux cospectra, emphasising particularly the effect of stability on the positions of the peaks along the frequency axis. More recently, (co)spectra obtained over a wide range of conditions and published by B.P. and P.M. show similar stability effects and could be reduced to one family of curves when normalised by Similarity Theory principles. These are discussed later in relation to the Lough Neagh curves. Also regarding (c), Berman (1965) attempted to normalise u spectra by appeal to the Similarity Theory, with some degree of success.

Over the sea, the presence of surface gravity waves, whose 'energy' (or vertical displacement) spectrum is characteristically narrow with a well-defined sharp peak (see § 6.3.) may result in modification of the turbulence at low levels at specific scales and thus modify spectra relative to those over a fixed boundary. In general it is expected that the relative contributions from the wide range of eddy scales to the flux and energy will depend, in varying degrees, upon height, stability (or Monin-Oboukhov length),

wind speed, surface roughness and (in the dissipation range) upon Reynold's Number.

The spectrum was defined in § 2.2.4. and the mechanics of spectral analysis of time series described in § 2.2.5., such an analysis giving information on the spectral and cospectral content for eddy periods between 1 minute and 0.2 seconds, though the spectra will be often described in terms of wavelength or wave number coordinate obtained from the frequency by a Taylor transform (§ 2.2.4.).

5.2. Use of the Similarity Theories

5.2.1. Application of the Monin-Oboukhov Similarity Theory

The physical principles upon which the Monin-Oboukhov theory is based were described in some detail in § 1.2. The theory concerns turbulence of scales outside (i.e. greater than those in) the dissipation range of the spectrum where molecular processes (viz. viscosity and conduction) are relatively unimportant viz. in the anisotropic region and inertial sub-range.

When considering the time spectra and cospectra it is necessary to take into account additionally the mean wind speed upon which the frequency, not being invariant, depends. Thus in the case of the velocity (u,w) spectra and momentum flux cospectrum Monin (1959) argues that the density $\phi(n)$ will be given by

$$\phi(n) \propto \frac{u_*^2 z}{\bar{u}} \psi_1 \left(\frac{nz}{u}, \frac{z}{L} \right) \qquad 5.1$$

where f will be written for $nz/u = zk/2\pi = z/\lambda$ a non-dimensional frequency. In the present work 5.1 has been modified as follows —

(a) A well-known representation of the (co)spectra is a plot of $n\phi(n)$ vs $\log_{10} n$; thus the area under the curve per unit logarithmic frequency band represents the contribution from that band to the total energy or flux —see § 2.2.4. Consequently each side of 5.1 is multiplied by n giving,

$n\phi(n) \propto u_*^2 \frac{nz}{u} \psi_1 \left(\frac{nz}{u}, \zeta\right)$ which may be written,

$$n\phi(n) \propto u_*^2 \psi_2 (f,\zeta) \qquad 5.1\,a$$

(b) On Similarity principles σ_u^2/u_*^2, σ_w^2/u_*^2 are Universal functions of ζ, and computation of a non-dimensional spectrum is facilitated by writing 5.1 a,

$$n\phi_{u,w}(n) \propto \sigma_{u,w}^2 \psi_3 (f,\zeta) \qquad 5.1\,b$$

(c) According to the Similarity Theory, Ri is a Universal function of ζ. Because Ri values are more readily available 5.1 b is written,

$$n\phi_{u,w}(n) \propto \sigma_{u,w}^2 \psi_4 (f, Ri) \qquad 5.1\,c$$

and,
$$n\phi_{uw}(n) \propto u_*^2 \psi_4 (f, Ri) \qquad 5.1\,d$$

An analogous equation applies to the temperature spectrum and heat-flux cospectrum. Thus in equation 5.1, for temperature u_*^2 is replaced by θ_*^2 and for heat flux by $u_*\theta_*$. The equation is then modified as for velocity, yielding,

$$n\phi_T(n) \propto \sigma_T^2 \psi_4(f, Ri) \qquad 5.1e$$

and,

$$n\phi_{wT}(n) \propto \sigma_{wT}^2 \psi_4(f, Ri) \qquad 5.1f$$

By plotting $n\phi(n)/\sigma^2$ vs $\log_{10} f$ we obtain, according to 5.1 c-f, Universal curves per Ri value. Because of the limited number of (co)spectra available and the inherent scatter of computed spectra, relations 5.1 c-f are investigated for 4 Ri ranges covering unstable ($Ri < -0.05$), near-neutral ($-.05 < Ri < 0$ and $0 < Ri < 0.05$) and stable ($Ri > 0.05$) conditions.

5.2.2. The Kolmogorov Similarity Theory

The well-known Kolmogorov theory of locally isotropic turbulence described in § 1.2. is a second Similarity Theory valid for the inertial sub-range and dissipation range. Thus the two Similarity Theories overlap in the inertial sub-range. In this region of the VELOCITY spectrum, $\phi_{u,w}(k)$ depends solely upon ε, k and $\phi_{u,w}(n)$ upon ε, n, u. Dimensional analysis then gives,

$$\phi_{u,w}(n) \propto \frac{u^4}{\varepsilon} \psi_5\left(\frac{nu^2}{\varepsilon}\right) \qquad 5.2$$

where it is expected that $\psi_5\left(\frac{nu^2}{\varepsilon}\right) \propto \left(\frac{nu^2}{\varepsilon}\right)^{-5/3}$. Relation 5.2 was suggested by Monin (1959) though it follows directly from the Kolmogorov hypotheses and the Taylor hypothesis for the space-time transform.

To investigate 5.2 using measured u' and w' spectra (Figs.5.1 and 5.2) the relation must be modified because ε is not

measured directly. Now on Monin-Oboukhov Similarity Theory,

$$\varepsilon \sim u_*^3 \, L^{-1} \, g_1(\zeta)$$

which may be written,

$$\varepsilon \sim u_*^3 \, z^{-1} \, g_2(\zeta)$$

a relation proposed in § 4.4.4.1. (equation 4.17). Further since $\bar{u} = \bar{u}(u_*, \zeta)$ this may be written,

$$\varepsilon \sim \bar{u}^3 \, z^{-1} \, g_3(\zeta) .$$

Thus it is possible to write 5.2,

$$\phi_{u,w}(n) \propto \bar{u} \; z \; g_4(\zeta) \; \psi_6(f) , \quad \text{or}$$

$$\phi_{u,w}(k) \propto u^2 \, z \; g_4(\zeta) \; \psi_6(f) , \quad \text{or}$$

$$\phi_{u,w}(k) \propto \sigma_{u,w}^2 \, z \, g_5(\zeta) \; \psi_6(f) \qquad 5.2a$$

Equation 5.2a also applies to the temperature spectrum. In this case, in the inertial sub-range, $\phi_T(k)$ depends upon ε, χ, k and $\phi_T(n)$ upon $\varepsilon, \chi, n, \bar{u}$. The analogous equation to 5.2 is then,

$$\phi_T(n) \propto \frac{u^4 \chi}{\varepsilon} \; \psi_5\left(\frac{nu^2}{\varepsilon}\right) \qquad 5.3$$

As with velocity, this is then modified, giving,

$$\phi_T(n) \propto u^{-2} \, z^2 \, \chi \, g_4(\zeta) \; \psi_6(f) , \quad \text{or}$$

$$\phi_T(k) \propto u^{-1} \, z^2 \, \chi \, g_4(\zeta) \; \psi_6(f) .$$

Further modification is required because χ is not measured directly, but on the Monin-Obukhov Similarity Theory,

$$\chi \sim u_* \theta_*^2 \, L^{-1} \, g_6(\zeta), \quad \text{or}$$

$$\chi \sim u_* \theta_*^2 \, z^{-1} \, g_7(\zeta).$$

As with velocity this may be written,

$$\chi \sim \bar{u} \theta_*^2 \, z^{-1} \, g_8(\zeta),$$

and assuming, again on a Similarity Theory basis that σ_T^2 / θ_*^2 is a Universal function of ζ, then $\chi \sim \bar{u} \, \sigma_T^2 \, z^{-1} \, g_9(\zeta)$. Therefore,

$$\phi_T(k) \propto \sigma_T^2 \, z \, g_9(\zeta) \, \psi_6(f) \qquad 5.3\,a$$

Equations 5.2 a, 5.3 a serve as convenient normalising relations for the non-dimensional spectral density $\phi(k) / z\sigma^2$ and frequency or wave number f, though there is expected to be a weak dependence upon ζ through the functions $g(\zeta)$. This occurs because of the replacement of ε in equation 5.2 and χ in 5.3.

The nature of the variation of $\phi_{u,w}(k)$ and $\phi_T(k)$ with k (see Figs. 5.1 - 5.3 inclusive) requires $\log_{10}\left(\phi(k) / z\sigma^2\right)$ to be plotted vs $\log_{10} f$. The investigation of relations 5.2 a, 5.3 a is made for three Ri ranges, $Ri < -0.10$, $-0.1 < Ri < 0$ and $0 < Ri < 0.1$.

5.2.3. Structure Function Behaviour

If the principles of § 5.2.1. are applied to the structure function then for the spatial function $D(x)$ the relation is, for temperature and velocity,

$$D(x)/\sigma^2 \propto \eta_1(x/z, Ri) \qquad 5.4\,a$$

which may be transformed to a corresponding temporal function. Of greater interest regarding the Lough Neagh results is the relation analogous to that for the spectrum in § 5.2.2., viz. in the inertial sub-range,

$$D(x)/\sigma^2 \propto \varepsilon_{10}(Ri)\eta_2(x/z) \qquad 5.4\,b$$

where $\eta_2(x/z)$ is expected to be $\propto (x/z)^{2/3}$. In practice, $\log_{10}\left(D(x)/\sigma^2\right)$ is plotted vs $\log_{10}(x/z)$ combining all runs according to whether Ri is positive or negative.

5.2.4. Characteristic Spectral Frequencies

The implication of § 5.2.1. is that, because the spectral form is a Universal function of Ri, then characteristic points on the spectrum should be determined solely by Ri. Such characteristic points considered are the wavelengths corresponding to maxima and to the low frequency limit of the -5/3 region.

5.3. Velocity Characteristics

5.3.1. Structure Function

The Kolmogorov hypotheses apply both to structure function and spectrum since one is the Fourier transform of the other and both depend upon the same physical process. In this respect the structure function defined in equation 4.12 is of interest i.e. $D_u(x) = 2\sigma_u^2\left(1 - r_u(x)\right)$ where $r_u(x) = r_u(\xi)$ for $\xi = x/\bar{u}$.

FIG. 5.1 LOGARITHMIC U SPECTRA

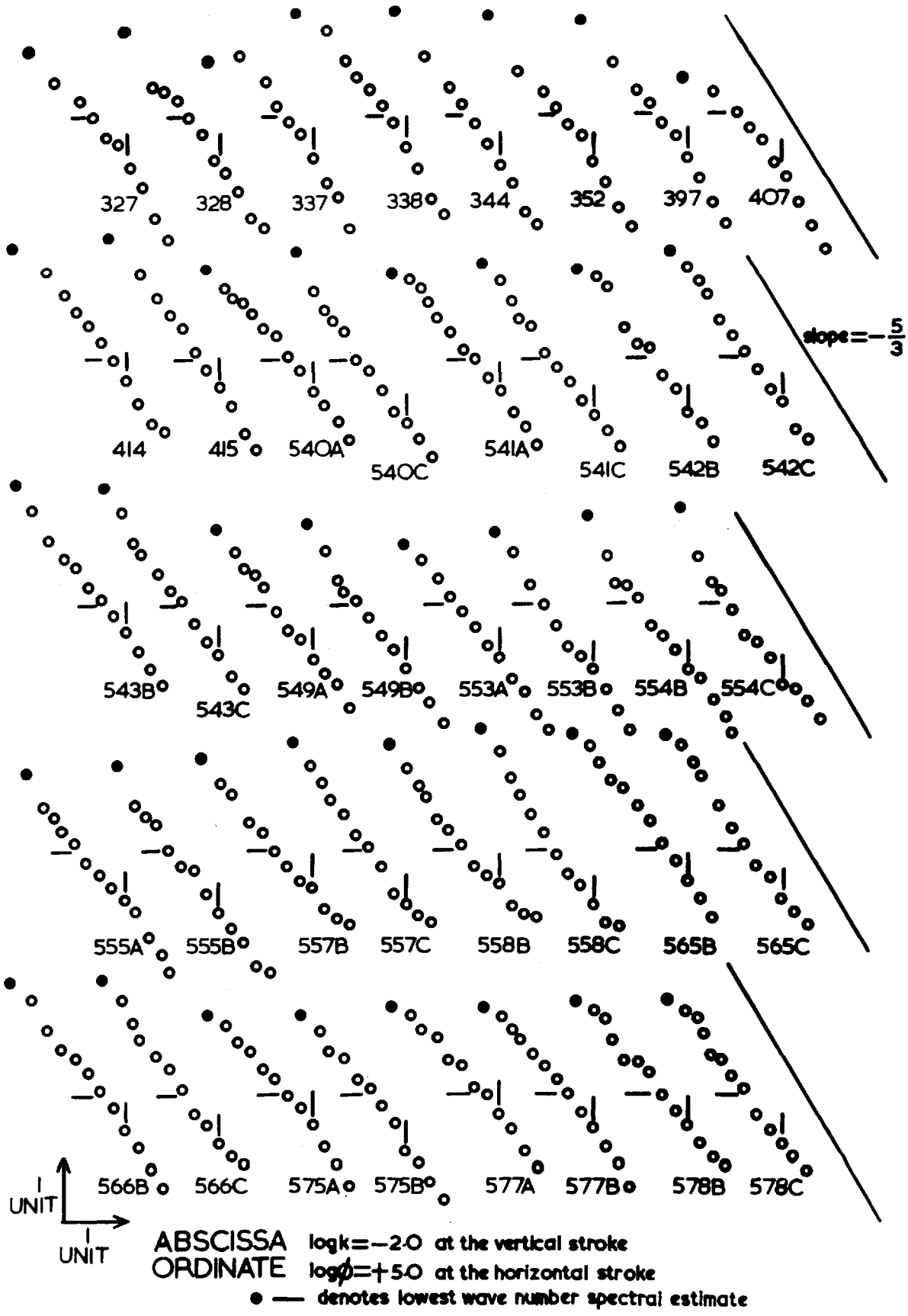

FIG.5.2 LOGARITHMIC W SPECTRA

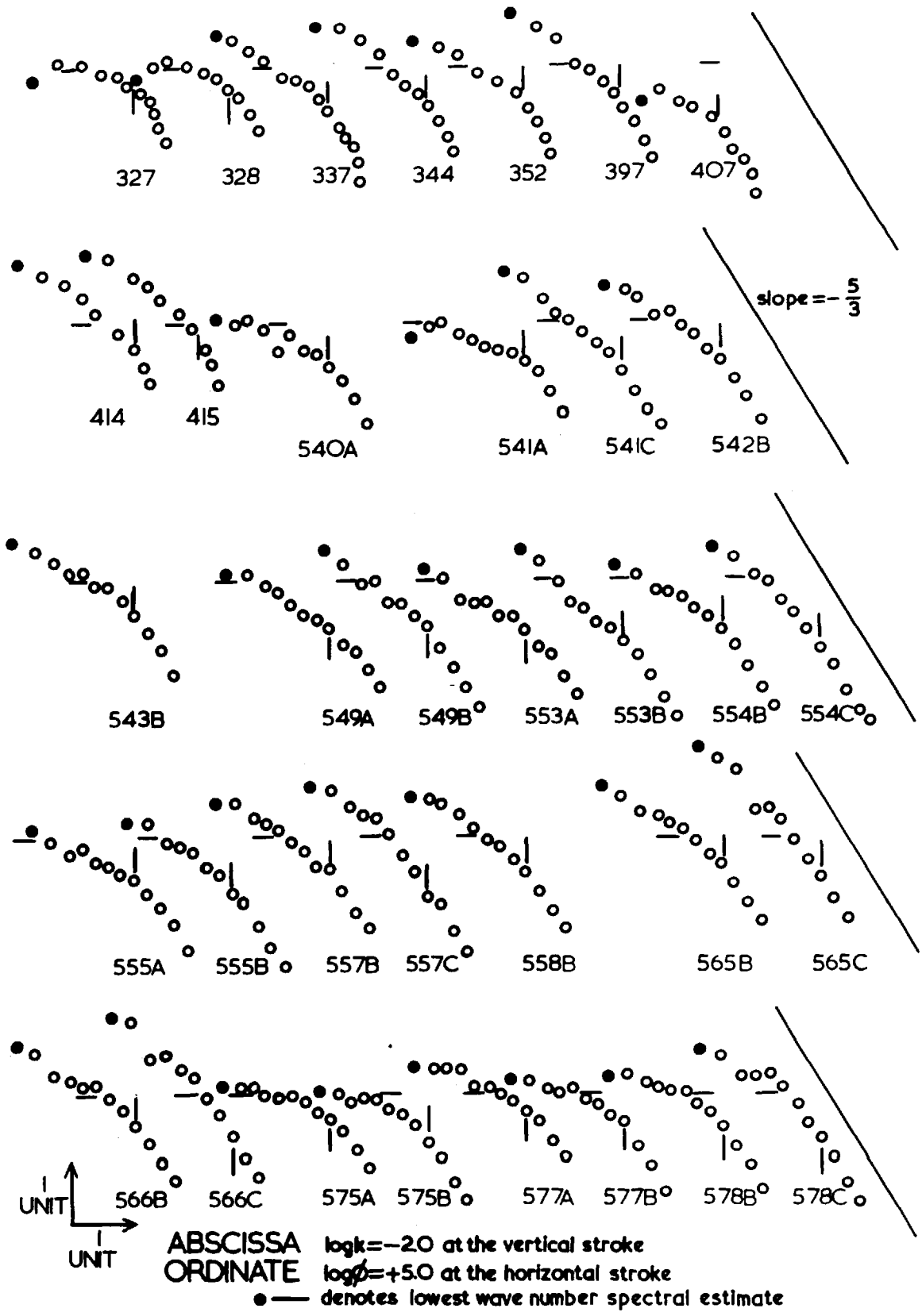

FIG.5.3 LOGARITHMIC T SPECTRA

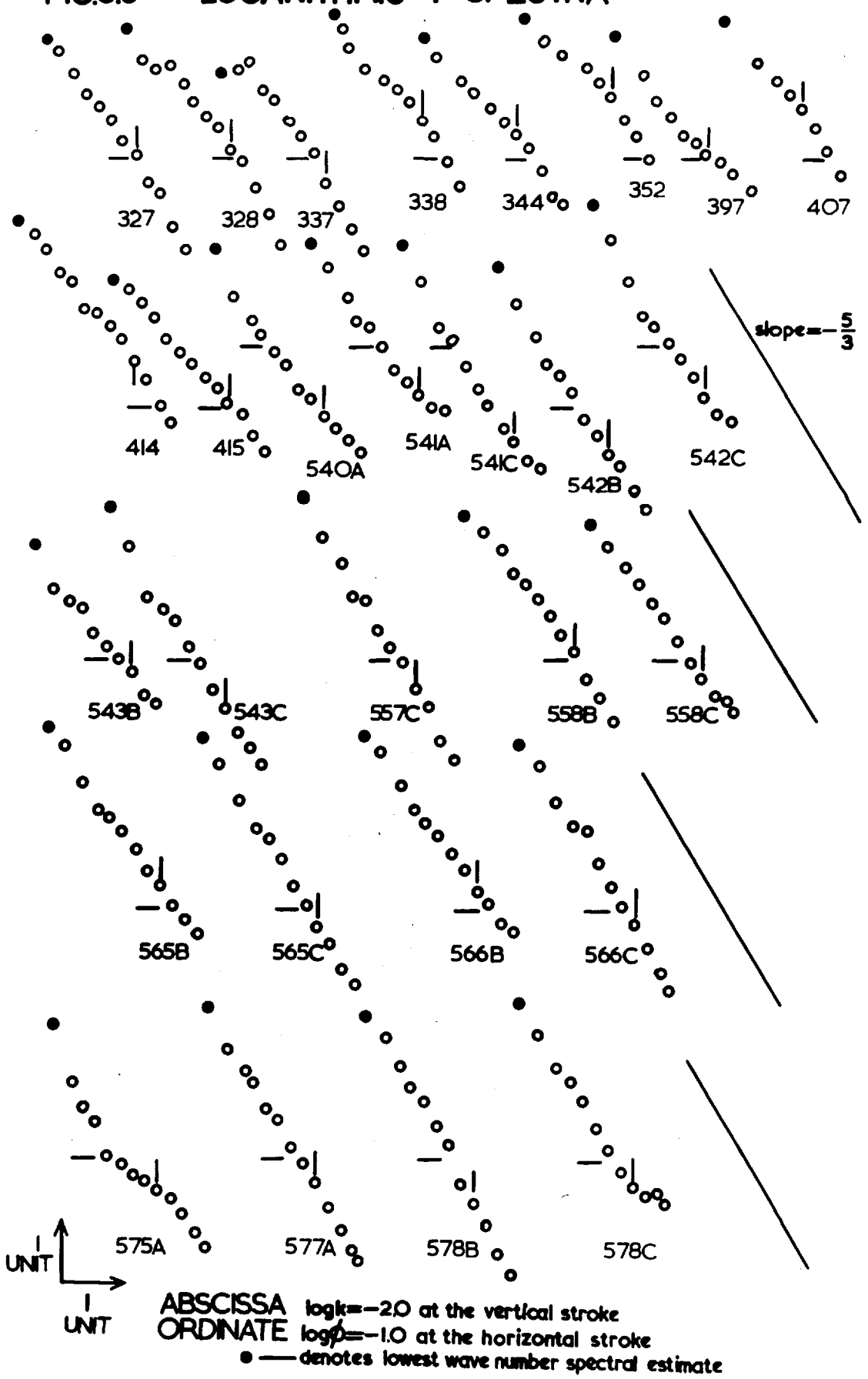

FIG.5.4 UW COSPECTRA (NORMALISED)

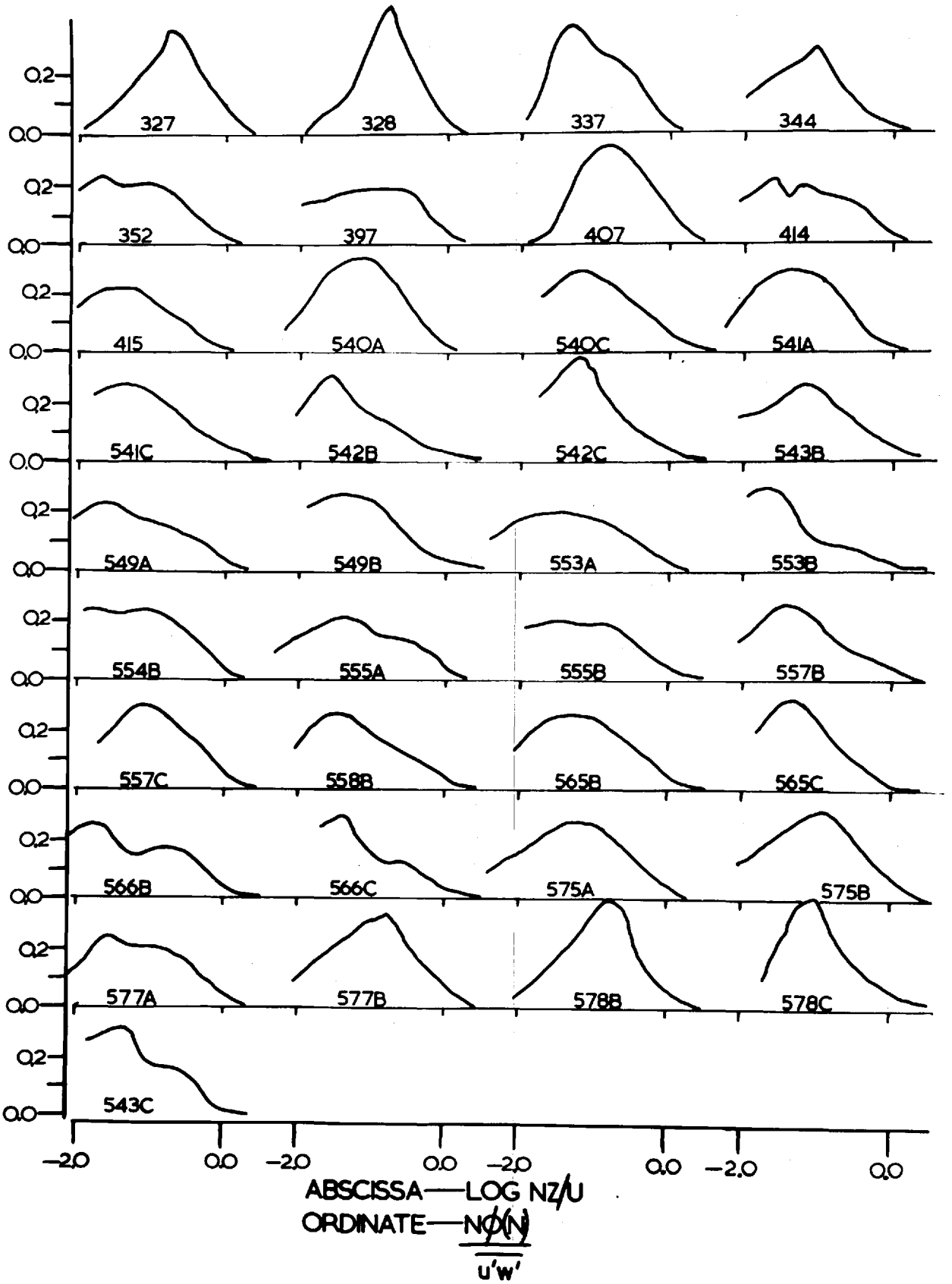

FIG.5.5 WT COSPECTRA (NORMALISED)

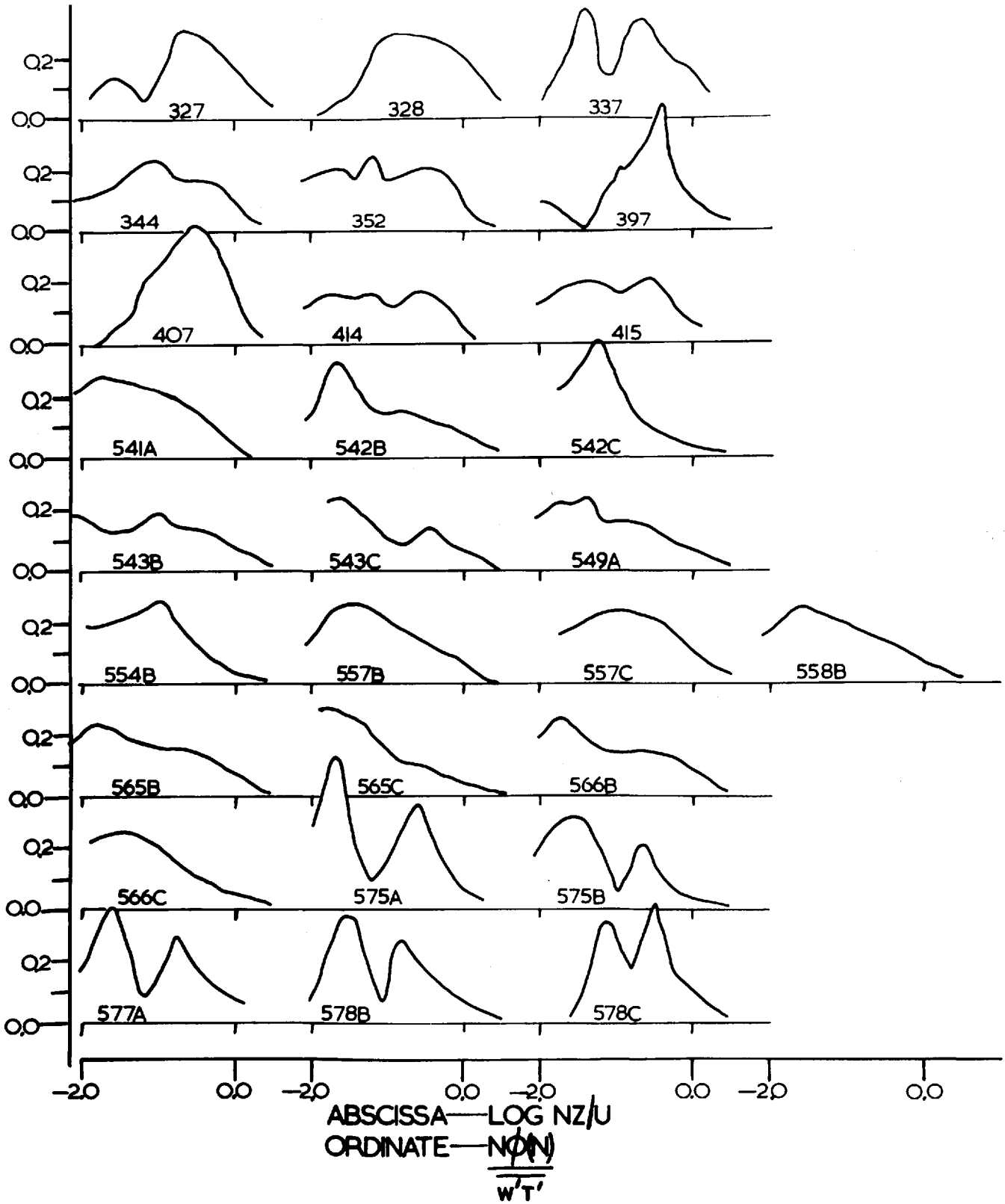

FIG.5.6 U AND T STRUCTURE FUNCTIONS

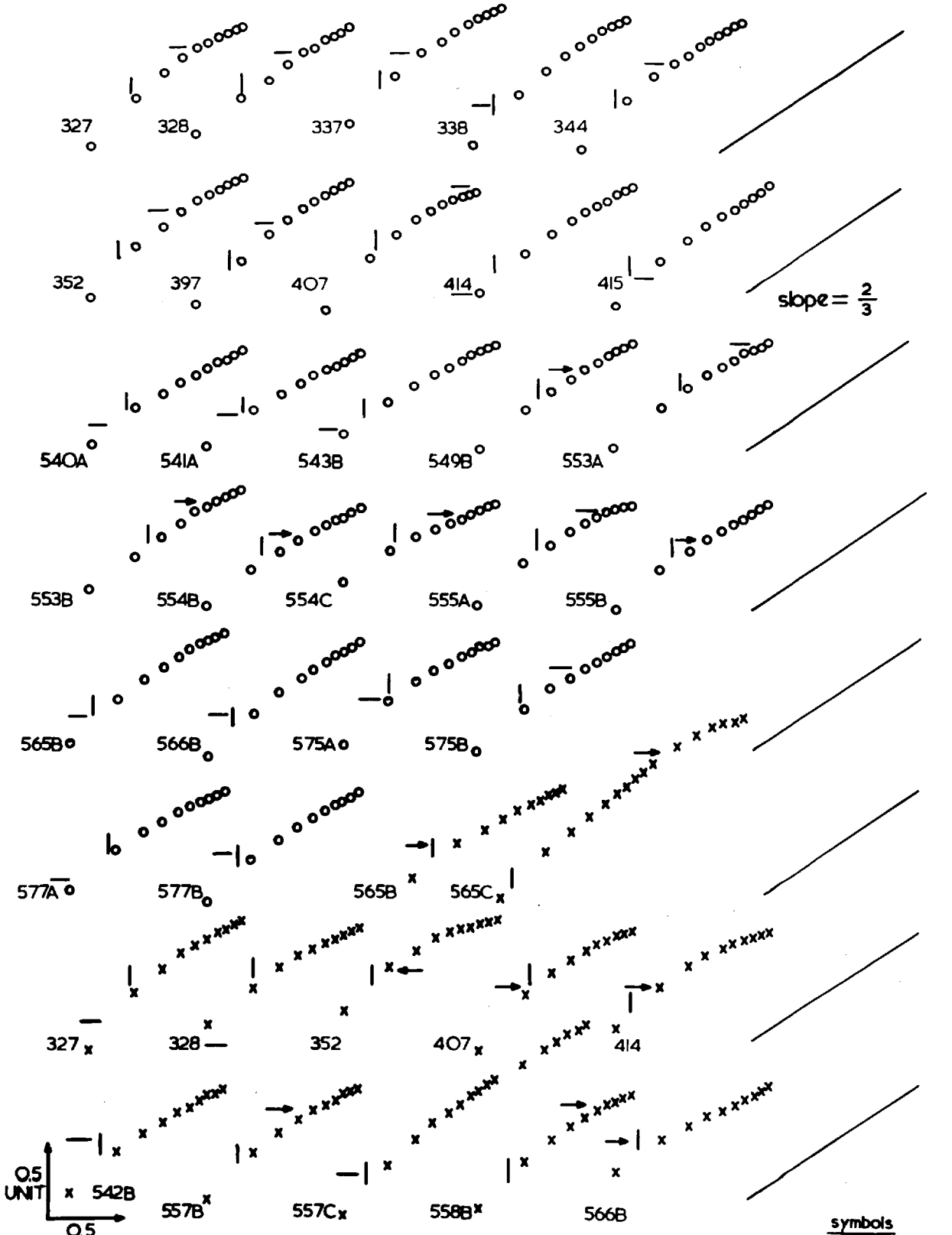

In Fig.5.6 is shown the function $D_u(x)$ vs x for runs where, over a range of x, the relation $D_u(x) \propto x^{2/3}$ is observed (Fig.5.6 also contains $D_T(x)$ whose properties are discussed in § 5.4.1.). For other runs the inertial sub-range does not extend to the observable x values, the minimum x being determined by $\bar{u}$ and $\xi = 0.1$ second. (The curves in Fig.5.6 are those used for the analysis reported in § 4.4. to obtain ε from the lines of slope 2/3.) For the w component the relation $D_w(x) \propto x^{2/3}$ is not observed over an appreciable x range and this is consistent with the restricted k range (observed) for which $\phi_w(k) \propto k^{-5/3}$ and the greater range for which $\phi_u(k) \propto k^{-5/3}$ —see § 5.3.2.

Mean values of $D_u(x) / \sigma_u^2$ are plotted vs x/z in Fig.5.7. as required by equation 5.4 b. Though considerable scatter exists, the effect of Ri in the region where $D/\sigma^2 \propto (x/z)^{2/3}$ is evidently small. The $(x/z)^{2/3}$ relation holds for $x/z < (x/z)_{max} \simeq 2$. At larger values of x/z the slope is significantly smaller than 2/3. The value of $(x/z)_{max}$ suggests a contribution to $D_u(x)$ here from anisotropic eddies since $D_u(x)$ depends mainly upon eddies of size $\sim x$ (§ 1.2.).

The relation $D_u(x) \propto x^p$ with $p \sim 2/3$ and $x_{max} \sim z$ has been observed and reported by Taylor (1955 and 1961) and Tatarskii (1961) in overland conditions at heights from 1 m. to 28 m. Record and Cramer (1966) also report $D_u(x) \propto x^{2/3}$ overland at heights of 15 m. —40 m. with $x_{max} \sim z$. An explanation of the apparent validity of the Kolmogorov relation beyond the inertial sub-range has been given by Gifford (1959) and was discussed in § 1.2.

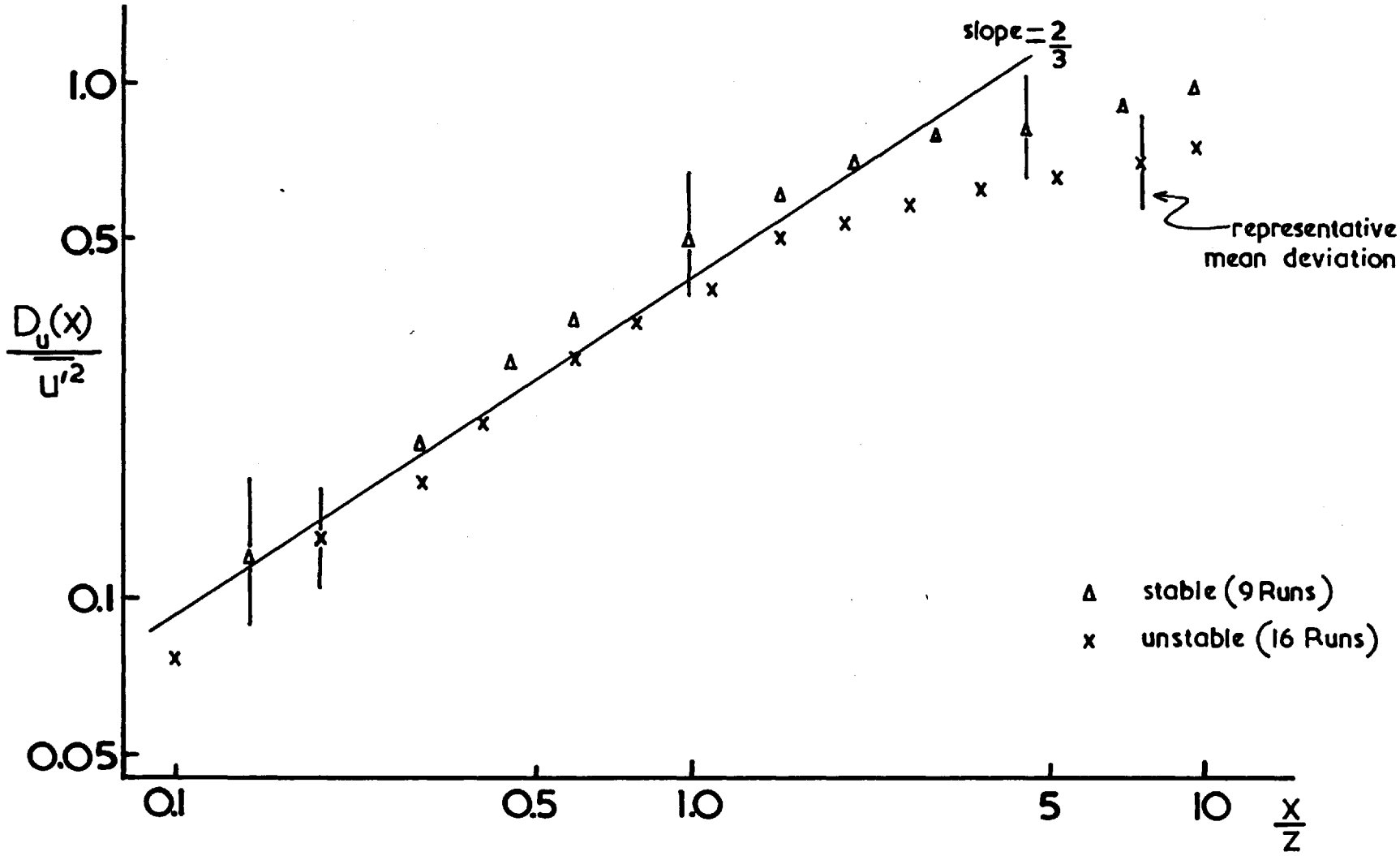
slope = 2/3
1.0
0.5
0.1
0.05
$\frac{D_u(x)}{\overline{u'^2}}$
0.1
0.5
1.0
5
10
$\frac{x}{z}$
representative mean deviation
Δ stable (9 Runs)
x unstable (16 Runs)

FIG. 5.7

5.3.2. Velocity Spectra

Log-log spectra for the u and w components are plotted in Figs.5.1 and 5.2 respectively . Lines of slope -5/3 are inserted for comparison with the spectra, and in the range of k investigated there is generally a region of higher k values in which $\phi(k) \propto k^{-5/3}$, though for some u spectra the slope is less than -5/3 in magnitude. The curves in Figs.5.1, 5.2 were used to estimate ε by drawing a 5/3 line through the high frequency part of the spectra — when the slope was obviously much different to -5/3 the spectra were not used. The results were presented in § 4.4. and 4.5.

Runs were grouped into three Ri ranges (as specified in § 5.2.2.) and $\phi_{u,w}/z\sigma^2_{u,w}$ plotted vs f as required by equation 5.2a. The averaged curves, together with mean deviations, are shown in Figs. 5.8(for u') and 5.9(for w'). The $f^{-5/3}$ domain is apparent for w' as well as u' and the ordinates show little dependence upon Ri. However the lower limit of f ($= f_L$) for which a $f^{-5/3}$ relation is observed does change with Ri as suggested in § 5.2.4. Close examination of Figs.5.8 and 5.9 gives the values f_L for each range of Ri shown in Table 5.1.

Table 5.1 Dependence of f_L upon Ri

Ri	f_L u	f_L w	f_L^{-1} u	f_L^{-1} w
< -0.1	0.3	0.6	3	1.6
-0.1 to 0	0.4	0.8	2.5	1.25
>0	0.5	0.8	2	1.25

The implication is clearly of an extension of the -5/3 law beyond the inertial sub-range enclosing wavelengths several times

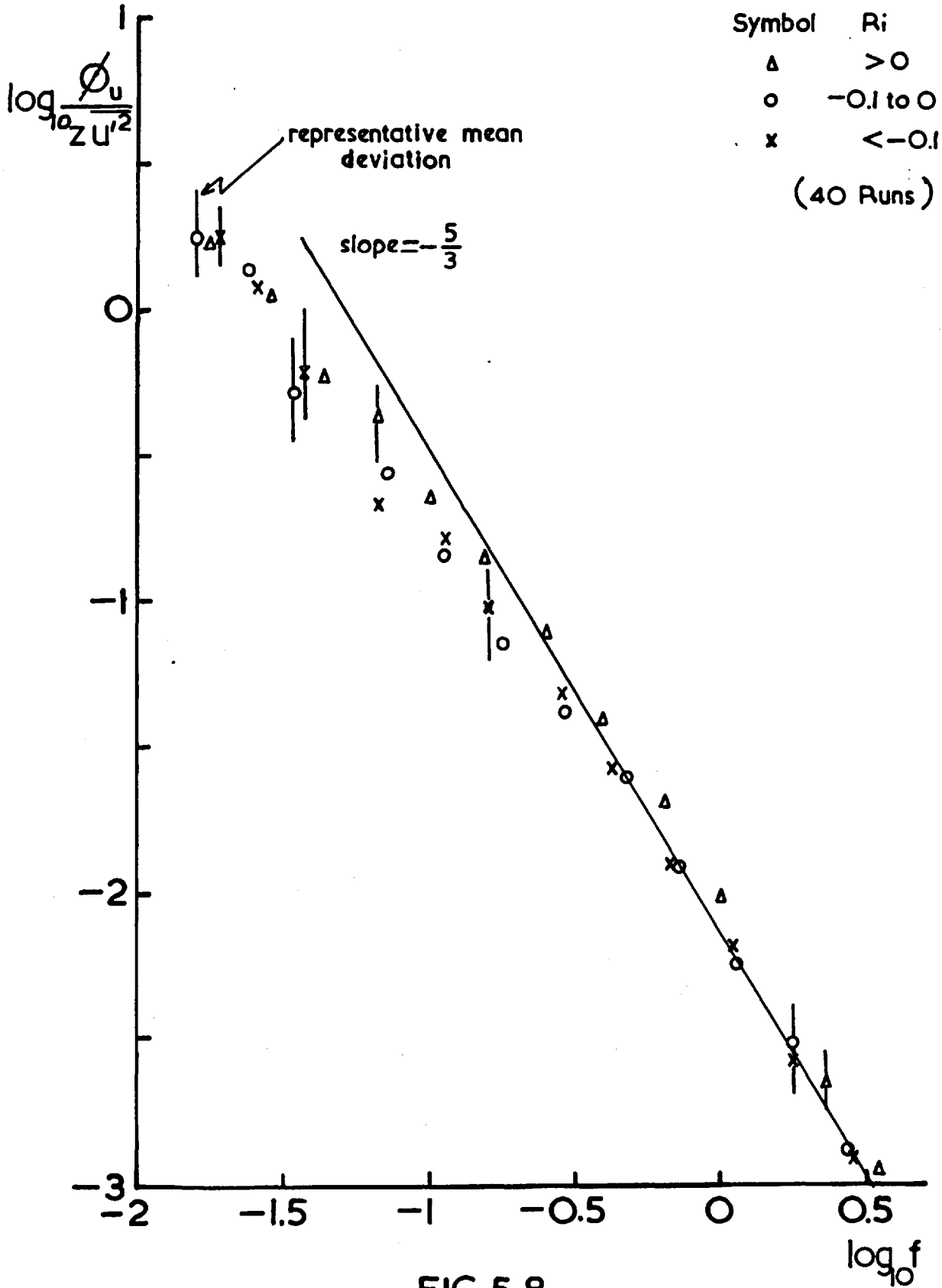
Symbol Ri
Δ >0
o −0.1 to 0
x <−0.1
(40 Runs)
representative mean deviation
slope = −5/3
1
0
−1
−2
−3
−2
−1.5
−1
−0.5
0
0.5
log10 f

FIG.5.8

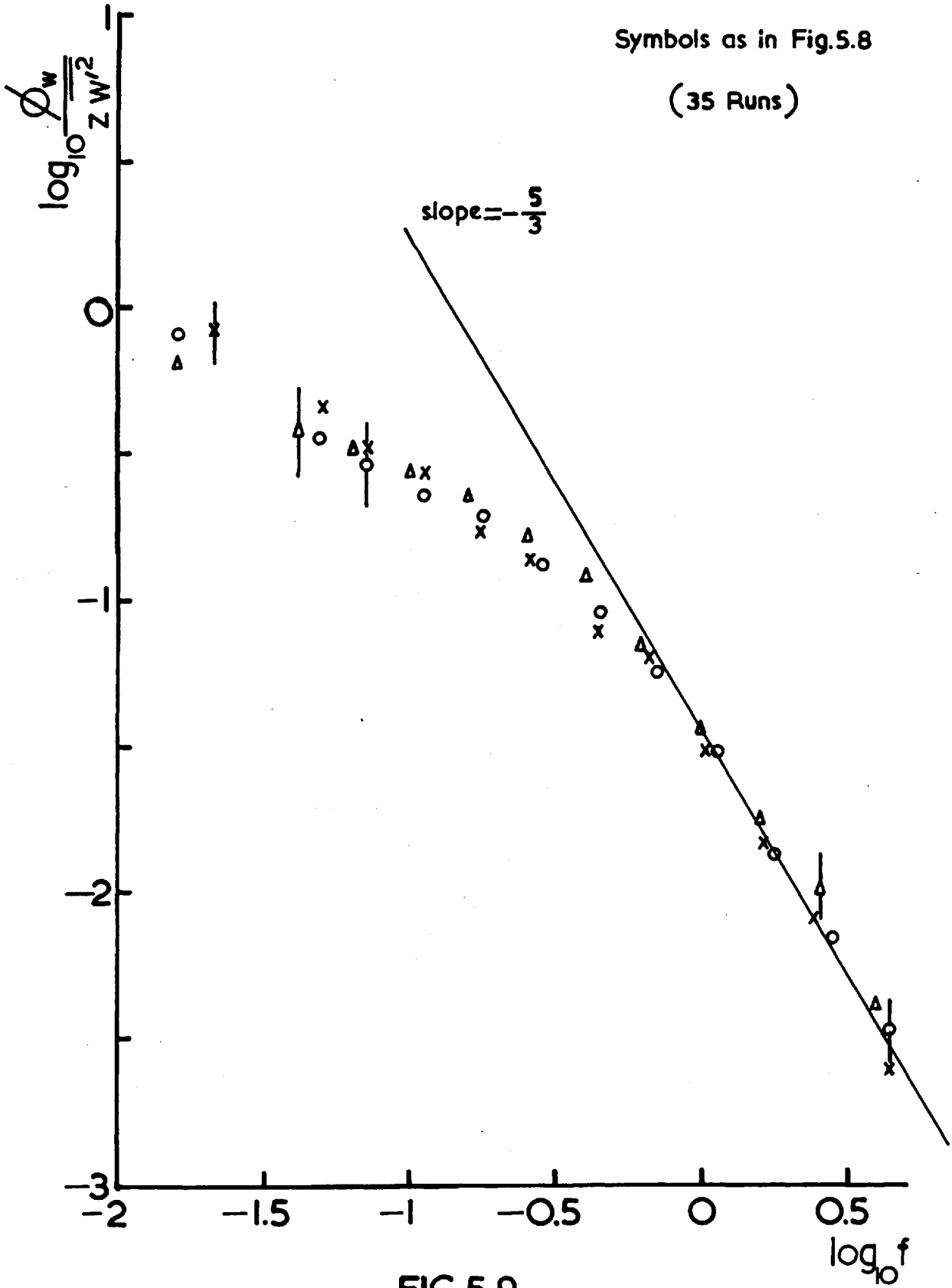
Symbols as in Fig.5.8
(35 Runs)
slope=-5/3
log10 φw / z w'^2
log10 f
1
0
-1
-2
-3
-2
-1.5
-1
-0.5
0
0.5

FIG.5.9

the height of observation. In fact measurement of the spectral correlation coefficient (see § 5.3.5.2.) implies that eddies of size ~z are anisotropic. The larger values of f_L in stable conditions are evidently related to a shift in spectral peak to smaller wavelength and the absence of convective energy (see § 5.3.4.). The magnitudes of f_L quoted in Table 5.1 are consistent with those of Gurvich (1960 a), MacCready (1962) for the w spectrum and Zubkovskii (1962) and Smith (1966) for the u spectrum, though the exact magnitude of the variation of f_L with Ri varies considerably from one author to the other. Note that $\lambda_L \sim x_{max}$ implying that $\phi(k_L)$ and $D(x_{max})$ are determined by eddies of comparable length and time scales as required for an inertial sub-range.

Spectral Densities in the -5/3 range

It is a consequence of Taylor's hypothesis, the assumption of local isotropy, the incompressibility of the flow and the Kolmogorov hypothesis that within the inertial sub-range for the one dimensional velocity spectra,

$$\phi_w(n)/\phi_u(n) = 4/3, \quad \text{and}$$

$$\phi_w(k)/\phi_u(k) = 4/3 \qquad 5.5$$

The equation 5.5 results from application of a Fourier transform to Von Karmen's equation (§ 4.4.2.1.) involving correlation functions and is a necessary but not sufficient condition for the existence of local isotropy. Local isotropy further requires that the

coherence between u' and w' be zero —see § 5.3.5.

The ratio of ϕ_w to ϕ_u in the -5/3 region of the Lough Neagh spectra can be evaluated from the normalised spectra in Figs.5.8, 5.9. Taking $\sigma_u^2/\sigma_w^2 = 3.18 \pm 0.15$ (§ 4.2.1.) the ratio $\phi_w/\phi_u = 1.38 \pm 0.15$ for all Ri. Thus one condition for the existence of locally isotropic turbulence is satisfied.

Experimental evidence for the existence of local isotropy within the surface layer is lacking. However results published by B.P. showed ϕ_w/ϕ_u approached 4/3 when $f_N >> 1$ (they evaluated ϕ_w/ϕ_u at $f = f_N$, the Nyquist frequency, for individual spectra). W.B., over the sea, found for comparable and higher frequencies (with $f_N \simeq 10 - 50$) that ϕ_w/ϕ_u was significantly less than 1.33 ($\simeq 1.0$) though additional evidence in the form of a spectral correlation coefficient suggested the approach to isotropy at much higher frequencies. Even so isotropy was not reached only one decade or less of wave numbers below the dissipation spectrum maximum. Thus, in toto, the results suggest that the value 4/3 is approached at high frequencies, though extensive investigations of inertial sub-range properties will require extensive and well-defined inertial sub-ranges (and hence -5/3 ranges).

5.3.3. Momentum Flux Cospectrum

Normalised uw cospectra are plotted in Fig.5.4. The curves are plotted so that $\int_{n_1}^{n_2} n F(n)\, d(\log_{10} n) = 0.43$ where $n_1 = 1/600$ and $n_2 = 10$ cps. The value of the integral follows from the fact that, over an infinite frequency range, $\int_0^\infty n F(n)\, d(\ln n) = 1$ and in the practical case of a finite range n_1 to n_2 $\int_{n_1}^{n_2} n F(n)\, d(\ln n) = 1$

as prescribed in the computational procedure. The conversion of $\ln n$ to $\log_{10} n$ involves a factor $\log_{10} e = 0.43$ since $\ln n = \log_{10} n / \log_{10} e$.

The most prominent feature is the peak, lying at a lower frequency than the w peak and whose position along the abscissa axis appears to vary considerably. Such behaviour is described in § 5.3.4. Of immediate interest is the high frequency behaviour, best described in an analogous way to the velocity spectra.

For many runs, $\phi_{uw}(k)$ shows large variations with k as k approaches its upper limit, and often changing sign. However smoothed curves generally show a similar power law relation. To investigate this equation 5.1 d can be manipulated to give $\phi_{uw}(k)/z\,u_*^2$ as a function of f and Ri. The normalised cospectral densities were computed for 37 runs, divided into 3 Ri ranges viz. $Ri < -0.10$, $-0.1 < Ri < 0$, $Ri > 0$ and averaged at several values of $\log_{10} k$ for ease of computation over as great a k range as possible. They are plotted in Fig.5.10 against $\log_{10} f$. For $\log_{10} f > -0.7$, the points are well described by a straight line of slope -2 implying

$$\phi_{uw}(k) \propto z\,u_*^2\,f^{-2} .$$

At lower frequencies there is a marked tendency for power to be greater the greater the instability. This is related to the fact that in unstable conditions the transfer is effected, in part, by convective turbulence located at lower frequencies than the mechanical turbulence effecting the transfer, in toto, in stable conditions. This is well illustrated in the cospectra of Fig.5.13

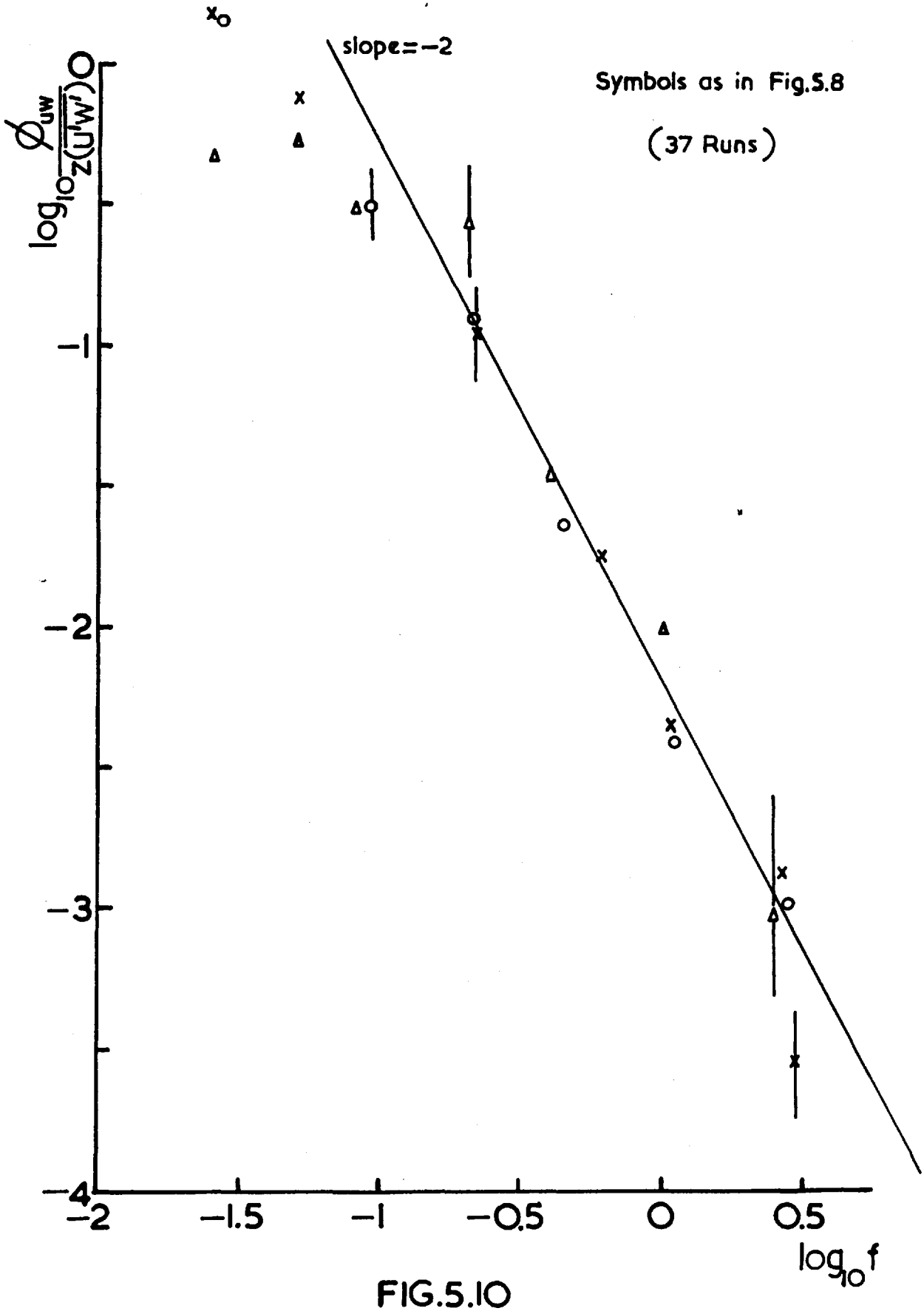
slope=−2
Symbols as in Fig.5.8
(37 Runs)
$\log_{10}\frac{\phi_{uw}}{z(\overline{u'w'})_0}$
−1
−2
−3
−4
−2
−1.5
−1
−0.5
0
0.5
$\log_{10} f$

FIG.5.10

to be described later.

Little previous experimental evidence is available regarding the dependence of ϕ_{uw} upon f at high frequencies; however L.P. (p.188) suggest that, on a theoretical basis, $\phi_{uw}(k)$ should depend upon $k^{-8/3}$, though they refer to data (of unknown source) as not confirming this prediction; nor does Fig.5.10. The f^{-2} dependence observed in Fig.5.10 occurs at values of f where the -5/3 law is obeyed for the velocity spectra. In fact,

$$\phi_{uw} \propto z\sigma_{uw}^2 f^{-2} \quad \text{for} \quad \log_{10} f > -0.7$$

$$\phi_{u} \propto z\sigma_{u}^2 f^{-5/3} \quad \text{for} \quad \log_{10} f > -0.6$$

$$\phi_{w} \propto z\sigma_{w}^2 f^{-5/3} \quad \text{for} \quad \log_{10} f > -0.2$$

The finiteness of ϕ_{uw} implies a small degree of anisotropy in the velocity field; this question of the -5/3 region and the inertial sub-range will be dealt with more fully later in connection with coherence (§ 5.3.5.). It is of some interest to find the relative sizes of the spectral and cospectral densities, by comparing Figs. 5.10 and 5.9, assuming $\sigma_w^2 / u_*^2 = 2.0$ (§ 4.2.1.) giving, for $\log_{10} f = 0$, $\phi_{uw}/\phi_w \simeq 0.1$. The ratio decreases rapidly with increasing f since ϕ_{uw} is decreasing faster than ϕ_w.

5.3.4. Spectra and Cospectra as Functions of Ri

The relation represented by equations 5.1 c, d will now be investigated for u,w spectra and the cospectra covering 2 to 4 Ri ranges as specified in § 5.2.1. The average curves, with

mean deviations, are presented, for u in Fig.5.11, for w in Fig.5.12 and uw in Fig.5.13.

5.3.4.1. u Spectra (Fig.5.11)

In this case only three Ri ranges were chosen. The unstable ($Ri < -0.05$) and neutral ($-0.05 < Ri < 0.05$) are similar in shape having a peak which is discernable through the scatter at $\lambda (= \bar{u}/n) \simeq 60\,z$. For the three very stable runs(Ri between 0.07 and 0.08) the effect of trend upon spectral distribution is most marked. For the run not affected by trend for which $Ri = 0.071$ the implication is that the energy peak is shifted to much higher frequencies in stable conditions, in the case illustrated (Run 407) at $\lambda \simeq 10\,z$. Note that the effect of trends in unstable conditions is much less evident in the spectrum because of the lower frequencies involved when stability damping is not present. The decrease in the ordinate with increase in f is related to the Kolmogorov Laws.

5.3.4.2. w Spectra (Fig.5.12)

The shape of the spectra is similar for all four Ri ranges. The effect of Ri is to shift the whole spectrum towards higher frequency with increase in stability, the scatter for each curve (one only has been drawn through the two sets of points for negative Ri) being sufficiently small to allow them to be distinguished from each other. Again the decrease of the ordinate with increase in f on the high frequency side of the peak relates to the Kolmogorov Laws. The position of the peak evidently depends upon Ri, as suggested in §5.2.4. For unstable and near-neutral spectra the maximum occurs

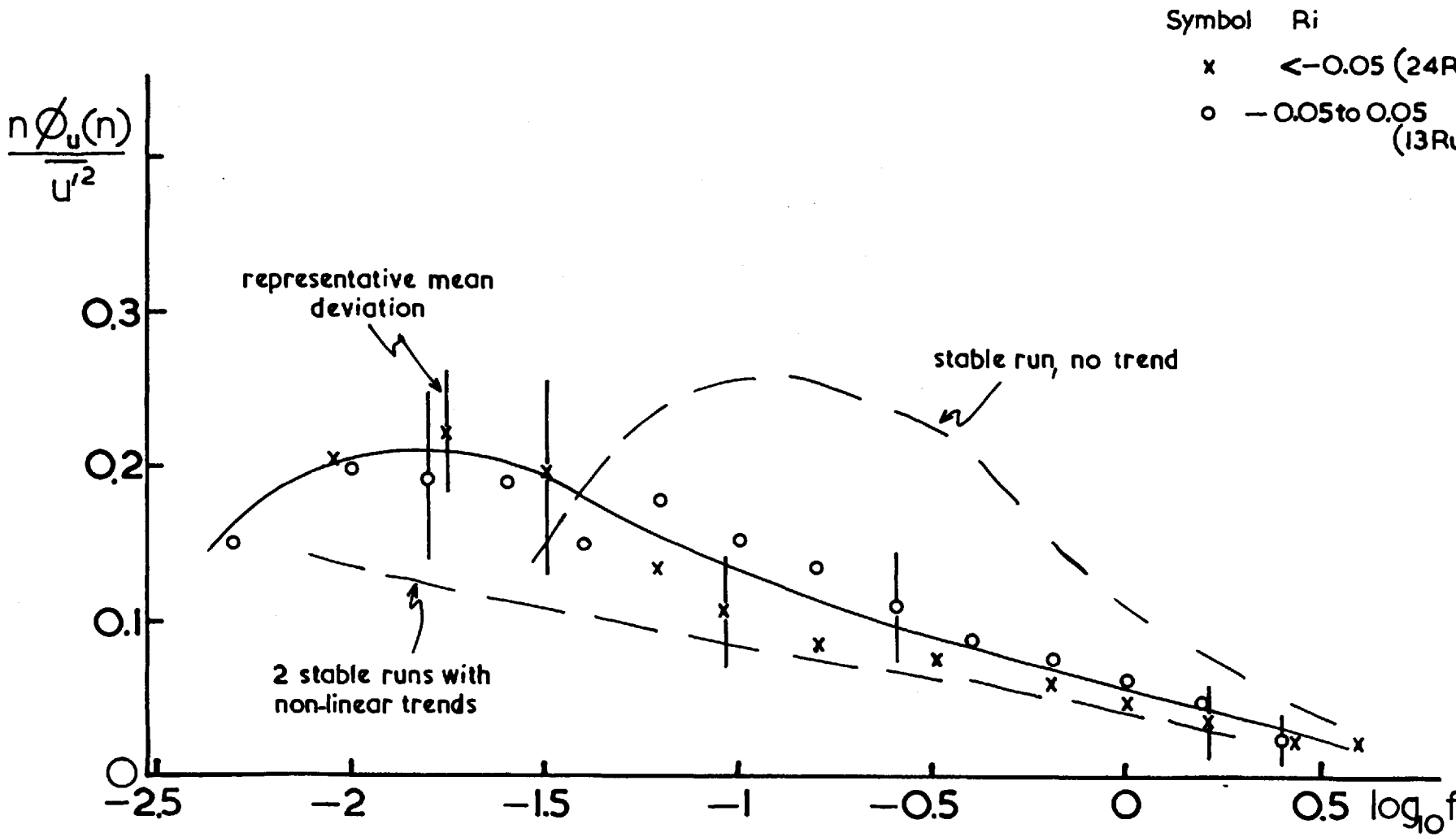
Symbol Ri
x <−0.05 (24 Runs)
o −0.05 to 0.05 (13 Runs)
$\frac{n\phi_u(n)}{\overline{u'^2}}$
representative mean deviation
stable run, no trend
2 stable runs with non-linear trends
0.3
0.2
0.1
0
−2.5
−2
−1.5
−1
−0.5
0
0.5
$\log_{10} f$

FIG.5.11

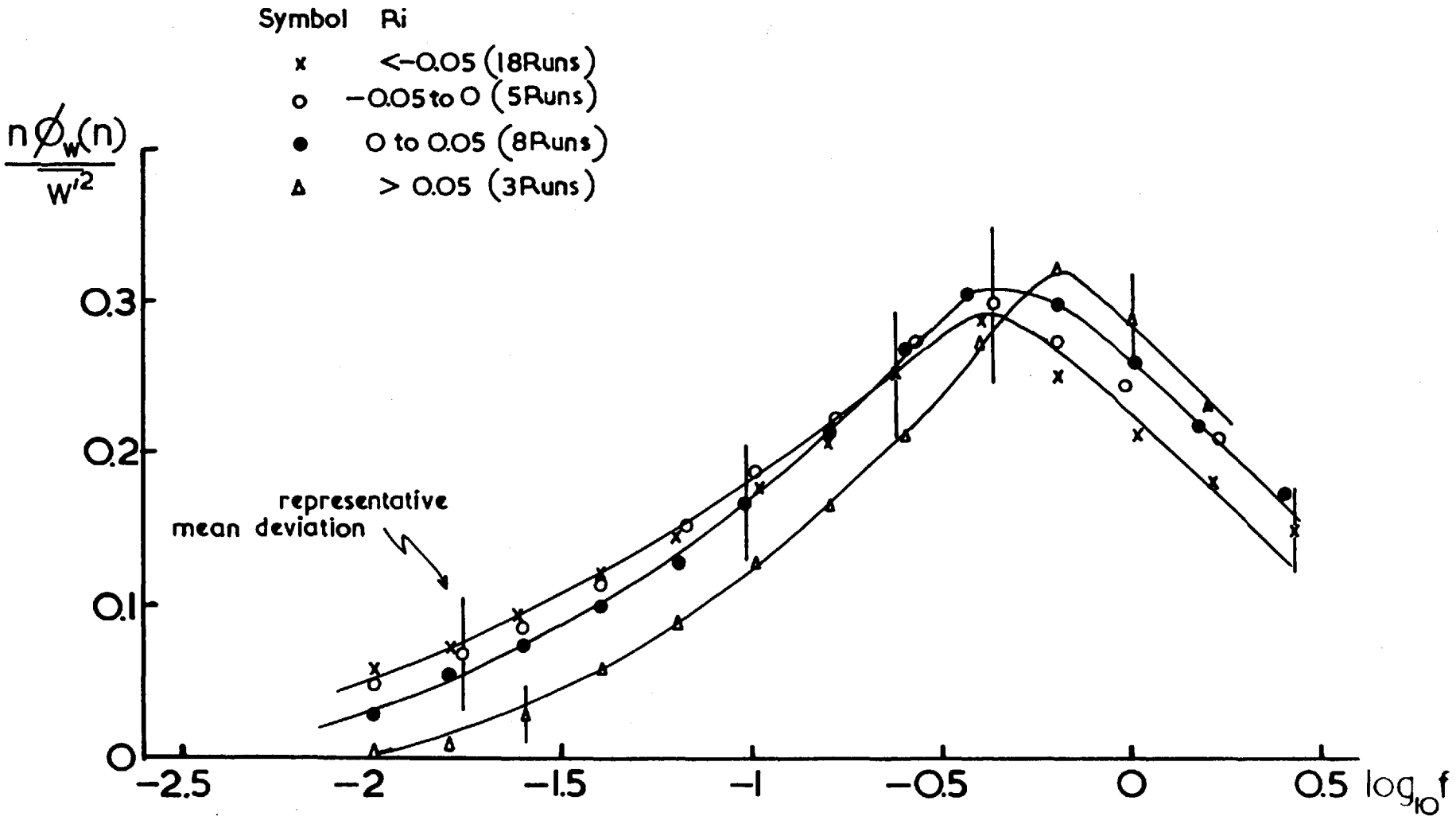
Symbol Ri
x <-0.05 (18Runs)
o -0.05 to 0 (5Runs)
● 0 to 0.05 (8Runs)
△ > 0.05 (3Runs)
$\frac{n\phi_w(n)}{\overline{w'^2}}$
0.3
0.2
0.1
0
representative
mean deviation
−2.5
−2
−1.5
−1
−0.5
0
0.5
$\log_{10} f$

FIG.5.12

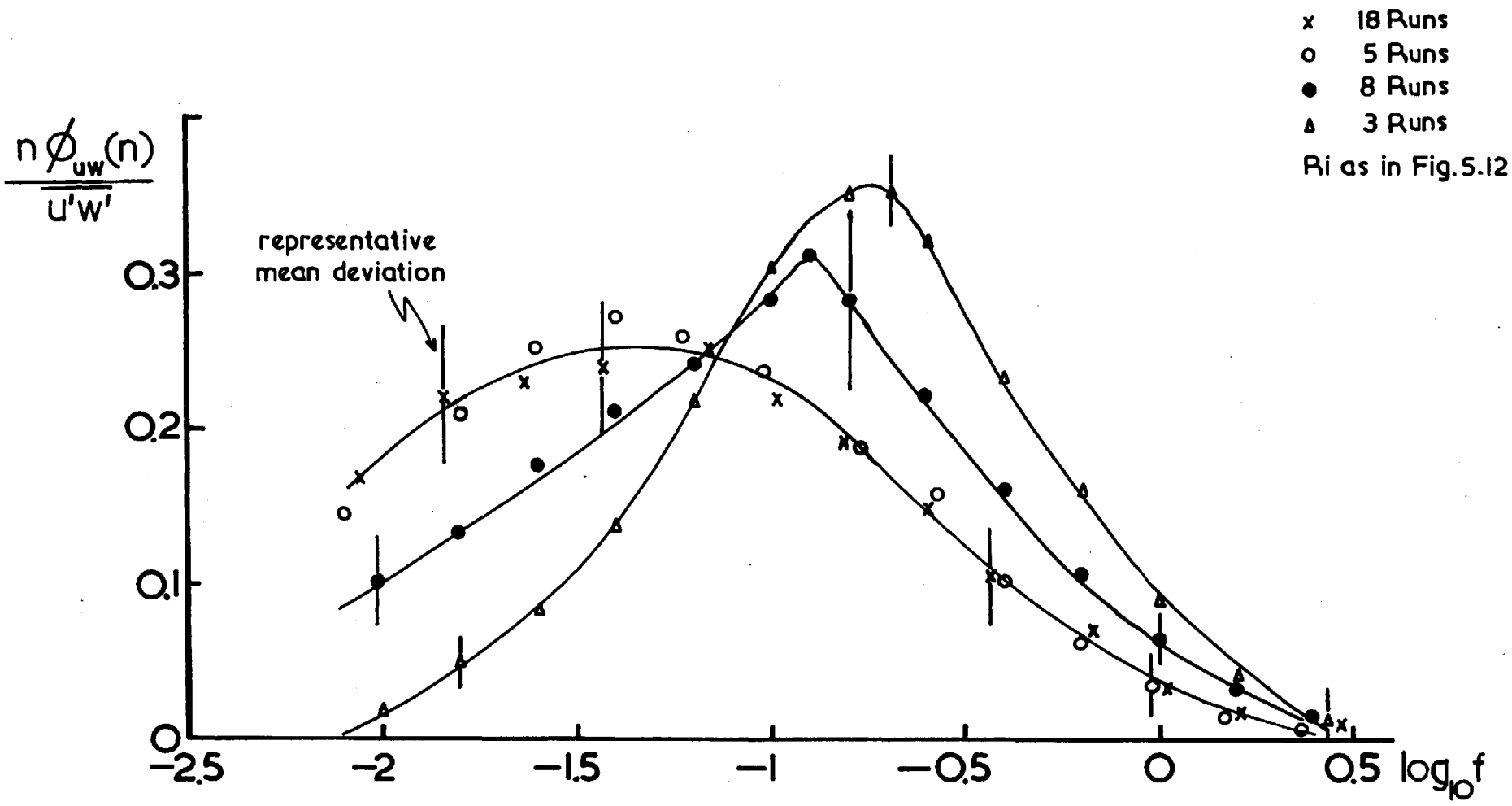
x 18 Runs
o 5 Runs
● 8 Runs
▲ 3 Runs
Ri as in Fig. 5.12
$\frac{n\phi_{uw}(n)}{\overline{u'w'}}$
representative mean deviation
0.3
0.2
0.1
0
−2.5
−2
−1.5
−1
−0.5
0
0.5
$\log_{10} f$

FIG. 5.13

at $\lambda_m = 2.5\,z$ and for stable spectra $\lambda_m = 1.6\,z$. This shift of λ_m with Ri is in the same direction as for the u component though of much smaller magnitude, the latter evidently due to the suppression of vertical turbulence at scales much greater than the height due to the proximity of the boundary. (Hence the larger eddies have scales greater in the horizontal than in the vertical, a reflection of the anisotropic nature of the turbulence.)

5.3.4.3. uw Cospectrum (Figs.5.13, 5.14)

The shape and position of the curves vary considerably with Ri, being almost constant when Ri is negative and showing considerable variation when Ri is positive. The peaks lie between those for the u and w spectra such that in unstable conditions $\lambda_m = 25\,z$, for slight stable conditions $\lambda_m = 8\,z$ and most stable ($Ri \simeq 0.08$) $\lambda_m = 5.5\,z$, a translation similar to that of the spectra. Fig.5.14 shows the variation of f_m with Ri for individual runs. The near-constancy of f_m for negative Ri with a rapid increase for positive Ri is a feature observed by P.M. for cospectra overland.

5.3.5. Coherence

This quantity was defined in § 2.2.4. through equation 2.19. It involves the cospectrum $\phi_{uw}(n)$ and quadrature spectrum $Q_{uw}(n)$ of u and w thus taking into account the correlation in amplitude and phase of the Fourier components of the fluctuations. The coherence can be divided into two parts (cf equation 2.19), viz.,

$$Coh\,(n) = \frac{\phi_{uw}(n)}{(\phi_u \phi_w)^{1/2}} + i\,\frac{Q_{uw}(n)}{(\phi_u \phi_w)^{1/2}} \qquad 5.6\,a$$

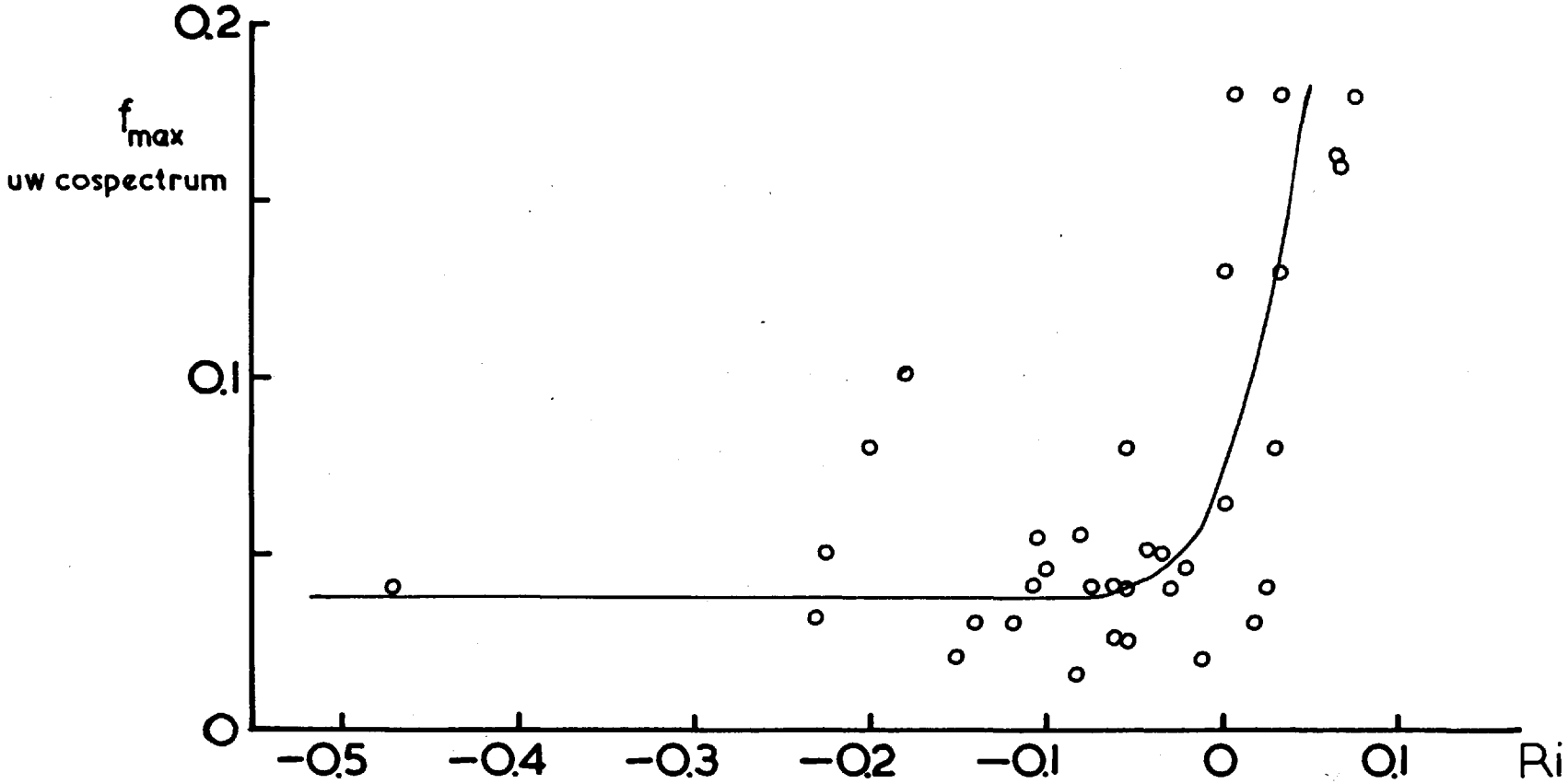

FIG. 5.14

or,
$$Coh(n)^2 = \frac{\phi_{uw}(n)^2}{\phi_u(n)\,\phi_w(n)} + \frac{Q_{uw}(n)^2}{\phi_u(n)\,\phi_w(n)} \qquad 5.6$$

5.3.5.1. The Quadrature Spectrum

A few estimates of the quadrature spectrum Q_{uw} were made on the basis of equation 2.17 described in § 2.2.4. chiefly to find its size relative to the cospectrum and hence its relative contribution to the coherence. Examples of the quadrature spectra (together with their corresponding cospectra) are shown in Fig.5.15. The spectra have been smoothed to a small degree at the high frequency end to reduce the characteristic scatter present in such measurements. In general $Q_{uw}(n)^2 << \phi_{uw}(n)^2$ at low frequencies where the ϕ_{uw} peak is observed but at higher frequencies $Q_{uw}(n)^2$ is often comparable with $\phi_{uw}(n)^2$. Measurements by Smith (1966) a few metres above the sea showed a negligible quadrature spectrum up to $n = 8$ cps though even here one could argue that the cospectrum has fallen to such a small value that $Q_{uw}(n)^2 \sim \phi_{uw}(n)^2$.

Regarding the Lough Neagh measurements it will be taken that the spectral correlation coefficient, in the range of frequencies investigated, is a good measure of the coherence with a possible underestimation at high frequencies.

An investigation of eddy structure using quadrature spectra is not being attempted because the latter show no consistent behaviour as regards Ri or z dependence.

5.3.5.2. The Spectral Correlation Coefficient

Fig.5.16 shows, for four Ri ranges ($Ri < -0.05$, $-0.05 < Ri < 0$, $0 < Ri < 0.05$, $Ri > 0.05$), average curves of correlation $R_{uw}(n)$ vs

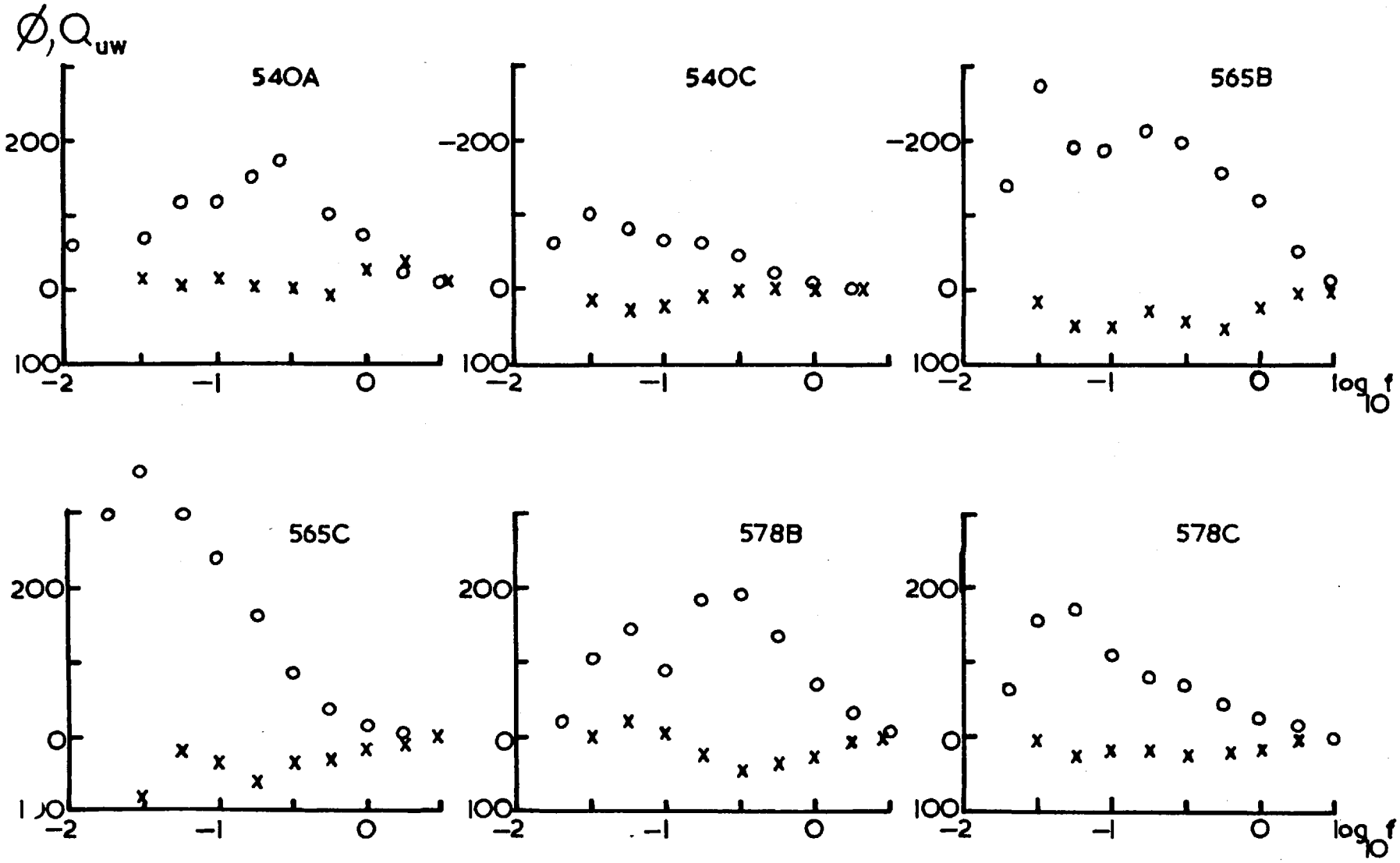
Ø, Q uw
540A
540C
565B
565C
578B
578C
200
0
100
−200
−2
−1
0
log 10 f
o cospectrum
x quadrature spectrum

FIG. 5.15

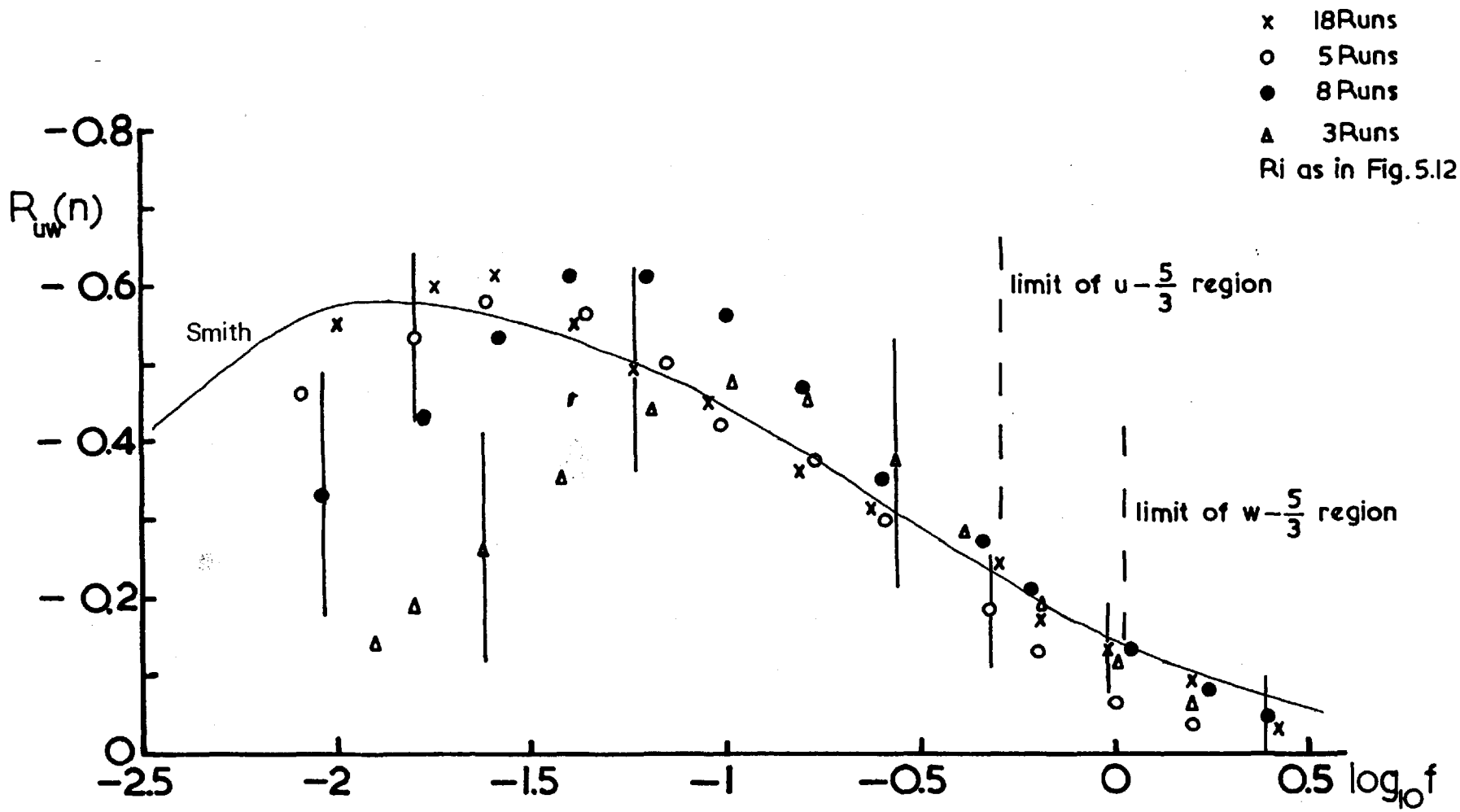
x 18Runs
o 5Runs
● 8Runs
Δ 3Runs
Ri as in Fig. 5.12
$R_{uw}(n)$
−0.8
−0.6
−0.4
−0.2
0
Smith
limit of $u-\frac{5}{3}$ region
limit of $w-\frac{5}{3}$ region
−2.5
−2
−1.5
−1
−0.5
0
0.5
$\log_{10} f$

FIG. 5.16

$\log_{10} f$ together with mean deviations. Sufficient scatter exists (being greatest at low frequencies) to suggest that other factors are important in determining $R_{uw}(n)$. A part of the scatter at low frequencies (similarly observed by W.B.) is due to the small value of $\phi_w(n)$ which approaches zero as the frequency decreases much faster than both $\phi_u(n)$ and $\phi_{uw}(n)$.

The shape of the curves depends considerably upon Ri, the peaks themselves approximately coinciding with the cospectral peaks. A main feature of the curves is the increase in correlation with increase in instability accompanied by a shift of the peak to lower frequencies. This suggests the existence of significant correlation at much lower frequencies and may be important in the choice of sampling period though these eddies may contribute little to the momentum flux because of the absence of vertical energy. An analogous (average) curve from data presented by Smith and W.B. is included in Fig.5.16. There is remarkably good agreement with the Lough Neagh data, the Vancouver curve being for Ri small and negative.

The second important feature of Fig.5.16 is the decrease of $R_{uw}(n)$ as f tends to its upper limit, for all Ri. A decrease of the coherence towards zero implies an approach to locally isotropic turbulence (at high frequencies) or absence of fluctuation energy (at low frequencies). The finiteness of R_{uw} at the upper limit of f (indeed it will be larger because of the quadrature contribution), together with the overlap with the -5/3 regions of the velocity spectra (lower limits indicated in the diagram) implies that, even though ϕ_w / ϕ_u was found to be consistent with isotropy,

nevertheless the observed -5/3 regions lie in an anisotropic turbulence field, as indeed is implied by $f_L < 1$.

5.3.6. Comparison with Other Results

Measurements of spectra and cospectra, both overland and over the sea, have been made by several authors in enough detail for them to be compared with the Lough Neagh curves in Similarity coordinates. Of particular value are those collected together by B.P. and P.M. —they are all Western data. Spectral data for the surface layer from the U.S.S.R. are often not accompanied by parameters required for the evaluation of the Similarity coordinates, but are valuable regarding a qualitative description of spectral characteristics.

In reducing all the spectra to the same coordinates viz. $n\phi(n)\sigma^{-2}$ vs $\log_{10} f$ use had to be made of the relation between $\sigma^2_{u,w}$ and u_*^2. § 4.2. indicates the use of $\sigma_w^2 / u_*^2 = 1.7$ and $\sigma_u^2 / u_*^2 = 6.0$ as mean observed values for several sites.

Attempts have been made in the past to represent spectra and cospectra with well-defined maxima, and obeying the Similarity Theory, by semi-empirical formulae based, initially, upon an exponential correlation function. The Fourier transform readily gives a spectrum, in terms of f say,

$$\frac{n\phi(n)}{\sigma^2} = \frac{\alpha f}{1 + \beta f^2} \qquad 5.7$$

To make the maximum dependent upon stability, and the spectrum $\phi(n)$ to depend upon $f^{-5/3}$ at high frequencies 5.7 is modified to,

$$\frac{n\phi(n)}{\sigma^2} = \frac{\alpha(f/f_m)}{1+\beta(f/f_m)^{5/3}} \qquad 5.8$$

with f_m varying with Ri. The constants α and β depend (a) upon the value of the ordinate when $f = f_m$, (b) upon the Kolmogorov relation when $f >> f_m$. The definition of $\phi(n)$ requires that the integral of the right hand side of 5.8 be equal to unity, and provides a test of the internal consistency of the formula.

5.3.6.1. u Spectrum (unstable)

Fig.5.17 shows normalised u spectra for 4 sites, including Lough Neagh. The inequality of the areas under the curves is the result of taking $\sigma_u^2 = 6u_*^2$, because as § 4.2. showed the relation may depend upon a factor varying from site to site (large-scale terrain factor). Consequently there is some uncertainty in the vertical position of each set of points. The smooth curves have been drawn by eye.

One important feature of the diagram is the relative positions of the peaks, viz. $\lambda_m = 100z$ for Vancouver (observations between 1.5m. and 4m. over the sea), $60z$ for Lough Neagh (2m. to 12m.), $45z$ for Hanford (3m. to 6m. over desert) and $30z$ for Round Hill (15m. to 40m. over 'rough' terrain). In addition Berman (1965) found that, for neutral conditions overland, $\lambda_m = 100z$ when $z = 2$m. and $\lambda_m = 4z$ when $z = 153$m. The variation in f_m is possibly due to the variation in the heights of observation, f_m increasing as z increases. Such a variation implies that the low frequency region of the u spectrum does not obey Similarity principles which require f_m to be invariant with height.

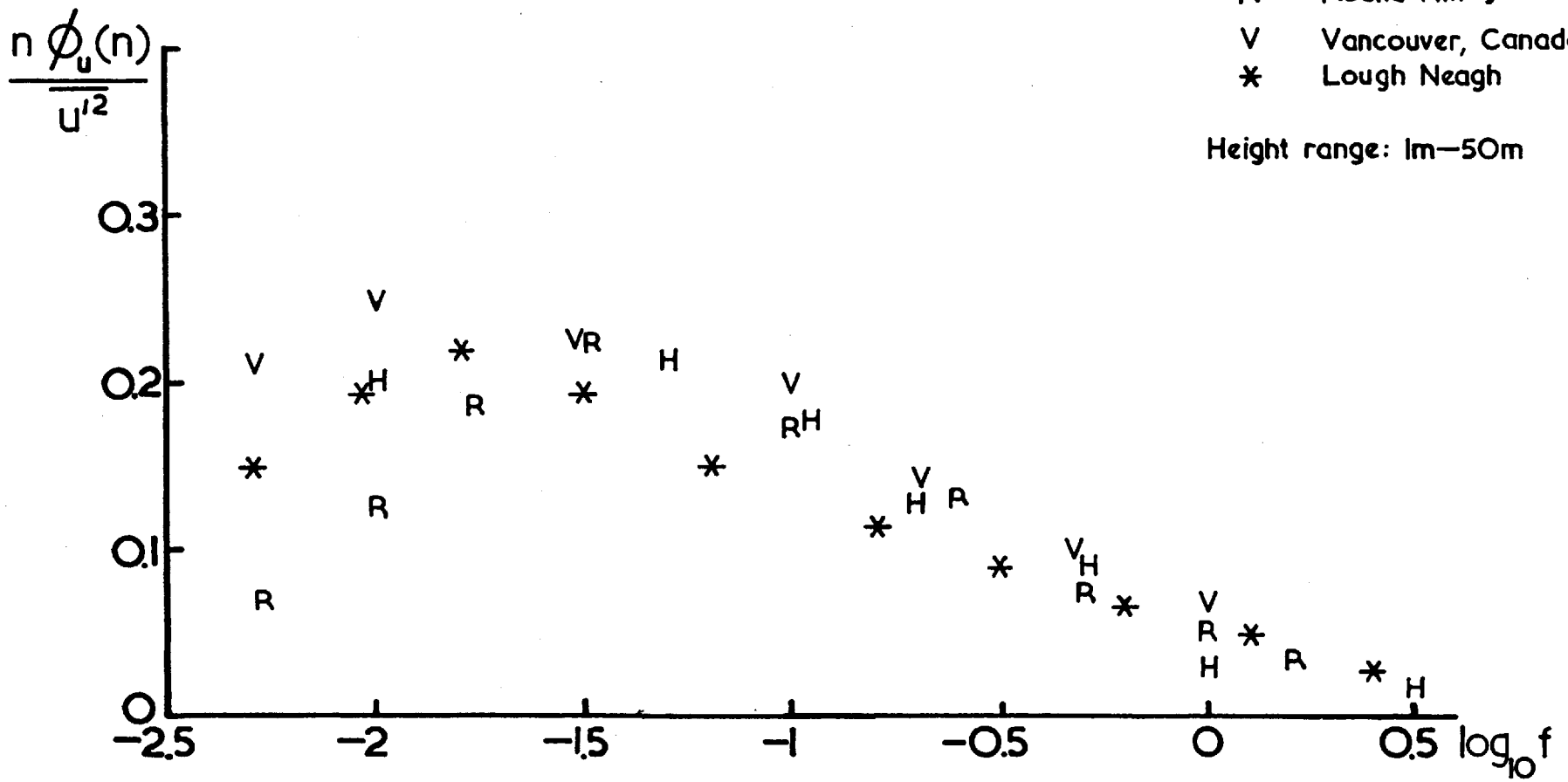

U Spectra in unstable and neutral air

FIG. 5.17

The scatter in the Lough Neagh data for negative Ri obscures evidence of the variation of f_m with height for the individual runs.

5.3.6.2. w Spectrum

Fig.5.18 shows normalised w spectra for 5 sites in unstable conditions, together with the position of the peak observed by Gurvich (1960 a) for Ri = -0.76. There is sufficiently small scatter to indicate a Universal form to the spectrum for Ri < -0.05 —the height range covered being from 1 m. to about 100 m. and there is a moderately good fit with the curve

$$\frac{n\phi_w(n)}{\overline{w'^2}} = \frac{0.68(f/f_m)}{1 + 1.5(f/f_m)^{5/3}} \qquad 5.9$$

with $\log_{10} f_m = -0.45$. Similarly Fig.5.19 shows data for stable conditions and covering a similar height range. Apart from the anomalous Hanford data (which appear to exaggerate the mid-frequency contributions) the data fit the relation,

$$\frac{n\phi_w(n)}{\overline{w'^2}} = \frac{0.75(f/f_m)}{1 + 1.5(f/f_m)^{5/3}} \qquad 5.10$$

with $\log_{10} f_m = -0.2$.

The above results slightly modify those of B.P. who used a similar relation but found the 'constant' in the numerator to be independent of Ri. Because of the small variation observed in Figs. 5.18, 5.19 the difference is not thought to be significant. Finally integration of the above relations yields a value of unity to within 5 - 10 per cent.

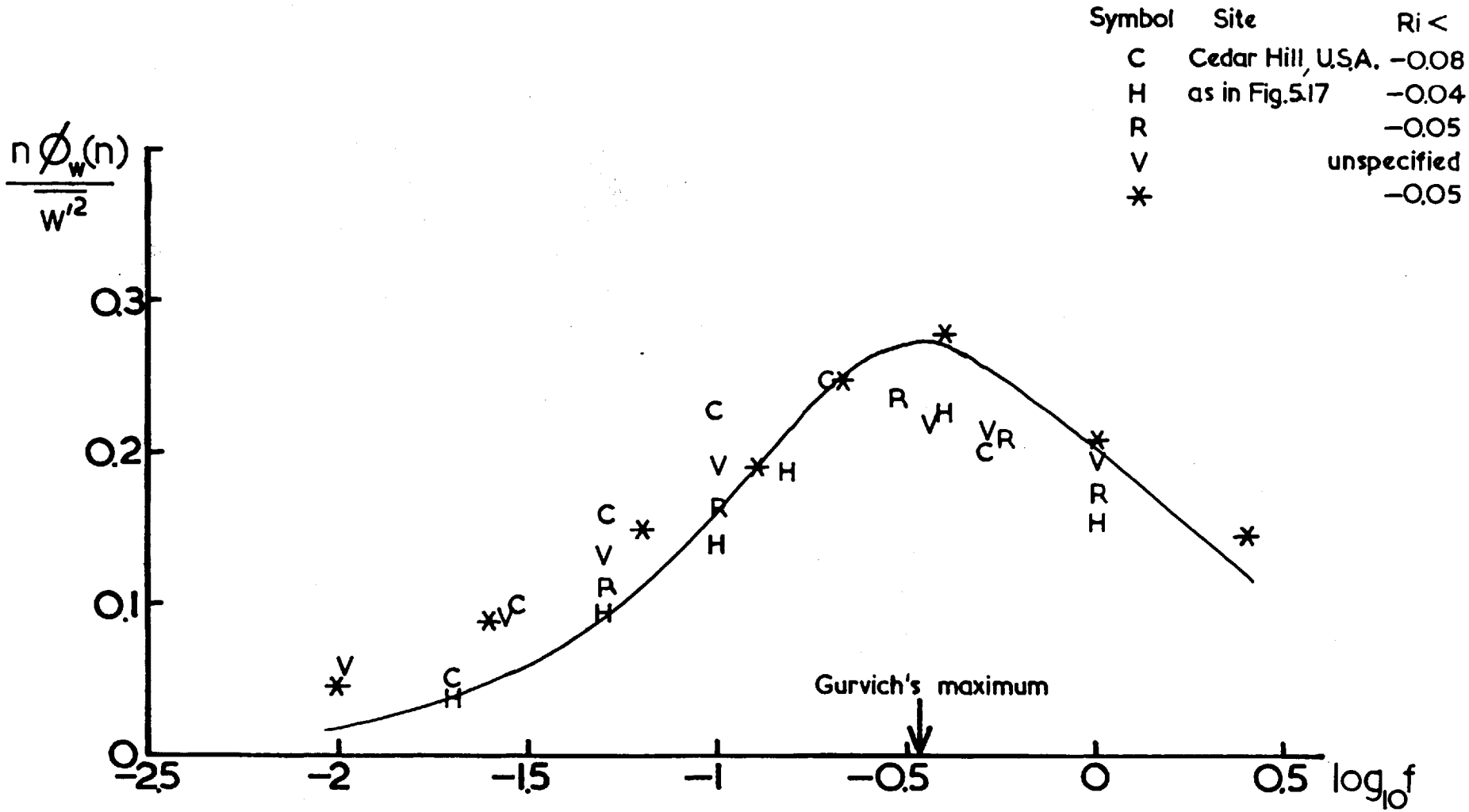

W spectra in unstable air

FIG.5.18

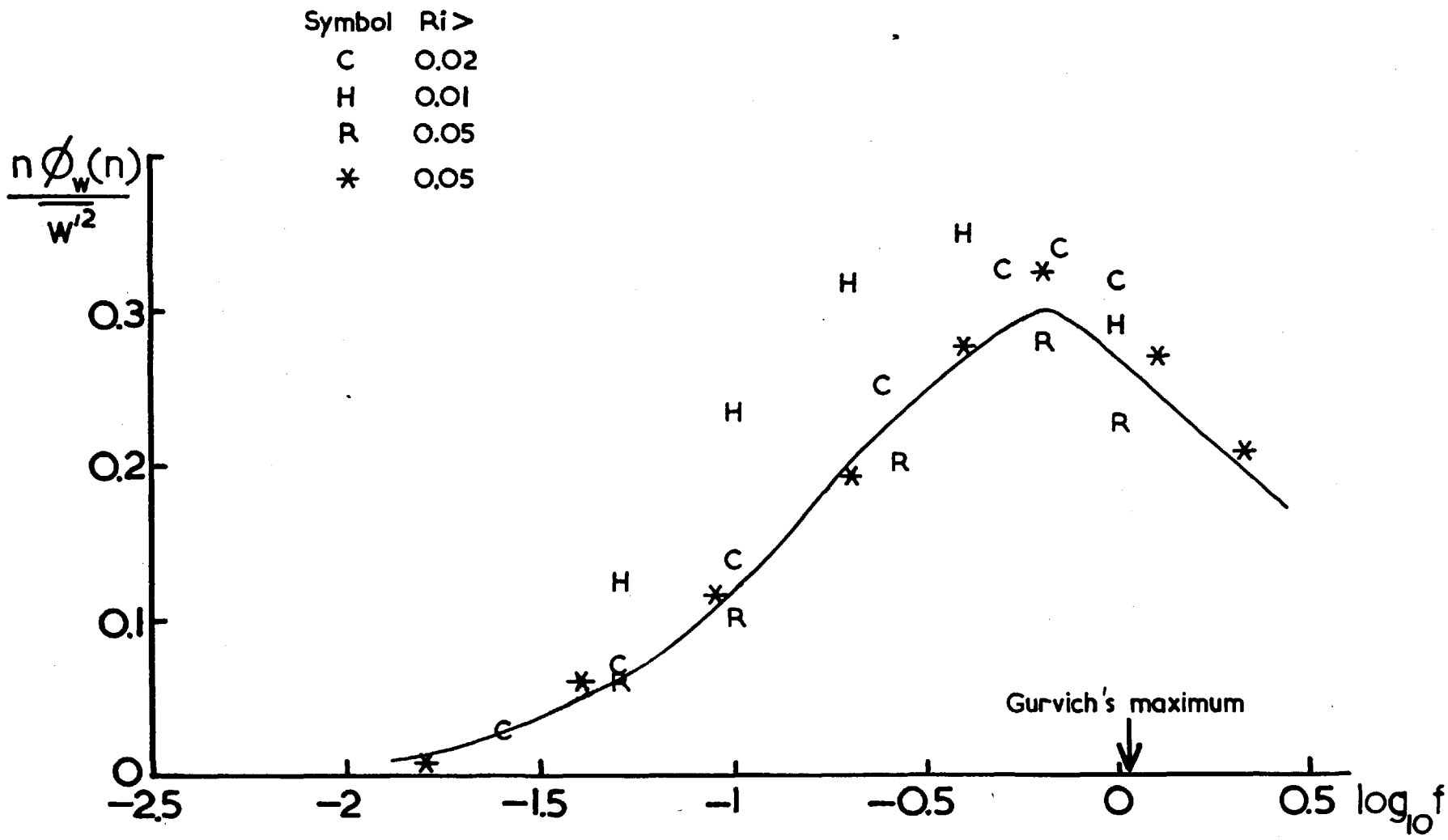

W spectra in stable air

FIG.5.19

5.3.6.3. uw Cospectrum

Fig.5.20 shows normalised uw cospectra for 4 sites in unstable conditions. The total height range covered is from 2m. to 90m. approximately. In the diagram is shown the curve represented by the relation,

$$-\frac{n\phi_{uw}(n)}{u_*^2} = \frac{0.45(f/f_m)}{1+0.6(f/f_m)^2} \qquad 5.11$$

with $\log_{10} f_m = -1.3$. It can be seen that the fit is tolerable except at low frequencies where 5.11 underestimates the contributions. Similarly Fig.5.21 shows data for stable conditions and as with the w spectra for Ri positive the Hanford data is anomalous, in this case shifted relative to the others to lower frequencies. The data can be represented by the relation,

$$-\frac{n\phi_{uw}(n)}{u_*^2} = \frac{0.48(f/f_m)}{1+0.6(f/f_m)^2} \qquad 5.12$$

with $\log_{10} f_m = -0.9$. Also shown in Fig.5.20 is the position of the peak found by Gurvich (1961) which is not inconsistent with the choice of $\log_{10} f_m = -1.3$. The empirical relations used to represent the cospectra differ from those proposed by P.M. in one important respect. viz. for $f >> f_m$ relations 5.11 and 5.12 reduce to $\phi_{uw}(n) \propto u_*^2 f^{-2}$ consistent with earlier results (cf § 5.3.3.) and appear to fit the heterogeneous data presented in Figs.5.20, 5.21 remarkably well at high frequencies. P.M. rather had $\phi_{uw}(n) \propto u_*^2 f^{-8/3}$ which does not fit the data as well. In addition the constant in the numerator varies slightly with Ri for a best fit of the observations.

Finally integration of the above relations yields a value of unity to within 5 per cent.

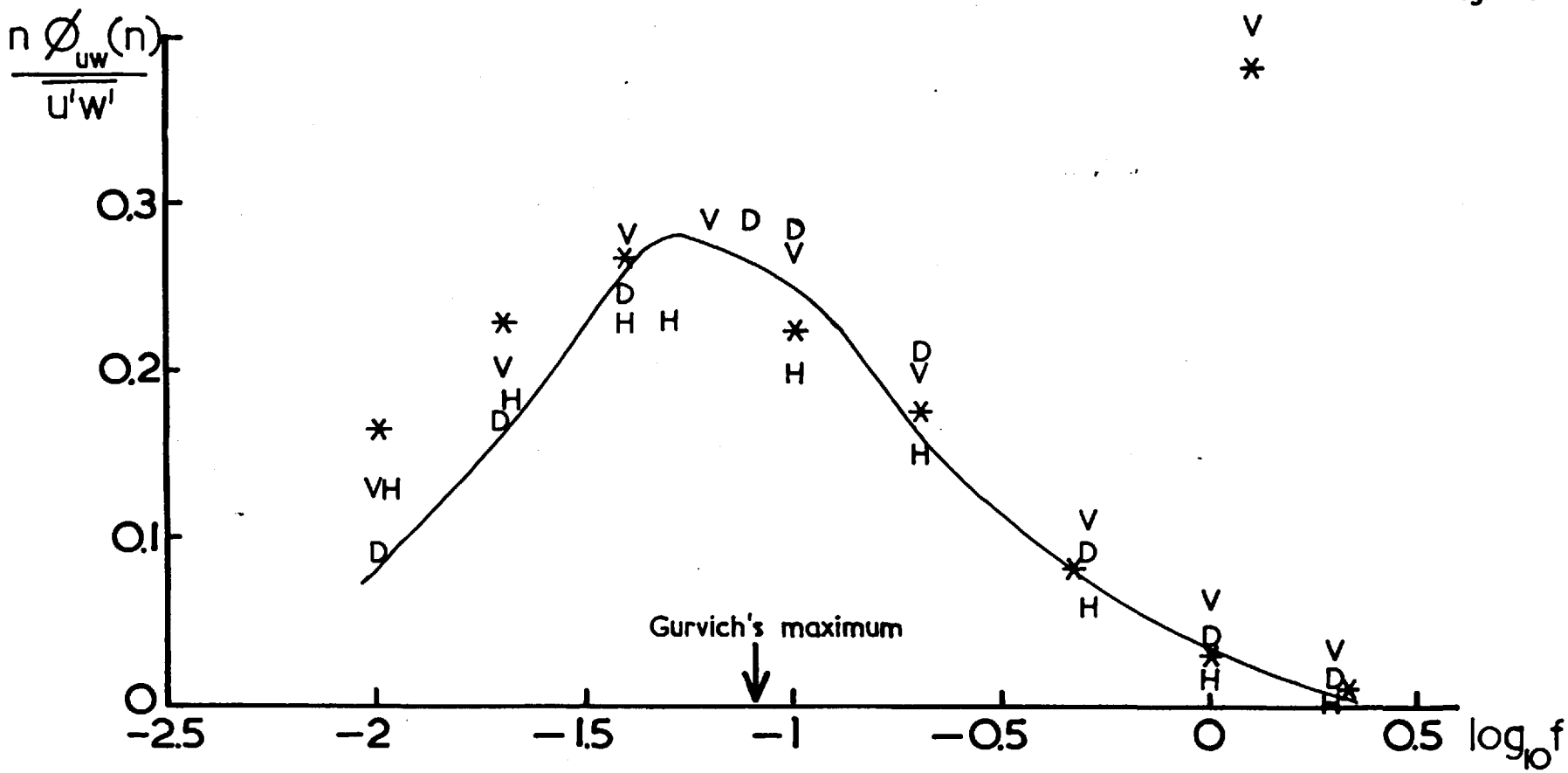

UW cospectra in unstable air

FIG. 5.20

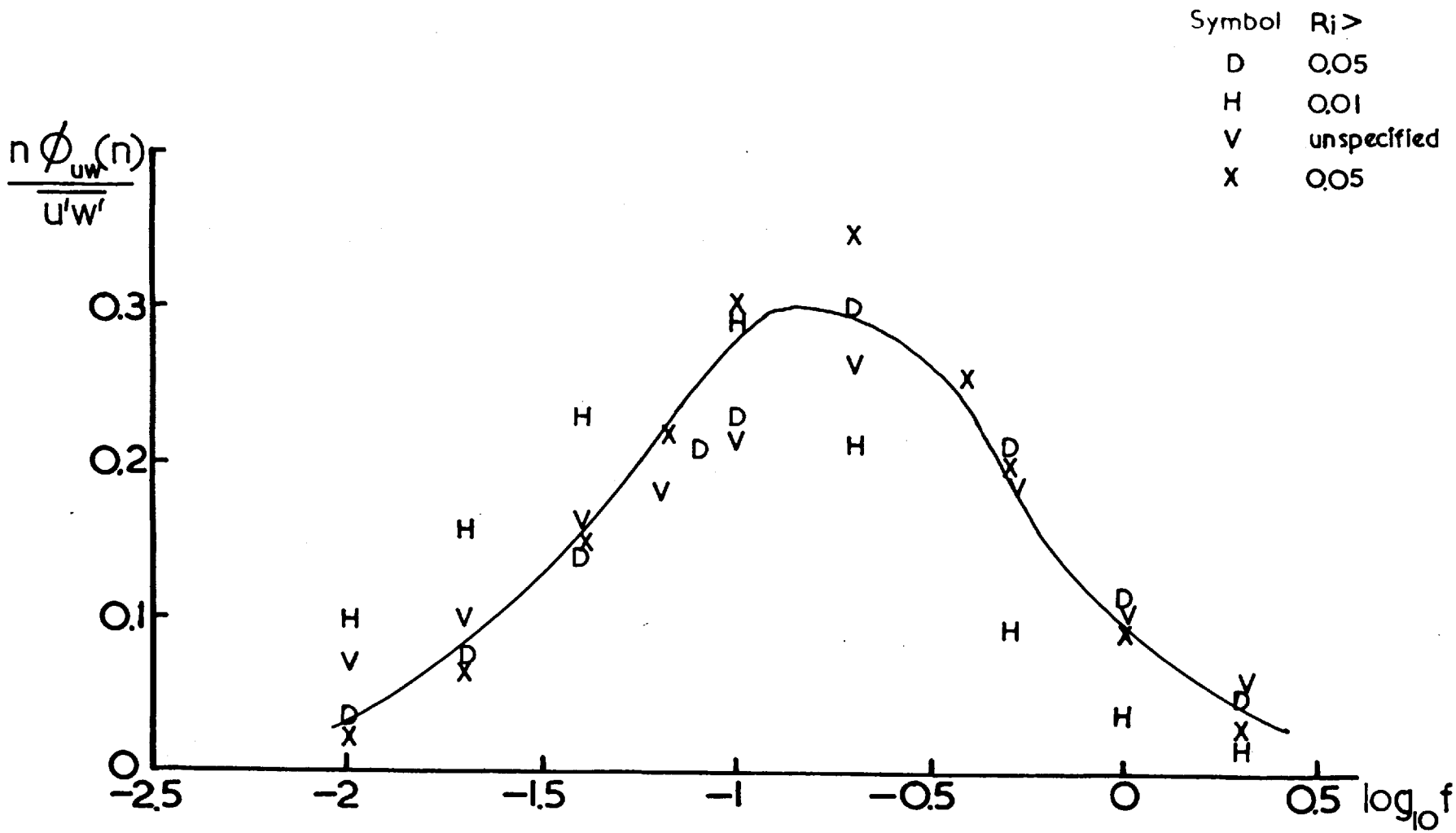

UW cospectra in stable air

FIG. 5.21

5.3.7. Summary

(a) Because of the relatively large low-frequency contributions to $\overline{u'^2}$, values of this quantity for a sampling time of 10 minutes may sometimes be unrepresentative.

(b) Because of the relatively large high-frequency contribution to $\overline{w'^2}$, values of this quantity for a data-spacing time of 0.1 seconds may be underestimated, in some cases by several per cent, by an amount greater the smaller z and the more positive is Ri. Values of $\overline{w'^2}$ used in § 4.2. were not corrected for this effect.

(c) The cospectral curves suggest that the greater part of the contribution to the flux is being recorded. Because of the relatively large correlation at low frequencies (for negative Ri) a sampling time much greater than 10 minutes is suggested to achieve completely stable values of $\overline{u'w'}$, consistent with the analysis in § 4.2.2. when 1 - 5 minute fluxes were compared to 10 minute fluxes to determine a flux variability. Choosing $R_{uw}(n) \ll$ peak value as a criterion for stable flux estimates one can extrapolate tentatively the curves (for negative Ri) in Fig.5.16 to lower frequencies giving a time period of the order of 30 - 60 minutes when R_{uw} is close to zero, suggesting a desirable sampling time of about 30 - 60 minutes.

(d) No evidence is present of the interaction of the water wave spectrum with the turbulence spectra (found by Preobrazhenskii (1968) at heights between 0.3 m. to 5 m.) as inferred by W.B. working at heights comparable to those at Lough Neagh. The Russians found individual, well-defined and narrow peaks that occurred on u and w spectra at frequencies corresponding to

that of the wave spectrum peak. It appears that the Lough Neagh spectra are not measured at a low enough height for such wave effects to be observed (though the vertical velocity maximum occurs at wave peak frequencies the w spectra are much wider with no evident anomalous peaks suggestive of wave interaction), a fact consistent with the discussion in § 4.2. regarding the relative sizes of $\overline{u'^2}$, $\overline{w'^2}$ with $-\overline{u'w'}$.

(e) Data from Lough Neagh and other sites provide substantial evidence for the existence of a Universal non-dimensional vertical velocity spectrum and momentum flux cospectrum described by relations 5.9 to 5.12 inclusive. They require the specification of Ri only which determines f_m. This is not so for the u spectrum which evidently depends upon other factors and therefore does not obey the Similarity Theory for low frequencies.

Finally there is an unexplained anomaly in the Hanford data in stable conditions.

5.4. Temperature Characteristics

5.4.1. Structure Function

The structure function for temperature is similarly defined as for velocity —see equation 2.13. As with velocity the function of particular practical interest is $D_T(x) = 2\sigma_T^2(1 - r_T(x))$ over a range of x important for the application of the Kolmogorov-Oboukhov Law of the inertial sub-range viz. the "2/3" law —see § 1.2. and § 5.5. In Fig.5.6 is shown the function $D_T(x)$ vs x, on a logarithmic scale, for runs where a 2/3 law is observed. The curves

are similar to those for velocity having an upper limit to the 2/3 behaviour at comparable values of x_{max}. Measurements from these curves are utilised in a later section (see § 5.5.).

When the curves are normalised according to equation 5.4 b and $D_T(x)/\sigma_T^2$ plotted vs x/z there is no tendency for them to group together, implying that the factors determining $D_T(x)$ in the range of x where $D_T(x) \propto x^{2/3}$ are not strongly correlated with σ_T^2 —the spectra behave in an analogous way (cf § 5.4.2.). For many runs the slope of the $D_T(x)$—x curve in the range $x/z \lesssim 1$ is less than 2/3 though there is no reason to doubt the existence of an inertial sub-range at smaller values of x with $x_{max} \sim$ the minimum observed x.

The relation $D_T(x) \propto x^p$ with $p \simeq 2/3$ has been observed and reported by Taylor (1961), Tatarskii (1961) and Record and Cramer (1966) in overland conditions at heights from 1 m. to 40 m. The results of the first two authors are discussed in a later section (§ 5.5.).

5.4.2. Temperature Spectrum

Log-log spectra are plotted in Fig.5.3, lines of slope -5/3 being inserted for comparison with the spectral slopes; there is an overall tendency for $\phi_T(k)$ to fall like $k^{-5/3}$ though some spectra have slopes considerably less than -5/3 in magnitude.

Runs were grouped as for velocity into three Ri ranges (viz. $Ri < -0.10$, $-0.10 < Ri < 0$, $0 < Ri$) and $\phi_T(k)/z\sigma_T^2$ plotted vs f as required by equation 5.3 a on a logarithmic scale. The average curves, together with the mean deviations, are shown in Fig.5.22

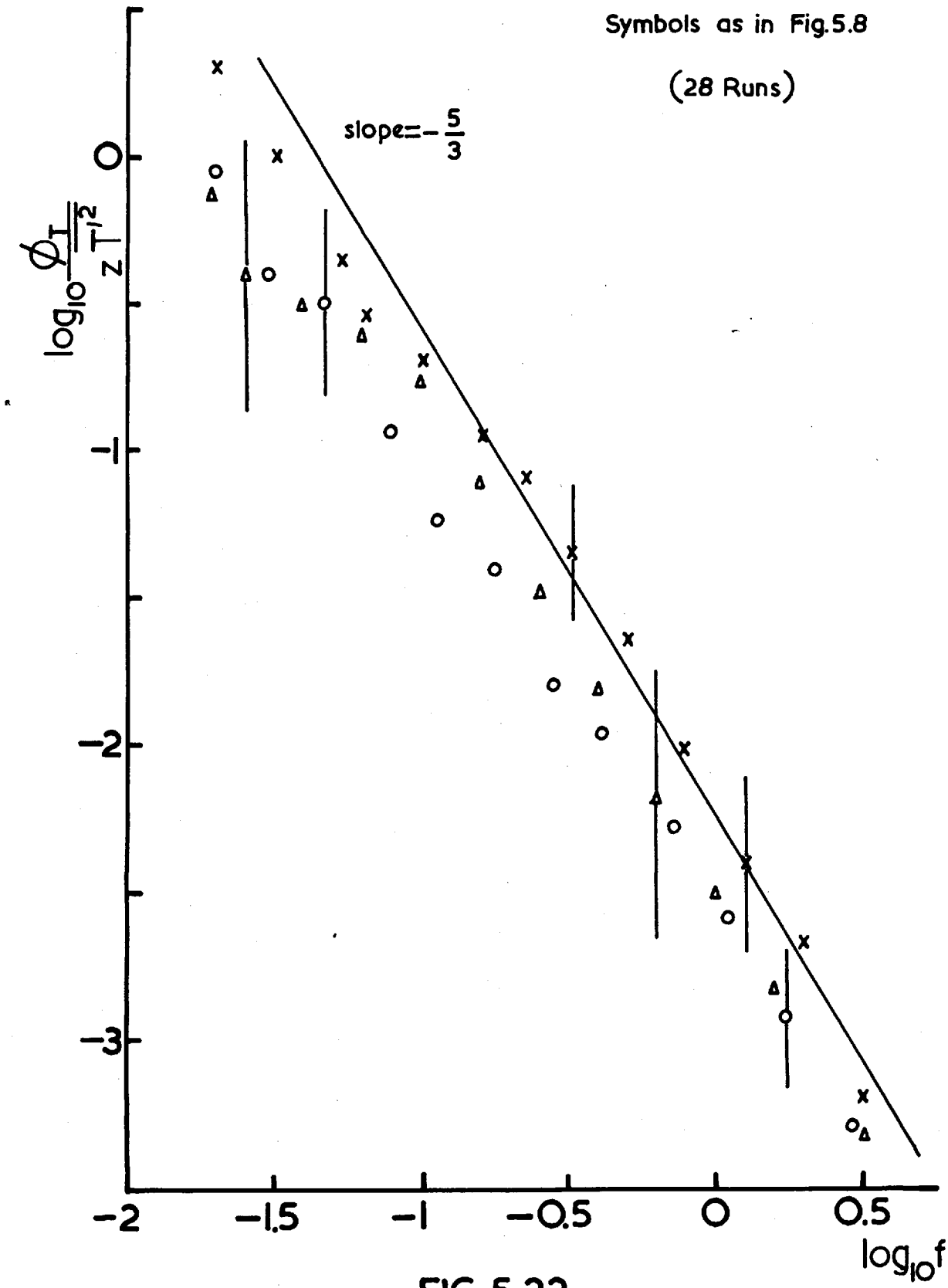
Symbols as in Fig.5.8
(28 Runs)
slope = $-\frac{5}{3}$
$\log_{10}\frac{\phi_I}{z\,T'^2}$
0
-1
-2
-3
-2
-1.5
-1
-0.5
0
0.5
$\log_{10} f$

FIG.5.22

and though over a relatively large f range $\phi_T(k) / z\sigma_T^2 \propto f^{-5/3}$ the curves do not group together as required by the Kolmogorov Similarity Theory. The reason for this may be that χ is not related to σ_T^2 in the way derived in § 5.2. on a Similarity basis; rather χ is only weakly correlated with σ_T^2. Consequently treating equation 5.3a as a normalising process, other normalisation factors were tried involving $\overline{w'T'}$, $\partial\theta/\partial z$ (upon which χ might be expected to depend) yet σ_T^2 proved to be the one giving least scatter. In conclusion the solution must evolve from equation 5.3 with direct measurements of χ from measurements of $\phi_T(k)$ in the dissipation region.

Close examination of Fig.5.22 allows for a determination of the dependence of f_L upon Ri, as suggested in § 5.2.4. Values of f_L for each Ri range are given in Table 5.2.

Table 5.2 Dependence of f_L upon Ri

Ri	f_L	f_L^{-1}
< -0.1	0.16	6.2
-0.1 to 0	0.4	2.5
> 0	0.1	10.0

Evidently f_L shows no dependence upon Ri, but the above values suggest that the -5/3 law extends further into the anisotropic region than for the u component of velocity. This is implied by the temperature spectra measured from an airplane at heights between 100m. and 1500m. by Zwang (1960).

5.4.3. Heat Flux Cospectrum

Normalised wT cospectra are plotted in Fig.5.5 on the same basis as the uw cospectra —see § 5.3.3. As with the momentum flux cospectra the most prominent feature is the peak, with two peaks occurring in slightly stable conditions though not so for momentum. These properties of the cospectra are described in § 5.4.5. In this section an investigation of the high frequency behaviour of the wT cospectra is made in analogy with the uw cospectra. Equation 5.1 f can be manipulated to give $\phi_{wT}(k) / z\,\sigma_{wT}^2$ as a function of f and Ri. The normalised cospectral densities were computed for a number of runs divided into 3 Ri ranges viz. $Ri < -0.10$, $-0.1 < Ri < 0$, $Ri > 0$ and averaged at several values of $\log_{10}k$ for ease of computation over as great a k range as possible. They are plotted in Fig.5.23 against $\log_{10}f$. For $\log_{10}f > -0.5$ the points are well described by a line of slope -2 implying

$$\phi_{wT}(k) \propto z\,\sigma_{wT}^2\, f^{-2}$$

Such a relation is analogous to that for momentum and as with the latter's flux cospectrum at low frequencies there is a marked tendency for power to be greater the greater the instability. This is better illustrated in the cospectra of Fig.5.24 to be described. The f^{-2} dependence occurs at values of f where the -5/3 law of the temperature spectrum is observed, viz.,

$$\phi_T(k) \propto z\,\sigma_T^2\, f^{-5/3} \qquad \text{for } \log_{10}f > -0.8$$

$$\phi_{wT}(k) \propto z\,\sigma_{wT}^2\, f^{-2} \qquad \text{for } \log_{10}f > -0.5$$

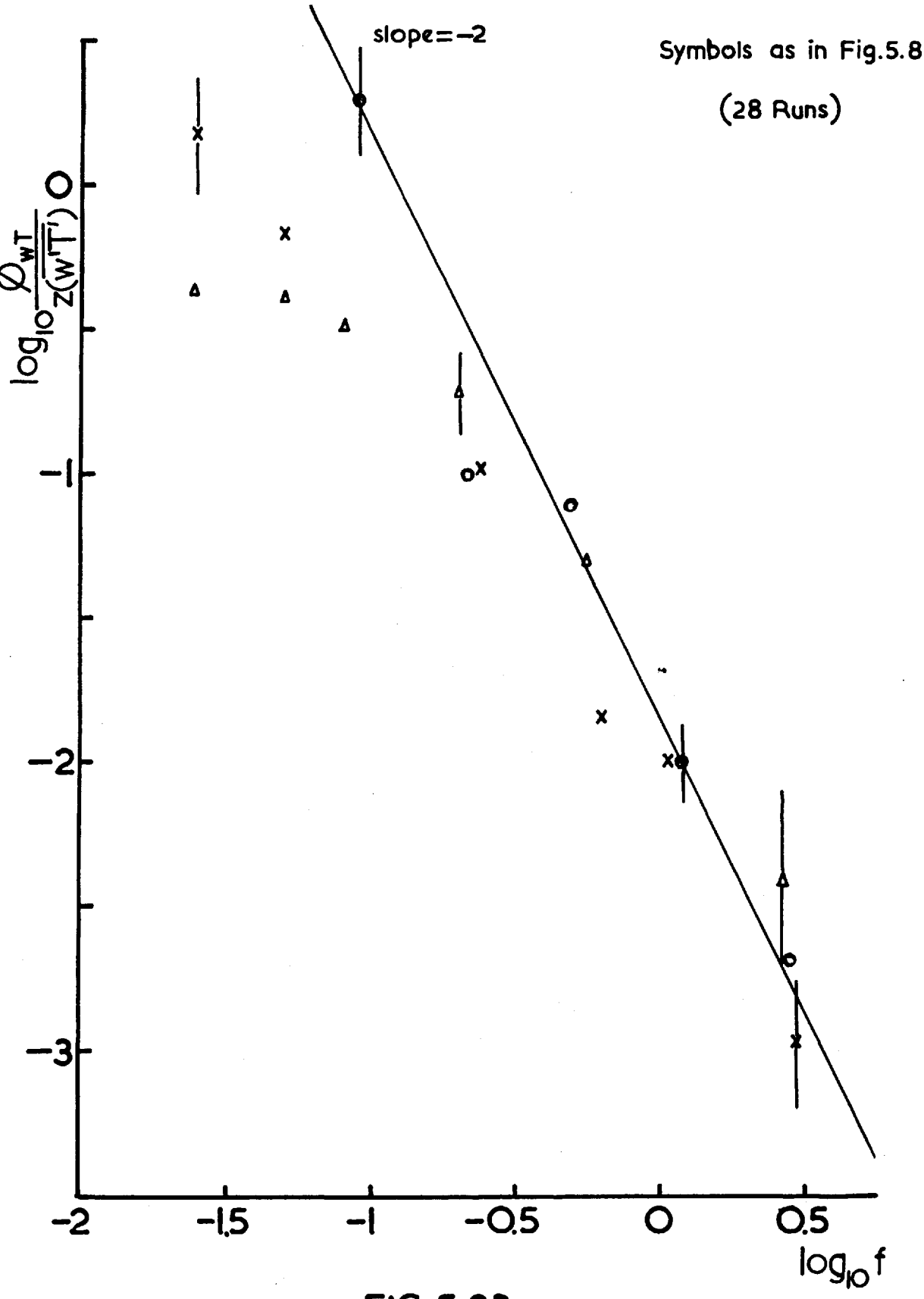
slope=−2
Symbols as in Fig.5.8
(28 Runs)
$\log_{10}\frac{\phi_{wT}}{Z(\overline{w'T'})}$
0
−1
−2
−3
−2
−1.5
−1
−0.5
0
0.5
$\log_{10} f$

FIG.5.23

Observations of heat-flux cospectra are relatively rare but regarding their high frequency behaviour the data published by P.M. for the South Dartmouth site indicate this is similar to that for the momentum flux cospectra with an index approximately equal to -2.

5.4.4. Heat Flux Cospectra as Functions of Ri

The relation represented by equation 5.1f is investigated for 4 Ri ranges specified in § 5.2.1. Temperature spectra computed from Lough Neagh data are not readily described by the analogous relation —see equation 5.1e — mainly because low frequency components of the temperature variance are very sensitive to unsteadiness, as is evident from pen recordings of the temporal variation of temperature. Indeed the requirement of steady conditions is a severe restriction placed upon the acceptability of temperature data since experience shows it is relatively more difficult to obtain steady temperature fields than velocity fields at Lough Neagh.

The average cospectra are shown in Fig.5.24 together with mean deviations. The shape and position of the curves vary considerably with Ri, with f_m showing a dependence upon Ri of similar form to the uw cospectrum —Fig.5.25 shows f_m vs Ri for the individual cases. From Fig.5.24, $\lambda_m = 40z$ in unstable conditions ($25z$ for momentum) and $\lambda_m = 3.5z$ for the most stable cases with $Ri \simeq 0.07 - 0.08$ ($5.5z$ for momentum). An unexpected feature of 5.24 is the existence of two peaks (at $\lambda_m = 40z$ and $4.5z$) in conditions close to neutral (on the stable side in Fig.5.24) when the power is necessarily small (relatively large mean deviations).

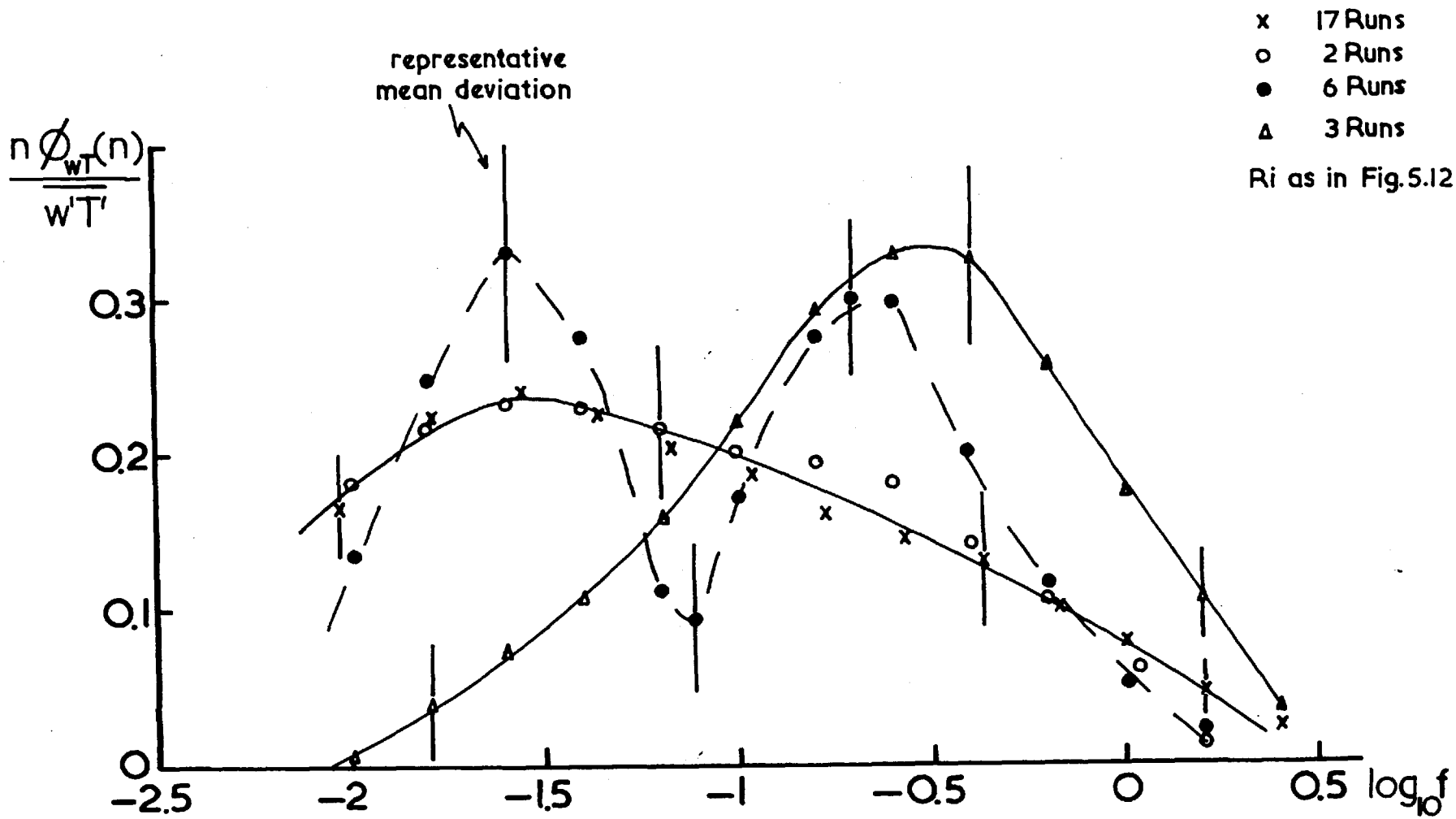
x 17 Runs
o 2 Runs
● 6 Runs
Δ 3 Runs
Ri as in Fig. 5.12
representative mean deviation
$\frac{n\phi_{wT}(n)}{\overline{w'T'}}$
0.3
0.2
0.1
0
−2.5
−2
−1.5
−1
−0.5
0
0.5
$\log_{10} f$

FIG. 5.24

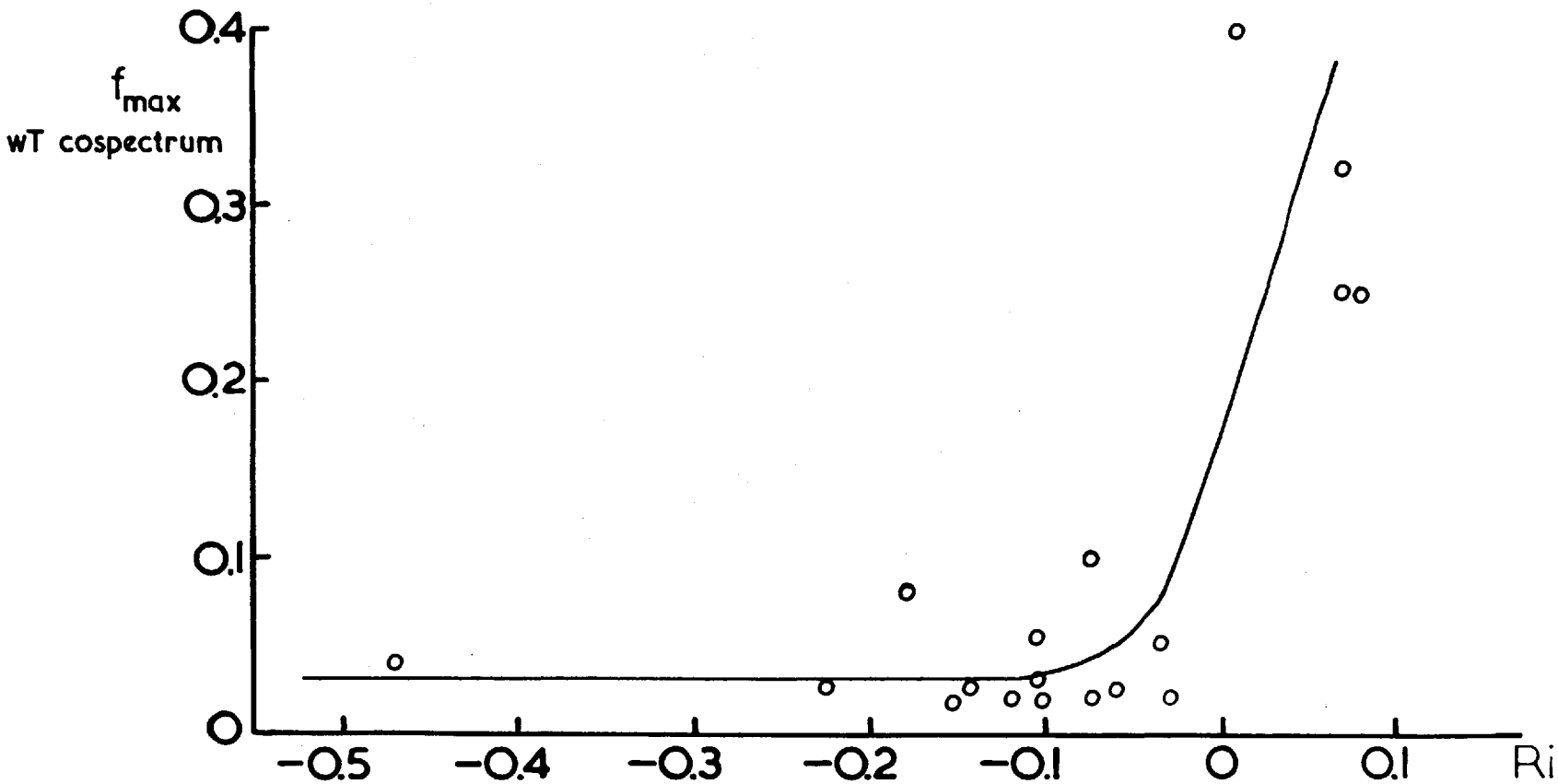

FIG.5.25

Nevertheless it is possible to resolve the two peaks. The author is not aware of similar behaviour being reported anywhere in the literature and this feature remains to be more fully confirmed and if confirmed, explained.

5.4.5. Coherence (Between w and T)

The coherence can be written, in analogy to equations 5.6, 5.6a for u and w,

$$Coh(n) = \frac{\phi_{wT}(n)}{(\phi_T \phi_w)^{1/2}} + i \frac{Q_{wT}(n)}{(\phi_T \phi_w)^{1/2}} \qquad 5.13a$$

or,

$$Coh(n)^2 = \frac{\phi_{wT}(n)^2}{\phi_T(n)\,\phi_w(n)} + \frac{Q_{wT}(n)^2}{\phi_T(n)\,\phi_w(n)} \qquad 5.13$$

5.4.5.1. The Quadrature Spectrum

Examples of quadrature spectra — defined for w and T from equation 2.17 — are shown in Fig.5.26 together with corresponding cospectra for comparison, smoothing of the spectral estimates having been made at high frequencies. For cases of significant heat flux, the inequality $Q_{wT}(n)^2 << \phi_{wT}(n)^2$ appears valid for all n (e.g. Run 565) but for small heat flux $Q_{wT}(n)^2 \sim \phi_{wT}(n)^2$ at low frequencies with negligible quadrature at high frequencies (e.g. Run 578).

As with the uw coherence, it will be assumed that, in the range of frequencies investigated, the spectral correlation coefficient $R_{wT}(n) = \phi_{wT}(n) / (\phi_T \phi_w)^{1/2}$ is a good measure of the

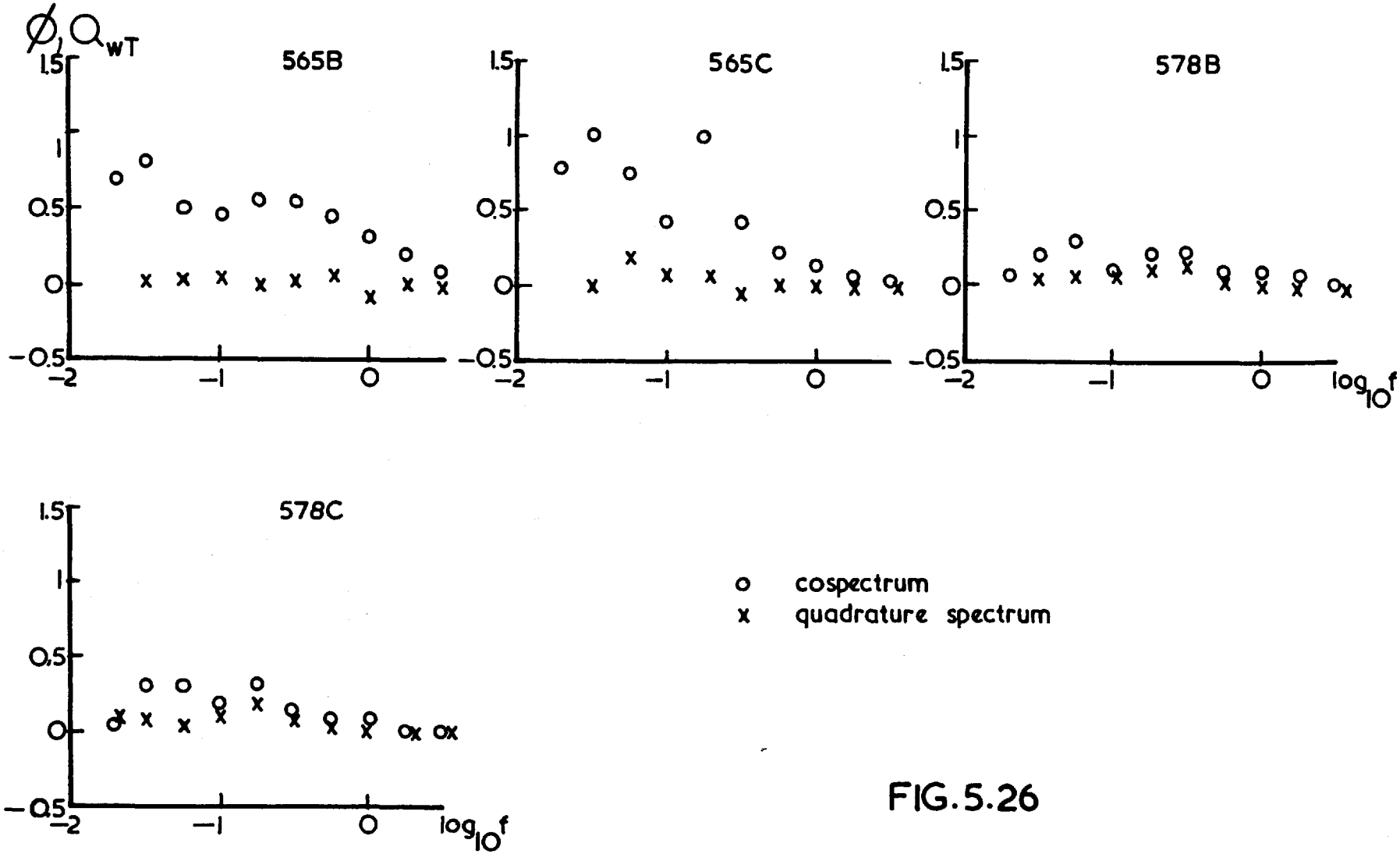
$\phi_1 Q_{wT}$
565B
565C
578B
578C
1.5
1
0.5
0
−0.5
−2
−1
0
$\log_{10} f$
o cospectrum
x quadrature spectrum

FIG. 5.26

coherence, though in near-neutral conditions (small heat flux) the quadrature may give significant contribution, especially at the low frequencies.

5.4.5.2. The Spectral Correlation Coefficient

Fig.5.27 shows for $Ri < -0.05$, $-0.05 < Ri < 0$, $Ri > 0.05$ average curves of correlation $R_{wT}(n)$ vs $\log_{10} f$ together with mean deviations. Sufficient scatter exists (being greatest at low frequencies) to suggest that other factors are important in determining $R_{wT}(n)$. As with R_{uw}, a part of the scatter at low frequencies will be due to the small value of ϕ_w. The shape and position of the curves depend upon Ri, with the peaks of the curves being approximately coincident with the cospectral peaks.

An important feature of the diagram is the overlap of the -5/3 region of the temperature spectrum with the finite R_{wT} to such an extent that, in stable conditions, f_L corresponds to the frequency of the correlation maximum. Thus the temperature inertial sub-range must occur at much higher frequencies than those in Fig.5.27, a result which is analogous to the velocity spectra behaviour.

5.4.6. Comparison of Heat Flux Cospectra

The only comprehensive set of heat flux cospectra known to the author are those published by P.M., obtained overland at South Dartmouth, U.S.A. at heights 15 m. — 90 m. Gurvich (1960 b) has also published a heat flux cospectrum obtained in weak instability at a height of 1 m. overland. Fig.5.28 shows normalised (in Similarity coordinates) wT cospectra for negative Ri for two sites, together

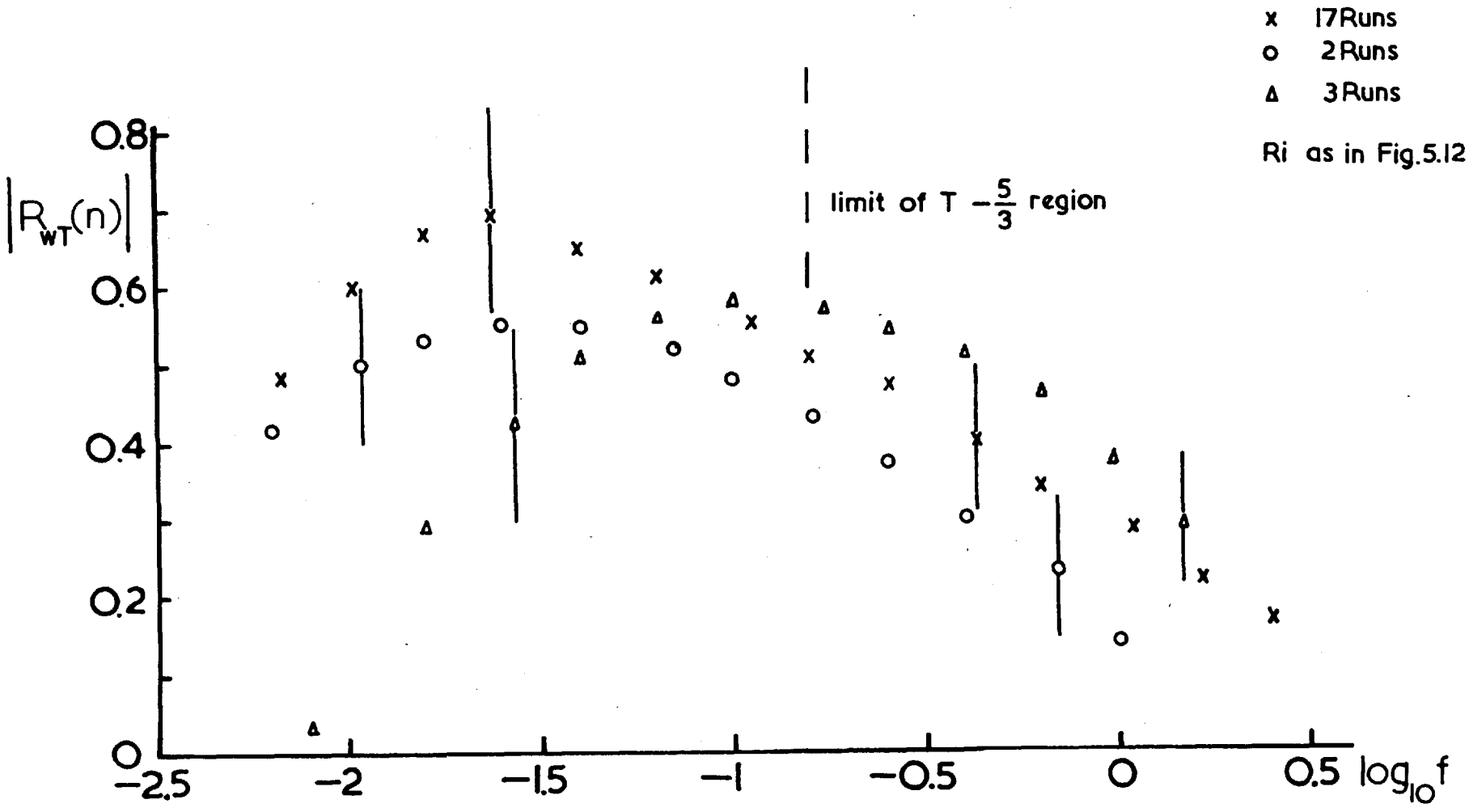
x 17 Runs
o 2 Runs
Δ 3 Runs
Ri as in Fig.5.12
limit of T $-\frac{5}{3}$ region
$|R_{WT}(n)|$
0.8
0.6
0.4
0.2
0
−2.5
−2
−1.5
−1
−0.5
0
0.5
$\log_{10} f$

FIG.5.27

Symbols and Ri as in Fig.5.20

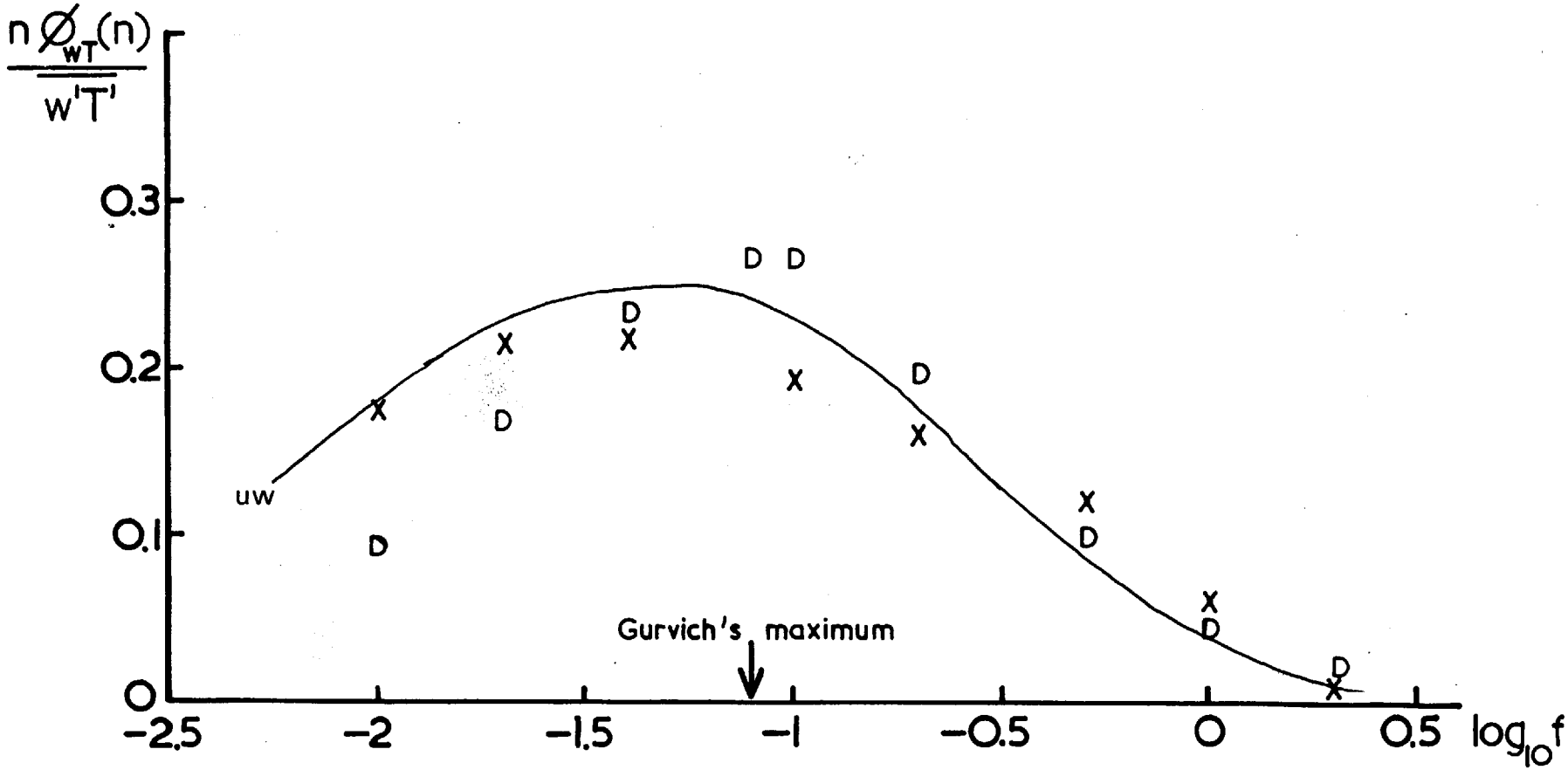

wT cospectra in unstable air

FIG. 5.28

with the position of the peak as observed by Gurvich. The latter lies close to that of P.M. whereas the Lough Neagh curve lies, evidently, at lower frequencies. Nevertheless a smooth curve has been drawn through the points by eye to represent them.

The agreement for positive Ri —Fig.5.29 — is better, though here again the Lough Neagh peak differs in position from the Dartmouth peak, in this case lying at a higher frequency. The smooth curve drawn by eye fits the data reasonably well.

Obviously more data from a variety of sites are required to establish a Universal form to the non-dimensional heat flux cospectrum.

5.4.7. Comparison of Lough Neagh Cospectra for Momentum and Heat Fluxes

It seems probable that if the transfers of heat and momentum are effected, under non-neutral stratification, by different mechanisms then the corresponding spectra will differ for a given Ri, since the predominant eddy scale concerned in the transfer will differ. Measurements of K_H, K_M —see § 4.3. — suggest that the transfers are unequal, such that $K_H > K_M$ (negative Ri) and $K_H < K_M$ (positive Ri).

A comparison of the Dartmouth cospectra for positive and negative Ri and of the cospectra of Gurvich shows no significant difference when plotted in Similarity coordinates. Included in Figs.5.28, 5.29 are the outlines of the uw cospectra for Lough Neagh taken from Fig.5.13 (a direct comparison being also possible between Fig.5.13 and Fig.5.24). For negative Ri $\lambda_m = 25\,z$ for momentum and $40\,z$ for heat flux whereas in stable conditions the heat flux

Symbols and Ri as in Fig.5.21

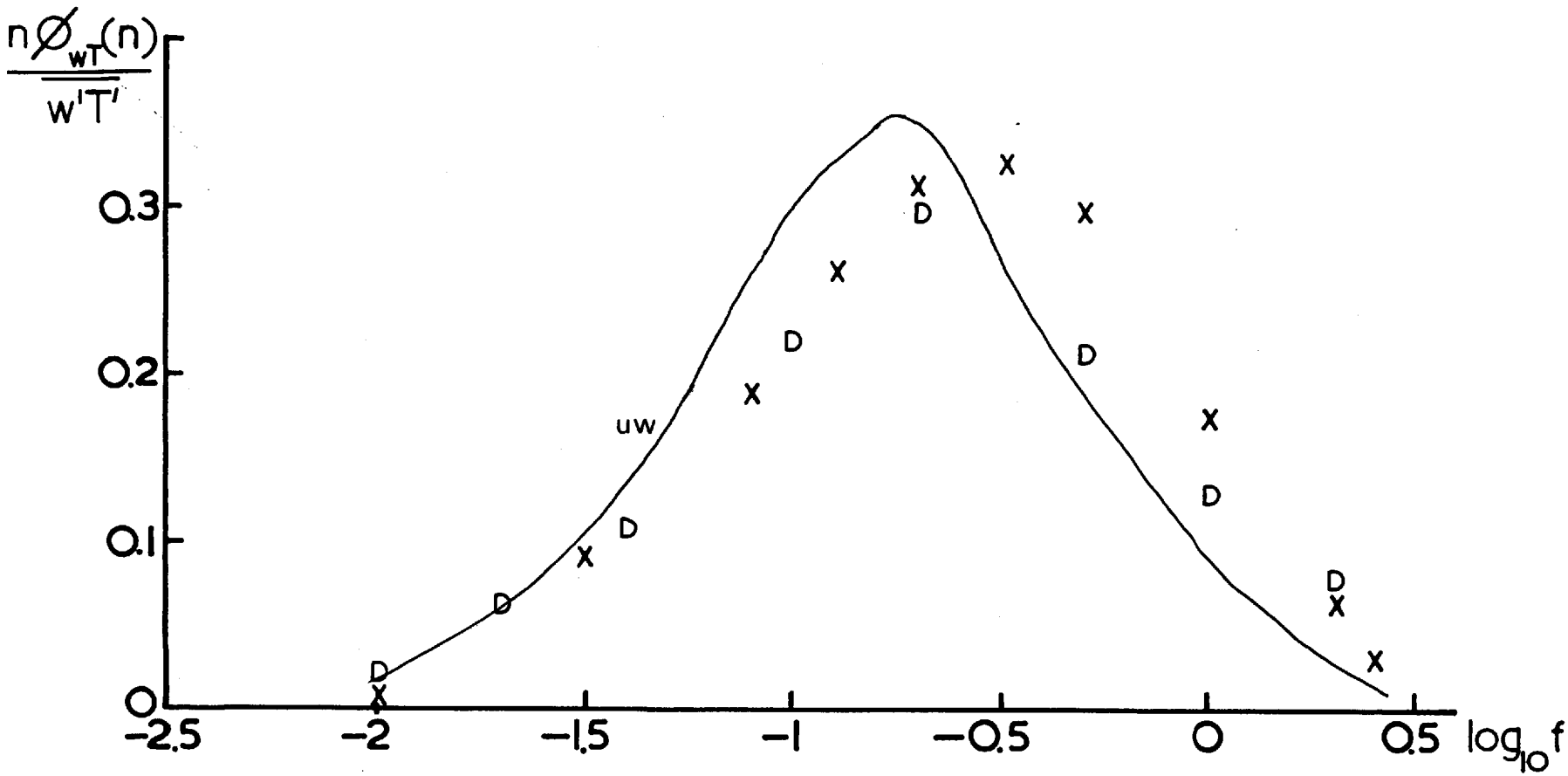

wT cospectra in stable air

FIG.5.29

peak ($\lambda_m = 3.5\,z$) lies at a higher frequency than the momentum flux peak ($\lambda_m = 5.5\,z$).

It can be expected that the smaller the wavelength of the cospectral peak the less efficient is the transfer (this is related to the decrease in spectral correlation as the wavelength decreases and isotropy is approached). Hence the differences in λ_m for heat and momentum flux observed at Lough Neagh in stable and unstable conditions are consistent with the measurements of the relative sizes of the transfer coefficients.

Unequivocal evidence for the differences in the two types of cospectra related to the different transfer mechanisms in non-neutral conditions is and will be difficult to obtain because of the inherent scatter of measured cospectra. This may account for its not being obtained by P.M. and for the tentative results of the Lough Neagh data described herein.

5.4.8. Summary

(a) There is a relatively large low-frequency contribution to $\overline{T'^2}$ such that values for a sampling time of 10 minutes may often be unrepresentative,

(b) The cospectral curves suggest that the greater part of the flux is being recorded. Because of the relatively large correlation at low frequencies when Ri is negative a sampling time much greater than 10 minutes is required to achieve completely stable values of $\overline{w'T'}$; $\simeq$ 30 - 60 minutes —cf § 5.3.7., part (c),

(c) It seems probable that, as for the momentum flux cospectrum, a Universal form exists describing the non-dimensional heat flux

cospectrum whose shape will differ little from that in Fig.5.28 and 5.29,

(d) The differences in f_m for the heat and momentum flux cospectra when Ri is positive and negative imply $K_H < K_M$, $K_H > K_M$ respectively consistent with direct measurements of K_H, K_M. This implication assumes that, the smaller the dominant eddy, the less efficient is the transfer mechanism because of the tendency for eddies, decreasing in size, to lose their anisotropic character and hence their transfer ability.

5.5. The Nature of Temperature Fluctuations

5.5.1. The Balance Equation of Temperature Fluctuations

The simplified balance equation for $\overline{T'^2}$ (Tatarskii, 1961) is,

$$\frac{\partial}{\partial t}\left(\frac{\overline{T'^2}}{2}\right) = -\chi - \overline{w'T'}\frac{\partial \theta}{\partial z} - \frac{\partial}{\partial z}\left(\frac{\overline{w'T'^2}}{2}\right) \qquad 5.14$$

In quasi-steady state conditions, the term expressing the local rate of change of T variance with time can generally be neglected since $\frac{\partial}{\partial t}\left(\overline{T'^2}/2\right) \sim \overline{T'^2}/\tau_s \sim 10^{-5}\ ^\circ C^2\ sec^{-1}$ compared to $\chi \sim 10^{-3}\ ^\circ C^2\ sec^{-1}$. Thus 5.14 becomes,

$$\chi = -\overline{w'T'}\frac{\partial \theta}{\partial z} - \frac{1}{2}\frac{\partial}{\partial z}\left(\overline{w'T'^2}\right) \qquad 5.15$$

The first two terms represent local rates of dissipation and production respectively whereas the flux divergence term may be positive or negative.

χ may be defined in terms of the dissipation spectrum viz.

$2\chi = \gamma \int_0^\infty k^2 \phi_T(k)\, dk$ but without the necessary spectrum measurements it may be estimated from knowledge of the spectrum in the inertial sub-range —see equations 1.3 and 1.4.

5.5.2. The Kolmogorov-Oboukhov Law of the Inertial Sub-Range

Writing equations 1.3 and 1.4 in full for k and x,

$$D_T(x) = C_T \chi \varepsilon^{-1/3} x^{2/3} \qquad 5.16$$

and,

$$\phi_T(k) = A_T \chi \varepsilon^{-1/3} k^{-5/3} \qquad 5.17$$

where C_T, A_T are Universal constants analogous to C_u, K_u for velocity. Because of the ill-defined ranges of x where the x dependence of $D_T(x)$ in 5.16 is observed for runs shown in Fig.5.6 χ will be estimated from the spectrum using equation 5.17 from known values of ε (velocity spectra) and requiring knowledge of A_T.

5.5.3. Measurement of the Universal Constant A_T

Estimates of the constant are few and are based primarily on the assumption that $\chi = -\overline{w'T'} \frac{\partial \theta}{\partial z}$. It will later be shown that such an assumption is wrong as indicated by observations made at Lough Neagh and inferred from the results of other workers.

Gurvich and Zubkovskii (1966) have shown, in a review paper, that there is no sufficiently accurate evaluation of either C_T or A_T (it is generally assumed that $C_T = 4 A_T$ though this may be invalid as was found in the case of velocity —see § 4.4.2.). Values of A_T so determined generally vary between 0.2 and 1.0 approximately.

For instance, Zwang (1962) found $C_T = 2.7$ ($A_T = 0.7$) and Gurvich et al. using skewness measurements derived $C_T = 3.5$ ($A_T = 0.9$). Taylor (1961) found $C_T = 1.0$ ($A_T = 0.25$) and Takeuchi (1962) $C_T = 1.2$ ($A_T = 0.3$). All these estimates relate to measurements overland in the near-surface layer of the atmosphere. Similar estimates of A_T were made using the author's spectra shown in Fig.5.3.

Lough Neagh Estimates

A_T was estimated for 23 runs where all the data required in equation 5.17 were available for its evaluation. It was assumed that the inertial sub-range law was valid in the observed -5/3 range and that $\chi = -\overline{w'T'}\,\frac{\partial\theta}{\partial z}$. The results for individual runs are shown in Table 5.3.

Table 5.3

RUN	A_T	RUN	A_T	RUN	A_T
327	0.14	540 A	1.70	565 C	0.32
328	0.17	542 B	0.33	566 B	0.50
337	0.17	542 C	1.15	566 C	0.28
344	1.55	543 B	0.38	575 A	4.0
352	1.78	543 C	0.80	577 A	0.17
407	0.58	557 C	0.68	578 B	0.14
414	0.79	558 B	0.33	578 C	0.89
415	0.65	565 B	0.45		

The mean value is 0.6 with a standard deviation of 0.4. Such a wide variation is however consistent with previous estimates where a local balance of fluctuation intensity has been assumed. Taking all the estimates together a value of $A_T = 0.50$ does not seem unreasonable, accurate to within 50 per cent.

5.5.4. The Terms in the Balance Equation

5.5.4.1. Previous Work

$\frac{1}{2}\frac{\partial}{\partial z}\left(\overline{w'T'^2}\right)$ will be abbreviated to D_z.

(1) The results of Taylor (1961) on heat flux estimates from $-\chi/\frac{\partial\theta}{\partial z}$ (χ from the T structure function) imply that D_z is finite and positive when Ri is negative.

(2) Record and Cramer (1966), assuming $\chi = -\overline{w'T'}\frac{\partial\theta}{\partial z}$ found a variation in A_T which, since it must be a Universal constant, implies a finite D_z, on average being negative and positive for Ri positive and negative respectively.

(3) Tatarskii (1961) published data showing $A_T^{1/2}\ \chi^{1/2}\ \varepsilon^{-1/6}$ vs $\kappa^{2/3}\ z^{2/3}\frac{\partial\theta}{\partial z}$ which reduces to $B\chi^{1/2}$ vs $B(-\overline{w'T'}\ \partial\theta/\partial z)^{1/2}$ where $B = u_*^{-1/6}(\kappa z)^{1/6}$. His diagram implies that D_z is negative and positive for Ri negative and positive respectively, in contradiction to (1) and (2) above. All three do, however, suggest that D_z is finite.

5.5.4.2. Lough Neagh Results

Values of χ and $-\overline{w'T'}\frac{\partial\theta}{\partial z}$ are shown in Table 5.4 together with Ri, and plotted against each other in Fig.5.30. With the probable error in χ estimated at 50 - 100 per cent, and that in $-\overline{w'T'}\frac{\partial\theta}{\partial z}$ at 20 - 50 per cent, the scatter is hardly surprising.

For several runs D_z was estimated from measurements of $\overline{w'T'^2}$ at two heights viz. $D_z \sim \Delta\left(\overline{w'T'^2}\right)/\Delta z$ with an order of magnitude accuracy*. Such values are included in Table 5.4 and show that,

(a) D_z is $\sim$ the other terms in the balance equation (5.15) confirming the inferences of § 5.5.4.1.,

*The factor of ½ has been omitted because of the approximate method used to find D_z.

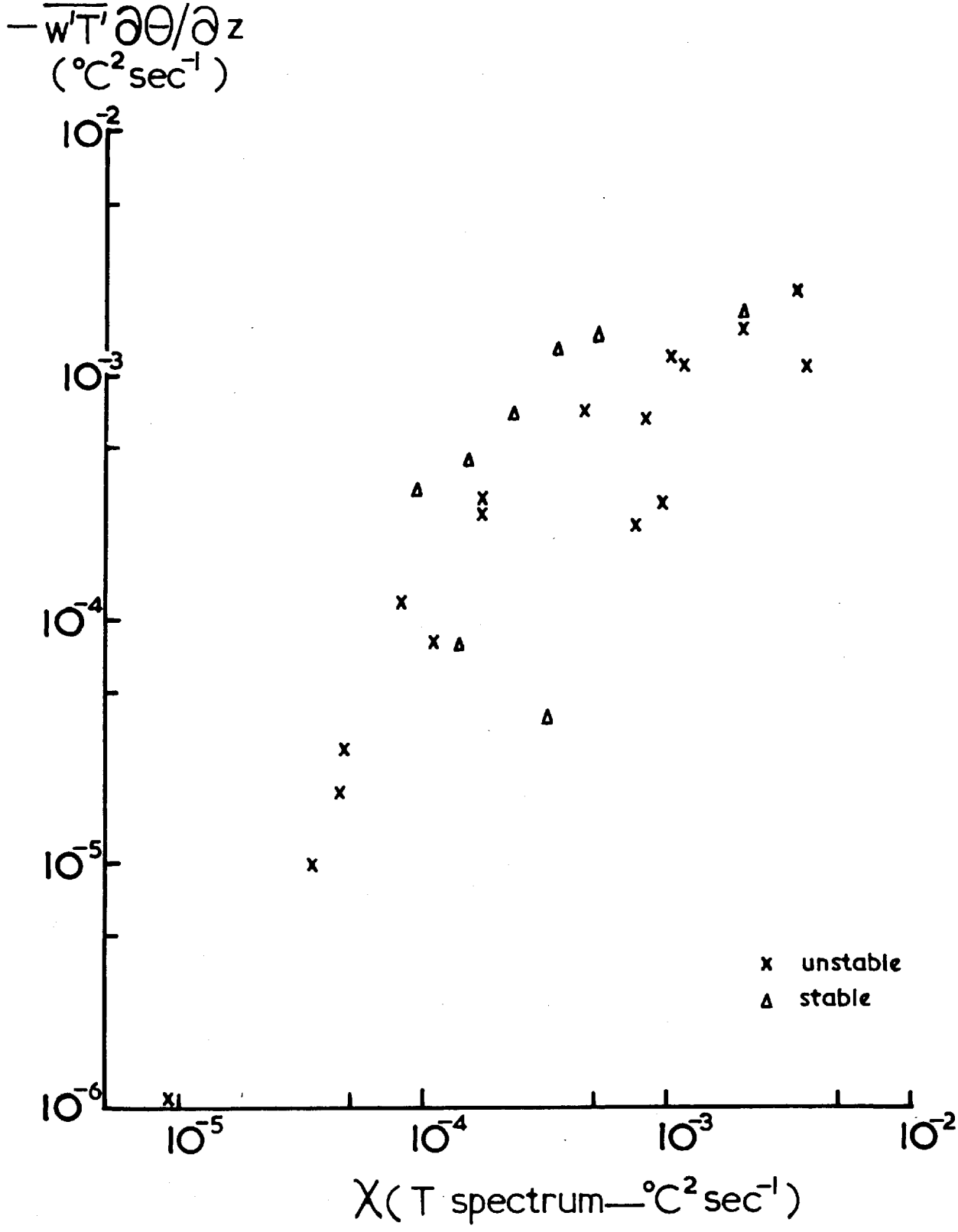
$-\overline{w'T'}\,\partial\theta/\partial z$
($°C^2 sec^{-1}$)
10^{-2}
10^{-3}
10^{-4}
10^{-5}
10^{-6}
10^{-5}
10^{-4}
10^{-3}
10^{-2}
χ(T spectrum—$°C^2 sec^{-1}$)
x unstable
Δ stable

FIG. 5.30

(b) D_z is, on average, positive in unstable conditions viz. $\overline{w'T'^2}$ increases with height agreeing with (1) and (2) in § 5.5.4.1.

RUN	Ri	$\chi \times 10^4$ $^\circ C^2\ s^{-1}$	$-\overline{w'T'}\frac{\partial\theta}{\partial z} \times 10^4$ $^\circ C^2\ s^{-1}$	$\overline{w'T'^2} \times 10^2$ $cm\ s^{-1}\ ^\circ C^2$	$\frac{\Delta\overline{w'T'^2}}{\Delta z} \times 10^4$ $^\circ C^2\ s^{-1}$
327	0.078	3.6	12.9		
328	0.071	5.2	15.2		
337	0.023	1.6	15.6		
344	-0.182	9.4	3.0		
352	-0.119	36.6	10.4		
407	+0.071	20.6	17.7		
414	-0.061	33.4	21.2		
415	-0.036	8.4	6.4		
540 A	-0.042	0.3	0.1	-0.3	
541 A	-0.032	-	-	-1.8	0.07
541 C	-0.054	0.1	0.004	-1.1	
542 B	-0.061	0.8	1.2	-2.8	0.9
542 C	-0.105	0.5	0.2	4.1	
543 B	-0.055	1.7	2.3	3.1	0.6
543 C	-0.075	0.5	0.3	7.8	
557 B	-0.106	-	6.5	15.6	-0.4
557 C	-0.201	1.1	0.8	12.7	
558 B	-0.144	4.5	6.7	23.2	
565 B	-0.102	10.3	11.5	57.0	2.5
565 C	-0.224	1.7	2.7	77.4	
566 B	-0.152	11.0	10.9	15.5	3.1
566 C	-0.469	1.7	3.1	40.2	
575 A	+0.003	3.2	0.4	-9.4	3.5
575 B	+0.001	-	-	-1.1	
577 A	+0.020	2.4	7.0	-8.3	
578 B	+0.034	0.9	3.4	5.5	-1.4
578 C	+0.030	1.4	0.8	-5.2	

Table 5.4

5.5.5. The Third Moment Term

Previous estimates of $\overline{w'T'^2}$ by Taylor (1961) and Businger and Miyake (1968) especially, suggest it has a negligible contribution to the turbulent heat flux with $C_p \overline{\rho w'T'}$ (proportional to $\overline{w'T'^2}$) $<< \rho C_p \overline{w'T'}$. In unstable conditions Businger et al. found average values of the quantity $\overline{w'T'^2}/(\overline{T}.\overline{w'T'})$ as 1.7×10^{-3} (Hay, Australia site) and 1.4×10^{-3} (Davis, California site). Over Lough Neagh in moderate convection, the value is 0.5×10^{-3} approximately thus confirming the negligible contribution of $\overline{w'T'^2}$ to the heat flux.

Values of $\overline{w'T'^2}$ in Table 5.4 show that, predominantly, the flux is positive and negative for Ri negative and positive respectively, being therefore of the same sign as $\overline{w'T'}$. This agrees with Businger et al.'s observations in unstable conditions.

In convection, over the sea in our case, the term, on average, represents a vertical flux of positive or negative temperature fluctuation and is related to the presence of positive buoyancy in such conditions. This is evident on analogue records two of which are shown in Figs.5.31 and 5.32. The relevant traces are the instantaneous products of $w'T'^2$ as a function of time. It can be seen that $w'T'^2$ occurs in bursts lasting $\sim$ 10 seconds separated by quiescent periods of virtually zero $w'T'^2$ lasting for a minute or more. These bursts are produced in upward moving air (see w trace) carrying a large positive temperature fluctuation (see T trace) in horizontally decelerating wind (see u trace) and averaged over a time period >> the quiescent period produce a finite value of $\overline{w'T'^2}$. The form of the temperature trace suggests a positive

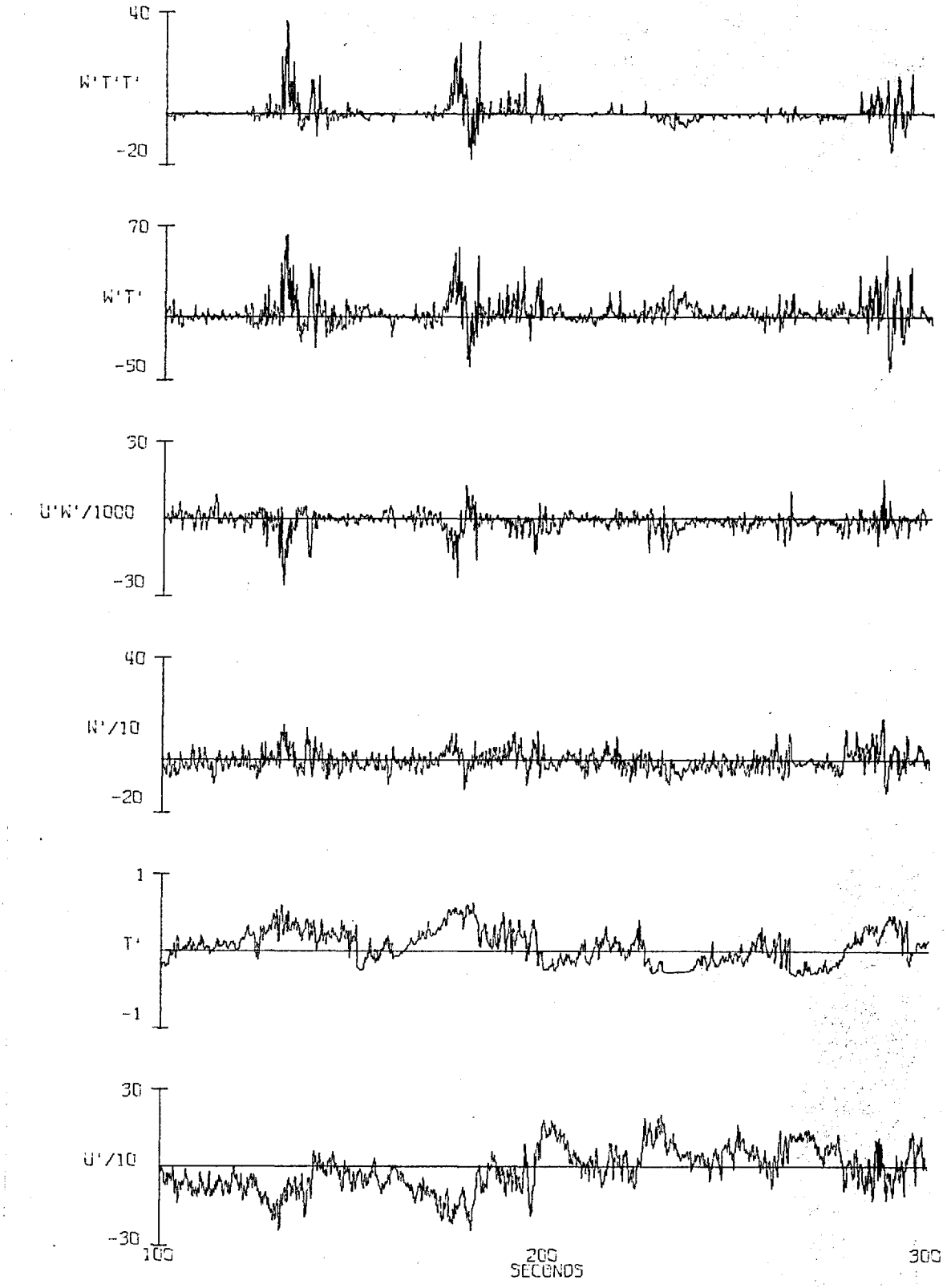
40
W'T'T'
-20
70
W'T'
-50
30
U'W'/1000
-30
40
W'/10
-20
1
T'
-1
30
U'/10
-30
100
200
SECONDS
300
Run 566B
U' AND W' IN CMS/SEC.
T' IN DEGREES C.

FIG.5.31

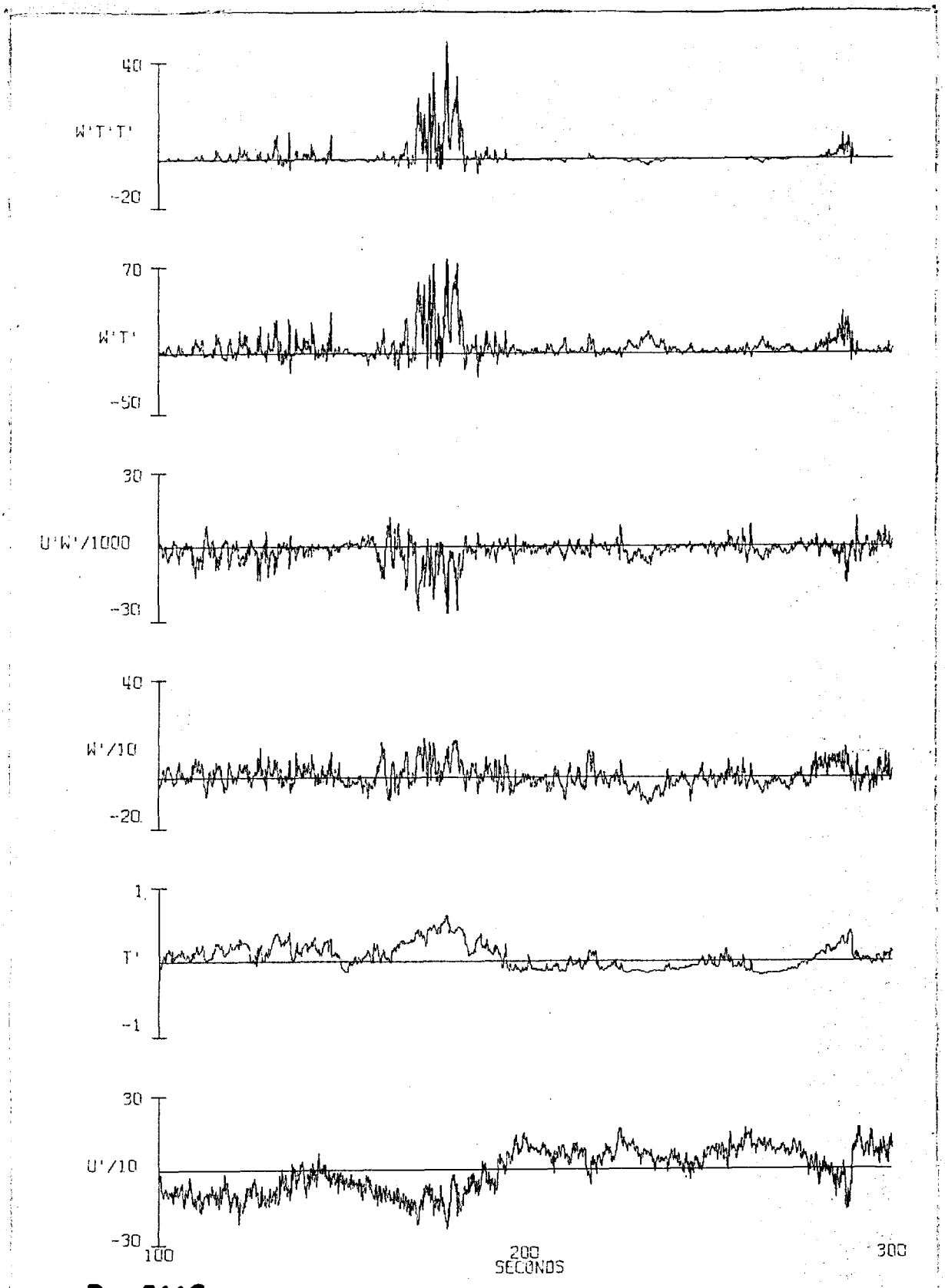
40
W'T'T'
-20
70
W'T'
-50
30
U'W'/1000
-30
40
W'/10
-20
1
T'
-1
30
U'/10
-30
100
200
SECONDS
300
Run 566C
U' AND W' IN CMS/SEC.
T' IN DEGREES C.

FIG. 5.32

skew temperature distribution which is what is observed —see Fig.5.33. Positive skewness is also observed in the w distribution (derived from the ϕ (angle) distribution) but the u distribution is nearly symmetrical.

On average, in unstable conditions, $\overline{w'T'^2}$ increases with height (§ 5.5.4.2.) suggesting buoyancy control. The temporal variation of $w'T'^2$ is related to the structure of turbulence in convective conditions.

5.5.6. Structure of Convection Over Lough Neagh

The form of spectra and cospectra as functions of Ri (§ 5.3., 5.4.) imply that heat flux is concentrated at the low frequency end of the w spectrum. A characteristic example is shown in Figs.5.31, 5.32, analogue records which are 200 second excerpts from 10 minute records. The association of the larger (positive) temperature fluctuations with the lower frequency fluctuations of (positive) w and their combined dominance of the heat flux (and $w'T'^2$) suggests a well-organised structure of the turbulence field dependent upon positive buoyancy for the transfer of heat and momentum by such large eddies. These eddies, characterised by horizontal decelerating air (negative anomaly —see u traces) and warm, upward moving air as they move past the point of observation carry the greater part of the heat flux $\overline{w'T'}$ and $\overline{w'T'^2}$ (and also $\overline{u'w'}$) over a sampling period of 10 minutes. In general, bursts of heat flux occur simultaneously with bursts of momentum flux due to the large negative correlation between u and T in the large eddies with positive w.

Similarities in the traces, and the bursts of flux, at

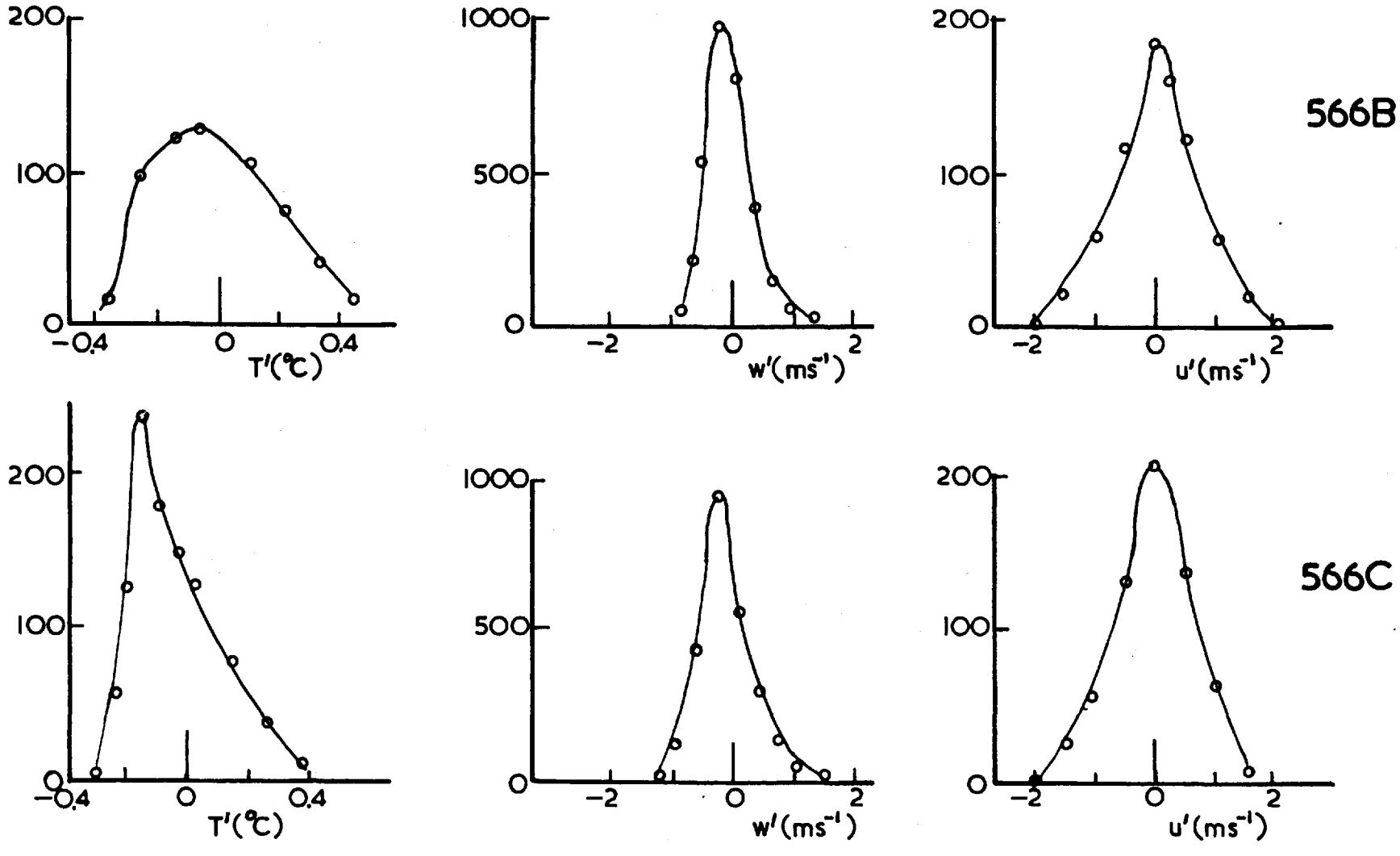

Ordinate—frequency of observations for total of 6000

FIG.5.33

the two heights are apparent though in this particular case a large burst of flux at time 130 seconds observable at level B does not appear in its entirety at level C. This is evidently due to a change with height of the temperature structure.

Because records are effectively line samples and the large eddies may be expected to occur randomly distributed their characteristic sizes and separations will be less than such quantities inferred from the records of Figs.5.31, 5.32 i.e. less than 100 - 150m. in size and separated by less than 500m. approximately.

Finally similar behaviour as observed in the turbulence structure in convection over Lough Neagh has been described in length by Priestley (1959) for records obtained at a height of 23m. overland, and has been reported by Haugen (private communication) though his bursts appear to be less frequent than those observed over Lough Neagh.

5.5.7. Summary

The section indicates that the temperature fluctuations in non-neutral conditions at one level are due to both a local production where the heat flux is directed along the temperature gradient and an advection of temperature anomaly from another level which, in unstable conditions at least, is dissipative in nature. The finiteness of the flux divergence term is related to an increase in height of the term $\overline{w'T'^2}$ due to the presence of positive buoyancy and whose finiteness relates to the skewness of temperature, in unstable conditions at least, being produced by large eddies carrying positive w and T anomalies and negative u anomalies and being the mechanism for the transport of heat and momentum vertically,

relatively little transfer occurring at other times.

For stable conditions $\overline{w'T'^2}$ is predominantly negative, so that in all conditions $\overline{w'T'^2}$ has the same sign, and is therefore in the same direction, as the heat flux $\overline{w'T'}$.

6.1. Introduction

The nature of the boundary can be specified in two distinct ways and the aim is to relate directly the two —

(i) Its aerodynamic properties can be specified by the aerodynamic roughness length z_o,

(ii) Dynamic properties can be specified through the wave frequency spectrum of the vertical surface displacement at a point.

There is also the question of the instantaneous spatial spectrum but this is beyond the scope of the present work. The present chapter is mainly concerned with (ii) but the question of the relation between (i) and (ii) is discussed (§ 6.4.) and that of the modification of turbulence in the air flow by wave motion (§ 6.5.). For reference purposes the reader should consult especially "Wind Waves" by B. Kinsman (1965) and "Dynamics of the Upper Ocean" by O.M. Phillips (1966).

6.2. Generation and Propagation of Wind Waves

6.2.1. Relevant Variables

An important relation exists between the wave period T, wavelength λ and wave phase velocity c for deep-sea gravity waves (waves with $\lambda \lesssim$ depth of water) viz.,

$$c = g(2\pi)^{-1} T \qquad 6.1$$

$$\lambda = cT = g(2\pi)^{-1} T^2 \qquad 6.2$$

Properties of the wind-driven gravity waves (i.e. we exclude

capillary waves) can be expected to depend upon four factors,

(i) the driving force through the wind speed $\bar{u}$ or friction velocity u_*,

(ii) the vertical gravity force per unit mass g,

(iii) the fetch F,

(iv) the duration of the wind t.

Considering only the fetch-limited situation, as for Lough Neagh, if the duration of the wind is long enough the wave system can be taken as being statistically steady in time, and independent of duration. In this situation Kitaigorodskii (1962) has suggested that a similarity-like theory could describe the characteristic features of the wave system. Thus for a fully developed sea any gravity wave property ρ would be given by

$$\rho = \rho\,(g,\ F,\ u_*) \qquad 6.3$$

or in the case of a spectral component,

$$\rho_n = \rho_n\,(g,\ F,\ u_*,\ n) \qquad 6.4$$

Properties are then described in terms of dimensionless quantities such as $n u_* g^{-1}$ (for frequency) and $g F u_*^{-2}$ (for fetch). The method has been used by Volkov (1968) with some degree of success. To be effective the method does require a large amount of data, comprehensive in form, which is not available up to date from Lough Neagh. Consequently the method is not fully exploited and for the available data equation 6.3 is considered qualitatively only.

Data from the wave recorder (§ 2.1.5.) whose position relative to the tower is shown schematically in Fig.6.1 have been processed in a way analogous to the wind fluctuation data to obtain wave frequency spectra.

6.2.2. The Equilibrium Range

In a steady, westerly wind of sufficiently long duration blowing over Lough Neagh initially capillary waves are produced over a range of frequencies with characteristic frequency $n_c = 4\ \rho_w g^3 \sigma_s^{-1}$, σ_s being the surface tension. Then the first gravity waves appear which grow, new ones being produced at lower frequencies as the fetch increases. The growth of such wave components cannot go on indefinitely (though this is not obvious for the longest waves) and the interesting possibility arises that an equilibrium range exists in the wave spectrum where the wave components have reached saturation energy level. Such a scheme was first presented by Phillips (1958). The existence of such an equilibrium range depends, not upon the existence of non linear interactions producing energy transfer between components as in turbulence, but upon the limiting configuration of a surface wave associated with discontinuities in the surface slope produced by an acceleration of -g at the crest. Excess energy is thus removed by the breaking of the surface, going into turbulent motion in the water. The physical parameters governing the asymptotic behaviour of the spectrum and those governing the surface stability must, to a first approximation, be the same; namely g . A dimensional analysis gives,

$$\phi_h(n) = \alpha\, g^2 n^{-5} \qquad 6.5$$

PLAN VIEW OF TOWER

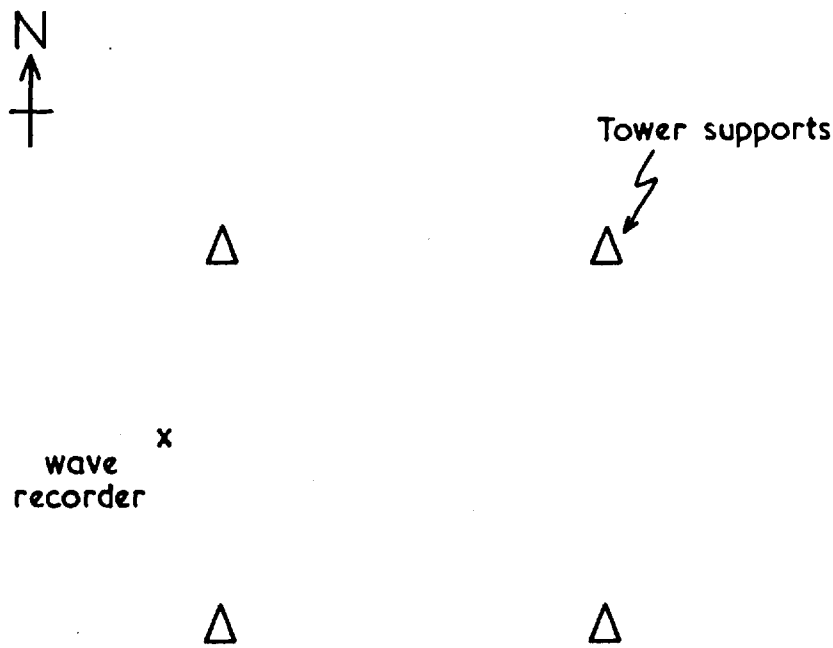

FIG.6.1

for $n_o < n < n_c$, n_o being the frequency of the spectral peak. It is perhaps of interest to compare this result of Phillips with the Kolmogorov law for turbulence.

In turbulence the energy input to the motion is primarily at low wave number from which it is transferred to high wave number by non linear interactions. The wave process is non linear and there is a similar transfer of energy to higher wave numbers (Kinsman, Chapter 13) but it is very small in comparison with the analogous flow in turbulence.

The wind seems to feed energy to waves of all frequencies and we can picture each component being fed separately by the wind until it reaches a saturation level, beyond which it rids itself of excess energy by the mechanism of breaking rather than to an adjacent component. Further it has been proposed (Kinsman, 1961) that for a sharply peaked spectrum the equilibrium range cannot be expected to appear until $n > 2n_o$ and that the effect of non-linear interactions amongst the wave components will be to produce secondary peaks at frequencies equal to integral multiples of n_o.

6.2.3. Mechanisms of Wave Growth

There exist two distinct theories of the mechanism of wave growth both published in the year 1957 and both now amalgamated to describe the growth and history of the whole wave spectrum.

The resonance theory of Phillips (1957) requires the supply of energy to the waves from convected pressure fluctuations on the surface arising from the turbulence in the wind, the most rapid growth taking place by resonance between the pressure fluctuations

and the modes of the free surface wave propagation in which case the convection velocities of the pressure pattern are of the order of the wave velocities. Such a theory is thought to apply to the early stages of wave growth, the energy in any component growing linearly with time.

The instability theory of Miles (1957) requires that the wind blowing over the corrugated water surface sets up a surface pressure distribution that is in phase with the surface slope and proportional to it, so that the energy in each component grows in the exponential manner characteristic of linearised instability models. In this theory is envisaged direct coupling between the air flow and waves, the rate of energy transfer depending directly upon the shape of the wind profile at the height where the wind speed equals the wave phase velocity.

From Miles' theory we would expect the greatest growth for wave components for which $c \ll \bar{u}_{10}$, and on the other hand for Phillips' theory the greatest growth will occur for wave components with $c \simeq \bar{u}_{10}$. By combining the two theories Phillips and Katz (1961) showed how the wave system could be envisaged as being initiated by the resonance mechanism with the energy in each component growing linearly until the component reached a size whereon the instability mechanism could act efficiently with the energy now growing exponentially with time until saturation occurs, with breaking of waves and significant non-linear effects. This appears to be the sequence of events for wave components with $c \ll \bar{u}_{10}$. However for components with $c \simeq \bar{u}_{10}$ the instability mechanism is very inefficient (Miles, 1960) so that the bulk of the energy observed

in these components must be provided by the resonance mechanism. One can then see that with a sufficient fetch there is an increase in the rate of growth from the linear to the exponential behaviour, the transition for any one component occurring at a particular fetch. In the fetch limited case with a steady wind and wave field, for a given fetch there exists a transition frequency below which energy is supplied by the resonance mechanism and above which it is supplied by the instability mechanism, the nature of the transition being a sudden acceleration in the wave growth. The curve AA in Fig.6.2 represents the theoretical relation predicted by Phillips and Katz (1961) on the basis of Miles' theory with number of waves before transition ($F\lambda_f^{-1}$) plotted vs $c_f \bar{u}_{10}^{-1}$.

It is now convenient to present the Lough Neagh data for the fetch limited case.

6.3. Data Presentation

6.3.1. Wave Spectra

Fig.6.3 shows data for twenty spectra plotted together according to fetch which ranges from 8 to 21 km. Characteristic of the individual spectra is the steep forward face, rising to a sharp maximum and falling off with increasing frequency. The features of Fig.6.3 are the large scatter at low frequencies and the tendency for the curves to fall together at high frequencies ($n > n_o$). The relatively large scatter occurring at the highest frequencies is thought to be related to the interference effect of the tower struts producing short secondary waves of amplitude 1 - 10 mm. superimposed upon the wind waves. Such waves have been observed on site, and

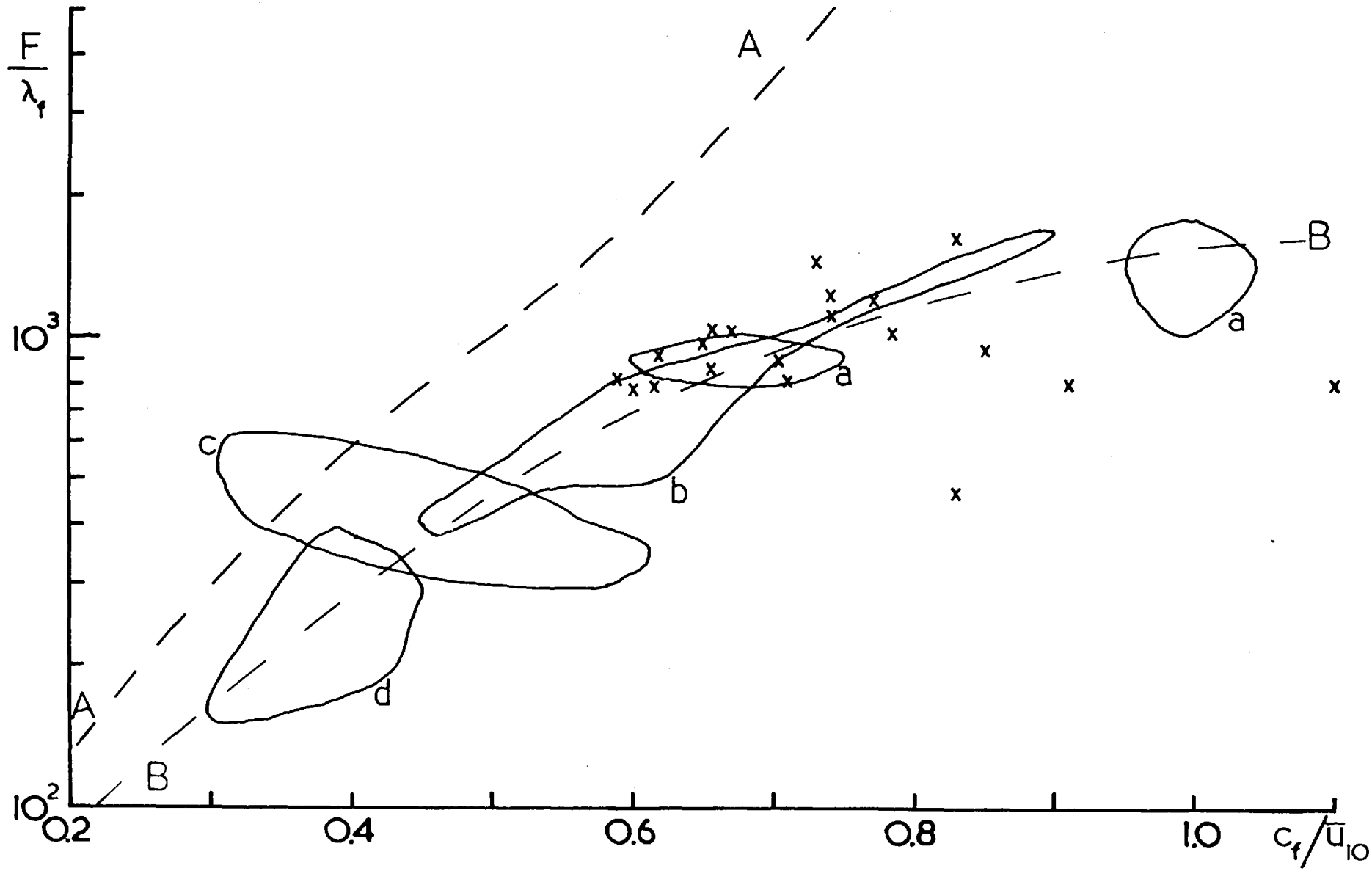

FIG.6.2

FIG.6.3 LOGARITHMIC WAVE SPECTRA

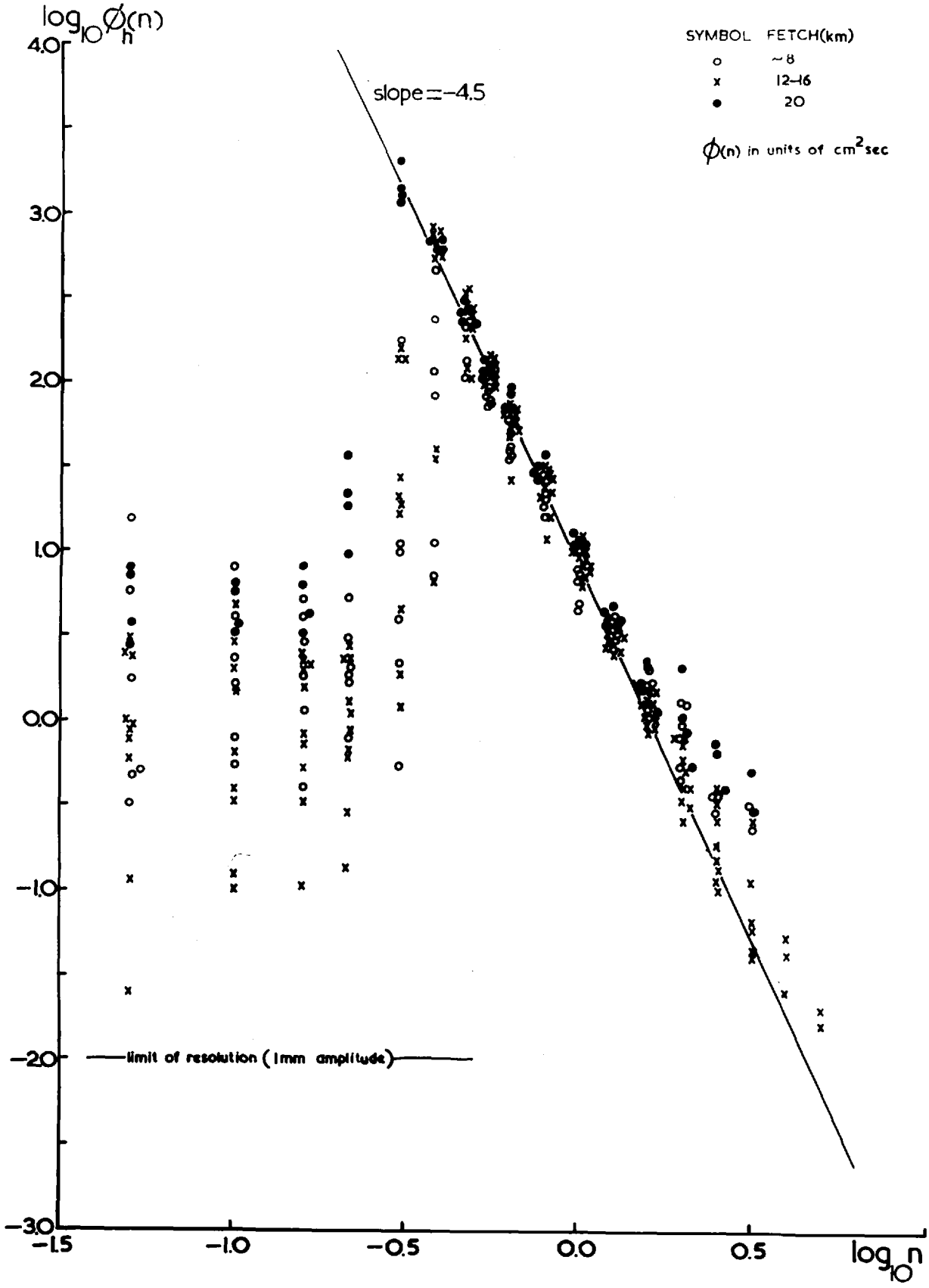

would be sensed by the wave recorder. The deviation of the points from a straight line (slope -4.5) in Fig.6.3 shows a correlation with wind direction such that it is minimum when direction is 270° and suggesting the secondary waves are attenuated significantly when travelling between strut and wave recorder against the wind, and a maximum when direction is near 200° and 350°, suggesting relatively little attenuation when travelling between strut and recorder with the wind (see Fig.6.1). Such ideas do require further evidence.

The values of $\phi_h(n)$ observed at the highest frequencies ($\sim 10^{-1}$ cm^2 sec at $n \sim 5$ cps) are an order of magnitude higher than that corresponding to the resolution limit of 1 mm. (§ 2.1.5.) equivalent to $\phi_h(n) = 10^{-2}$ cm^2 sec.

6.3.2. High Frequency Behaviour

The high frequency behaviour of the spectra represented by the straight line in Fig.6.3 is,

$$\phi_h(n) = \beta n^{-4.5} \qquad 6.6$$

with $\beta = 8.0 \pm 0.5$.

The difference between relations 6.6 and 6.5 might be expected according to Kinsman's argument that variations in the index result from spectra whose observed high frequency range is not sufficiently extensive, but it is relevant that other workers have found an index lying between -4.5 (Kinsman, 1961 and Hicks, 1960) and -5.5 (Burling, 1955). In the individual spectra there is no

evidence of secondary maxima at $n = 2n_o, 3n_o, \ldots$ but Kinsman (1961) has observed them and they are also apparent in the spectra published by Volkov et al. (1967). It is not however certain under what particular conditions these secondary maxima appear.

Of particular importance is the value of the constants appearing in equations 6.5 and 6.6. In comparing the constants there is the problem of unequal indices to contend with. However with only a ten per cent difference between the indices no great error is introduced by equating β and αg^2. Indeed such a practice was adopted by Phillips (1966) for comparing the constants measured by several workers where the index varied between -4.5 and -5.5. With $\beta = \alpha g^2$ and $\beta = 8.0 \pm 0.5$,

$$\alpha = (8.3 \pm 0.5) \times 10^{-6} \quad \text{for } n \text{ in cps,}$$

or

$$\alpha = (1.3 \pm 0.1) \times 10^{-2} \quad \text{for } n \text{ in rdns sec}^{-1}.$$

Phillips' overall mean value of several sets of results is $\alpha = (1.17 \pm 0.12) \times 10^{-2}$ —see footnote. The very good agreement implies that $\phi(n)$ in equation 6.6 represents a saturation value appropriate to an equilibrium range.

6.3.3. Characteristic Frequencies and Low Frequency Behaviour

In all the individual spectra measured, and presented in Fig.6.3, there are two characteristic frequencies, viz. n_o, the frequency of the spectral peak and n_f, the frequency of the steep

FOOTNOTE Phillips (monograph, p.114) quotes $\alpha = 1.17 \times 10^{-2}$ (n in rdns sec^{-1}) but wrongly infers $\alpha = 18.3$ (n in cps) by multiplying 1.17×10^{-2} by $(2\pi)^4$ instead of $(2\pi)^{-4}$ whence 18.3 should be replaced by 7.6×10^{-6}. (Compare this with $\alpha = 8.3 \times 10^{-6}$ for the Lough Neagh spectra.)

forward face. The data obtained at Lough Neagh show a high correlation between n_o and n_f such that

$$n_o = 1.1\ n_f \qquad 6.7$$

to a few per cent.

The Frequency n_f

The existence of the steep forward face (and therefore a definable n_f) is particularly important regarding the theory of wave growth (§ 6.2.) and the transition from one mechanism to the other. It strongly suggests identification of n_f with the transition frequency (Phillips and Katz, 1961); further a characteristic property of the measured spectra is a decrease in n_f as F increases which would be expected as a result of transition from a linear growth rate to an exponential one. To correspond to the ordinate in Fig.6.2 F/λ_f was evaluated ($\lambda_f = c_f n_f^{-1}$) and plotted vs $c_f/\bar{u}_{10}$, together with the data of Barnett and Wilkonson (1967) enclosed by boundary a, Snyder and Cox (1966) by boundary b, Kinsman (1960) by boundary c and Burling (1955) by boundary d. All the points lie to one side of the curve AA such that transition is observed earlier than predicted. Curve AA assumes the initial motion is at rest yet if there is some small wave motion at the windward edge of the generating region this may provide a more effective trigger for transition; additionally the wind may be unsteady (see Phillips' monograph). The scatter of the points in Fig.6.2 will be due in part to uncertainty in the fetch and in the wind duration. Nevertheless all the data suggest a Universal curve BB relating

F and n_f in a given wind, n_f being approximately the transition frequency in any real situation.

The Frequency n_o

Fig.6.4 shows values of T_{obs} (being the period of the dominant wave, computed from ten minute pen records) vs $\bar{u}_{10}$, according to fetch; also shown are the corresponding values of c, λ calculated using relations 6.1 and 6.2. Clearly the wave period depends a great deal upon $\bar{u}$ and F which is implied also in Fig.6.3. T_{obs} is clearly identifiable with $T_o = n_o^{-1}$ obtained from the spectra. Comparison of the two shows T_{obs} invariably $< T_o$ the reason being that T_{obs} represents an average time period over the wave peak necessarily weighted to the smaller times by virtue of the asymmetry of the peak.

Low Frequency Behaviour

Fig.6.5 shows averaged spectra (from nine individual spectra) with a variation of fetch at approximately constant wind speed. They are normalised and indicate that an increase in F produces a shift in the relative contribution to $\overline{h'^2}$ to lower frequencies whilst that at the peak remains constant. Similarly Fig.6.6 shows normalised (individual) spectra with a variation in wind speed at constant fetch. Here an increase in wind speed produces a shift in the relative contribution to lower frequencies whilst that at the peak increases also.

Significance of Increase in $\overline{h'^2}$

$\overline{h'^2}$ increases in two ways; by an increase in $\bar{u}$ which imparts

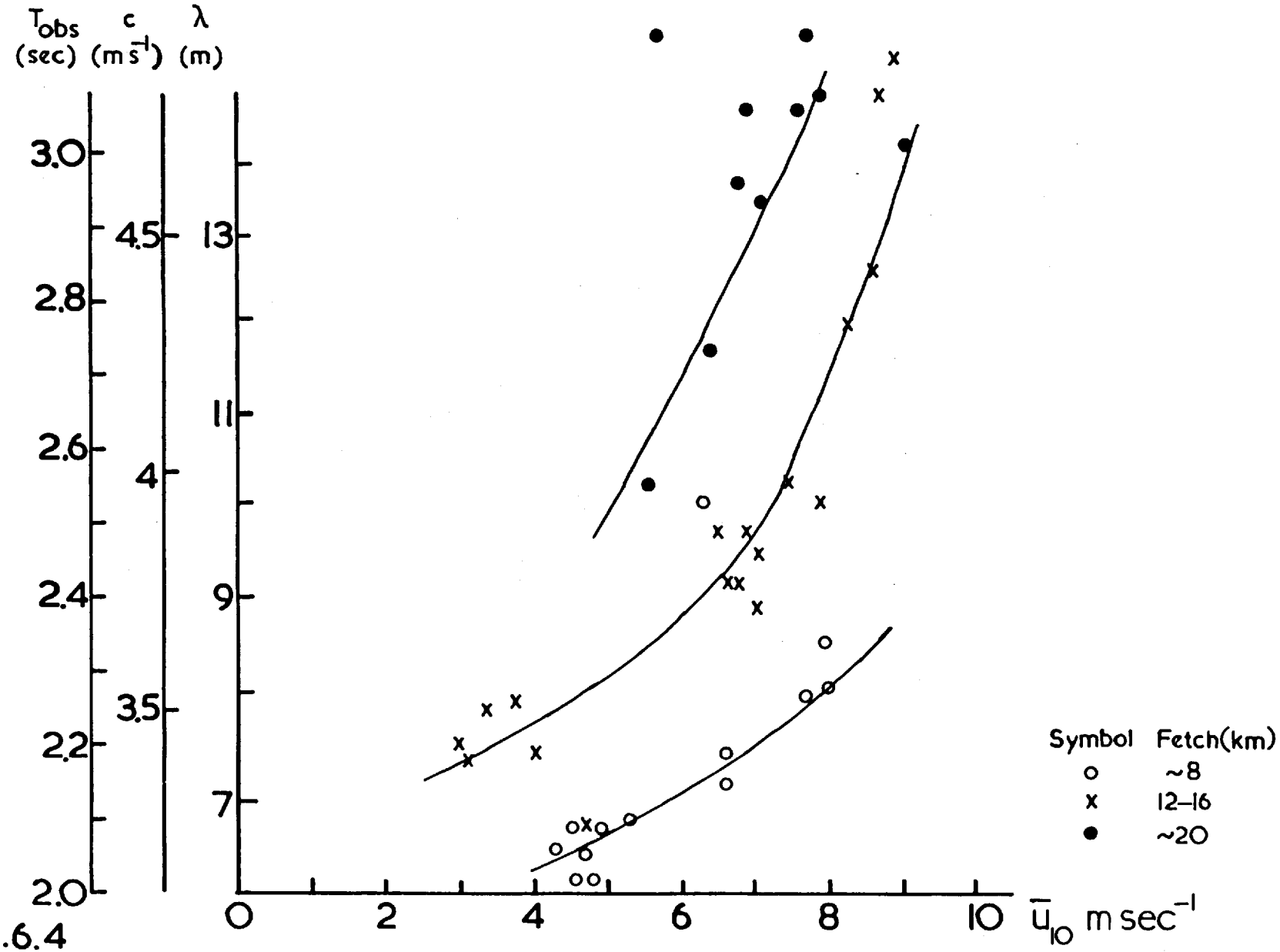
T_{obs} (sec)
c ($m\,s^{-1}$)
λ (m)
3.0
2.8
2.6
2.4
2.2
2.0
4.5
4
3.5
13
11
9
7
0
2
4
6
8
10
$\bar{u}_{10}$ m sec^{-1}
Symbol
Fetch(km)
~8
12–16
~20

FIG.6.4

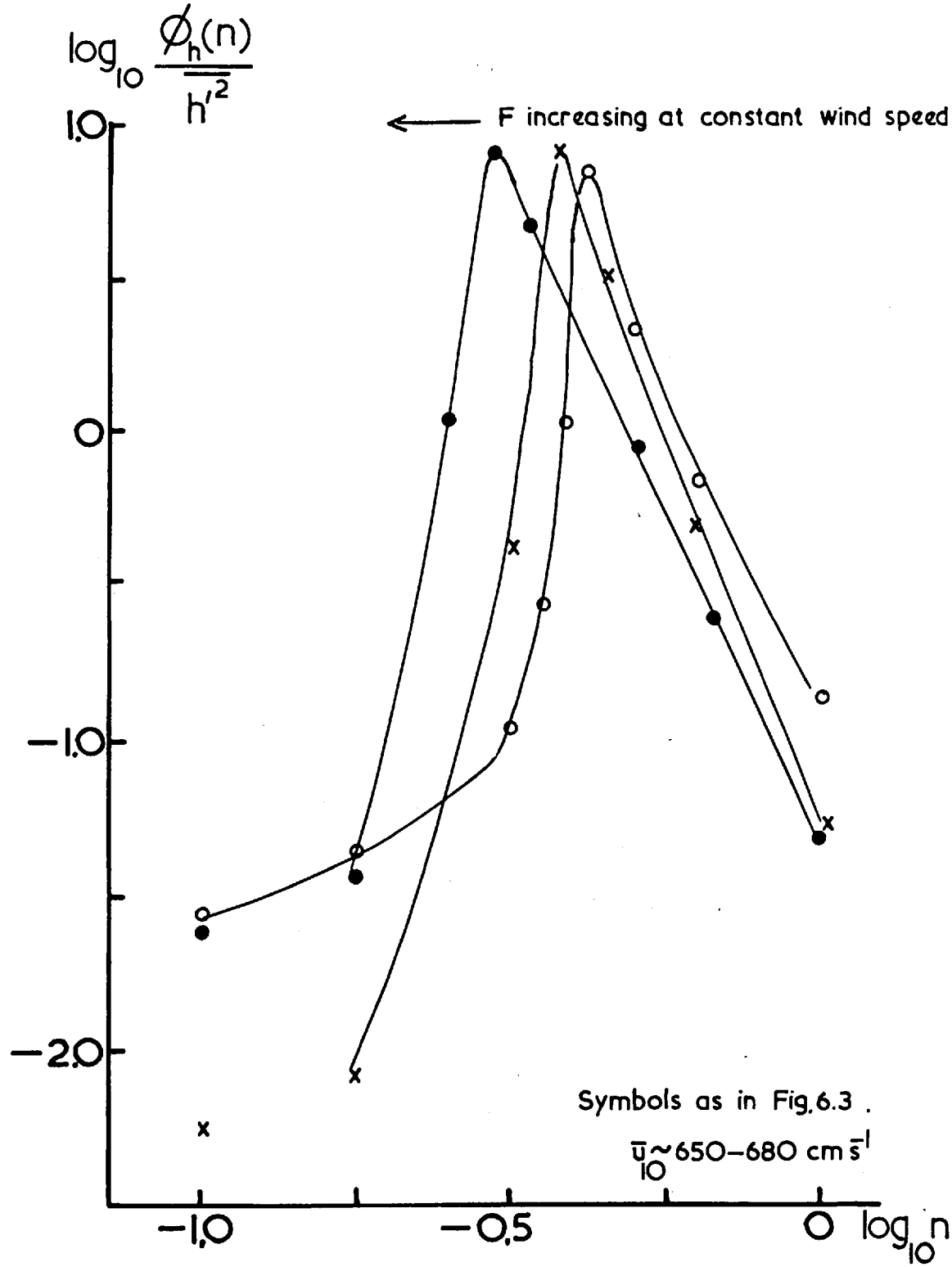
log10 Øh(n) / h'2
F increasing at constant wind speed
1.0
0
−1.0
−2.0
Symbols as in Fig.6.3 .
ū10 ~ 650–680 cm s−1
−1.0
−0.5
0
log10 n

FIG.6.5

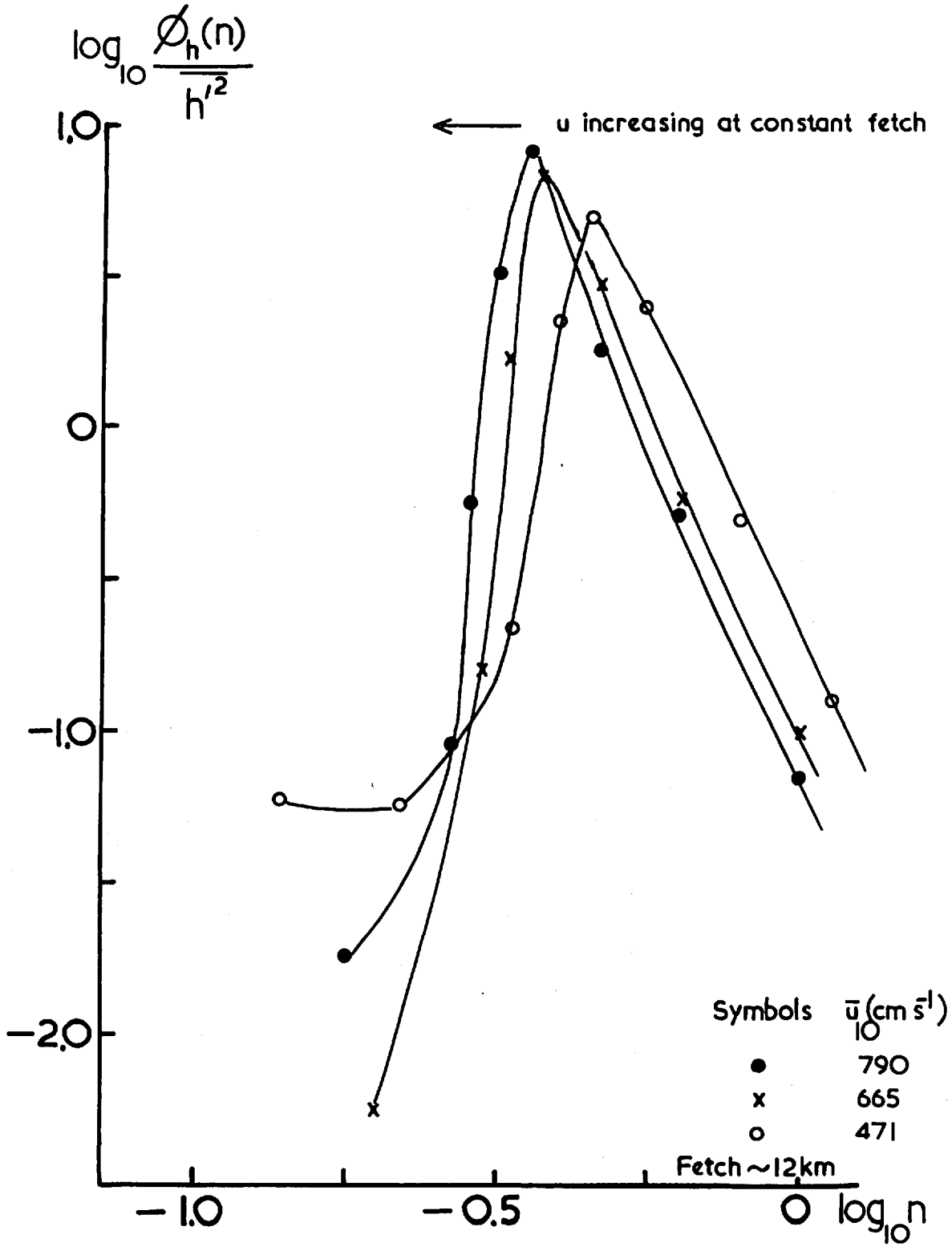
$\log_{10} \frac{\phi_h(n)}{\overline{h'^2}}$
u increasing at constant fetch
1.0
0
-1.0
-2.0
-1.0
-0.5
0
$\log_{10} n$
Symbols
$\bar{u}_{10}$ (cm s^{-1})
790
665
471
Fetch ~12km

FIG.6.6

additional energy to all wave components. Thus successive wave components of increasingly lower frequency reach saturation thereby extending the equilibrium range and decreasing n_o; by an increase in F which provides a longer time for injection of energy to waves from the wind, the transition frequency decreasing thereby extending the equilibrium range. Thus the increase in $\overline{h'^2}$ and decrease in n_o is a consequence of the saturation at higher frequencies constituting the equilibrium range. There is also an increase in $\phi_h(n_o)$.

Now, $$\overline{h'^2} = \int_0^\infty \phi_h(n)\, dn = \int_0^{n_o} \phi_1(n)\, dn + \int_{n_o}^\infty \phi_2(n)\, dn$$

The form of $\phi_2(n)$ in the capillary range is not important in this context and may be written as βn^{-a}. Therefore,

$$\overline{h'^2} = I_1 + \frac{\beta}{a-1} n_o^{1-a} \qquad 6.8$$

where $I_1 = \int_0^{n_o} \phi_1(n)\, dn \simeq 0.$ i.e. $\overline{h'^2} = \frac{\beta}{a-1} n_o^{1-a}$

For $a = 5$, $\beta = 8$, $\overline{h'^2} = 2n_o^{-4}$

and $a = 4.5$, $\beta = 8$, $\overline{h'^2} = 2.3\, n_o^{-3.5}$ 6.9

Relation 6.9 would be appropriate for the Lough Neagh data.

Fig.6.7 shows $\overline{h'^2}$ vs n_o^{-1} together with the curve representing relation 6.9. The deviation at high values of $\overline{h'^2}$ suggests the non-negligeability of I_1, due to the growth of the

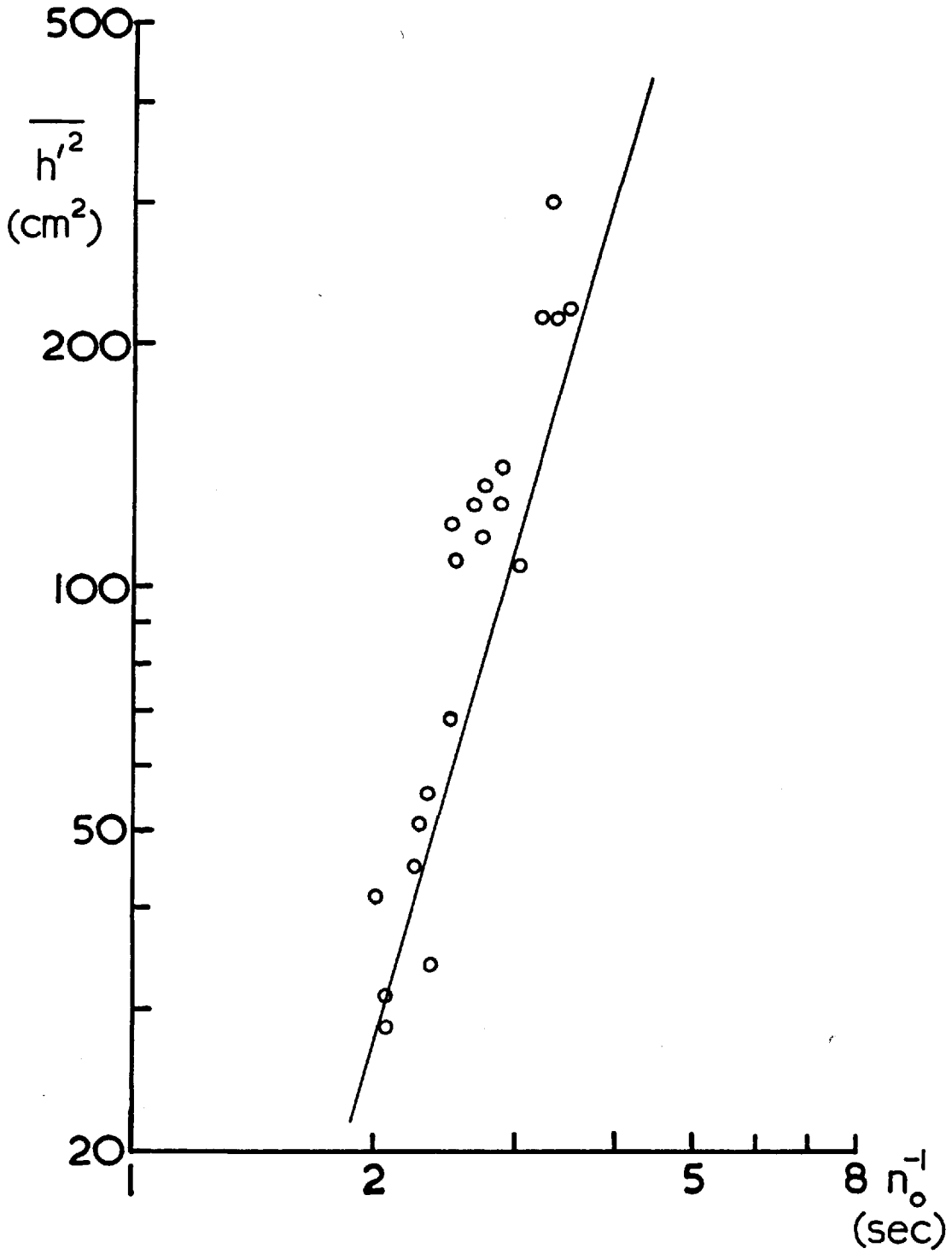

FIG.6.7

low frequency components with increase in fetch. Certainly 6.9 could be used to estimate $\overline{h'^2}$ given n_o from observation.

6.4. The Aerodynamic Roughness and Wave Statistics

It has been conjectured (see Phillips, 1958 for instance) that z_o will be determined principally by the wave components with the greatest contribution to the mean square surface slope and not to $\overline{h'^2}$; such components will have frequencies $n >> n_o$. The components that support the bulk of the surface stress must then be those for which $c < c_1$ where $c_1 \simeq 5 u_*$ (see Phillips' monograph, p.143) and for these the mean square surface displacement can be written,

$$\left(\overline{h'^2}\right)_r = \int_{n_1}^{\infty} \phi_h(n)\, dn \qquad 6.10$$

following Phillips with $n_1 = g(2\pi c_1)^{-1} = g(10\pi u_*)^{-1}$.

The contribution of the capillary components is negligible and using relation 6.5,

$$\left(\overline{h'^2}\right)_r = \alpha g^2 \int_{n_1}^{\infty} n^{-5}\, dn = \frac{\alpha g^2 n_1^{-4}}{4} = \frac{\alpha g^2 g^{-4} (2\pi c_1)^4}{4} = \alpha g^{-2} 4\pi^4 c_1^4.$$

If the flow was aerodynamically rough, z_o being independent of ν would be proportional to $\left(\overline{h'^2}\right)_r^{\frac{1}{2}}$ viz.,

$$z_o \propto \alpha^{\frac{1}{2}} g^{-1} 2\pi^2 c_1^2 = 50\pi^2 \alpha^{\frac{1}{2}} u_*^2 g^{-1}.$$

The relation $z_o \propto u_*^2 g^{-1}$ was suggested originally (on purely dimensional grounds) by Charnock (1955).

For a transitional flow (between aerodynamically smooth and rough) one can postulate,

$$z_o = f\left(\left(\overline{h'^2}\right)_r^{1/2}, \quad \nu u_*^{-1}\right) \qquad 6.11$$

where νu_*^{-1} characterises the thickness of the viscous sub-layer.

Kitaigorodskii (1968) approaches the problem through consideration of the stage of wave development, the degree of which can be described by $c_o u_*^{-1}$ or $g \sigma_h u_*^{-2}$, σ_h^2 being equal to $\overline{h'^2}$.

For small development, $c_o/u_* \ll 1$ and $g \sigma_h u_*^{-2} \ll 1$, he predicts $z_o \sim \sigma_h$. At moderate development $c_o/u_* \sim 1$, $g \sigma_h u_*^{-2} \sim 1 - 10$, then $z_o \sim \sigma_h \exp(-\kappa c_o u_*^{-1})$ and for very large development $c_o/u_* \gg 1$, $g \sigma_h u_*^{-2} > 10^2$, then $z_o \propto u_*^2 g^{-1}$ where the flow is now aerodynamically rough. Further for moderate and large development the relation

$$\frac{z_o u_*}{\nu} = f\left(\frac{u_*^3}{g\nu}\right) \qquad 6.12$$

equivalent to 6.11 should depend in its form upon the degree of wave development represented by $g \sigma_h u_*^{-2}$, viz.,

$$\frac{z_o u_*}{\nu} = f\left(\frac{u_*^3}{g\nu}, \quad \frac{g\sigma_h}{u_*^2}\right) \qquad 6.13$$

Thus the existence of different stages of wave development will result in a large scattering on the graph of the function $z_o(u_*)$. This is especially evident when plotting $z_o u_*/\nu$ vs $u_*^3/g\nu$, as was done by Kitaigorodskii (1968) for values of $g \sigma_h u_*^{-2}$ equal to

60 and 120. His results are shown in Fig.6.8 and for the present set of Lough Neagh data similar quantities were computed —see Table 6.1 — and plotted in Fig.6.8.

Table 6.1

RUN	c_o/u_*	$g\sigma/u_*^2$	$z_o u_*/\nu$	$u_*^3/g\nu$
540	21	20.2	0.047	47
541	19	13.6	0.028	72
542	14	9.1	0.16	176
543	—	—	0.063	158
549	—	—	5.1	60
553	17.5	17.2	5.2	48
555	—		8.2	58
557	19.5	22.6	0.29	73
565	14.5	10.0	1.4	268
566	15	10.6	1.3	228
575	29	37.8	0.024	66
577	20.5	18.4	0.069	149
578	25	29.5	0.25	72

Apart from the three odd points with $z_o u_*/\nu >> 1$ the relation is consistent with that of Kitaigorodskii taking into consideration the value of $g\sigma_h u_*^{-2} \simeq 20$ compared to that for the Russian work. Thus the state of the sea at Lough Neagh can be described as only moderately developed and z_o should be given by $\sigma_h \exp(-\kappa c_o u_*^{-1})$. Values of this quantity compared to values measured from wind profiles are shown in Table 6.2 using $\kappa = 0.4$. The values are of the same order as z_o, but more data would be required to derive the constant of proportionality connecting z_o and $\sigma_h \exp(-\kappa c_o u_*^{-1})$.

The dependence of z_o upon u_* requires specification of

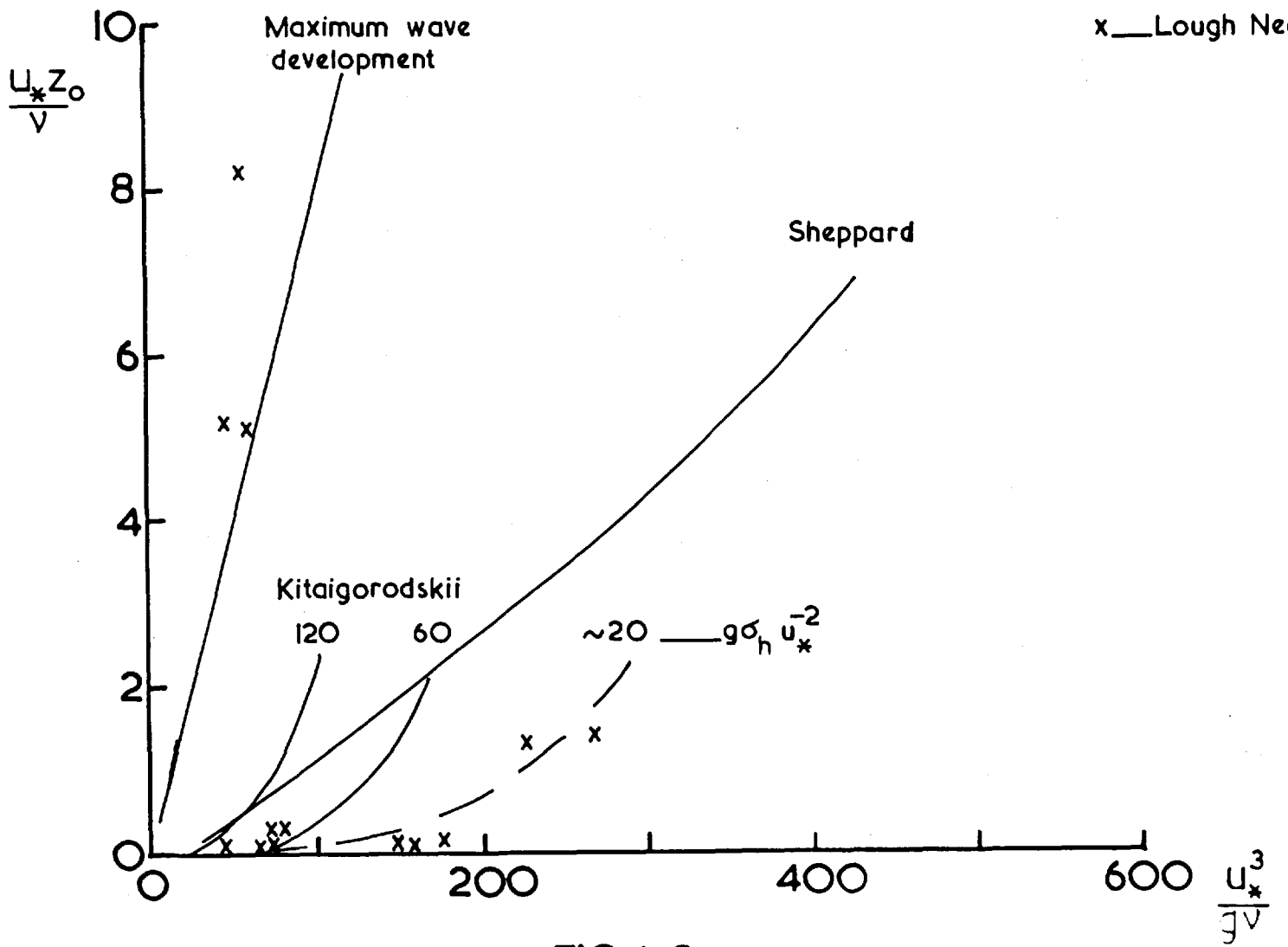
Maximum wave development
x__Lough Neagh
Sheppard
Kitaigorodskii
120
60
~20 ___ $g\sigma_h u_*^{-2}$
$\frac{u_* z_o}{\nu}$
$\frac{u_*^3}{g\nu}$
0
2
4
6
8
10
200
400
600

FIG.6.8

Table 6.2

RUN	$\ln z_o$	$\ln(q_h \exp(-\kappa c_o u_*^{-1}))$
540	-7.9	-6.4
541	-8.5	-5.6
542	-7.1	-3.5
553	-3.2	-5.1
557	-6.2	-5.4
565	-5.1	-3.3
566	-5.1	-3.6
575	-8.7	-8.6
577	-7.9	-5.5
578	-7.1	-7.3

the degree of wave development through the quantity $g \sigma_h u_*^{-2}$. Values of this quantity in Table 6.1 are seen to be not widely varying (between 10 and 40). Indeed inspection of Table 6.1 suggests $c_o u_*^{-1} \simeq g \sigma_h u_*^{-2}$, the quantity $c_o u_*^{-1}$ varying between 15 and 30. The near-constancy of this parameter may be a good reason why Sheppard obtained a very good correlation between z_o and u_* obtained from neutral wind profiles with $z_o \propto u_*^{2.7}$. Unfortunately his relation when plotted in the correct coordinates for Fig.6.8 is not altogether consistent with the other data which show a consistent variation with degree of wave development.

Since Sheppard data was taken at the same site as the author's data a value of $g \sigma_h u_*^{-2} \simeq 20$ can be assigned to the former. Because a much greater amount of data is involved greater emphasis should be placed on Sheppard's curve in Fig.6.8 than the author's, drawn through sparsely distributed points. Having made this readjustment, comparison of the Sheppard curve to those of

Kitaigorodskii taking into account the values of $g\,\sigma_h\,u_*^{-2}$ does not yield total disagreement, and their positions relative to that occupied by the curve representing maximum wave development viz. for $z_o = 7.8 \times 10^{-2}\,u_*^2\,g^{-1}$ (from Phillips) should be noted.

6.5. Modification of Turbulence Spectra by the Wave Motion

Stewart (1967) has shown by application of Miles' theory that significant horizontal and vertical fluctuation energy should exist due to the wave motion, and should result in a relatively large spectral contribution in the turbulence spectra over a frequency range corresponding to the width of the wave spectral peak. That such peaks are absent from the spectra of Smith (1966), measured at the British Columbia site from a fixed mast, leads him to cast doubt upon the Miles' theory of wave generation. However Preobrazhenskii (1968) has reported such wave effects upon the turbulence spectra measured from a floating buoy. Here there is the added complication of the oscillatory motion of the instrument buoy and, as Stewart has pointed out, since the wave motion is large compared with the air velocities at wave frequencies, even a small contamination of the signal by wave motion will introduce a large spurious peak in the turbulence spectrum.

It seems reasonable to expect a significant modification of the u' and w' spectra at frequencies $\sim n_o$ up to heights z such that the ratio $\frac{a}{}$ of the height z to the wave amplitude is $\lesssim 1$.

In the case of the Lough Neagh data, for Runs 575 A, 577 A there exist the optimum conditions viz. a minimum value of $\frac{a}{}$ amongst the runs for observing the anomalous spectral energy peaks,

with the height of observation 1.6 m. and the wave amplitude 49 and 40 cm. respectively. Thus values of $\underline{a}$ were 3.3 and 4.0 respectively. Careful scrutiny of the turbulence spectra for these, and other, runs revealed no evidence that the wave power impresses itself upon the turbulence spectra.

Smith's value of $\underline{a}$ was about 4.5 whilst that of Preobrazhenskii was comparable; this would imply that the peaks observed by Preobrazhenskii were largely due to spurious effects introduced by the oscillatory motions of the instrument buoy. The measurement of spectra at materially smaller values of $\underline{a}$ would require a special mounting of u,w sensors allowing sampling below the highest wave crests —a difficult operation.

Summary of Results

The thesis was written to provide a comprehensive, and at the same time quantitative, description of many aspects of turbulence in the surface layer of the atmosphere above the sea surface, together with a description of the properties of the wind driven sea waves. Data collected over the past few years at Lough Neagh, after analysis, allowed the following to be assessed,

(a) Relations of the vertical profiles of u, θ, q to the turbulent transfers of momentum, heat and water vapour, and their relative efficiences as a function of Richardson Number.

(b) Bulk properties of the turbulence in relation to the nature of the vertical fluxes of heat and momentum.

(c) Properties of the dissipation rate of kinetic energy.

(d) Spectral properties in relation to the Kolmogorov Theory of locally isotropic turbulence and the Monin-Oboukhov Similarity Theory.

(e) Properties of the sea surface.

Analysis of the profiles of u and θ and the eddy fluxes of heat and momentum confirm results overland that K_H/K_M varies with Ri such that $K_H > K_M$ when Ri is negative and $K_H < K_M$ when Ri is positive. In the former case there is a greater correlation between w' and T' than for u' and w' ($r_{wT} > r_{uw}$) and in the latter it is found $r_{wT} < r_{uw}$. The relative positions of the cospectral peaks for heat and momentum fluxes for different values of Ri are consistent with the relative sizes of K_H and K_M. Analogue records of the instantaneous products u'w' and w'T' suggest that the large eddies effect the greater part of the heat and

momentum transfer in convection as found earlier by Priestley overland, periods of intense eddy transfer associated with the large eddies being separated by periods with relatively little vertical transfer present.

Computed fluxes of heat and momentum indicate that a sampling period of 10 minutes is sufficient to measure the greater part of the contribution under the conditions met at Lough Neagh but such a sampling period implies a high statistical variability because of the relatively high spectral correlation coefficient at low frequencies. This arises not from a high cospectral density but from small values of the vertical velocity energy at these frequencies. Extrapolation of the spectral correlation curves suggest a sampling period of 30 - 60 minutes for statistically stable flux estimates. For the majority of runs $\overline{u'w'}$ and $\overline{w'T'}$ are approximately constant with height, the remainder having a variation implying horizontal gradients of wind speed and temperature ~ 1 m s^{-1} km^{-1} and 0.2°C km^{-1} respectively which are large on a synoptic scale but can occur at smaller scales locally. The separation of the runs is found to be significant because only when the momentum flux is approximately constant with height is there close agreement with the friction velocity evaluated independently from the wind profile.

Thus in conditions of near-constancy of flux with height and non-extreme stabilities u_* found using the log-linear formula gives the momentum flux to within 20 per cent. In addition measurements of $\overline{u'^2}$ and/or $\overline{w'^2}$ allow $-\overline{u'w'}$ to be inferred with a probable error of 5 - 10 per cent.

A heat transfer coefficient relating $\overline{w'T'}$ to $\bar{u}_{10}$, $\theta_{10} - \theta_o$ was found empirically and though the relation has unacceptable physical consequences in neutral and stable conditions, it serves to determine the heat flux to within 10 per cent from relatively simple measurements. Knowledge of the coefficient also allows for the determination of evaporation if $q_{10} - q_o$ is known. There is close agreement between the heat flux $-u_*\theta_*$, estimated from the profiles using the log-linear formula, and the eddy flux $\overline{w'T'}$.

The Kolmogorov -5/3 Law is found to exist in the anisotropic region of the spectrum, though the ratio of the spectral densities for w and u in the -5/3 region is close to 4/3, appropriate to locally isotropic turbulence. However this is a necessary but not sufficient condition for the existence of local isotropy. The Universal constants for the u spectrum and structure function were evaluated and values of the dissipation rate then computed. This quantity depends upon $\bar{u}$, z, Ri and roughness, and in a non-dimensional form viz. $\varepsilon z u_*^{-3}$ gives a Von Karman constant of 0.4. The dissipation rate is balanced approximately by the rates of production of mechanical and buoyant energy, with the vertical flux divergence estimated to be small on most occasions.

The -5/3 law of the temperature spectrum was also confirmed, allowing for a determination of the dissipation rate of temperature fluctuations, χ. Measurements suggest that on occasions the vertical flux divergence is significant, and comparable in size to the local terms.

The spectra and cospectra are described by the Similarity Theory and with data from other sources they indicate a set of

Universal non-dimensional spectra and cospectra for any type of underlying surface and described (according to the Ri) by a set of empirical relations.

The sea surface at Lough Neagh is characterised by wind induced gravity waves of period 2 to 4 seconds and a wave spectrum depending upon wind speed and fetch, with a sharp peak and high frequency region with saturation "energy" proportional to frequency to the power -4.5. The Universal constant appropriate to this equilibrium range is close to that given by Phillips. The degree of wave development is specified through the theory of Kitaigorodskii and found to vary only slightly about a value well below the maximum possible for the open ocean. The implication is that z_o and u_* are closely related as found by Sheppard for Lough Neagh viz. $z_o \propto u_*^{2.7}$, and the limiting configuration is represented by Charnock's relation $z_o \propto u_*^2 g^{-1}$.

There is no evidence that wave power impresses itself upon the turbulence spectra and it is suggested that any such effect will occur only at levels at or below the level of the wave crests.

Appendix 1. Turbulence Data

RUN	Date	Time G.M.T.	Azimuth degrees	T_o °C	z cm	$\bar{u}$ cm s^{-1}	$\bar{u}_{10}$ cm s^{-1}	$\theta - \theta_o$ °C	$\theta_{10} - \theta_o$ °C
327	10.10.63	1550	250	11.3	400	535	610	1.98	2.32
328	10.10.63	1610	240	11.6	400	497	587	2.21	2.60
337	11.10.63	1320	220	11.7	400	635	731	1.24	1.50
338	12.10.63	0810	190	11.7	400	748	773	-3.33	-3.46
344	14.10.63	1335	190	11.7	400	600	611	-2.03	-2.04
352	16.10.63	0800	220	11.7	400	658	690	-3.16	-3.24
397	16.10.64	1555	300	10.7	400	600	657	1.00	1.10
407	19.10.64	1418	200	10.8	400	452	555	2.42	3.16
414	22.10.64	0811	200	10.5	400	788	842	-2.58	-2.69
415	22.10.64	0853	195	10.4	400	768	821	-1.86	-1.88
540 A	23. 7.68	1627	340	17.3	180	581	663	-0.52	-0.56
540 C	"				1210	675		-0.57	
541 A	"	1642	340	17.4	180	585	664	-0.58	-0.61
541 C	"				1210	677		-0.61	
542 B	"	1707	330	17.3	420	624	665	-0.89	-0.93
542 C	"				1210	674		-0.94	
543 B	"	1724	335	17.2	420	723	771	-1.33	-1.37
543 C	"				1210	781		-1.37	
549 A	25. 7.68	1400	325	17.4	180	383	423	-0.83	-0.90
549 B	"				420	405		-0.86	
553 A	"	1519	320	17.4	180	379	432	-0.54	-0.57
553 B	"				420	409		-0.56	
554 B	"	1535	330	17.4	420	430	454	-0.45	-0.47
554 C	"				1210	457		-0.47	
555 A	"	1550	320	17.4	180	407	457	-0.37	-0.40
555 B	"				420	437		-0.38	
557 B	13. 8.68	0927	270	18.0	425	619	660	-2.34	-2.44
557 C	"				1220	669		-2.46	
558 B	"	0942	270	18.1	430	615	649	-2.25	-2.33
558 C	"				1220	656		-2.35	
565 B	14. 8.68	1456	310	18.3	430	739	790	-2.56	-2.65
565 C	"				1220	800		-2.67	
566 B	"	1512	320	18.3	430	702	746	-2.10	-2.21
566 C	"				1220	756		-2.23	
575 A	20. 8.68	1525	220	17.2	160	489	570	0.26	0.34
575 B	"				400	527		0.30	
577 A	"	1557	225	17.2	160	566	682	1.13	1.39
577 B	"				395	619		1.26	
578 B	"	1612	230	17.3	400	634	709	1.53	1.70
578 C	"				1210	724		1.74	

RUN	G_u sec^{-1}	G_θ $°C\ cm^{-1}$	G_q cm^{-1}	Ri_D	Q	Ri_v	$Ri_v(4)$	BR(4)
327	0.178	7.58	-1.56	0.081	-.003	0.078	0.078	-1.95
328	0.197	8.45	-1.88	0.074	-.003	0.071	0.071	-1.80
337	0.264	5.17	-2.75	0.025	-.002	0.023	0.023	-0.75
338	0.110	-3.94	-2.84	-0.111	-.014	-0.125	-0.125	0.55
344	0.068	-2.02	-2.61	-0.148	-.034	-0.182	-0.182	0.31
352	0.109	-3.71	-2.57	-0.106	-.013	-0.119	-0.119	0.58
397	0.160	1.19	-3.76	0.016	-.009	0.007	0.007	-0.13
407	0.244	12.6	-0.83	0.072	-.001	0.071	0.071	-6.1
414	0.160	-3.94	-3.39	-0.053	-.008	-0.061	-0.061	0.47
415	0.165	-2.34	-3.03	-0.029	-.007	-0.036	-0.036	0.31
540 A	0.214	-1.44	-23.6	-0.011	-.031	-0.042	-0.053	0.033
540 C	0.051	-0.20	-2.21	-0.026	-.055	-0.081		
541 A	0.248	-1.68	-24.0	-0.009	-.023	-0.032	-0.054	0.014
541 C	0.047	-0.06	-2.01	~0	-.054	-0.054		
542 B	0.117	-1.19	-7.07	-0.030	-.031	-0.061	-0.061	0.067
542 C	0.038	-0.20	-1.41	-0.047	-.058	-0.105		
543 B	0.134	-1.47	-8.13	-0.028	-.027	-0.055	-0.055	0.072
543 C	0.050	-0.20	-2.01	-0.027	-.048	-0.075		
549 A	0.197	-2.40	-21.2	-0.021	-.031	-0.052	-0.229	0.048
549 B	0.058	-0.92	-7.66	-0.093	-.136	-0.229		
553 A	0.231	-0.96	-20.7	-0.006	-.002	-0.008	-0.081	0.023
553 B	0.079	-0.37	-6.32	-0.020	-.061	-0.081		
554 B	0.089	-0.51	-6.88	-0.022	-.052	-0.074	-0.073	0.030
554 C	0.011	-0.20	-1.51	-0.561	-1.31	-1.87		
555 A	0.240	-0.96	-21.2	-0.005	-.017	-0.022	-0.099	0.020
555 B	0.075	-0.37	-7.25	-0.022	-.077	-0.099		
557 B	0.124	-3.39	-8.03	-0.075	-.031	-0.106	-0.106	0.169
557 C	0.038	-0.50	-2.01	-0.118	-.083	-0.201		
558 B	0.106	-3.22	-6.97	-0.107	-.037	-0.144	-0.147	0.185
558 C	0.030	-0.50	-1.61	-0.189	-.107	-0.296		
565 B	0.145	-3.35	-10.1	-0.054	-.048	-0.102	-0.102	0.133
565 C	0.038	-0.60	-2.01	-0.141	-.083	-0.224		
566 B	0.125	-3.95	-10.3	-0.086	-.066	-0.152	-0.152	0.155
566 C	0.030	-0.81	-2.42	-0.308	-.161	-0.469		
575 A	0.216	2.40	-11.8	0.018	-.015	0.003	0.001	-0.073
575 B	0.108	0.92	-5.13	0.027	-.026	0.001		
577 A	0.298	6.97	-11.0	0.027	-.007	0.020	0.033	-0.248
577 B	0.158	3.35	-5.40	0.046	-.013	0.033		
578 B	0.180	4.22	-6.14	0.045	-.011	0.034	0.034	-0.276
578 C	0.080	1.91	-4.53	0.102	-.072	0.030		

RUN	u_*^2 $cm^2\ s^{-2}$	θ_* °C	$\overline{u'^2}$ $cm^2 s^{-2}$	$\overline{w'^2}$ $cm^2 s^{-2}$	$-\overline{u'w'}$ $cm^2 s^{-2}$	τ dynes cm^{-2}	$\overline{T'^2}$ $°C^2$	$\overline{w'T'}$ $cm\ s^{-1}$ °C	H_v m cal cm^{-2} min^{-1}
327	625	0.080	2720	1600	315	0.40	.0625	-1.7	-31
328	780	0.074	4210	1740	413	0.52	.0196	-1.8	-33
337	1850	0.059	1870	850	466	0.59	.0049	-0.9	-17
338	—	—	5270	—	—	—	.0324	—	—
344	—	—	4510	1280	451	0.56	.0169	1.5	28
352	1370	-0.085	3680	920	575	0.72	.0625	2.8	52
397	680	0.014	3560	1380	671	0.84	.0121	-0.5	-10
407	730	—	780	370	172	0.22	.0576	-1.4	-26
414	960	-0.102	6830	2040	1080	1.35	.0900	5.4	100
415	900	-0.054	6810	2880	1575	1.98	.0121	2.8	52
540 A	336	-0.011	3648	717	403	0.50	.0035	0.07	1.3
540 C			4000	862	317	0.40	—	—	—
541 A	307	-0.014	3145	707	426	0.53	.0040	0.28	5.2
541 C			2496	942	598	0.75	.0030	0.06	1.1
542 B	376	-0.030	2592	942	602	0.75	.0130	1.00	19
542 C			3773	1189	1150	1.44	.0126	1.18	22
543 B	455	-0.047	5630	1056	925	1.16	.0197	1.56	29
543 C			4423	1354	709	0.89	.0145	1.49	28
549 A	303	-0.017	2316	723	484	0.61	.043	0.61	12
549 B			2015	740	373	0.47	—	—	—
553 A	331	-0.007	1530	583	376	0.47	—	—	—
553 B			1507	540	353	0.44	—	—	—
554 B	442	-0.007	2681	587	255	0.32	.0017	0.19	3.5
554 C			3352	—	—	—	—	—	—
555 A	416	-0.007	2400	734	427	0.53	—	—	—
555 B			2651	606	410	0.51	—	—	—
557 B	645	-0.078	2923	1008	477	0.60	.0216	1.90	35
557 C			3956	1038	492	0.62	.0277	1.53	28
558 B	900	-0.069	4375	1115	577	0.72	.0195	2.07	39
558 C			5331	—	—	—	.0124	—	—
565 B	1030	-0.093	5264	1433	1034	1.29	.0424	3.44	64
565 C			4156	2253	1285	1.61	.0231	4.43	83
566 B	940	-0.090	5391	1349	929	1.16	.0408	2.76	51
566 C			4876	1918	1150	1.44	.0236	3.79	71
575 A	216	0.018	2714	1289	568	0.71	.0148	-0.15	-2.8
575 B			2190	641	341	0.43	.0070	-0.15	-2.8
577 A	335	0.052	3739	1891	1019	1.28	.0202	-1.00	-19
577 B			2859	960	568	0.71	—	—	—
578 B	440	0.067	3628	1055	510	0.64	.0140	-0.80	-15
578 C			3038	1055	456	0.57	.0216	-0.95	-7.8

RUN	$\overline{u'T'}$ cm s^{-1} °C	H_h m cal cm^{-2} min^{-1}	$\lvert L_v \rvert$ m	z/L_v	K_H cm^2 s^{-1}	K_M cm^2 s^{-1}	K_H/K_M	$\overline{u'^2}/\overline{w'^2}$	$\overline{u'^2}/-\overline{u'w'}$
327	10.5	195	24.8	0.161	2240	1770	1.26	1.69	8.6
328	7.9	147	35.2	0.114	2130	2100	1.01	2.40	10.0
337	1.9	35	91.6	0.044	1740	1760	0.99	2.19	3.3
338	-5.1	-95	—	—	—	—	—	—	—
344	-4.0	-75	37.5	-0.117	7450	6650	1.12	3.54	9.9
352	-9.7	-180	31.4	-0.127	7550	5280	1.43	4.00	6.4
397	3.7	69	580	0.007	4450	4200	1.06	2.72	5.6
407	3.4	63	11.7	0.34	1110	705	1.58	2.07	4.3
414	-6.8	-126	46.5	-0.086	13700	6750	2.03	3.32	6.3
415	-5.8	-108	132.5	-0.030	11750	9550	1.23	2.38	4.3
540 A	-1.65	-31	208	-0.009	485	1880	0.26	5.10	9.1
540 C	-1.92	-36	—	—	—	—	—	4.65	12.6
541 A	-1.01	-19	65.5	-0.027	1670	1720	0.97	4.45	7.4
541 C	0.27	5	297	-0.041	10000	12700	0.79	2.65	4.2
542 B	-2.52	-47	76.3	-0.055	5800	5150	1.13	2.75	4.3
542 C	-3.62	-67	156.5	-0.078	59050	30250	1.95	2.11	3.3
543 B	-1.97	-36	65.3	-0.065	10600	6900	1.54	5.35	6.1
543 C	-1.24	-23	33.0	-0.368	74500	14200	5.25	3.26	6.3
549 A	-1.84	-34	—	—	—	—	—	3.20	4.8
549 B	-1.44	-27	—	—	—	—	—	2.72	5.4
553 A	-0.79	-15	—	—	—	—	—	2.63	4.1
553 B	-0.57	-11	—	—	—	—	—	2.80	4.3
554 B	-0.17	-3.2	45.5	-0.092	3730	2860	1.30	4.66	10.5
554 C	1.06	20	—	—	—	—	—	—	—
555 A	1.00	19	—	—	—	—	—	3.27	5.6
555 B	-1.31	-24	—	—	—	—	—	4.37	6.5
557 B	-2.34	-43	28.5	-0.149	5600	3850	1.45	2.92	6.1
557 C	0.42	7.8	30.0	-0.405	30600	12950	2.36	3.82	8.0
558 B	-2.79	-52	32.5	-0.132	6450	5440	1.18	3.93	7.6
558 C	-2.01	-37	—	—	—	—	—	—	—
565 B	-7.30	-136	37.0	-0.116	10250	7150	1.44	3.67	5.1
565 C	-3.78	-71	47.1	-0.258	73800	33800	2.18	1.85	3.2
566 B	-8.50	-158	49.6	-0.087	7000	7450	0.94	4.00	5.8
566 C	-5.97	-111	48.5	-0.252	46800	38400	1.22	2.54	4.3
575 A	0.47	8.8	3300	0.001	625	2630	0.24	2.11	4.8
575 B	0.46	8.6	8000	0.001	1630	3160	0.52	3.42	6.4
577 A	3.71	69	350	0.005	1440	3420	0.42	1.98	3.7
577 B	3.04	57	—	—	—	—	—	2.98	5.1
578 B	4.79	89	74.5	0.054	1900	2830	0.67	3.44	7.1
578 C	4.78	89	400	0.030	5000	5710	0.97	2.88	6.7

RUN	$w^2/-\overline{u'w'}$	$\overline{u'T'}/\overline{w'T'}$	$\sigma_T^2/\left(z\frac{\partial\theta}{\partial z}\right)^2$	r_{uw}	r_{wT}	r_{uT}	$\lvert r_{wT}/r_{uw}\rvert$
327	5.1	-6.2	1.44	0.15	-0.17	0.81	1.13
328	4.2	-4.4	5.81	0.15	-0.32	0.87	2.13
337	1.5	-2.1	8.65	0.37	-0.42	0.64	1.13
338	—	—	0.77	—	—	-0.39	—
344	2.8	-2.7	0.38	0.19	0.34	-0.46	1.79
352	1.6	-3.5	0.36	0.31	0.37	-0.64	1.19
397	2.1	-7	0.18	0.30	-0.41	0.55	1.36
407	2.1	-2.4	4.45	0.32	-0.30	0.51	0.94
414	1.9	-1.3	0.29	0.29	0.40	-0.87	1.37
415	1.8	-2.1	0.72	0.36	0.47	-0.64	1.30
540 A	1.8	-23.6	0.19	0.25	0.14	-0.46	0.56
540 C	2.7	—	—	0.17	—	—	—
541 A	1.7	-3.6	0.23	0.29	0.17	-0.29	0.59
541 C	1.6	4.4	0.02	0.39	0.11	0.31	0.28
542 B	1.6	-2.5	0.19	0.39	0.29	-0.43	0.75
542 C	1.6	-3.1	0.03	0.44	0.30	-0.53	0.68
543 B	1.1	-1.3	0.19	0.38	0.34	-0.59	0.90
543 C	1.9	-0.8	0.04	0.29	0.34	-0.49	1.17
549 A	1.5	-3.0	0.02	0.37	—	-0.58	—
549 B	2.0	—	—	0.31	—	—	—
553 A	1.6	—	—	0.40	—	—	—
553 B	1.5	—	—	0.39	—	—	—
554 B	2.3	-0.9	0.03	0.21	0.19	-0.08	0.90
554 C	—	—	—	—	—	—	—
555 A	1.7	—	—	0.32	—	—	—
555 B	1.5	—	—	0.47	—	—	—
557 B	2.1	-1.2	0.98	0.28	0.41	-0.28	1.46
557 C	2.1	+0.3	0.14	0.25	0.29	0.04	1.16
558 B	1.9	-1.3	0.96	0.26	0.44	-0.30	1.69
558 C	—	—	0.30	—	—	-0.25	—
565 B	1.4	-2.1	0.49	0.38	0.44	-0.49	1.16
565 C	1.8	-0.9	0.24	0.42	0.61	-0.39	1.45
566 B	1.5	-3.1	0.72	0.35	0.37	-0.57	1.06
566 C	1.7	-1.6	0.42	0.38	0.56	-0.55	1.47
575 A	2.3	-3.1	0.10	0.31	-0.11	0.23	0.36
575 B	1.9	-3.1	0.19	0.29	-0.22	0.37	0.76
577 A	1.9	-3.7	0.61	0.38	-0.16	0.42	0.42
577 B	1.7	—	—	0.34	—	—	—
578 B	2.1	-6.0	2.02	0.26	-0.21	0.67	0.81
578 C	2.3	-5.0	2.41	0.26	-0.18	0.59	0.69

RUN	E cm^2s^{-2}	ε_1 cm^2s^{-3}	ε_2 cm^2s^{-3}	ε_3 cm^2s^{-3}	$E/\bar{\varepsilon}$ sec	$uE/\bar{\varepsilon}$ m
327	3240	52	53	—	62	332
328	4460	60	63	—	73	373
337	2040	94	86	—	23	133
338	—	152	150	—	35	261
344	4340	64	59	—	71	414
352	3450	63	61	—	56	362
397	3700	86	77	—	45	270
407	865	41	41	—	21	97
414	6650	268	251	—	26	197
415	7270	191	199	—	37	291
540 A	3270	204	204	64	21	122
540 C	3650	15	—	—	243	1640
541 A	2880	138	150	122	21	123
541 C	2580	33	45	46	63	426
542 B	2650	48	—	74	44	275
542 C	3760	45	—	—	84	566
543 B	5010	197	211	96	30	217
543 C	4330	38	—	—	114	890
549 A	2280	68	—	132	23	88
549 B	2060	27	28	50	59	239
553 A	1590	53	53	78	26	99
553 B	1540	21	22	31	55	225
554 B	2450	28	28	53	68	292
554 C	—	18	21	—	163	745
555 A	2350	59	61	138	27	110
555 B	2440	35	32	46	64	280
557 B	2950	68	—	100	35	216
557 C	3750	36	—	35	104	695
558 B	4110	83	—	86	49	301
558 C	5070	35	—	—	145	950
565 B	5020	184	172	160	29	214
565 C	4810	70	—	65	71	569
566 B	5060	160	135	135	36	252
566 C	5090	57	—	63	85	643
575 A	3000	185	155	320	14	69
575 B	2120	72	65	57	33	174
577 A	4220	331	299	450	12	68
577 B	2860	138	126	140	21	130
578 B	3510	193	—	130	22	139
578 C	3070	68	—	59	48	348

RUN	u_{16}	u_8	u_4	u_2	u_1	$\theta_{16}-\theta_o$	$\theta_8-\theta_o$	$\theta_4-\theta_o$	$\theta_2-\theta_o$	$\theta_1-\theta_o$
	cm s^{-1}					°C				
327	659	588	535	487	440	2.52	2.23	2.00	1.81	1.68
328	650	560	497	450	410	2.87	2.51	2.24	2.04	1.90
337	781	708	635	561	488	1.64	1.45	1.28	1.16	1.05
338	780	769	748	706	(650)	-3.46	-3.39	-3.29	-3.17	-3.02
344	617	609	600	565	(481)	-2.07	-2.03	-1.99	-1.92	-1.83
352	705	682	658	620	(537)	-3.28	-3.21	-3.11	-3.00	-2.86
397	687	643	600	556	512	1.13	1.09	1.05	1.02	0.99
407	613	529	452	395	340	3.62	2.96	2.51	2.26	2.02
414	859	830	788	740	681	-2.72	-2.67	-2.59	-2.45	-2.30
415	844	810	768	721	657	-1.92	-1.87	-1.81	-1.74	-1.65
540	695	652	619	586	554	-0.57	-0.56	-0.54	-0.52	-0.50
541	691	652	621	590	559	-0.61	-0.61	-0.60	-0.59	-0.56
542	688	655	622	589	556	-0.95	-0.93	-0.89	-0.85	-0.80
543	797	758	720	684	647	-1.39	-1.36	-1.33	-1.28	-1.20
545	480	466	450	430	402	-0.86	-0.83	-0.81	-0.78	-0.74
546	544	524	503	480	451	-0.94	-0.91	-0.88	-0.85	-0.81
549	429	420	406	387	356	-0.92	-0.89	-0.86	-0.83	-0.81
550	474	461	439	412	378	-0.87	-0.85	-0.83	-0.81	-0.79
551	495	485	465	437	402	-0.82	-0.79	-0.77	-0.75	-0.72
553	439	426	407	383	353	-0.58	-0.57	-0.56	-0.55	-0.53
554	460	448	429	403	367	-0.48	-0.46	-0.45	-0.44	-0.43
555	464	453	436	413	377	-0.41	-0.39	-0.38	-0.37	-0.36
556	680	657	628	592	543	-2.62	-2.57	-2.49	-2.40	-2.27
557	682	650	617	584	536	-2.48	-2.42	-2.34	-2.23	-2.11
558	665	643	615	580	526	-2.37	-2.32	-2.24	-2.15	-2.04
559	708	680	650	613	560	-2.23	-2.18	-2.10	-1.99	-1.88
563	640	620	595	563	516	-2.42	-2.36	-2.27	-2.15	-2.04
564	728	695	660	620	568	-2.45	-2.37	-2.26	-2.14	-2.03
565	809	776	739	696	640	-2.68	-2.64	-2.56	-2.45	-2.30
566	759	733	702	664	610	-2.27	-2.19	-2.09	-1.97	-1.83
575	595	556	525	496	470	0.36	0.33	0.30	0.27	0.24
576	733	669	623	585	552	1.16	1.08	1.01	0.94	0.86
577	731	666	618	579	543	1.49	1.35	1.26	1.16	1.07
578	751	685	636	593	554	1.81	1.65	1.54	1.42	1.30

RUN	$q_o - q_{16}$	$q_o - q_8$	$q_o - q_4$	$q_o - q_2$	$q_o - q_1$
	gm/Kg				
327	—	—	—	—	—
328	—	—	—	—	—
337	0.80	0.69	0.61	0.54	0.48
338	1.86	1.78	1.70	1.62	1.54
344	1.35	1.30	1.23	1.15	1.06
352	1.21	1.14	1.06	0.99	0.92
397	1.37	1.22	1.10	1.01	0.93
407	—	—	—	—	—
414	2.16	2.09	2.00	1.90	1.79
415	1.77	1.69	1.60	1.52	1.44
540	5.08	4.90	4.67	4.39	-4.09
541	5.01	4.82	4.59	4.32	4.07
542	4.70	4.58	4.41	4.19	3.92
543	4.47	4.27	4.06	3.84	3.58
545	4.93	4.79	4.64	4.45	4.18
546	4.97	4.82	4.65	4.45	4.18
549	5.00	4.91	4.74	4.50	4.22
550	5.05	4.93	4.76	4.51	4.25
551	4.83	4.71	4.52	4.28	4.03
553	4.85	4.76	4.62	4.40	4.13
554	4.75	4.61	4.43	4.22	3.95
555	4.87	4.74	4.56	4.34	4.06
556	4.95	4.83	4.65	4.41	4.17
557	4.98	4.81	4.60	4.36	4.12
558	4.97	4.83	4.65	4.43	4.18
559	4.92	4.78	4.57	4.31	4.03
563	5.07	4.90	4.68	4.34	3.89
564	5.93	5.73	5.45	5.04	4.52
565	5.83	5.66	5.42	5.10	4.64
566	5.22	5.01	4.76	4.43	3.98
575	3.44	3.24	3.09	2.94	2.79
576	3.09	2.85	2.71	2.56	2.42
577	2.97	2.70	2.52	2.39	2.25
578	3.21	2.86	2.68	2.52	2.35

Symbols

$G_u \equiv \partial U/\partial z$

$G_\theta = \partial\theta/\partial z \times 10^4$

$G_q = \partial q/\partial z \times 10^4$

BR(4) = Bowen Ratio defined as $\dfrac{4 \times 10^{-4}\ \partial\theta/\partial z}{\partial q/\partial z}$

$H_v = \rho C_p \overline{w'T'}$

$H_h = \rho C_p \overline{u'T'}$

$\tau = \rho(-\overline{u'w'})$

$r_{xy}^2 = \dfrac{(\overline{x'y'})^2}{\overline{x'^2}\ \overline{y'^2}}$

$E = \dfrac{3}{4}(\overline{u'^2} + \overline{w'^2})$

ε_1 = ε evaluated from u spectrum 5/3 law

ε_2 = ε evaluated from u structure function 2/3 law

ε_3 = ε evaluated from w spectrum 5/3 law.

Appendix 2: Wave Data

RUN	Fetch km	$\bar{u}_{10}$ cm s^{-1}	T_{obs} sec	T_o sec	T_f sec	n_o sec^{-1}	c_o cm s^{-1}	λ_o cm	$c_f/\bar{u}_{10}$	F/λ_f^3 x 10^{-3}
540	8	663	2.19	2.32	2.56	0.43	361	839	0.601	0.78
541	8	664	2.15	2.27	2.50	0.44	354	805	0.590	0.82
542	8 - 9	665	2.23	2.50	2.62	0.40	390	976	0.615	0.79
545	16	471	2.09	2.22	2.50	0.45	346	769	0.828	1.64
546	8 -16	529	2.10	2.32	2.50	0.43	361	839	0.739	1.23
550	8	466	2.05	2.06	2.22	0.49	321	661	0.743	1.11
551	8 -16	489	2.09	2.06	2.28	0.49	321	661	0.728	1.48
553	8	432	2.06	2.00	2.13	0.50	312	624	0.770	1.20
556	12.5	665	2.42	2.70	3.00	0.37	421	1136	0.705	0.89
557	12.5	660	2.42	2.62	2.78	0.38	409	1071	0.657	1.04
558	12.5	649	2.49	2.50	2.78	0.40	390	976	0.670	1.04
559	12.5	686	2.49	2.50	2.85	0.40	390	976	0.650	0.99
563	8	627	2.53	3.00	3.33	0.33	468	1401	0.830	0.46
564	9 -16	705	2.46	2.71	3.20	0.37	422	1140	0.710	0.81
565	14	790	2.53	2.86	3.12	0.35	446	1279	0.617	0.92
566	9 -16	746	2.56	2.86	3.12	0.35	446	1279	0.653	0.86
575	20	570	3.16	3.33	4.00	0.30	520	1730	1.100	0.80
576	20	688	3.06	3.33	4.00	0.30	520	1730	0.910	0.80
577	20	682	2.96	3.45	3.70	0.29	539	1858	0.850	0.94
578	20	709	2.93	3.22	3.56	0.31	502	1615	0.785	1.01

RUN	$\overline{h'^2}$ cm^2	$\lvert\overline{h'}\rvert$ cm	$\lvert h'\rvert_{max}$ cm	$\phi^{**}(n_o)$ $cm^2 sec$	$\phi(n_o)/\overline{h'^2}$ sec	β^*
540	55.0	5.7	23.7	370	6.7	7.8
541	51.0	5.6	19.6	310	6.1	7.6
542	67.8	6.4	26.8	460	6.8	7.4
545	45.3	5.1	37.0	220	4.9	8.7
546	33.5	4.6	22.7	130	3.9	6.5
550	31.0	4.4	20.0	210	6.8	7.1
551	28.5	4.2	16.3	175	6.2	7.4
553	41.3	5.0	21.5	210	5.1	7.2
556	113	8.4	44.4	780	6.9	9.8
557	126	9.0	42.6	1400	11.1	9.6
558	119	8.7	44.2	1140	9.5	7.5
559	108	8.3	43.5	815	7.5	9.8
563	106	8.2	42.4	700	6.6	9.8
564	131	9.1	52.5	900	6.9	9.8
565	140	9.4	45.5	1150	8.2	8.1
566	125	8.9	42.0	1110	8.9	9.8
575	299	13.8	61.3	2380	7.9	9.1
576	213	11.6	60.0	1690	8.0	11.5
577	218	11.6	62.5	1620	7.8	10.5
578	211	11.5	59.1	1840	8.7	12.6

* $\log\beta = \log \phi_h(n)$ at $n = 1$ cps

** single spectral estimates: $\Delta h = 1/60$ cps

Ratio of Structure Function and Spectral (Inertial Sub-Range) Constants

In § 4.4.2.2. the ratio C_u/K_u was found to be 3.30 ± 0.16. It will be shown that such a value, rather than 4.03 assumed by many authors in the past, is consistent with a theoretical prediction requiring knowledge of the observed limits of the inertial sub-range.

The Fourier transform relationship between $D(x)$ and $\phi(k)$ is,

$$D(x) = 2\int_0^{\infty} \phi(k)\,(1 - \cos kx)\,dk \qquad 4.18$$

The integral will be considered for three wave number ranges viz.,

$0 < k < k_L$ (the energy production region)

$k_L < k < k_u$ (where $\phi(k) = K_u \varepsilon^{2/3} k^{-5/3}$)

$k_u < k < \infty$ (the energy dissipation region)

Equation 4.18 can then be written,

$$\frac{1}{2}D(x) = \int_0^{k_L} \phi_1(k)\,(1 - \cos kx)\,dk + \int_{k_L}^{k_u} \phi_2(k)\,(1 - \cos kx)\,dk + \int_{k_u}^{\infty} \phi_3(k)\,(1 - \cos kx)\,dk \qquad 4.19$$

Now consider the hypothetical case of the spectral form $\phi_2(k) = \alpha k^{-5/3}$ extending over all wave numbers; this allows 4.19 to be written in terms of the integral $\int_0^{\infty} \phi_2(k)\,(1 - \cos kx)\,dk$

viz.

$$\frac{1}{2}D(x) = \int_0^{k_L} (\phi_1 - \alpha k^{-5/3})(1 - \cos kx)\,dk + \int_0^{\infty} \alpha k^{-5/3}(1 - \cos kx)\,dk$$

$$+ \int_{k_u}^{\infty} (\phi_3 - \alpha k^{-5/3})(1 - \cos kx)\,dk \qquad 4.20$$

The middle integral equals $2\alpha x^{2/3}$ (Webb, 1964). From the known shape of the spectrum, then for $k < k_L$, $\alpha k^{-5/3} >> \phi_1(k)$ and $k > k_u$, $\alpha k^{-5/3} >> \phi_3(k)$. The first and third integrals in 4.20 can then be approximated using these inequalities. Nevertheless they are still unintegrable over finite k ranges and further approximations are necessary to assess their relative importance regarding the form of $D(x)$ over a range of x constituting the inertial sub-range. 4.20 becomes now,

$$\frac{1}{2}D(x) = 2\alpha x^{2/3} + I_p + I_D \qquad 4.21$$

where

$$I_p = -\int_0^{k_L} \alpha k^{-5/3}(1 - \cos kx)\,dk$$

$$I_D = -\int_{k_u}^{\infty} \alpha k^{-5/3}(1 - \cos kx)\,dk$$

For $k > k_u$, the maximum value of I_D equals $\alpha x^{2/3}\left(3/(k_u x)^{2/3}\right)$. By expanding $1 - \cos kx$ as $(kx)^2/2$ for $kx \lesssim 1$, I_p becomes,

$$I_p \simeq -\frac{3}{8}(k_L x)^{4/3}\,\alpha x^{2/3}$$

Therefore,

$$D(x) = 4\alpha x^{2/3}\left(1 - \frac{3}{16}(k_L x)^{4/3} \pm \frac{3}{2(k_u x)^{2/3}} \cdots\cdots\right) \qquad 4.22$$

In practice it is observed that $D(x) = \beta x^{2/3}$ when $x_{min} < x < x_{max}$, and so,

$$\beta \simeq 4\alpha \left(1 - \frac{3}{16}(k_L x)^{4/3} \pm \frac{3}{2(k_u x)^{2/3}}\right)$$

so long as x lies between x_{min} and x_{max}.
If this range is such that,

$$k_L x_{max} << 1$$
$$k_u x_{min} >> 1$$

then, $\beta = 4\alpha$ i.e. $C_u/K_u = 4$. The latter inequality is observed in practice where typically $k_u x_{min} \sim 100$. However $k_L x_{max}$ is typically ~ 1. With $k_L x = 1$,

$$\beta = 4\alpha \left(1 - \frac{3}{16}\right) = 3.25\,\alpha$$

i.e. $\beta/\alpha = C_u/K_u = 3.25$.

This is close to the value found by experiment viz., 3.30 ± 0.16.

Acknowledgements

Particular thanks are due to Mr. R.A. Drayton for programming and computing; Mr. E.G. Jennings for the photographic work and Miss M. Street who took on the typing at short notice.

Also to Mr. D. Tribble, Senior Experimental Scientist in the Department who designed most of the instrumentation and electronics and carried out much of the experimental work on site, and who kindly made available to me most of the technical details in § 2.1.

Finally to my supervisor Professor P.A. Sheppard for his guidance, and inexorable criticism of my work.

Bibliography

Batchelor, G.K.	1953	The Theory of Homogeneous Turbulence. (Cambridge University Press).
Blackman, R.B. and Tukey, J.W.	1958	Measurement of Power Spectra. (Dover Publications, New York).
Hinze, J.O.	1959	Turbulence. (McGraw Hill).
Kinsman, B.	1965	Wind Waves. (Prentice Hall, New Jersey).
Lumley, J.L. and Panofsky, H.A.	1964	The Structure of Atmospheric Turbulence. (Wiley & Sons, New York).
Pasquill, F.	1962	Atmospheric Diffusion. (D. Van Nostrand, London).
Phillips, O.M.	1966	Dynamics of the Upper Ocean. (Cambridge University Press).
Priestley, C.H.B.	1959	Turbulent Transfer in the Lower Atmosphere. (University of Chicago Press).
Roll, H.U.	1965	Physics of the Marine Atmosphere. (Academic Press, New York).
Tatarskii, V.I.	1961	Wave Propogation in a Turbulent Medium. (Science Press).

References

Ball, F.K.	1961	J.Met., 18, p.553.
Barad, M.L.	1958	Geo.Res.Pap.No.59, A.F.C.R.C.
Barnett, T.P. and Wilkonson, J.C.	1967	J.Mar.Res., 25, p.292.
Batchelor, G.K.	1947	Proc.Camb.Phil.Soc., 43, p.533.
	1950	Q.J.R.Met.Soc., 76, p.133.
Berman, S.	1965	Ibid, 91, p.302.
Brocks, K.	1966	Beit.Phys.Atmos., 39, 2-4.
Burling, R.W.	1955	Ph.D. Thesis, University of London.
Busch, N.E. and Panofsky, H.A.	1968	Q.J.R.Met.Soc., 94, p.132.
Businger, J.A. and Miyake, M.	1968	Ibid, 94, p.206.
Bye, J.A.T.	1967	J.Mar.Res., 75, p.95.
Charnock, H.	1955	Q.J.R.Met.Soc., 81, p.639.
	1967	Ibid, 93, p.97.
Chou Min-Yui	1966	Bull.Acad.Sci.(U.S.S.R.) Atmospheric and Oceanic Physics, 2, p.291.
Deacon, E.L.	1955	C.S.I.R.O. Div.Met.Phys. Tech.Paper No.4.
Deacon, E.L., Sheppard, P.A. and Webb, E.K.	1956	Aust.J.Phys., 9, p.511.
Dyer, A.J.	1967	Q.J.R.Met.Soc., 93, p.501.
Elagina, E.G.	1963	Bull.Acad.Sci.(U.S.S.R.) Geo.Ser. p.1133.
Elliot, W.P.	1958	Trans.Amer.Geophys.Union, 39, p.1048.
Eleagle, R.G., Deardorff, J.W. and Badgley, F.I.	1958	J.Mar.Res., 17, p.141.
Gibsen, M.M.	1963	J.Fluid Mech., 15, p.161.
Gibsen, M.M. and Schwartz, W.H.	1963	Ibid, 16, p.365.

Gifford, F.	1959	J.Met., 16, p.344.
Gill, G.C.	1967	Proc.First Canadian Conference on Micrometeorology, Part 1, p.1.
Grant, H.L., Stewart, R.W. and Moilliet, A.	1962	J.Fluid Mech., 12, p.241.
Gurvich, A.S.	1960a	Bull.Acad.Sci.(U.S.S.R.) Geo.Ser., p.695.
	1960b	Ibid, p.1033.
	1961	Ibid, p.1031.
Gurvich, A.S. and Zubkovskii, S.L.	1966	Bull.Acad.Sci.(U.S.S.R.) A.O.P., 2, p.118.
Hasse, L., Brocks, K., Dunckel, M. and Görner, U.	1966	Beit.Phys.Atmos., 39, p.254.
Hess, G.D. and Panofsky, H.A.	1966	Q.J.R.Met.Soc., 92, p.277.
Hicks, B.C.	1960	see Phillips (1960).
Ivanov, V.N.	1962	Bull.Acad.Sci.(U.S.S.R.) Geo.Ser., p.788.
Jex, H.R. and MacCready, P.B.	1964	J.App.Met., 3, p.182.
Kinsman, B.	1960	see Phillips (1960).
	1961	J.Geo.Res., 66, p.2411.
Kitaigorodskii, S.A.	1962	Bull.Acad.Sci.(U.S.S.R.) Geo.Ser. p.73.
	1967	Bull.Acad.Sci.(U.S.S.R.) A.O.P., 3, p.769.
	1968	Ibid, 4, p.498.
Kolesnikova, V.N.and Monin, A.S.	1965	Ibid, 1, p.377.
MacCready, P.B.	1962	J.Geo.Res., 67, p.1051.
Miles, J.W.	1957	J.Fluid Mech., 3, p.185.
	1960	Ibid, 7, p.469.
Monin, A.S.	1959	J.Geo.Res., 64, p.2196.
	1962	Ibid, 67, p.3103.
Monin, A.S. and Oboukhov, A.M.	1954	U.S.S.R. Acad.Sci., Works of the Geophys. Inst., No.24 (151).
Mordukovitch, M.I. and Zwang, L.R.	1966	Bull.Acad.Sci.(U.S.S.R.) A.O.P., 2, p.477.

Oboukhov, A.M.	1951	Bull.Acad.Sci.(U.S.S.R.) Geo.Ser. p.49.
	1962	J.Geo.Res., 67, p.3011; also J.Fluid Mech., 13, p.77.
Oboukhov, A.M. and Yaglom, A.M.	1959	Q.J.R.Met.Soc., 85, p.81.
Panofsky, H.A.	1962	J.Geo.Res., 67, p.3161.
Panofsky, H.A. and Deland, R.J.	1959	Advances in Geophysics (6) p.41.
Panofsky, H.A. and Mares, E.	1968	Q.J.R.Met.Soc., 94, p.581.
Panofsky, H.A. and McCormick, R.A.	1960	Ibid, 86, p.495.
Panofsky, H.A. and Townsend, A.A.	1964	Ibid, 90, p.147.
Panofsky, H.A. and Van de Hoven, I.	1955	Ibid, 81, p.603.
Pasquill, F.	1949	Q.J.R.Met.Soc., 75, p.239.
	1962	J.Geo.Res., 67, p.231.
Phillips, O.M.	1957	J.Mar.Res., 16, p.231.
	1958	J.Fluid Mech., 4, p.426.
Phillips, O.M. and Katz, E.J.	1961	J.Mar.Res., 19, p.57.
Pond, S.	1968a	Bull.A.Met.Soc., 49, p.832.
	1968b	J.Geo.Res., 73, p.507.
Pond, S., Stewart, R.W. and Burling, R.W.	1963	J.Atm.Sci., 20, p.319.
Pond, S., Smith, S.D., Hamblin, P.F. and Burling, R.W.	1966	Ibid, 23, p.376.
Preobrazhenskii, L.Yu	1968	Bull.Acad.Sci.(U.S.S.R.) A.O.P., 4, p.569.
Priestley, C.H.B.	1967	Physics of Fluids, 10, No.9, p.538.
Priestley, C.H.B.and Swinbank, W.C.	1947	Proc.Roy.Soc.A, 189, p.543.
Record, F.A. and	1966	Q.J.R.Met.Soc., 92, p.519.

Reynolds, O.	1895	Phil.Trans.Roy.Soc.A, 186, p.123.
Rider, N.E.	1954	Q.J.R.Met.Soc., 80, p.198.
Rider, N.E., Phillips, I.R. and Bradley, E.F.	1963	Ibid, 89, p.507.
Sheppard, P.A.	1958	Ibid, 84, p.205.
Smith, S.D.	1966	J.Mar.Res., 25, p.239.
Snyder, R.L. and Cox, C.S.	1966	Ibid, 24, p.141.
Stewart, R.W.	1967	Boundary Layers and Turbulence, Physics of Fluids Supplement, p.547.
Swinbank, W.C.	1955 1964	C.S.I.R.O. Div.Met.Phys.Tech.Paper No.2. Q.J.R.Met.Soc., 90, p.119.
Swinbank, W.C. and Dyer, A.J.	1967	Ibid, 93, p.494.
Takahashi, T.	1962	J.Ocean.Soc.Japan, 20, p.257.
Takeuchi, K.	1962	J.Met.Soc.Japan, 40, p.127.
Taylor, G.I.	1938	Proc.Roy.Soc.A, 164, p.476.
Taylor, R.J.	1952 1955 1960 1961	Q.J.R.Met.Soc., 78, p.179. J.Aust.Phys., 8, p.535. Bull.Acad.Sci.(U.S.S.R.) Geo.Ser. p.1218. J.Fluid Mech., 10, p.449.
Van de Hoven, I.	1957	J.Met., 14, p.160.
Volkov, Yu A.	1968	Bull.Acad.Sci.(U.S.S.R.) A.O.P., 4, p.555.
Volkov, Yu A., Karpovich, Yu V.and Kestner, A.P.	1967	Ibid, 3, p.577.
Webb, E.K.	1964	Q.J.R.Met.Soc., 90, p.344.
Weiler, H.S. and Burling, R.W.	1968	J.Atm.Sci., 24, p.653.
Zilitinkevich, S.S.	1966 1967	Bull.Acad.Sci.(U.S.S.R.) A.O.P., 2, p.655. Ibid, 3, p.627.
Zilitinkevich, S.S. and Chalikov, D.V.	1968	Ibid, 4, p.165.

Zubkovskii, S.L. 1962 Bull.Acad.Sci.(U.S.S.R.) Geo.Ser. p.887.

Zubkovskii, S.L.and Kravchenko, T.K. 1967 Bull.Acad.Sci.(U.S.S.R.) A.O.P., 3, p.73.

Zubkovskii, S.L.and Zwang, L.R. 1966 Ibid, 2, p.798

Zwang, L.R. 1960 Bull.Acad.Sci.(U.S.S.R.) Geo.Ser., p.833.
1962 Trans.Inst.Atmos.Phys., Acad.Sci.U.S.S.R.,4.